Spatiotemporal Model of the Asymmetric Division Cycle of *Caulobacter crescentus*

Kartik Subramanian

Dissertation submitted to the faculty of the Virginia Polytechnic Institute and State University in partial fulfillment of the requirements for the degree of

Doctor of Philosophy
in
Genetics, Bioinformatics and Computational Biology

John J. Tyson, Chair
Mark R. Paul, Co-Chair
Yang Cao
Birgit Scharf

September 03, 2014
Blacksburg, VA

Keywords: Mathematical modeling, *Caulobacter* cell cycle, protein regulatory networks, reaction-diffusion models

Spatiotemporal Model of the Asymmetric Division Cycle of *Caulobacter crescentus*

Kartik Subramanian

ABSTRACT

The life cycle of *Caulobacter crescentus* is of interest because of the asymmetric nature of cell division that gives rise to progeny that have distinct morphology and function. One daughter called the stalked cell is sessile and capable of DNA replication, while the second daughter called the swarmer cell is motile but quiescent. Advances in microscopy combined with molecular biology techniques have revealed that macromolecules are localized in a non-homogeneous fashion in the cell cytoplasm, and that dynamic localization of proteins is critical for cell cycle progression and asymmetry. However, the molecular-level mechanisms that govern protein localization, and enable the cell to exploit subcellular localization towards orchestrating an asymmetric life cycle remain obscure. There are also instances of researchers using intuitive reasoning to develop very different verbal explanations of the same biological process. To provide a complementary view of the molecular mechanism controlling the asymmetric division cycle of *Caulobacter*, we have developed a mathematical model of the cell cycle regulatory network.

Our reaction-diffusion models provide additional insight into specific mechanism regulating different aspects of the cell cycle. We describe a molecular mechanism by which the bifunctional histidine kinase PleC exhibits bistable transitions between phosphatase and kinase forms. We demonstrate that the kinase form of PleC is crucial for both swarmer-to-stalked cell morphogenesis, and for replicative asymmetry in the predivisional cell. We propose that localization of the scaffolding protein PopZ can be explained by a Turing-type mechanism. Finally, we discuss a preliminary model of ParA-dependent chromosome segregation. Our model simulations are in agreement with experimentally observed protein distributions in wild-type and mutant cells. In addition to predicting novel mutants that can be tested in the laboratory, we use our models to reconcile competing hypotheses and provide a unified view of the regulatory mechanisms that direct the *Caulobacter* cell cycle.

DEDICATION

Dedicated to my parents, Latha Subramanian and Dr. R. Subramanian. Your love and unconditional support allowed me to follow a path of my own choosing.

ACKNOWLEDGEMENTS

The work presented in this dissertation would not have been possible without the contributions of my mentors, teachers, friends, and family. First and foremost, I would like to express my deepest gratitude to my advisor John Tyson, for the expert training, guidance, and encouragement I have received over the past five years. He has inspired me with his passion for science, his oratory skills, and impeccable work ethic. I could not have asked for a better advisor.

I would also like to thank my co-advisor, Mark Paul, who has always been available to patiently discuss fledgling ideas on modeling strategies. His critique and insight have been valuable to my ongoing development as a researcher. I would like to express appreciation to my committee members, Dr. Yang Cao and Dr. Birgit Scharf, who have been more than eager to discuss the progression of my research project, and offer suggestions when I was in a tangle. I am grateful for the time invested by all members of my committee, and the confidence they have placed in me to carry out research in an independent manner. With their assistance, I have learned how to view and investigate biological systems from the perspective of multiple disciplines.

I would like to acknowledge the support of members in the Tyson lab, past and present. Janani (& Arjun), whose enthusiasm for science was infectious, spawned many discussions over lunch and coffee. Anael, who is both friend and mentor, was a great source of support with his timely advice and perspectives on performing research. I was fortunate to be in the company of, and learn from other talented members of the Tyson lab, including Oak, Rajat, Tian, Iman, Mobaserra, TC Jones, Chun, Kenneth, Chiara, Pavel, Jignesh, Sandip, Debashis, Cihan, and Alida. Last but not the least, I express my most sincere gratitude to the wonderful Kathy Chen. Apart from her scientific insight and personal support, she ensured the supplies of cookies, coffee, home-baked brownies, banana bread, and homegrown tomatoes never ran out, helping me to put in the extra hour everyday.

I would like to thank the GBCB program; in particular, Dr. Bevan, and the peerless Dennie Munson for help with administrative affairs. I would also like to thank the kind Sue Rasmussen, who managed salaries and accounts during my stay as a graduate student.

Blacksburg is a place I grew to love, and my stay here was made more enjoyable thanks to the wonderful people I met. Pritesh, Vandana, Ravi, Govind, Gaurav, Asmita, Jaideep, Balaji, Hardik, Priya, Manasa, Saloni, Keyur and the PK's karaoke gang including Bobby, Lukas, Shantala, and Bandy.

I would like to thank my dearest friends Ajay, Aalok, Karan, Sahil, Mayuresh, Amruta, & Shyamala. I had a wonderful time discovering the United States with you.

I would like to thank members of my family: amma, appa, Kavita, Myra and Gaurav. I was comforted knowing that you will always be there for me.

Blacksburg is also the place where I first saw the most wonderful girl I would ever meet. Sudeeksha, it is debatable whether your presence in my life hastened or delayed my PhD, but I would have it no other way. Lots of likes!!

Lastly, I would like to thank *Caulobacter crescentus*. While you were a challenging and at times frustrating organism to study, you cannot be blamed of being dull, and kept me interested throughout our collaboration of five years. Thank you!!

ATTRIBUTIONS

Funding:

The work described in this dissertation is supported by a grant from the National Science Foundation (DMS-1225160). The funders had no role in study design, data collection and analysis, decision to publish, or preparation of the manuscript.

Chapters 2-5 in this dissertation are manuscripts that have either been published or will be submitted shortly.

Chapter 2: Kartik Subramanian, Mark R. Paul, John J. Tyson (2013) Potential Role of a Bistable Histidine Kinase Switch in the Asymmetric Division Cycle of *Caulobacter crescentus*. PLOS Comput.Biol 9(9): e1003221

Chapter 3: Kartik Subramanian, Mark R. Paul, John J. Tyson. Dynamic Localization of DivL and PleC in the Asymmetric Division Cycle of *Caulobacter crescentus*: A Theoretical Investigation of Alternative Models. (To be submitted)

Chapter 4: Kartik Subramanian, Mark R. Paul, John J. Tyson (2014) *De novo* Production of Turing Activator Generates Polarity in Pattern Formation. Proceedings of the Evry Spring School on Modelling Complex Biological systems in the context of Genomics (Evry, France) pp. 131-142

Chapter 5: Kartik Subramanian, Fei Li, Yang Cao, Mark R. Paul, John J. Tyson. Turing Mechanism Explains PopZ Localization in *Caulobacter crescentus*. (To be submitted)

The contributions of co-authors are as follows:

Dr. John J. Tyson is the corresponding author on all manuscripts. He provided guidance for the conception and design of all mathematical models described in the dissertation. He also helped analyze and interpret the simulation results, and contributed to the revision of the various drafts of the manuscripts. He significantly contributed to the formulation of the PleC-DivK biochemical network based on principles of thermodynamics and allostery (Chapter 2). He provided material (computers/ software) used for the simulations.

Dr. Mark R. Paul is a co-author on all manuscripts. He provided valuable advice regarding the formulation of the reaction-diffusion models and the ODE solvers used in the simulations. He helped critique the simulation results, and contributed to the analysis of the same. He reviewed all manuscripts and made suggestions that helped strengthen the readability of the manuscripts.

Dr. Yang Cao is a co-author of the manuscript presented as Chapter 5 in this dissertation. He contributed significantly to the development of the stochastic algorithm used to model PopZ distribution. He helped critique and analyze the results of the stochastic simulations obtained by his graduate student Fei Li.

Fei Li is a graduate student in Dr Yang Cao's Lab at Virginia Tech. He is a co-author of the manuscript presented as Chapter 5 in this dissertation. He helped develop the stochastic version of the PopZ model. He performed the stochastic simulations and contributed to the analysis and interpretation of the results. Along with Dr Yang Cao, he helped write the description of the stochastic model and the corresponding results.

Table of Contents

List of Figures

List of Tables

Chapter 1 Preface

1.1 Introduction

1.1.1 Asymmetric protein localization and division cycle in prokaryotes

A textbook description of the differences between eukaryotes and prokaryotes would mention that unlike in eukaryotes, the components in the bacterial cytoplasm are homogeneously distributed. However, this notion has been dispelled; improvements in imaging techniques have revealed that proteins [1,2], RNA [3], and chromosomes [4] are localized at specific subcellular domains of the bacterial cytoplasm. Moreover, the distribution profiles of these macromolecules change during the cell cycle. Protein localization has been observed in many bacteria, including *E.coli* [5], *B.subtilis* [6,7]*, V. cholerae* [8], and *S.flexnerii* [9,10]. However, it is probably most significant to the life cycle of *Caulobacter crescentus*; affecting a range of physiological processes such as growth [11,12], cell shape [13,14], differentiation [15], motility [16,17], stringent response [18,19], and cell division [20].

Caulobacter is a free-living, oligotrophic bacterium that resides in aquatic environments. In order to survive on limited nutrients, it has evolved a dimorphic life cycle (**Figure 1.1**) [21]. Cell division gives rise to two morphologically and functionally different daughters: a sessile but replication competent 'stalked cell' that remains anchored to the substratum; and a motile but quiescent 'swarmer cell' that can disperse in search of fresh nutrients. By separating the two daughters, the bacterial population within a geographic location may be maintained below carrying capacity afforded by the low-nutrient environment. The obligate swarmer stage may also offer a competitive advantage by enabling the slow growing *Caulobacter* population to find new nutrient-rich regions before other microbial communities [22]. In response to nutritional cues, the swarmer cell ejects its flagellum, retracts the pili and grows a stalk at the site where the motility apparatus used to be present. The morphological transitions are accompanied by exit from G1-phase and entry into S-phase of the cell cycle. Later, the stalked cell undergoes a second morphological transition, as it acquires a new flagellum at the opposite pole. At this predivisional stage, one half of the cell resembles the stalked cell while the other resembles the swarmer cell.

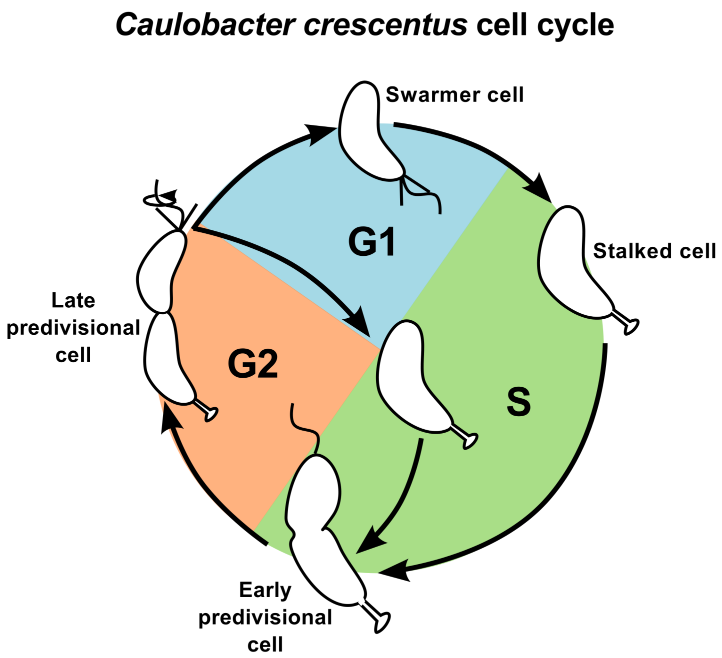

Figure 1.1: Life cycle of *Caulobacter crescentus.*

The motile swarmer cell contains a flagellum and pili, and it cannot undergo DNA replication (G1 phase, blue region). The stalked cell remains attached to substratum by its stalk, and undergoes active DNA replication (S phase, green region). The predivisional cell is equipped with a stalk at one end and a flagellum/pili at the other. It is preparing for cell division (G2 phase, orange region).

1.1.2 *Caulobacter crescentus* is a model organism

The underlying cause for the morphological transitions in *Caulobacter* is the cell cycle-dependent changes in the localization of asymmetrically distributed proteins [2,15]. In the laboratory, it is relatively easy to synchronize *Caulobacter* cells and study the temporal dynamics of proteins [23]. *Caulobacter* strains are also amenable to manipulation and investigation using genetics, biochemical assays and microscopy techniques [24]. The experimental tractability combined with the fact that subcellular localization is intrinsic to its life cycle makes *Caulobacter crescentus* a model organism for understanding asymmetric cell division in prokaryotes.

Caulobacter crescentus in an alpha-proteobacterium. Other members belonging to this class of proteobacteria include the nitrogen-fixing *Sinorhizobium meliloti*, the plant pathogen *Agrobacterium* *tumefaciens*, and the mammalian pathogens *Rickettsia prowazekii* and *Brucella abortus.* Many cell cycle-related genes are shared between different species of alpha-proteobacteria [25,26]. The *Caulobacter* cell cycle also bears resemblance to the division cycle of stem cells, with the stalked cell likened to an asymmetrically dividing stem cell [27]. Therefore, fundamental research using *Caulobacter crescentus* may provide clues to how heterogeneous protein distributions and asymmetric division cycles are regulated in other systems of importance to agriculture and medicine.

1.1.3 The need for a computational model of the cell cycle regulatory network

In most prokaryotes that exhibit non-homogeneous distributions, proteins localize at one or both poles of the cell cytoplasm [8,10,28,29]. The observation of subcellular localization in bacterial cells has stimulated research on discovering the underlying mechanisms that drive the spatial organization of macromolecules in prokaryotes. How do proteins recognize cell poles? What are the mechanisms that govern the temporal regulation of localization? How does the bacterium exploit spatial organization in order to control physiological processes such as differentiation and cell division? Molecular biologists are currently trying to answer these questions by observing changes in cell physiology and in spatiotemporal distributions of proteins in mutant strains of *Caulobacter* [22,24,30]. Based on their results, they hypothesize models that are verbal explanations of how a molecular interaction network can regulate the outcome of a certain physiological process [31–36]. However, the underlying biochemical network that orchestrates the cell cycle is comprised of a large number of proteins that interact in nonlinear fashion. These networks consist of feedback loops that ensure regulated and robust response to environmental stimuli and perturbations [31,37–42]. The inherent complexity of these regulatory networks means that one cannot solely rely on intuition or verbal models to explain the mechanism behind a certain physiological outcome. Not surprisingly, there are instances of researchers producing similar experimental results but proposing very different mechanisms as the cause of a certain physiological process [29,33–36,43,44].

An advantage of a mathematical modeling approach is that it can be used to compare hypothetical models and establish which proposed hypothesis, if any, is better suited to explain the experimental observations. An *in silico* approach also allows modelers to decompose a large biochemical network into smaller sub-networks or 'modules', that can be modeled and analyzed independently. An end-point of a modeling study should also be to tease out underlying design principles that enable the cell to perform tasks in an efficient and robust fashion. A computational model that is successful in reproducing a majority of the experimental evidence can also be used to make predictions regarding the behavior of the control system under novel conditions. Hence, models can also be cross-validated by experimental tests of predictions made by the model.

The development of high-throughput imaging techniques have accelerated the identification and quantification of localization factors in *Caulobacter crescentus* [44–46]. The extensive amount of data that is available on spatiotemporal distribution of proteins in wild-type and mutant cells, and the need for rigorous mathematical analysis of competing hypotheses warrant the development of a reaction-diffusion model of the cell cycle regulatory network of *Caulobacter crescentus*.

1.2 Research overview

My aim has been to formulate a spatiotemporal model of the cell cycle regulatory network that can prove useful in furthering our understanding of the control mechanism governing the asymmetric division cycle of *Caulobacter crescentus*. Each chapter in this dissertation describes a computational model pertaining to a module of the regulatory network. In each case, I give an overview of the biological system and discuss important questions that can be answered using a modeling approach. I present my hypothesis and assumptions that are the basis of the model formulation. Simulation results are discussed in the light of experimental observations, and model predictions are proposed to stimulate future experimental research. Finally, based on computational analysis, I discuss new insight that emerge regarding the nature of the control system and its role in directing cell cycle progression and cell fate asymmetry.

In **chapter 2**, we propose a molecular mechanism to explain DivK-induced conformational changes in the histidine kinase PleC. The elementary chemical reactions proposed in our mechanism are consistent with the general principles of thermodynamics, allostery and enzyme-substrate reactions. A temporal model (ordinary differential equations only) based on our mechanism shows that the transition of PleC from a phosphatase to kinase is a bistable switch driven by DivJ. Bistability allows the swarmer-to-stalked transition to be robust to small perturbations in nutrient level, and ensures that the stalked cell does not transition back to the swarmer stage. The kinase form of PleC was considered non-essential under physiological conditions [47]. Our model suggests otherwise, indicating that the kinase form of PleC may be required to prevent premature swarmer pole development.

During the swarmer-to-stalked transition, DivK gets phosphorylated and binds to DivL in order to inactivate DivL. Consequently, CtrA~P gets dephosphorylated in the stalked cell [32,48]. The inhibitory relation between DivL and DivK~P ensures that CtrA~P level is high in swarmer cells but low in replication-competent stalked cells. Paradoxically in the predivisional cell stage, DivL is reactivated in spite of co-localizing with its inhibitor DivK~P. To resolve this conundrum, informal models propose that co-localized PleC is a phosphatase that dephosphorylates approaching DivK~P, thereby creating a "protection zone" for DivL [32]. We investigated this hypothesis by including spatial aspects to the mechanistic model proposed in Chapter 2. **Chapter 3** describes the spatiotemporal model of the DivJ-PleC-DivK and DivL-CckA-CtrA sub-networks. Our simulations show that PleC cannot be a phosphatase in the predivisional cell prior to compartmentalization. Instead, we propose that predivisional-cell PleC is a kinase that sequesters DivK~P away from DivL, thereby maintaining DivL in an active state. Simulation results support our hypothesis of "inhibitor sequestration". Our model suggests that the rationale for varying subcellular localization of DivL and PleC is to exploit dynamic spatial localization in order to progress through the stalked and predivisional cell without resorting to any changes in the reaction network topology.

The PopZ polymer is considered as a 'landmark' protein that self-assembles in a cell cycle-regulated fashion [36]. In the swarmer cell, PopZ is present only at one pole of the cell, before assuming bipolar localization in the early predivisional cell. Based on the observed distribution pattern in wild-type and mutant cells, we speculated that an Activator-Substrate depletion (A-SD) type Turing mechanism is responsible for the localization of PopZ polymer. The polymer is the activator and the monomeric form of PopZ is the substrate. However, the classical Gierer-Meinhardt equations of an A-SD Turing pattern do not exhibit activator localization at the poles, unless a nucleating factor is present to bias the distribution. The evidence for a nucleating factor for PopZ is debatable. In **Chapter 4**, we formulate a generic A-SD reaction-diffusion model and describe modifications that generate activator peaks that localize at the poles instead of mid-cell.

In **Chapter 5**, we describe our models of PopZ localization as they have evolved over time. The classical equations of Gierer and Meinhardt suffice to explain PopZ localization if we assume ParA is a nucleating factor. This property of ParA is still being debated [36,43]. When we used our modified scheme and parameter constraints as described in Chapter 4, our simulations show that PopZ unipolar-to-bipolar localization is independent of other proteins, and only depends on cell size. However, PopZ localization is not autonomous, but requires the completion of chromosome replication and segregation [29,36]. By accounting for the reportedly slow diffusion and localization of *Caulobacter* mRNA [49], we are able to reconcile the Turing mechanism of PopZ localization with chromosome segregation and cell cycle control. We propose that the cell exploits the slow diffusion of mRNA to fine-tune the timing of PopZ bipolar localization with other cell cycle events, such as the completion of chromosome segregation. Bipolar PopZ localization may be a checkpoint for the completion of S-phase of the cell division cycle.

Completion of chromosome segregation is required not only for PopZ localization but also for localization of DivL and CckA [50] and for the release of cell division protein FtsZ from the new pole to the mid-cell [36]. Given the importance of these proteins to the cell cycle, we sought to understand the cause of varying translocation speeds of the chromosome in mutant strains of *Caulobacter*. In **Chapter 6**, we describe a reaction-diffusion-advection model of the ParABS-mediated chromosome segregation system. Our simulation results are in agreement with the observed translocation times for chromosome segregation in wild-type and mutant strains of *Caulobacter* [33,34]. Based on our analysis of simulated mutants, we propose that PopZ polymers bind excess ParA dimers, thus maintaining an optimal level of nucleoid-bound ParA in the cell cytoplasm. However, our model cannot capture all features of the segregation process. The advection term in our model is phenomenological and cannot be used to compare between the different mechanisms suggested for ParA-dependent segregation. The erratic movement exhibited by the chromosome front [33,34] and the elastic motion of bulk DNA [44] are also not accessible to our deterministic description of segregation. I outline ongoing and future efforts to address these issues.

1.3 References

1. Shapiro L, McAdams HH, Losick R (2009) Why and how bacteria localize proteins. Science 326: 1225–1228. doi:10.1126/science.1175685.

2. Goley ED, Iniesta AA, Shapiro L (2007) Cell cycle regulation in *Caulobacter*: location, location, location. J Cell Sci 120: 3501–3507. doi:10.1242/jcs.005967.

3. Nevo-Dinur K, Govindarajan S, Amster-Choder O (2012) Subcellular localization of RNA and proteins in prokaryotes. Trends Genet 28: 314–322.

4. Thanbichler M, Shapiro L (2006) Chromosome organization and segregation in bacteria. J Struct Biol 156: 292–303.

5. Winkler J, Seybert A, König L, Pruggnaller S, Haselmann U, et al. (2010) Quantitative and spatio-temporal features of protein aggregation in Escherichia coli and consequences on protein quality control and cellular ageing. EMBO J 29: 910–923.

6. Wu LJ, Errington J (2003) RacA and the Soj-Spo0J system combine to effect polar chromosome segregation in sporulating Bacillus subtilis. Mol Microbiol 49: 1463–1475.

7. Dos Santos VT, Bisson-Filho AW, Gueiros-Filho FJ (2012) DivIVA-Mediated Polar Localization of ComN, a Posttranscriptional Regulator of Bacillus subtilis. J Bacteriol 194: 3661–3669. doi:10.1128/JB.05879-11.

8. Yamaichi Y, Bruckner R, Ringgaard S, Moll A, Cameron DE, et al. (2012) A multidomain hub anchors the chromosome segregation and chemotactic machinery to the bacterial pole. Genes Dev 26: 2348–2360.

9. Goldberg MB, Bârzu O, Parsot C, Sansonetti PJ (1993) Unipolar localization and ATPase activity of IcsA, a Shigella flexneri protein involved in intracellular movement. J Bacteriol 175: 2189–2196.

10. Steinhauer J, Agha R, Pham T, Varga AW, Goldberg MB (1999) The unipolar Shigella surface protein IcsA is targeted directly to the bacterial old pole: IcsP cleavage of IcsA occurs over the entire bacterial surface. Mol Microbiol 32: 367–377.

11. Aaron M, Charbon G, Lam H, Schwarz H, Vollmer W, et al. (2007) The tubulin homologue FtsZ contributes to cell elongation by guiding cell wall precursor synthesis in *Caulobacter crescentus*. Mol Microbiol 64: 938–952. doi:10.1111/j.1365-2958.2007.05720.x.

12. Kühn J, Briegel A, Mörschel E, Kahnt J, Leser K, et al. (2010) Bactofilins, a ubiquitous class of cytoskeletal proteins mediating polar localization of a cell wall synthase in *Caulobacter crescentus*. EMBO J 29: 327–339.

13. Charbon G, Cabeen MT, Jacobs-Wagner C (2009) Bacterial intermediate filaments: in vivo assembly, organization, and dynamics of crescentin. Genes Dev 23: 1131–1144.

14. Jin SK, Sun SX (2009) Morphology of *Caulobacter crescentus* and the mechanical role of crescentin. Biophys J 96.

15. Lam H, Matroule J-Y, Jacobs-Wagner C (2003) The asymmetric spatial distribution of bacterial signal transduction proteins coordinates cell cycle events. Dev Cell 5: 149–159. Available: http://www.ncbi.nlm.nih.gov/entrez/query.fcgi?cmd=Retrieve&db=PubMed&dopt=Citation&list_uids=12852859.

16. Lam H, Schofield WB, Jacobs-Wagner C (2006) A landmark protein essential for establishing and perpetuating the polarity of a bacterial cell. Cell 124: 1011–1023. Available: http://www.ncbi.nlm.nih.gov/pubmed/16530047.

17. Briegel A, Ding HJ, Li Z, Werner J, Gitai Z, et al. (2008) Location and architecture of the *Caulobacter crescentus* chemoreceptor array. Mol Microbiol 69: 30–41.

18. Boutte CC, Henry JT, Crosson S (2012) ppGpp and polyphosphate modulate cell cycle progression in *Caulobacter crescentus*. J Bacteriol 194: 28–35. Available: http://www.ncbi.nlm.nih.gov/pubmed/22020649.

19. Henry JT, Crosson S (2013) Chromosome replication and segregation govern the biogenesis and inheritance of inorganic polyphosphate granules. Mol Biol Cell 24: 3177–3186. Available: http://www.pubmedcentral.nih.gov/articlerender.fcgi?artid=3806658&tool=pmcentrez&rendertype=abstract.

20. Goley ED, Yeh YC, Hong SH, Fero MJ, Abeliuk E, et al. (2011) Assembly of the *Caulobacter* cell division machine. Mol Microbiol 80: 1680–1698.

21. Poindexter JS (1981) The *Caulobacter*s: ubiquitous unusual bacteria. Microbiol Rev 45: 123–179.

22. Curtis PD, Brun Y V (2010) Getting in the Loop: Regulation of Development in *Caulobacter crescentus*. Microbiol Mol Biol Rev 74: 13–41. Available: http://mmbr.asm.org/cgi/content/abstract/74/1/13.

23. Evinger M, Agabian N (1977) Envelope-associated nucleoid from *Caulobacter crescentus* stalked and swarmer cells. J Bacteriol 132: 294–301.

24. Skerker JM, Laub MT (2004) Cell-cycle progression and the generation of asymmetry in *Caulobacter crescentus*. Nat Rev Microbiol 2: 325–337. doi:10.1038/nrmicro864.

25. Hallez R, Bellefontaine A-F, Letesson J-J, De Bolle X (2004) Morphological and functional asymmetry in alpha-proteobacteria. Trends Microbiol 12: 361–365. doi:10.1016/j.tim.2004.06.002.

26. Brilli M, Fondi M, Fani R, Mengoni A, Ferri L, et al. (2010) The diversity and evolution of cell cycle regulation in alpha-proteobacteria: a comparative genomic analysis. BMC Syst Biol

4: 52. Available:
http://www.pubmedcentral.nih.gov/articlerender.fcgi?artid=2877005&tool=pmcentrez&rendertype=abstract.

27. Nierman WC, Feldblyum T V, Laub MT, Paulsen IT, Nelson KE, et al. (2001) Complete genome sequence of *Caulobacter crescentus*. Proc Natl Acad Sci U S A 98: 4136–4141.

28. Shapiro L, McAdams HH, Losick R (2002) Generating and exploiting polarity in bacteria. Science 298: 1942–1946. doi:10.1126/science.1072163.

29. Bowman GR, Comolli LR, Gaietta GM, Fero M, Hong S-H, et al. (2010) *Caulobacter* PopZ forms a polar subdomain dictating sequential changes in pole composition and function. Mol Microbiol 76: 173–189. Available:
http://www.pubmedcentral.nih.gov/articlerender.fcgi?artid=2935252&tool=pmcentrez&rendertype=abstract.

30. Ausmees N, Jacobs-Wagner C (2003) Spatial and temporal control of differentiation and cell cycle progression in *Caulobacter crescentus*. Annu Rev Microbiol 57: 225–247. Available: http://www.ncbi.nlm.nih.gov/pubmed/14527278.

31. Paul R, Jaeger T, Abel S, Wiederkehr I, Folcher M, et al. (2008) Allosteric regulation of histidine kinases by their cognate response regulator determines cell fate. Cell 133: 452–461. Available:
http://www.pubmedcentral.nih.gov/articlerender.fcgi?artid=2804905&tool=pmcentrez&rendertype=abstract.

32. Tsokos CG, Perchuk BS, Laub MT (2011) A dynamic complex of signaling proteins uses polar localization to regulate cell fate asymmetry in *Caulobacter crescentus*. Dev Cell 20: 329–341.

33. Schofield WB, Lim HC, Jacobs-Wagner C (2010) Cell cycle coordination and regulation of bacterial chromosome segregation dynamics by polarly localized proteins. Eur Mol Biol Organ J 29: 3068–3081. Available: http://www.ncbi.nlm.nih.gov/pubmed/20802464.

34. Ptacin JL, Lee SF, Garner EC, Toro E, Eckart M, et al. (2010) A spindle-like apparatus guides bacterial chromosome segregation. Nat Cell Biol 12: 791–798. Available: http://www.ncbi.nlm.nih.gov/pubmed/20657594.

35. Ebersbach G, Briegel A, Jensen GJ, Jacobs-Wagner C (2008) A self-associating protein critical for chromosome attachment, division, and polar organization in *Caulobacter*. Cell 134: 956–968. Available: http://www.pubmedcentral.nih.gov/articlerender.fcgi?artid=2614312&tool=pmcentrez&rendertype=abstract.

36. Laloux G, Jacobs-Wagner C (2013) Spatiotemporal control of PopZ localization through cell cycle-coupled multimerization. J Cell Biol 201: 827–841. Available: http://www.mendeley.com/research/spatiotemporal-control-popz-localization-through-cell-cyclecoupled-multimerization/. Accessed 17 October 2013.

37. Domian IJ, Reisenauer A, Shapiro L (1999) Feedback control of a master bacterial cell-cycle regulator. Proc Natl Acad Sci U S A 96: 6648–6653. Available: http://www.pubmedcentral.nih.gov/articlerender.fcgi?artid=21969&tool=pmcentrez&rendertype=abstract.

38. Tan MH, Kozdon JB, Shen X, Shapiro L, McAdams HH (2010) An essential transcription factor, SciP, enhances robustness of *Caulobacter* cell cycle regulation. Proc Natl Acad Sci U S A 107: 18985–18990. Available: http://www.ncbi.nlm.nih.gov/pubmed/20956288.

39. Brazhnik P, Tyson JJ (2006) Cell cycle control in bacteria and yeast: a case of convergent evolution? Cell cycle Georg Tex 5: 522–529. Available: http://cat.inist.fr/?aModele=afficheN&cpsidt=17794220.

40. Subramanian K, Paul MR, Tyson JJ (2013) Potential Role of a Bistable Histidine Kinase Switch in the Asymmetric Division Cycle of *Caulobacter crescentus*. PLoS Comput Biol 9.

41. Li S, Brazhnik P, Sobral B, Tyson JJ (2008) A Quantitative Study of the Division Cycle of *Caulobacter crescentus* Stalked Cells. PLoS Comput Biol 4: 19. Available: http://www.pubmedcentral.nih.gov/articlerender.fcgi?artid=2217572&tool=pmcentrez&rendertype=abstract.

42. Li S, Brazhnik P, Sobral B, Tyson JJ (2009) Temporal Controls of the Asymmetric Cell Division Cycle in *Caulobacter crescentus*. PLoS Comput Biol 5: 15. Available: http://www.ncbi.nlm.nih.gov/pubmed/19680425.

43. Ptacin JL, Gahlmann A, Bowman GR, Perez AM, von Diezmann ARS, et al. (2014) Bacterial scaffold directs pole-specific centromere segregation. Proc Natl Acad Sci U S A. Available: http://www.ncbi.nlm.nih.gov/pubmed/24778223.

44. Lim HC, Surovtsev VI, Beltran BG, HUang F, Bewesdorf Jorg, et al. (2014) Evidence for a DNA-relay mechanism in ParABS-mediated chromosome segregation. Elife 3.

45. Werner JN, Chen EY, Guberman JM, Zippilli AR, Irgon JJ, et al. (2009) Quantitative genome-scale analysis of protein localization in an asymmetric bacterium. Proc Natl Acad Sci U S A 106: 7858–7863.

46. Sliusarenko O, Heinritz J, Emonet T, Jacobs-Wagner C (2011) High-throughput, subpixel precision analysis of bacterial morphogenesis and intracellular spatio-temporal dynamics. Mol Microbiol 80: 612–627.

47. Matroule J-Y, Lam H, Burnette DT, Jacobs-Wagner C (2004) Cytokinesis monitoring during development; rapid pole-to-pole shuttling of a signaling protein by localized kinase and phosphatase in *Caulobacter*. Cell 118: 579–590. Available: http://www.ncbi.nlm.nih.gov/pubmed/15339663.

48. Chen YE, Tropini C, Jonas K, Tsokos CG, Huang KC, et al. (2011) Spatial gradient of protein phosphorylation underlies replicative asymmetry in a bacterium. Proc Natl Acad Sci U S A 108: 1052–1057. Available: http://www.pubmedcentral.nih.gov/articlerender.fcgi?artid=298695&tool=pmcentrez&rendertype=abstract.

49. Montero Llopis P, Jackson AF, Sliusarenko O, Surovtsev I, Heinritz J, et al. (2010) Spatial organization of the flow of genetic information in bacteria. Nature 466: 77–81.

50. Iniesta AA, Hillson NJ, Shapiro L (2010) Polar Remodeling and Histidine Kinase Activation, Which Is Essential for *Caulobacter* Cell Cycle Progression, Are Dependent on DNA Replication Initiation. J Bacteriol 192: 3893–3902. Available: http://www.pubmedcentral.nih.gov/articlerender.fcgi?artid=2916389&tool=pmcentrez&rendertype=abstract.

Chapter 2 Potential Role of Bistable Histidine Kinase Switch in the Asymmetric Division Cycle of *Caulobacter crescentus*

Kartik Subramanian[1], Mark R. Paul[2] and John J. Tyson[3,4,*]

[1]Graduate Program in Genetics, Bioinformatics and Computational Biology, [2]Department of Mechanical Engineering, [3]Department of Biological Sciences, and [4]Virginia Bioinformatics Institute, Virginia Polytechnic Institute and State University, Blacksburg VA 24061

2.1 Abstract

The free-living aquatic bacterium, *Caulobacter crescentus*, exhibits two different morphologies during its life cycle. The morphological change from swarmer cell to stalked cell is a result of changes of function of two bi-functional histidine kinases, PleC and CckA. Here, we describe a detailed molecular mechanism by which the function of PleC changes between phosphatase and kinase state. By mathematical modeling of our proposed molecular interactions, we derive conditions under which PleC, CckA and its response regulators exhibit bistable behavior, thus providing a scenario for robust switching between swarmer and stalked states. Our simulations are in reasonable agreement with *in vitro* and *in vivo* experimental observations of wild-type and mutant phenotypes. According to our model, the kinase form of PleC is essential for the swarmer-to-stalked transition and to prevent premature development of the swarmer pole. Based on our results, we reconcile some published experimental observations and suggest novel mutants to test our predictions.

2.2 Introduction

The function of the cell division cycle of both prokaryotes and eukaryotes is to produce two nearly identical copies of a progenitor cell. The two progeny cells have identical genomes (modulo unavoidable mutations in the DNA replication process), and they are usually quite similar in all other aspects (called ‘‘symmetric’’ cell division). However, there are many cases of asymmetric cell division, in which the two progeny cells are notably different from each other [1]. An interesting example of asymmetric cell division is the freshwater bacterium, *Caulobacter crescentus*. Because *Caulobacter* populations typically live in low-nutrient environments, they have developed a strategy of asymmetric cell division to limit intraspecific competition [2]. During the cell division process, proteins are unequally distributed to the two halves of the cell, giving rise to two morphologically distinct daughter cells. One daughter cell (the stalked cell) is anchored to its place of birth via an appendage called the stalk, while the other daughter cell (the swarmer cell) is equipped with a flagellum and pilus that allows it to swim away from its place of birth. Hence, even though the total number of cells doubles, the number of stalked cells at a specific location stays the same. Another key difference is that, after cell division, the stalked cell immediately initiates a new round of DNA replication and cell division, while the wandering swarmer cell is not competent for DNA replication (it is in a prokaryote version of G1 phase). Once the swarmer cell finds a nutritionally suitable location, it will differentiate into an immobile stalked cell, initiate DNA replication, and establish a new population.

Orchestration of this asymmetric cell division cycle requires proper temporal and spatial regulation of several key proteins (see **Figure 2.1 A**). The temporal dynamics of these proteins was captured in a pair of papers by Li et al. [3,4]. At least two of these proteins, PleC and CckA, are bifunctional, capable of acting as either phosphatase or kinase. PleC kinase activity is up- regulated by its own response regulator, DivK. It is unknown how DivK alters the activity of its own phosphorylating enzyme, PleC. DivK is present at roughly constant level throughout the cell cycle [5]. However, PleC is a phosphatase during the swarmer stage of the cell cycle and kinase during the stalked stage (see Figure 1B). It would be interesting to know how this cross-talk between PleC-kinase and its substrate, DivK, is restricted to the stalked stage of the cell cycle.

At the level of physiology, whether a cell has a stalk or a flagellum depends on the phosphorylation status of the proteins DivK, PleD and CtrA. In the swarmer cell, CtrA~P (the active, phosphorylated form of CtrA) binds to the origin of replication on the *Caulobacter* chromosome and inhibits initiation of DNA replication [6]. During the transition from swarmer to stalked cell, CtrA gets dephosphorylated and degraded, thereby lifting the block on DNA replication. In addition, CtrA affects the transcription of over 125 genes, so periodic changes in CtrA activity causes widespread changes in the expression profile of *Caulobacter* genes during the cell division cycle [7,8]. DivK, on the other hand, is unphosphorylated in the swarmer cell and gets phosphorylated during the transition to the stalked cell. In the phosphorylated state, DivK initiates a pathway for stalk formation [9]. It is also responsible (indirectly) for the dephosphorylation and proteolysis of CtrA [10–12].

The phosphorylation states of DivK and CtrA are governed by the bifunctional histidine kinases PleC and CckA, respectively. Both PleC and CckA can switch between two conformations: a kinase conformation and a phosphatase conformation [9], [11] (see **Figure 2.1 B**). Typically, in bacteria the change in activity of a bifunctional histidine kinase is brought about by an external signal molecule binding to the sensor region of the protein [13]. However, the change in PleC from a phosphatase to a kinase is brought about by its substrate, DivK [9]. In fact, the sensor domain of PleC is not essential for its function [14]. This interaction, where substrate binding to a bifunctional histidine kinase changes its function, has, to our knowledge, been observed only for PleC in *Caulobacter*. It has been suggested that DivK up-regulates PleC kinase activity preferentially in stalked cells because it is in stalked cells where DivK~P and PleC are co-localized at the poles [9].

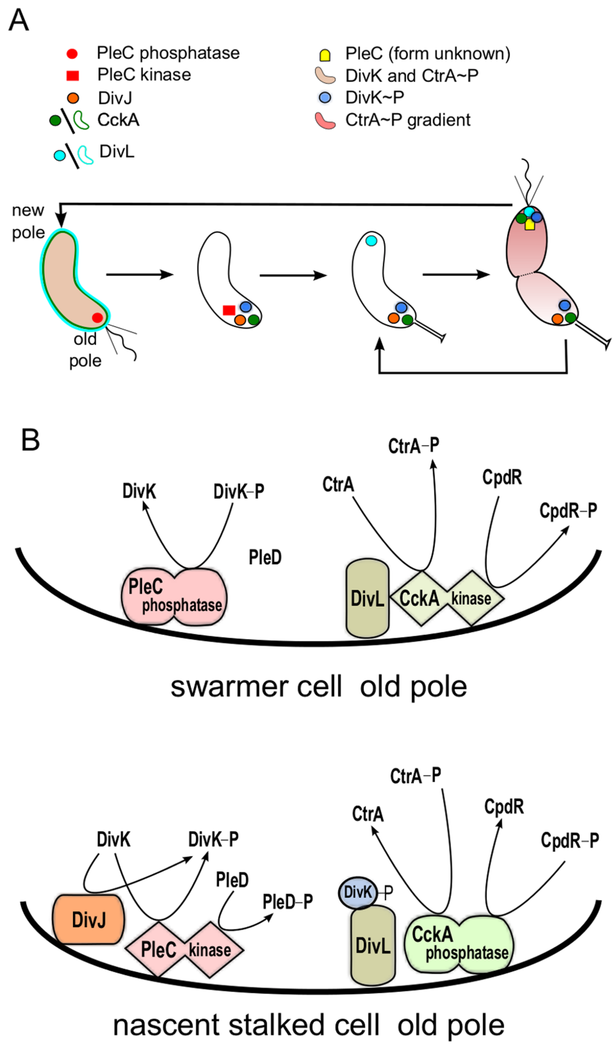

Figure 2.1: Morphological transitions in *Caulobacter crescentus* are governed by changes in localization and activity of proteins.

(A) Schematic representation of the *Caulobacter crescentus* cell cycle. The cell undergoes a series of morphological changes from swarmer cell (left)→nascent stalked cell→stalked cell→pre-divisonal cell (right). These events are driven by changes in the activity and localization of cell cycle proteins. In particular, notice that DivL (light blue) and CckA (green) are uniformly distributed on the membrane in the swarmer cell but localized at the poles in the stalked cell. (B) Model of the status of PleC and CckA activity at the old pole in the swarmer cell and in the nascent stalked cell. In the swarmer cell, DivJ is not localized or activated. As a result, PleC is a phosphatase and CckA is a kinase. In the stalked cell, DivJ is localized to the old pole, causing PleC to flip to the kinase form, which in turn induces CckA to switch to a phosphatase.

CckA acts as a kinase in the swarmer cell, keeping the level of CtrA~P high, which in turn blocks DNA replication [22]. In the stalked cell, CckA becomes a phosphatase, and CtrA gets dephosphorylated, allowing initiation of DNA replication [23]. DivL, a tyrosine kinase has been implicated in maintaining CckA in the kinase state [11], [12], [24], [25]. DivL can phosphorylate CtrA *in vitro* [18]. However, *in vivo* its role in maintaining a high level of CtrA~P is indirect [24]. Multiple lines of evidence support the idea that DivL promotes CtrA phosphorylation via activation of CckA kinase. (a) *divL* mutants show marked reduction not only in CtrA~P but also in CckA~P [24], [26] and CpdR~P [26]. (b) The phenotype of *divJ* over-expression mutants is alleviated by mutations in *divL* [20]. (c) DivK~P is known to bind to DivL and interfere with its ability to activate CckA kinase [11]. Although the mechanism by which DivL influences CckA is unclear, DivL seems to be the intermediate by which the PleC-DivJ-DivK~P axis regulates the level of CtrA~P.

CckA's second substrate, CpdR, is phosphorylated and inactive in swarmer cells [23]. When CckA becomes a phosphatase in the stalked cell, active CpdR turns on the ClpXP proteolytic machinery for degrading CtrA [27], [28]. In this manner, CckA governs both dephosphorylation and proteolysis of CtrA.

Taken together, these observations suggest that PleC-DivJ-DivK and DivL-CckA-CtrA are crucial drivers of the swarmer-to-stalked transition, as summarized in **Figure 2.1** and **Figure 2.2**.

Here, we propose a mechanism for ligand-dependent modifications of the bifunctional histidine kinase, PleC. The mechanism consists of elementary chemical reactions describing ligands (either DivK or DivK~P) binding to the histidine kinase dimer in either its phosphatase or kinase form. The binding states determine the rates of the autophosphorylation, phosphotransfer, and phosphatase reactions catalyzed by PleC. If DivK~P is more efficient than unphosphorylated DivK at promoting the transition of PleC from phosphatase to kinase, then PleC and DivK~P would be involved in a positive feedback loop. Such positive feedback loops are well known for their tendency to function as bistable toggle switches [29], and toggle switches are well known for their roles in cellular decision-making [30]–[32] including critical transitions in the eukaryotic cell cycle [33]–[35].

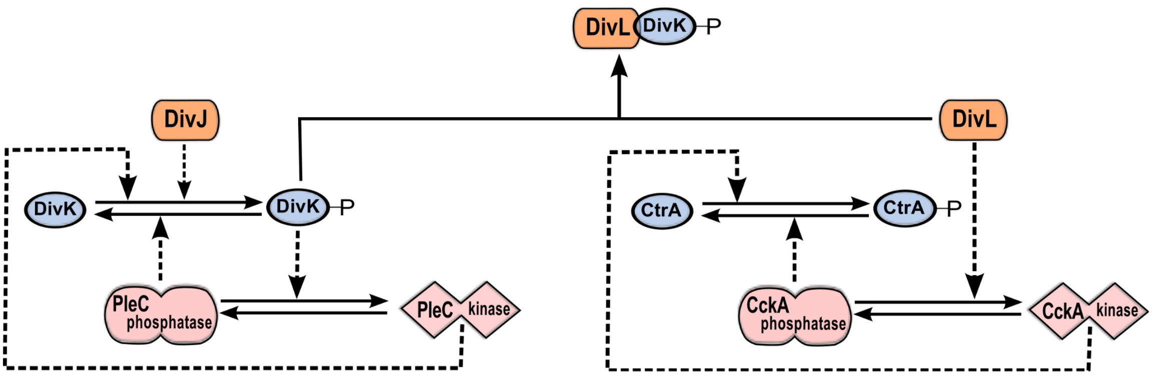

Figure 2.2: The DivJ-PleC-DivK and DivL-CckA-CtrA modules are coupled via DivK~P-DivL interaction.

PleC kinase and DivK~P are involved in a positive feedback loop. By phosphorylating DivK, DivJ biases the positive feedback loop toward the PleC kinase state. DivL up-regulates the kinase form of CckA, which in turn phosphorylates CtrA. The phosphorylated form of DivK~P binds to and inactivates DivL, causing CckA to revert to the phosphatase form and dephosphorylate CtrA.

In the Supplementary Material (**Appendix A.1**), we show that a detailed model of the interactions between DivK and PleC, under reasonable conditions on the rate constants (or propensities) of these reactions, exhibits robust bistability as a function of DivJ activity. That is, by carrying out the initial, limited phosphorylation of DivK, DivJ can function as the "toggle bar" for flipping the bistable switch from the PleC-phosphatase state to the PleC-kinase state. When DivJ activity is low (swarmer cell), PleC is a phosphatase and DivK is predominantly dephosphorylated. As DivJ activity rises, enough DivK gets phosphorylated to flip the PleC switch to the kinase form (stalked cell). By coupling DivK~P to DivL, we show that the PleC switch can induce the transition of CckA from kinase to phosphatase form, causing CtrA~P and CpdR~P levels to drop in the nascent stalked cell (**Figure 2.1 B**).

This model of a PleC bistable switch is an intermediate step on the way to a full spatial model of the asymmetric division cycle in *Caulobacter* cells (in preparation). Using a model based on ordinary differential equations (biochemical kinetics of spatially homogeneous reactions), we address in this paper only certain features of the control system that are independent of the complex spatio-temporal choreography of the cell cycle control system. In particular, we validate our model of the PleC switch against known mutant phenotypes, and then we discuss some predictions of the model: (a) over-expressing DivK should result in a loss of asymmetry and cell cycle arrest in the stalked cell stage, (b) PleC kinase is required to ensure that the nascent swarmer pole will mature only after cytokinesis, and (c) the swarmer-to-stalked transition is robust to fluctuations in nutrients available in the environment.

2.3 Methods

The complete reaction network (**Figure A.1**) was translated into a system of 52 non-linear ordinary differential equations (**Table A.4**) using the mass-action law of chemical kinetics, with one exception. The mechanism by which DivL promotes the kinase form of CckA is unknown, so we modeled this step phenomenologically with a Hill function. Because there are many closed loops of elementary chemical reactions in **Figure A.1**, we must choose rate constant values that respect the thermodynamic principle of detailed balance, as explained in **Appendix A.1**. As long as we satisfy these thermodynamic constraints, we find that the reaction network exhibits bistability over a robust range of parameter values. The parameter values that we use for our simulations of the full model (**Table A.4**) are given in **Table A.5**.

The full model can be simplified slightly by reducing the first 28 equations in **Table A.4** to the first 20 equations in **Table A.6**, as explained in **Appendix A.1**, section D, and confirmed in **Figure A.4**.

The equations for both the full model and the reduced model were encoded as .ode files and simulated using the freely available software, XPP-AUT. The signal-response curves were drawn using the AUTO facility of XPP-AUT. From the data points generated by XPP-AUT, the plots shown in the figures were generated using the python library, Matplotlib [47]. **Figure 2.3** is a simulation of the full model described in **Table A.4**, while **Figures 2.4–2.9** are simulations of the reduced model and its corresponding mutants (**Table A.4** and **Table A.8**).

2.4 Results

2.4.1 Proposed mechanism of substrate-induced conformational changes in PleC

Our detailed mechanism of substrate-induced conformational changes in PleC is presented in the Supplementary Material (**Appendix A.1**). The model is based on the following considerations. PleC is a homodimeric, bifunctional histidine kinase. It can bind to either DivK or DivK~P. As a kinase, it phosphorylates DivK to DivK~P, and as a phosphatase it hydrolyzes DivK~P back to DivK. We assume that, when DivK or DivK~P are bound to both subunits of PleC, the enzyme undergoes a concerted conformational change from its phosphatase form to its kinase form. The conformational change is described in the manner of the Monod-Wyman-Changeux [36] theory of allosteric enzymes. A detailed model of PleC-DivJ-DivK-PleD interactions contains 38 biochemical species (**Table A.4**, Eq. 1–38; **Figure A.1 A** and **B**), many of which are involved in null-cycles. To build a kinetic model of this reaction network, we must assign reasonable values to all the forward and reverse rate constants (k_f and k_r), respecting the fact that $k_f/k_r = K_{eq} = \exp(-\Delta G^0/RT)$, where ΔG^0 is the standard

Gibbs free energy change and K_{eq} is the equilibrium constant for the reaction. In the Supplementary Material **(Appendix A.1)** we assign reasonable ΔG^0 values to every reaction in the network, and then assign k_f and k_r values consistent with the computed equilibrium constants. In this way, we are assured that our kinetic model satisfies the Principle of Detailed Balance around all null-cycles. (For a null cycle, $\Delta G^0 = 0$ and $K_{eq} = 1$; hence, the product of forward rate constants around the cycle = the product of reverse rate constants around the cycle.) Having built a kinetic model that is consistent with the thermodynamic requirements of the histidine kinase (PleC)—response regulator (DivK) system, we then show (see **Figure 2.3**) that the 'two component' system does indeed exhibit bistability as a function of DivJ activity.

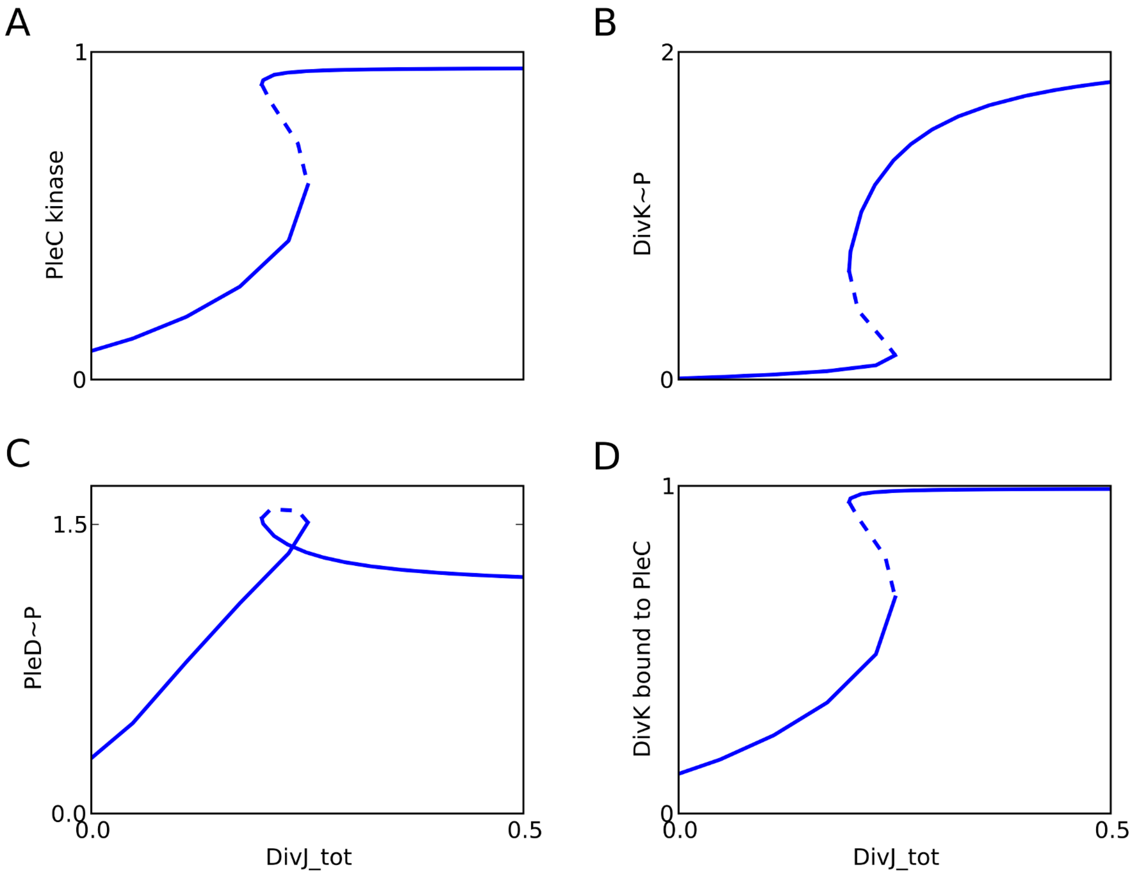

Figure 2.3: DivJ initiates the PleC phosphatase-to-kinase transition.

For the full model (Figure A.1), we plot signal-response curves (one-parameter bifurcation diagrams) for the steady state levels of (A) PleC kinase, (B) DivK~P, (C) PleD~P, and (D) DivK bound to PleC as functions of total DivJ (the parameter DivJ_tot in the model). Solid lines, stable steady states; dashed lines, unstable steady states. In our model, PleC_tot = constant = 1.0, but total DivK, total CtrA, and total PleD depends on DivJ_tot (see Figure A.6).

In the next subsections, we examine biochemically relevant features of this bistable control system.

2.4.2 DivJ-dependent phosphorylation of DivK is crucial for switching PleC from a phosphatase to a kinase

ΔdivJ cells are filamentous [20], [21], show mislocalized stalks and delocalized DivK [5]. In addition, the level of phosphorylation of DivK in *ΔdivJ* cells is reported to be only 44% of wild-type level [21]. Not surprisingly, CtrA~P level is higher in this deletion mutant [20]. Furthermore, mutations in *divJ* have an adverse effect on cell division rate [20], [37], [38]. Hence, DivJ is considered to be a cell-fate determinant, essential for a smooth swarmer-to-stalked transition [39].

Paul *et al.* [9] suggested that DivJ initiates the PleC phosphatase-to-kinase transition, by a positive feedback loop: DivK, on being phosphorylated by DivJ, activates PleC autokinase, and PleC kinase makes more DivK~P. Their experiments, however, indicate that PleC kinase activity is up-regulated by DivK irrespective of DivK's phosphorylation state. Given that the total concentration of DivK remains the same throughout the cell cycle [5], why isn't PleC a kinase at all times?

Presumably, the phosphatase form of PleC has a higher affinity for its substrate DivK~P than for its product DivK. Therefore, even though the PleC phosphatase-to-kinase transition may be promoted by either DivK~P or DivK, DivK~P has a greater propensity than DivK to induce the conformational change. Once PleC becomes a kinase, it produces more DivK~P, which enhances the rate of change from phosphatase to kinase. This self-reinforcing positive feedback loop between DivK~P and PleC kinase can turn the PleC transition into a bistable "toggle" switch [29].

As shown in **Figure 2.3 A**, DivJ can function as the lever of this toggle switch. As the activity of DivJ increases, PleC switches abruptly from a steady state of low kinase activity to a steady state of high kinase activity. DivK also transitions from a mostly-unphosphorylated steady state to a mostly-phosphorylated steady state (**Figure 2.3 B** and **Figure A.6 B**), as does PleD as well (**Figure 2.3 C** and **Figure A.6 F**). We propose that this toggle switch underlies the swarmer-to-stalked transition, where the arrival of DivJ at the old pole triggers PleC to switch to its kinase form, thereby triggering a new stalk end through PleD phosphorylation. It has been shown that upon glucose starvation, DivJ localization is inhibited, and the proportion of swarmer cells in the population doubles [39]. To test the signal-response curves in our model, it would be interesting to see if single cells can toggle between swarmer and stalked morphology upon changing nutrient composition.

According to Paul *et al.*, accumulation of DivK~P at the poles causes its local concentration to increase beyond a threshold required for the activation of PleC kinase. Our model does not address this possibility because (at present) it does not take space into account. While we cannot rule out the contribution of polar localization, our model shows that it is not essential for the phosphatase-to-kinase transition. Our simulations indicate that a large fraction of PleC kinase is bound to DivK (**Figure 3D**). Hence, it is possible that localization of DivK~P is not the cause but the consequence of PleC kinase up-regulation. PleC kinase molecules may serve as docking sites for DivK molecules at the flagellar pole. PleC phosphatase on the other hand need not have any bound DivK. This picture is in agreement with observations that PleC, DivJ and DivL contribute to localization of DivK~P to the poles [19], [40].

2.4.3 Over-expressing DivK may block the cell cycle in the stalked cell stage

In vitro experiments show that PleC kinase activity increases in response to increasing DivK concentration, even in the absence of DivJ [9]. The specific activity of PleD in forming cyclic di-GMP was used as a proxy to measure PleC kinase activity. Surprisingly, the specific activity of PleC kinase *in vitro* is two-fold greater in the presence of $DivK_{D53N}$, a mutant form of DivK that does not get phosphorylated. This indicates that DivK need not be phosphorylated to induce a conformational change in PleC. *In vivo*, however, PleC remains a phosphatase in the DivK-rich swarmer cell. Another odd result of the assay is that the specific activity of PleC kinase drops sharply at high DivK concentrations.

To reproduce these results in Δ*divJ* mutants, we set [DivJ] = 0 in our simulations (**Table A.8**). To simulate the $divK_{D53N}$ mutation, we set the rates of all phosphotransfer reactions to zero (**Table A.8**). In **Figure 2.4** we plot steady-state PleD phosphorylation level against increasing total concentration of DivK (from 0.3 to 30). Our simulations show a qualitative similarity to the experiments [9]. PleD~P level rises at first and then drops at high [DivK] (**Figure 2.4 A–C**). PleD~P levels in Δ*divJ* $divK_{D53N}$ simulations (**Figure 2.4 A**) are comparable to PleD~P levels in Δ*divJ* (**Figure 2.4 B**) and wild-type (**Figure 2.4 C**) simulations. These results support the findings by Paul *et al.* [9] that unphosphorylated DivK is also able to up-regulate PleC kinase. There is a sharp drop in PleD phosphorylation at high [DivK] because PleC shifts predominantly to DivK-bound forms that do not have a free binding site for PleD (**Figure 2.3 D**) and therefore cannot phosphorylate it. Product inhibition by cyclic di-GMP may also play a significant role [41], but this effect is not included in our model.

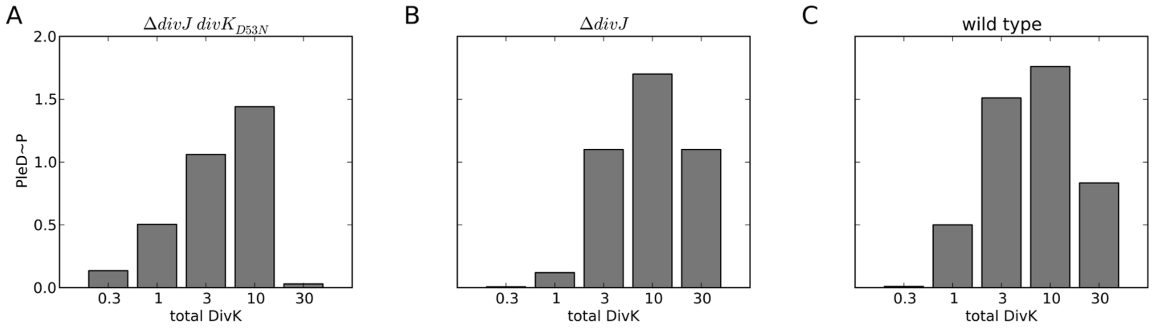

Figure 2.4: Over-expressing DivK causes a drop in PleD phosphorylation.

The steady state level of PleD~P is plotted against increasing amount of total DivK for (A) *ΔdivJ divK*$_{D53N}$, **(B)** *ΔdivJ*, and (C) wild type background. Although the absolute levels vary among the three cell types, in each case PleD~P level shows an initial increase followed by a drop at high DivK.

Since DivK is capable of activating PleC kinase in the absence of DivJ, we plotted a two-parameter bifurcation diagram to estimate the effect of varying concentrations of DivJ and DivK on PleC activity (**Figure 2.5 A**). The enclosed bistable region tapers off as we increase either total DivJ or total DivK (k_{syndk}). This implies that at moderate concentrations of DivK (e.g., $k_{\mathrm{syndk}} = 0.015$), the PleC phosphatase-to-kinase transition is robust and dependent on the activity and localization of DivJ (**Figure 2.5 B**). However, increasing DivK in the cell would lead to transitions that are less robust and independent of DivJ. We predict that a 5- to 10-fold increase in DivK concentration will result in PleC being locked in the kinase form, and the cell will be blocked in the stalked stage of the cell cycle. We propose that *in vivo* the total concentration of DivK is low enough that it needs to be phosphorylated in order to induce PleC to become a kinase. In this case, the bistable PleC switch becomes reliant on the appearance of DivJ activity rather than on the polar accumulation of DivK.

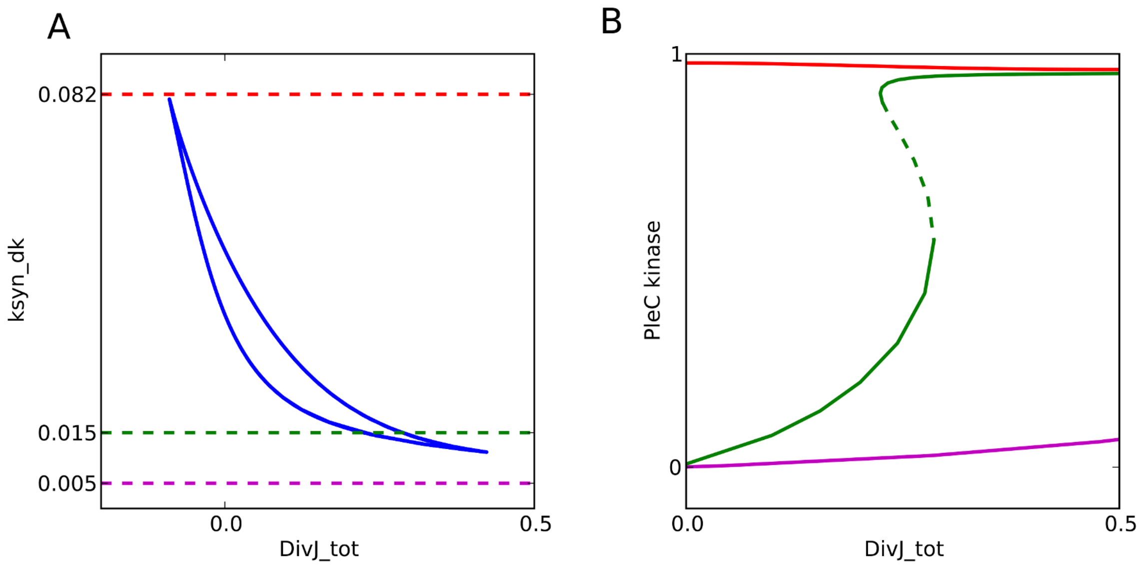

Figure 2.5: Over-expressing DivK causes activation the PleC switch independent of DivJ.

(A) Two-parameter bifurcation diagram, indicating how the PleC switch behaves in cells expressing different levels of DivJ_tot and DivK_total ($\boldsymbol{k}_{syn\_dk}$ is the rate constant for synthesis of DivK). PleC exhibits bistability within the crescent-shaped region bounded by the blue lines. (B) One-parameter bifurcation diagrams (signal-response curves) for three different values of $\boldsymbol{k}_{syn\_dk}$, indicated by the dashed horizontal lines in panel A. Notice that PleC kinase level is always low if $\boldsymbol{k}_{syn\_dk}<0.011$ and always high if $\boldsymbol{k}_{syn\_dk}>0.082$.

2.4.4 The PleC-DivJ-DivK switch confers bistability to the DivL-CckA-CtrA module

The DivL-CckA-CtrA module bears a striking resemblance to DivJ-PleC-DivK switch. Nonetheless, there are important differences. DivL can phosphorylate CtrA *in vitro*, but this reaction is of no significance *in vivo* [22], [42]. Unlike PleC, which directly transfers its phosphoryl group to an aspartate residue on DivK, CckA relies on a series of phospho-transfer events [23]. To this end, it has an additional aspartate-containing domain which first picks up the phosphoryl group from the histidine residue and passes it on to the histidine residue of a downstream histidine phosphotransfer (HPt) protein called ChpT [43]. Finally, ChpT relays the phosphoryl group to the aspartate residue on the response regulator CtrA. In our mathematical equations, we model ChpT and CckA as a single protein, CckA, whose transition from phosphatase to kinase is promoted by DivL. The third difference is that CtrA is not known to up-regulate CckA kinase, so there is no reason to expect bistability in the CckA-ChpT-CtrA phospho-relay system.

It is a well-established fact that DivK~P inhibits CtrA activity, and the mechanistic details of this process have become progressively clear. Initial experiments showed that DivK~P down-regulates

CckA kinase activity [12]. Later experiments indicated that DivL is required for maintaining CckA as a kinase, and that DivK~P binding to DivL inhibits this effect [11], [44]. Since the mechanistic details regarding how DivL influences CckA activity are currently unknown, we model this process phenomenologically, using a Hill function to describe how DivL promotes CckA kinase. We couple the PleC-DivK~P bistable switch to the CckA kinase-to-phosphatase transition by having DivK~P bind to and inactivate DivL. In the swarmer cell, DivJ is absent and the PleC switch is in the phosphatase state (DivK unphosphorylated). Hence, DivL is active and maintains CckA in the kinase state (CtrA phosphorylated). The up-regulation of DivJ is the trigger for the swarmer-to-stalked transition. DivJ activity flips the PleC switch to the kinase state; DivK gets phosphorylated and binds to DivL. DivL activity drops abruptly (**Figure 2.6 A**), and consequently CckA returns to its default phosphatase form (**Figure 2.6 B**). As a result, CtrA becomes dephosphorylated and inactive (**Figure 2.6 C** and **Figure A.6 D**), and CpdR becomes dephosphorylated and active (**Figure 2.6 D**).

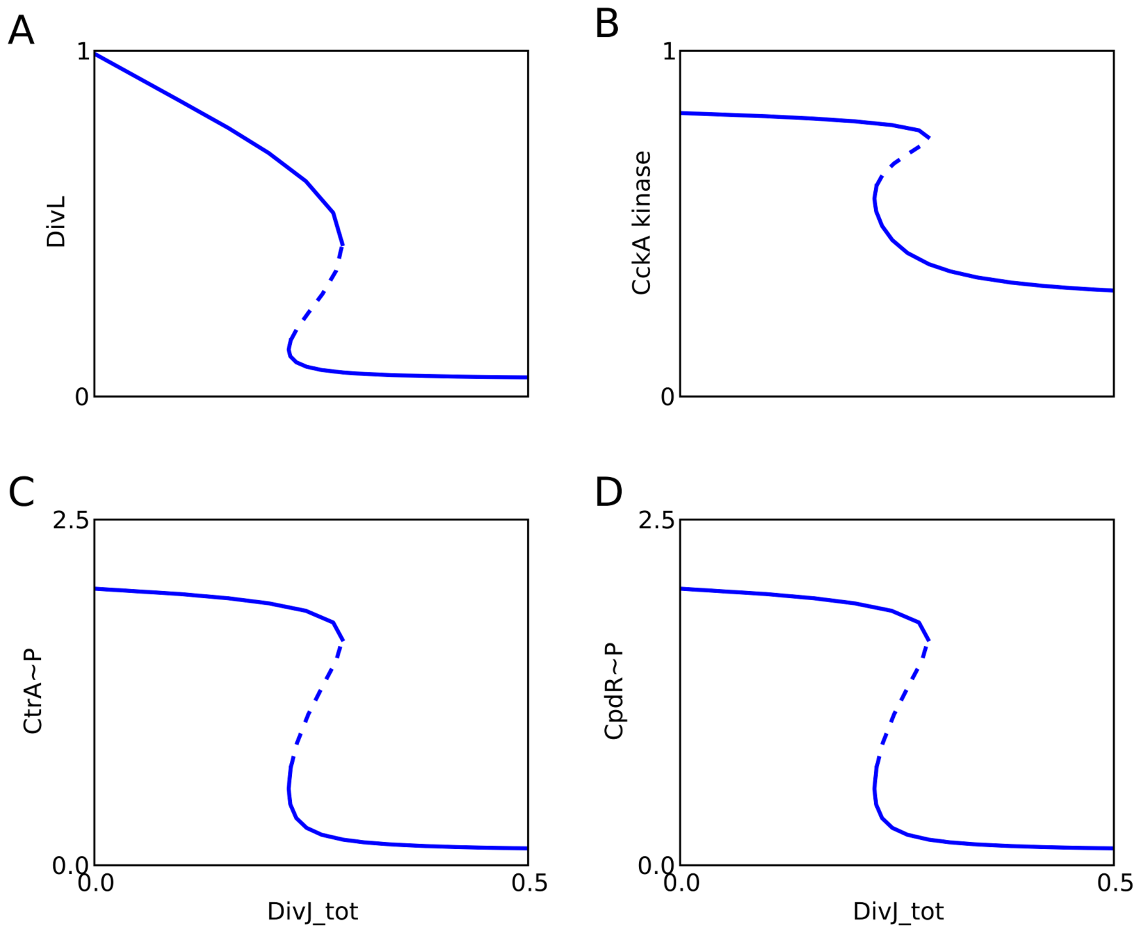

Figure 2.6: The DivJ-PleC-DivK module controls the DivL-CckA-CtrA module.

When the PleC switch is activated, DivK~P binds to DivL and inactivates components of the CckA module. One parameter bifurcation diagrams show the steady state levels of (A) DivL, (B) CckA kinase, (C) CtrA~P, and (D) CpdR~P as functions of DivJ_tot.

The proposed coupling of these switches is supported by experimental evidence that a Δ*divJ* mutant can be rescued by point mutations in *divL* and *cckA* genes [20]. CtrA activity, which is high in Δ*divJ* cells (**Figure 2.7 A**), is restored to normalcy by point mutations in *divL* and *cckA* that interfere with CtrA phosphorylation (**Figure 2.7 B–D**). As expected, CtrA~P level in a Δ*divJ* mutant can be reduced by decreasing the specific activity of DivL (**Figure 2.7 B**). Interestingly, our simulations show that decreasing the specific activity of CckA kinase lowers the level of CtrA~P (**Figure 2.7 C**), but increasing the specific activity of CckA phosphatase does not restore CtrA~P level (**Figure 2.7 D**). Hence, we predict that the point mutations in CckA that rescue Δ*divJ* mutants do so by reducing the kinase activity of CckA.

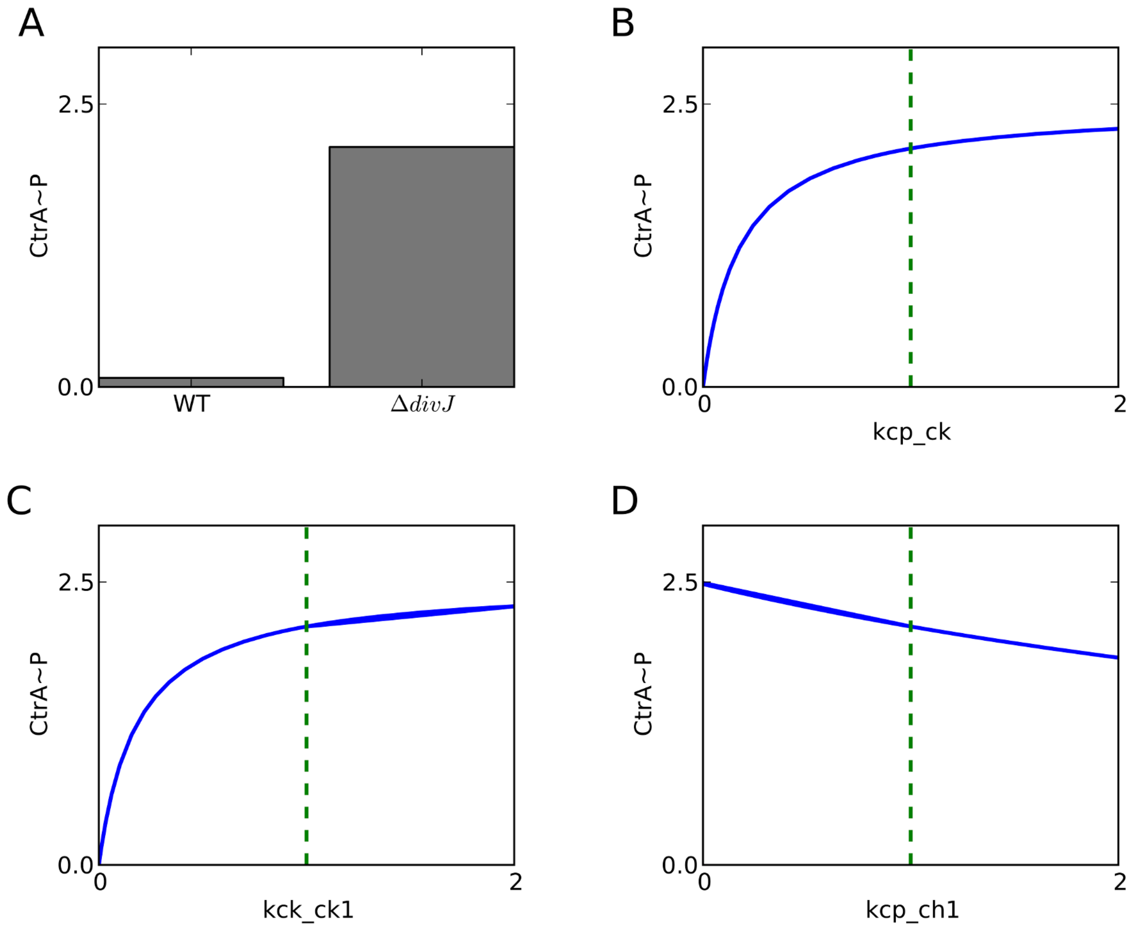

Figure 2.7: Point mutations in CckA suppress the *ΔdivJ* mutant phenotype by affecting CckA kinase activity.

(A) *ΔdivJ* cells show higher CtrA~P level than their wild type counterpart. Point mutations in CckA and DivL are known to suppress the mutant phenotype. To understand how, we plot the steady-state level of CtrA~P as a function of rate constants governing (B) DivL activating CckA kinase ($k_{\text{cp-ck}}$), (C) CckA kinase activity ($k_{\text{ck-ck1}}$), and (D) CckA phosphatase activity ($k_{\text{cp-ch1}}$). The vertical green lines indicate the values of the rate constants in the *ΔdivJ* background. Reducing the value of $k_{\text{cp-ck}}$ or $k_{\text{ck\_ck1}}$ causes a corresponding reduction in CtrA~P level. However, increasing $k_{\text{cp\_ch1}}$ does not cause CtrA~P to fall to its wild-type level.

2.4.5 Simulations of divK$_{D90G}$ are consistent with observed phenotypes

To simulate the consequences of the *divK$_{D90G}$* mutation, we make note of the fact that, *in vitro*, autophosphorylation of PleC is markedly reduced in the presence of DivK$_{D90G}$ [9]. This fact indicates that DivK$_{D90G}$, unlike its wild-type counterpart, is unable to up-regulate the kinase form of PleC. Since DivK$_{D90G}$ is not an allosteric ligand, we set $\Delta G°_{\text{TL}} = 0$, and accordingly updated the equilibrium constants and parameters for all the concerned reactions (**Table A.8**). In addition, although DivK$_{D90G}$

is phosphorylated to the same extent as wild type DivK, it is unable to bind to DivL [11]. Hence, we altered the binding equilibrium of $DivK_{D90G}$ to DivL (**Table A.8**).

Using the altered parameter set, we tried to reproduce two known phenotypes of $divK_{D90G}$ cells. Filamentous $divK_{D90G}$ cells initiate swarmer progeny-specific development (SPD) prematurely. SPD defines a range of cell cycle events, including activation of the flagellum, development of pili, release of the flagellum and ultimately development of the stalk [45]. It is important that these events take place in a timely manner and that they are restricted to the newborn swarmer cell. Filamentous $divK_{D90G}$ mutants, however, initiate SPD in the predivisional cell. In particular, pilin synthesis (a part of SPD) requires CtrA~P. Hence, we examined whether CtrA~P level is increased in simulations of $divK_{D90G}$ mutant cells. **Figure 2.8** compares one-parameter bifurcation diagrams for wild-type (green) and mutant (red) cells. The levels of DivK~P (**Figure 2.8 A**), PleD~P (**Figure 2.8 B**) and PleC kinase (**Figure 2.8 C**) are much lower in mutant cells, while CtrA~P level remains high (**Figure 2.8 D**). This could potentially lead to initiation of SPD.

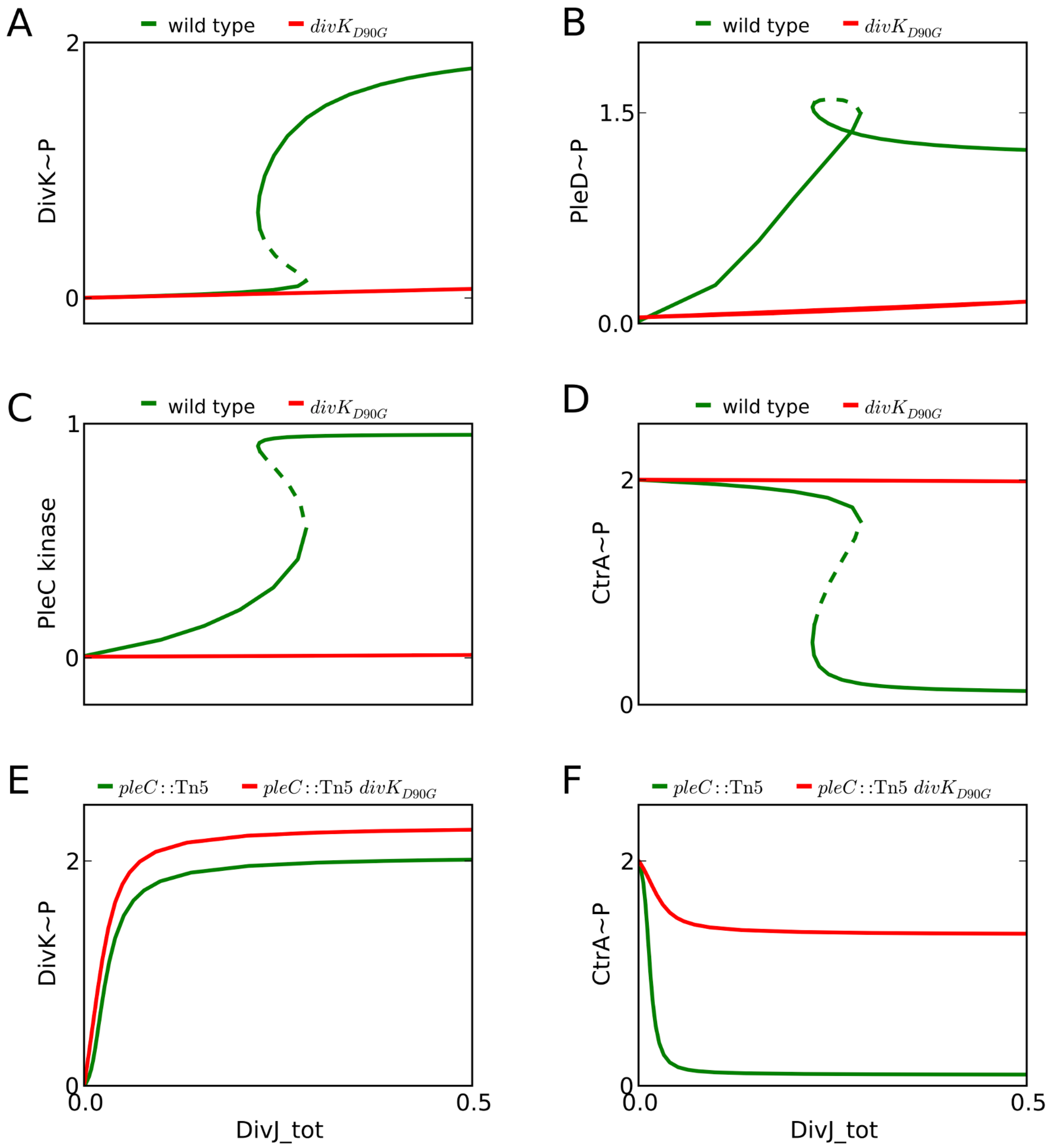

Figure 2.8: Simulations capture the physiological effects of $divK_{\mathbf{D90G}}$ mutants

$divK_{D90G}$ mutants are unable to activate PleC kinase or bind to and inactivate DivL. One parameter bifurcation diagrams compare the wild type (green line) and mutant level (red line) of (A) DivK~P, (B) PleD~P, (C) PleC kinase, and (D) CtrA~P. $divK_{\mathrm{D90G}}$ mutants also suppress the effects of *pleC*:Tn*5* mutants. Our simulations show that (E) the steady state levels of DivK~P are the same in *pleC*::Tn*5* (green line) mutant cells and in *pleC*:Tn*5* $divK_{\mathrm{D90G}}$ double mutants (red line). However, (F) CtrA~P is restored to wild-type level in the double mutant.

The $divK_{D90G}$ mutation is a suppressor of the *pleC*::Tn*5* mutant phenotype. Cells lacking PleC show extended periods of bipolar localization of DivK~P and also fail to develop stalks. A *pleC*::Tn*5* *divK*$_{D90G}$ double mutant does not show any of these defects [45]. Our simulations show that DivK~P level increases and CtrA~P level drops in *pleC*::Tn*5* background (**Figure 2.8 E and F**). Since DivK remains phosphorylated in the absence of PleC, it is not dislodged from the poles [19]. DivK~P binds to DivL and suppresses CtrA phosphorylation (**Figure 2.8 F**), thus preventing SPD. However, in the *pleC*::Tn*5* *divK*$_{D90G}$ double mutant, CtrA~P level remains high in spite of elevated DivK~P (**Figure 2.8 E–F**, red line). This result is in accordance with the finding that CckA~P, CtrA~P and Cpdr~P levels are high when the binding of DivK~P to DivL is weakened [11]. Restoration of CtrA~P in the double mutant allows flagellar pole development. Hence, the restoration of unipolar localization of DivK in *pleC*::Tn*5* *divK*$_{D90G}$ double mutant may be a natural consequence of the inability of DivK$_{D90G}$ to bind to DivL.

2.4.6 The PleC kinase activity may prevent premature swarmer progeny-specific development

Although PleC is bifunctional, its designation in the cell has primarily been that of a phosphatase. This view has been fostered by results showing an elevation in DivK~P in *pleC*::Tn*5* mutants [21]. Furthermore, *pleC*$_{F778L}$ mutants, which lack autokinase activity, appear to have a normal cell cycle [45]. However, later experiments have shown that, although cells possessing PleC$_{F778L}$ progress through the cell cycle without any problems, they show a marked reduction in holdfast attachment [9]. These cells also show lower c-di-GMP levels, indicating that PleD is not sufficiently phosphorylated and activated in the absence of PleC kinase activity. Another mutant that reduces PleC autokinase activity is *divK*$_{D90G}$ [9]. In contrast to the *pleC*$_{F778L}$ mutants, cells possessing the *divK*$_{D90G}$ mutation do not require cytokinesis to initiate SPD.

If both mutations result in loss of PleC autokinase activity, why does only one of them exhibit premature SPD? One may argue that premature SPD is not due to the loss of PleC kinase activity, but is instead a consequence of inability of DivK$_{D90G}$ to bind to DivL. However, we found that altering the rate constants governing the binding reaction had no effect on the phenotype, because DivK$_{D90G}$~P is low at all times and hence does not inhibit DivL. To shed light on this discrepancy, we propose a novel mutant strain of DivK, which we call *divK*$_X$. The novel mutant deviates from *divK*$_{D90G}$ in that it retains wild type ability to bind to DivL. By simulations, we compare the phenotypes of *divK*$_{D90G}$, *divK*$_X$ and *pleC*$_{F778L}$ (see **Figure 2.9**). To model the *pleC*$_{F778L}$ mutant, we set the autophosphorylation rates to zero (**Table A.8**).

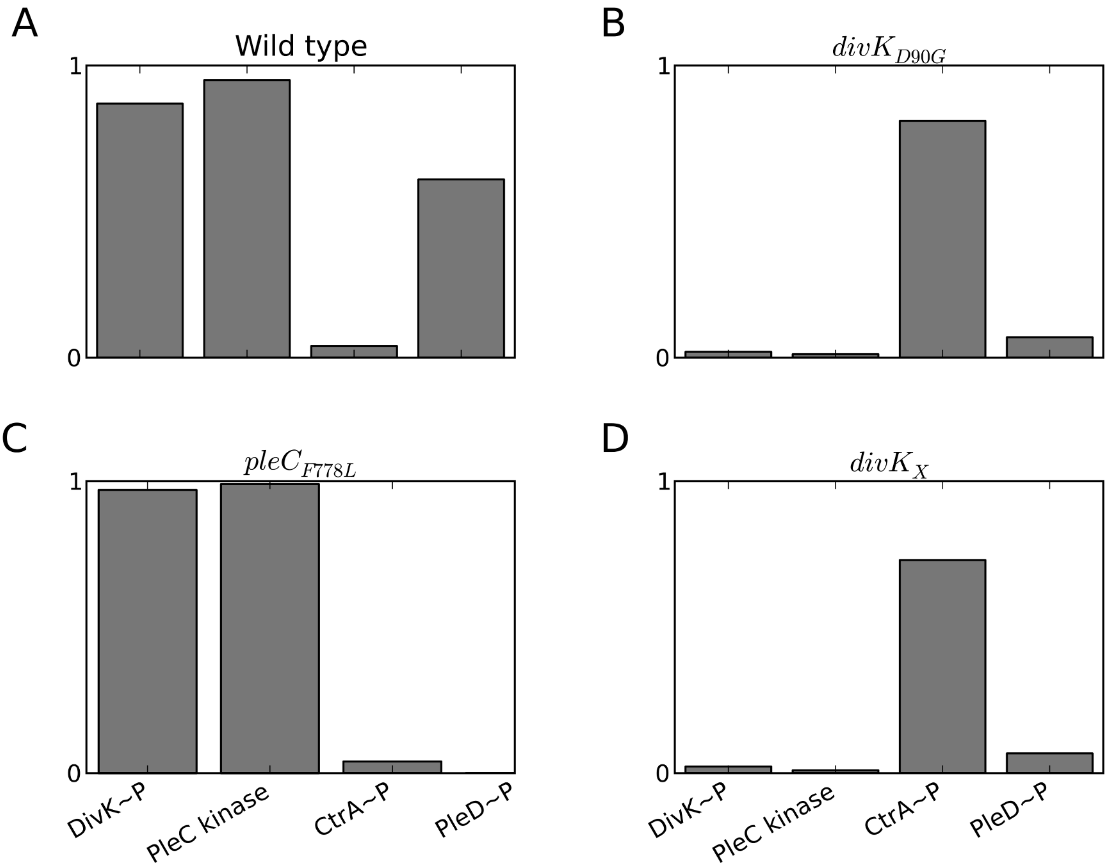

Figure 2.9: Comparison of *pleC*$_{F778L}$ and *divK*$_{\mathbf{D90G}}$ mutants reveals the importance of the PleC kinase state.

For wild-type cells (A) and three different mutants (B–D), we plot the steady-state fractions of four variables: PleC kinase, DivK~P, CtrA~P and PleD~P. $DivK_X$ is a hypothetical mutant form of DivK which is still phosphorylated and dephosphorylated by PleC but does not induce the conformational change of PleC from phosphatase to kinase.

In comparison to wild type, $pleC_{F778L}$ cells show a reduction in the level of PleD~P; but DivK~P and PleC kinase levels show only modest difference (**Figure 2.9 A and C**). This simulated comparison agrees with experimental observations, which show that $pleC_{F778L}$ cells have reduced surface attachments but otherwise cycle normally. We reason that, although $pleC_{F778L}$ does not have kinase activity, it still retains its ability to switch to the kinase form. Hence, in stalked and predivisional cells, the majority of PleC is locked in the inactive kinase conformation. It follows that the PleC phosphatase to DivJ ratio is low and most of the DivK is phosphorylated. In comparison, $divK_{D90G}$ and a $divK_X$ show a reduction in the PleC kinase level **(Figure 2.9 B and D)**. Since most PleC is in the phosphatase form, DivK~P level is low and CtrA~P level remains high throughout the cell cycle, thereby initiating SPD prematurely. Based on these simulation results, we propose that PleC kinase is important to prevent premature SPD. In the predivisional cell prior to compartmentalization, DivJ maintains PleC as a kinase while DivK is phosphorylated and bound to the pole/s. Once cytokinesis occurs, DivJ and PleC find themselves in different compartments, causing PleC to switch back to a phosphatase and allowing SPD.

2.5 Discussion

We propose a model of the *Caulobacter* swarmer-to-stalked (G1-to-S) transition based on a pair of bifunctional histidine kinases, PleC and CckA. We suggest that the phosphatase-to-kinase transition of the PleC bifunctional enzyme is governed by concerted conformational changes brought about by homotropic interaction with its response regulator, DivK. By formulating a mathematical model based on a set of elementary chemical reactions, we show that the transition from phosphatase to kinase can function as a bistable switch driven by the starter kinase, DivJ. Our simulations reproduce the *in vitro* experimental observation that DivK and/or DivK~P up-regulate PleC kinase activity. We hypothesize that even if DivK and DivK~P have equal potential for causing the conformational change of PleC, DivK~P is a more efficient inducer as a natural consequence of it being a substrate to the relaxed form, the phosphatase form of PleC. That DivK~P is a more efficient inducer of the phosphatase-to-kinase transition creates a positive feedback loop and the potential for bistability, and bistability would explain why the swarmer-to-stalked transition is irreversible [35].

The swarmer-to-stalked transition is triggered by a rise in activity of the starter kinase DivJ. Evidence suggests that DivJ accumulates in response to nutritional signals [39]. Compared to well-fed cells, a greater fraction of *Caulobacter* cells are devoid of DivJ foci and exist as swarmer cells under conditions of glucose exhaustion. Hence, we consider DivJ as a nutritional proxy and use it as a control parameter in our model. As observed in our bifurcation diagrams, as total DivJ accumulates, the proteins that drive the swarmer-to-stalked transition show abrupt and irreversible changes in activity at the boundary of the bistable region. Once the transition has occurred, the control system will not permit a reverse transition (stalked-to-swarmer) in response to a marginal drop in nutritional level (i.e., in total DivJ concentration). In our view, once the PleC flips to the kinase form, the cell is committed to a new round of DNA synthesis before it can make a new motility apparatus in the predivisional stage. While bistability is not an essential feature of the morphological transitions in the *Caulobacter* division cycle, we propose that bistability in the PleC phosphatase-to-kinase transition may ensure that the swarmer-to-stalked transition is robust and does not undergo a reverse transition in response to small fluctuations in nutrient levels.

Our model is able to reproduce phenotypes of known experimental mutants and provide additional insight into the underlying physiology. Mutants overexpressing DivK show a decrease in CckA phosphorylation, in addition to filamentous growth and chromosomal over-replication [43]. Our two-parameter bifurcation diagrams indicate that cells with elevated DivK can no longer be regulated by DivJ. At higher concentrations, DivK can drive the positive feedback even in the absence of DivJ, resulting in PleC being in the kinase form and CtrA~P being down-regulated. This prediction can be tested by overexpressing DivK in a Δ*divJ* background. Conversely Δ*divJ* mutants with a normal level of DivK are blocked in G1 phase owing to high CtrA~P, while point mutations in *divL* and *cckA* rescue Δ*divJ* mutants [20]. Our simulations suggest that Δ*divJ* mutants can be rescued by point mutations that down-regulate CckA kinase activity, but not by mutants that up-regulate CckA's phosphatase activity.

Prior experiments and a mathematical model [46] dealing with the PleC-DivJ-DivK system have focused almost exclusively on the phosphatase form of PleC, while the kinase form has been considered inconsequential. We argue on the contrary that PleC kinase activity is important for proper progression through the *Caulobacter* cell cycle. To demonstrate this claim, we make an important distinction between two mutants $pleC_{F778L}$ and $divK_{D90G}$. Our simulations show that while $\mathrm{PleC_{F778L}}$ has no autokinase activity, the majority of $\mathrm{PleC_{F778L}}$ molecules in stalked cells are in an inactive kinase form. These cells would therefore, appear normal. On the other hand, most PleC molecules remain in the phosphatase form in cells containing $\mathrm{DivK_{D90G}}$. We predict that in wild-type predivisional cells, PleC localized at the new pole is in the kinase form. Compartmentalization has the effect of withdrawing DivJ, causing PleC to switch back to the phosphatase form, as seen in our signal-response curves. The PleC-containing compartment, in the absence of DivJ, transitions into a swarmer cell. In mutant $divK_{D90G}$ cells, we predict that PleC at the new pole is always a phosphatase. This, we reason, would cause the premature presence of CtrA~P in predivisional cells resulting in premature swarmer progeny-specific development (SPD). This conclusion is supported by the fact that filamentous $divK_{D90G}$ mutants show SPD in the absence of compartmentalization [45]. We are aware that $divK_{D90G}$ has a pleotropic effect of binding weakly to DivL. Hence, we hypothesize a novel mutant, $divK_X$, which is similar to $divK_{D90G}$ but retains its ability to bind DivL. We simulate such a mutant and find its behavior to be comparable to $divK_{D90G}$.

In this work, we are focusing on a small window in the *Caulobacter* cell cycle, the G1-to-S transition. We have not explored here how these coupled switches would function in a spatio-temporal context and whether they play a role in generating asymmetry in the two halves of the cell at a later stage in the division cycle. To explore these questions requires a spatio-temporal model that tracks the location of proteins in the cell and takes into account the effects of protein diffusion through the cytoplasm, as in [12], [46]. Without an accurate spatio-temporal model of these molecular interactions, we are still a long way from understanding the network of molecular interactions that governs the asymmetric life cycle of *Caulobacter crescentus*.

2.6 References

1. Jacobs C, Shapiro L (1998) Microbial asymmetric cell division: localization of cell fate determinants. Current opinion in genetics development 8: 386–391. Available: http://www.sciencedirect.com/science?_ob=ArticleURL&_udi=B6VS0-45MFJ3Y-2T&_user=126524&_coverDate=08/31/1998&_alid=1568942021&_rdoc=64&_fmt=high&_orig=mlkt&_origin=mlkt&_zone=rslt_list_item&_cdi=6248&_sort=v&_st=17&_docanchor=&view=c&_ct=23585&_acct=C000010360&_version=1&_urlVersion=0&_userid=126524&md5=286896b52402f031c9b3723a9747e995&searchtype=a.

2. Curtis PD, Brun Y V (2010) Getting in the Loop: Regulation of Development in *Caulobacter crescentus*. Microbiol Mol Biol Rev 74: 13–41. Available: http://mmbr.asm.org/cgi/content/abstract/74/1/13.

3. Li S, Brazhnik P, Sobral B, Tyson JJ (2008) A Quantitative Study of the Division Cycle of *Caulobacter crescentus* Stalked Cells. PLoS Computational Biology 4(1): e9. Available: http://www.pubmedcentral.nih.gov/articlerender.fcgi?artid=2217572&tool=pmcentrez&rendertype=abstract.

4. Li S, Brazhnik P, Sobral B, Tyson JJ (2009) Temporal Controls of the Asymmetric Cell Division Cycle in *Caulobacter crescentus*. PLoS Computational Biology 5(8): e1000463. Available: http://www.ncbi.nlm.nih.gov/pubmed/19680425.

5. Jacobs C, Hung D, Shapiro L (2001) Dynamic localization of a cytoplasmic signal transduction response regulator controls morphogenesis during the *Caulobacter* cell cycle. Proceedings of the National Academy of Sciences of the United States of America 98: 4095–4100. Available: http://www.pubmedcentral.nih.gov/articlerender.fcgi?artid=31185&tool=pmcentrez&rendertype=abstract.

6. Quon KC, Yang B, Domian IJ, Shapiro L, Marczynski GT (1998) Negative control of bacterial DNA replication by a cell cycle regulatory protein that binds at the chromosome origin.

Proceedings of the National Academy of Sciences of the United States of America 95: 120–125. Available: http://www.ncbi.nlm.nih.gov/cgi-bin/Entrez/referer?http://www.pnas.org/cgi/content/full/95/1/120.

7. Domian IJ, Quon KC, Shapiro L (1996) The control of temporal and spatial organization during the *Caulobacter* cell cycle. Current opinion in genetics development 6: 538–544. Available: http://www.ncbi.nlm.nih.gov/entrez/query.fcgi?cmd=Retrieve&db=PubMed&dopt=Citation&list_uids=8939718.

8. Laub MT, Chen SL, Shapiro L, McAdams HH (2002) Genes directly controlled by CtrA, a master regulator of the *Caulobacter* cell cycle. Proceedings of the National Academy of Sciences of the United States of America 99: 4632–4637. Available: http://www.pubmedcentral.nih.gov/articlerender.fcgi?artid=123699&tool=pmcentrez&rendertype=abstract.

9. Paul R, Jaeger T, Abel S, Wiederkehr I, Folcher M, et al. (2008) Allosteric regulation of histidine kinases by their cognate response regulator determines cell fate. Cell 133: 452–461. Available: http://www.pubmedcentral.nih.gov/articlerender.fcgi?artid=2804905&tool=pmcentrez&rendertype=abstract.

10. Hung DY, Shapiro L (2002) A signal transduction protein cues proteolytic events critical to *Caulobacter* cell cycle progression. Proceedings of the National Academy of Sciences of the United States of America 99: 13160–13165. Available: http://www.pubmedcentral.nih.gov/articlerender.fcgi?artid=130603&tool=pmcentrez&rendertype=abstract.

11. Tsokos CG, Perchuk BS, Laub MT (2011) A dynamic complex of signaling proteins uses polar localization to regulate cell fate asymmetry in *Caulobacter crescentus*. Dev Cell 20: 329–341.

12. Chen YE, Tropini C, Jonas K, Tsokos CG, Huang KC, et al. (2011) Spatial gradient of protein phosphorylation underlies replicative asymmetry in a bacterium. Proceedings of the National Academy of Sciences of the United States of America 108: 1052–1057. Available: http://www.pubmedcentral.nih.gov/articlerender.fcgi?artid=298695&tool=pmcentrez&rendertype=abstract.

13. Stewart RC (2010) Protein histidine kinases: assembly of active sites and their regulation in signaling pathways. Current Opinion in Microbiology 13: 133–141. Available: http://www.pubmedcentral.nih.gov/articlerender.fcgi?artid=2847664&tool=pmcentrez&rendertype=abstract.

14. Hecht GB, Lane T, Ohta N, Sommer JM, Newton A (1995) An essential single domain response regulator required for normal cell division and differentiation in *Caulobacter crescentus*. the The European Molecular Biology Organization Journal 14: 3915–3924. Available: http://www.pubmedcentral.nih.gov/articlerender.fcgi?artid=394470&tool=pmcentrez&rendertype=abstract.

15. Ohta N, Lane T, Ninfa EG, Sommer JM, Newton A (1992) A histidine protein kinase homologue required for regulation of bacterial cell division and differentiation. Proceedings of the National Academy of Sciences of the United States of America 89: 10297–10301. Available: http://www.pubmedcentral.nih.gov/articlerender.fcgi?artid=50325&tool=pmcentrez&rendertype=abstract.

16. Wu J, Ohta N, Newton A (1998) An essential, multicomponent signal transduction pathway required for cell cycle regulation in *Caulobacter*. Proceedings of the National Academy of Sciences of the United States of America 95: 1443–1448. Available: http://www.pubmedcentral.nih.gov/articlerender.fcgi?artid=19037&tool=pmcentrez&rendertype=abstract.

17. Aldridge P, Paul R, Goymer P, Rainey P, Jenal U (2003) Role of the GGDEF regulator PleD in polar development of *Caulobacter crescentus*. Molecular Microbiology 47: 1695–1708. Available: http://www.ncbi.nlm.nih.gov/pubmed/12622822.

18. Wu J, Ohta N, Zhao J-L, Newton A (1999) A novel bacterial tyrosine kinase essential for cell division and differentiation. Proceedings of the National Academy of Sciences of the United States of America 96: 13068–13073. Available: http://www.pubmedcentral.nih.gov/articlerender.fcgi?artid=23901&tool=pmcentrez&rendertype=abstract.

19. Lam H, Matroule J-Y, Jacobs-Wagner C (2003) The asymmetric spatial distribution of bacterial signal transduction proteins coordinates cell cycle events. Developmental Cell 5:

149–159. Available:
http://www.ncbi.nlm.nih.gov/entrez/query.fcgi?cmd=Retrieve&db=PubMed&dopt=Citation&list_uids=12852859.

20. Pierce DL, O'Donnol DS, Allen RC, Javens JW, Quardokus EM, et al. (2006) Mutations in DivL and CckA rescue a divJ null mutant of *Caulobacter crescentus* by reducing the activity of CtrA. Journal Of Bacteriology 188: 2473–2482. Available: http://jb.asm.org/cgi/content/abstract/188/7/2473.

21. Wheeler RT, Shapiro L (1999) Differential localization of two histidine kinases controlling bacterial cell differentiation. Molecular Cell 4: 683–694. Available: http://www.ncbi.nlm.nih.gov/pubmed/10619016.

22. Jacobs C, Ausmees N, Cordwell SJ, Shapiro L, Laub MT (2003) Functions of the CckA histidine kinase in *Caulobacter* cell cycle control. Molecular Microbiology 47: 1279–1290. Available: http://www.ncbi.nlm.nih.gov/pubmed/12603734.

23. Chen YE, Tsokos CG, Biondi EG, Perchuk BS, Laub MT (2009) Dynamics of two Phosphorelays controlling cell cycle progression in *Caulobacter crescentus*. Journal of bacteriology 191: 7417–7429. Available: http://www.pubmedcentral.nih.gov/articlerender.fcgi?artid=2786585&tool=pmcentrez&rendertype=abstract. Accessed 28 July 2011.

24. Reisinger SJ, Huntwork S, Viollier PH, Ryan KR (2007) DivL Performs Critical Cell Cycle Functions in *Caulobacter crescentus* Independent of Kinase Activity. Journal Of Bacteriology 189: 8308–8320. Available: http://www.pubmedcentral.nih.gov/articlerender.fcgi?artid=2168681&tool=pmcentrez&rendertype=abstract.

25. Iniesta AA, Hillson NJ, Shapiro L (2010) Polar Remodeling and Histidine Kinase Activation, Which Is Essential for *Caulobacter* Cell Cycle Progression, Are Dependent on DNA Replication Initiation. Journal Of Bacteriology 192: 3893–3902. Available: http://www.pubmedcentral.nih.gov/articlerender.fcgi?artid=2916389&tool=pmcentrez&rendertype=abstract.

26. Gora KG, Tsokos CG, Chen YE, Srinivasan BS, Perchuk BS, et al. (2010) A cell-type-specific protein-protein interaction modulates transcriptional activity of a master regulator in

Caulobacter crescentus. Molecular Cell 39: 455–467. Available: http://www.ncbi.nlm.nih.gov/pubmed/20598601.

27. Iniesta AA, Shapiro L (2008) A bacterial control circuit integrates polar localization and proteolysis of key regulatory proteins with a phospho-signaling cascade. Proceedings of the National Academy of Sciences of the United States of America 105: 16602–16607. Available: http://www.pubmedcentral.nih.gov/articlerender.fcgi?artid=2575466&tool=pmcentrez&rendertype=abstract.

28. Iniesta AA, McGrath PT, Reisenauer A, McAdams HH, Shapiro L (2006) A phospho-signaling pathway controls the localization and activity of a protease complex critical for bacterial cell cycle progression. Proceedings of the National Academy of Sciences of the United States of America 103: 10935–10940. Available: http://www.pubmedcentral.nih.gov/articlerender.fcgi?artid=1544152&tool=pmcentrez&rendertype=abstract.

29. Tyson J (2003) Sniffers, buzzers, toggles and blinkers: dynamics of regulatory and signaling pathways in the cell. Current Opinion in Cell Biology 15: 221–231. Available: http://linkinghub.elsevier.com/retrieve/pii/S0955067403000176.

30. Atkinson MR, Savageau MA, Myers JT, Ninfa AJ (2003) Development of genetic circuitry exhibiting toggle switch or oscillatory behavior in Escherichia coli. Cell 113: 597–607. Available: http://www.ncbi.nlm.nih.gov/pubmed/12787501.

31. Gardner TS, Cantor CR, Collins JJ (2000) Construction of a genetic toggle switch in Escherichia coli. Nature 403: 339–342. Available: http://www.ncbi.nlm.nih.gov/pubmed/10659857.

32. Arkin A, Ross J, McAdams HH (1998) Stochastic kinetic analysis of developmental pathway bifurcation in phage lambda-infected Escherichia coli cells. Genetics 149: 1633–1648. Available: http://www.pubmedcentral.nih.gov/articlerender.fcgi?artid=1460268&tool=pmcentrez&rendertype=abstract.

33. Sha W, Moore J, Chen K, Lassaletta AD, Yi C-S, et al. (2003) Hysteresis drives cell-cycle transitions in Xenopus laevis egg extracts. Proceedings of the National Academy of Sciences of the United States of America 100: 975–980. Available:

http://www.pubmedcentral.nih.gov/articlerender.fcgi?artid=298711&tool=pmcentrez&rendertype=abstract.

34. Yao G, Lee TJ, Mori S, Nevins JR, You L (2008) A bistable Rb-E2F switch underlies the restriction point. Nature Cell Biology 10: 476–482. Available: http://www.ncbi.nlm.nih.gov/pubmed/18364697.

35. Novak B, Tyson JJ, Gyorffy B, Csikasz-Nagy A (2007) Irreversible cell-cycle transitions are due to systems-level feedback. Nature Cell Biology 9: 724–728. Available: http://www.ncbi.nlm.nih.gov/pubmed/17603504.

36. Changeux J-P (2011) Allostery and the Monod-Wyman-Changeux Model After 50 Years. Annual review of biophysics: 41,103-133. Available: http://www.ncbi.nlm.nih.gov/pubmed/22224598.

37. Siegal-Gaskins D, Crosson S (2008) Tightly Regulated and Heritable Division Control in Single Bacterial Cells. Biophysical Journal 95: 2063–2072. Available: http://www.pubmedcentral.nih.gov/articlerender.fcgi?artid=2483777&tool=pmcentrez&rendertype=abstract.

38. Lin Y, Crosson S, Scherer NF (2010) Single-gene tuning of *Caulobacter* cell cycle period and noise, swarming motility, and surface adhesion. Molecular Systems Biology 6: 445. Available: http://www.nature.com/doifinder/10.1038/msb.2010.95.

39. Boutte CC, Henry JT, Crosson S (2012) ppGpp and polyphosphate modulate cell cycle progression in *Caulobacter crescentus*. Journal Of Bacteriology 194: 28–35. Available: http://www.ncbi.nlm.nih.gov/pubmed/22020649.

40. Ohta N, Newton A (2003) The Core Dimerization Domains of Histidine Kinases Contain Recognition Specificity for the Cognate Response Regulator. Journal of bacteriology 185: 4424–4431.

41. Paul R, Abel S, Wassmann P, Beck A, Heerklotz H, et al. (2007) Activation of the diguanylate cyclase PleD by phosphorylation-mediated dimerization. The Journal of Biological Chemistry 282: 29170–29177. Available: http://www.ncbi.nlm.nih.gov/pubmed/17640875.

42. Jacobs C, Domian IJ, Maddock JR, Shapiro L (1999) Cell cycle-dependent polar localization of an essential bacterial histidine kinase that controls DNA replication and cell division. Cell 97: 111–120. Available: http://www.ncbi.nlm.nih.gov/pubmed/10199407.

43. Biondi EG, Reisinger SJ, Skerker JM, Arif M, Perchuk BS, et al. (2006) Regulation of the bacterial cell cycle by an integrated genetic circuit. Nature 444: 899–904. Available: http://www.ncbi.nlm.nih.gov/pubmed/17136100.

44. Iniesta AA, Hillson NJ, Shapiro L (2010) Cell pole-specific activation of a critical bacterial cell cycle kinase. Proceedings of the National Academy of Sciences of the United States of America 107: 7012–7017. Available: http://www.pubmedcentral.nih.gov/articlerender.fcgi?artid=2872457&tool=pmcentrez&rendertype=abstract.

45. Matroule J-Y, Lam H, Burnette DT, Jacobs-Wagner C (2004) Cytokinesis monitoring during development; rapid pole-to-pole shuttling of a signaling protein by localized kinase and phosphatase in *Caulobacter*. Cell 118: 579–590. Available: http://www.ncbi.nlm.nih.gov/pubmed/15339663.

46. Tropini C, Huang KC (2012) Interplay between the Localization and Kinetics of Phosphorylation in Flagellar Pole Development of the Bacterium *Caulobacter crescentus*. PLoS Computational Biology 8(8): e1002602. Available: http://www.pubmedcentral.nih.gov/articlerender.fcgi?artid=3410866&tool=pmcentrez&rendertype=abstract.

47. Hunter JD (2007) Matplotlib: A 2D Graphics Environment. Computing in Science Engineering 9: 90–95. Available: http://ieeexplore.ieee.org/lpdocs/epic03/wrapper.htm?arnumber=4160265.

Chapter 3 Dynamical Localization of DivL and PleC in the Asymmetric Division Cycle of *Caulobacter crescentus*: A Theoretical Investigation of Alternative Models

Kartik Subramanian[1], Mark R. Paul[2] and John J. Tyson[3,4,*]

[1]Graduate Program in Genetics, Bioinformatics and Computational Biology, [2]Department of Mechanical Engineering, [3]Department of Biological Sciences, and [4]Virginia Bioinformatics Institute, Virginia Polytechnic Institute and State University, Blacksburg VA 24061

3.1 Abstract

Replicative asymmetry in the predivisional cell of *Caulobacter crescentus* requires that the regulatory protein DivL localizes to the new pole of the cell, where it up-regulates CckA kinase, prompting CckA to phosphorylate CtrA in the "swarmer" half of the predivisional cell. At division, CtrA~P inhibits DNA synthesis in the newborn swarmer cell, whereas CtrA (unphosphorylated) is permissive of DNA synthesis in the newborn stalked cell. It has been suggested that co-localization of DivL with PleC phosphatase at the new pole is essential to DivL's activity there. However, there are contrasting views on whether the bifunctional enzyme, PleC, is functioning as a kinase or phosphatase at the new pole. To explore this ambiguity, we formulate a mathematical model of the spatiotemporal distributions of DivL, PleC and associated proteins during the asymmetric division cycle of a *Caulobacter* cell. Our results show that changes in the localization and activities of DivL and PleC drive the G1-to-S transition early in the cell division cycle (at the swarmer-to-stalked cell transition), while promoting S-phase asymmetry in the predivisional cell. Our simulations reproduce the experimentally observed spatial distribution and phosphorylation status of CtrA in wild-type and mutant cells. Based on the model, we explore novel combinations of mutant alleles, making predictions that can be tested experimentally.

3.2 Introduction

The bacterium *Caulobacter crescentus* undergoes asymmetric division to give daughter cells (a stalked cell and a swarmer cell) with distinct morphologies and functionalities. The sessile and replication-competent stalked cell is anchored to the substratum, while the motile but replication-quiescent swarmer cell swims to a new location, before shedding its flagellum and differentiating into a stalked cell. This dimorphism enables the bacterial population to disperse and survive in the low-nutrient, aquatic environments where *Caulobacter* is naturally found [1]. The precursor to asymmetric division is the predivisional cell, which is characterized by a stalk at one pole and nascent swarmer apparatus at the opposite pole. The swarmer, stalked and predivisional cells represent three distinct developmental stages that define the *Caulobacter* cell cycle.

3.2.1 The conundrum of phosphorylation status of PleC and DivK in the predivisional cell

Progression through the *Caulobacter* cell cycle is dictated by the phosphorylation status of two proteins, DivK and CtrA. These two proteins are response regulators at the termini of two phosphotransfer modules (DivJ-PleC-DivK and DivL-CckA-CtrA) **(Figure 3.1 A)**. PleC and CckA are bifunctional histidine-modifying enzymes that may act as either kinases or phosphatases [2,3]. Both PleC and DivJ can phosphorylate DivK, while the role of DivL is to up-regulate CckA's kinase activity [4]. DivL is a tyrosine kinase, but its kinase activity is not involved in the up-regulation of CckA [4]; how DivL promotes CckA activity is still unknown. DivK~P binds to and inhibits DivL [5]. In a swarmer cell, DivJ is absent, PleC is a phosphatase, and DivK is unphosphorylated. Consequently, DivL is actively up-regulating CckA kinase activity [6], which in turn maintains CtrA in its phosphorylated form, thereby inhibiting DNA replication in the swarmer cell [7]. The introduction of DivJ during the swarmer-to-stalked transition enables the phosphorylation of DivK~P, triggering a pathway that culminates in the dephosphorylation of CtrA~P in stalked cells [8–10]. Therefore, at the molecular level, swarmer and stalked cells can be distinguished based on which response regulator – CtrA or DivK – is phosphorylated.

The schematic in **Figure 3.1A** suggests that DivK and CtrA cannot be concurrently phosphorylated during the cell cycle. Therefore, it is surprising that both response regulators are phosphorylated in predivisional cells **(Figure 3.1 B)**. While the level of DivK~P remains fairly constant in the stalked and predivisional stages [11], CtrA~P level changes sharply from lowest in the stalked cell stage to peak activity in the predivisional stage [3,12]. Recent experimental observations [5,6] favor a model where DivL is active (up-regulating CckA kinase) in the predivisional *Caulobacter* cell. Hence, DivL, inactivated by DivK~P during the swarmer-to-stalked transition, appears to be reactivated in the predivisional cell, despite the continuing presence of DivK~P. It is unclear how the inhibitory interaction between DivK~P and DivL that is required for swarmer-to-stalked transition early in the cell cycle is circumvented in the predivisional stage of the cell cycle.

3.2.2 Contrasting models of PleC function

While the dual roles of CckA as a phosphatase and kinase are acknowledged and understood [3–6,13], there are contrasting opinions regarding the function of the histidine kinase/phosphatase, PleC, in predivisional cells. *In vitro* experiments revealed that the kinase form of PleC is up-regulated by DivK~P [2]. Based on this important finding, informal models were proposed, suggesting that the DivJ-dependent increase in the level of DivK~P that occurs during the swarmer-to-stalked transition induces PleC to become a kinase. As a kinase, PleC phosphorylates PleD, which in turn initiates a pathway for stalked-cell development [14]. Further, the model suggests that, in the predivisional cell, PleC remains a kinase until cytokinesis separates PleC and DivJ into separate compartments [15–17]. (We refer to verbal explanations of experimental findings as “informal models” to distinguish them from the mathematical models we explore in this paper.)

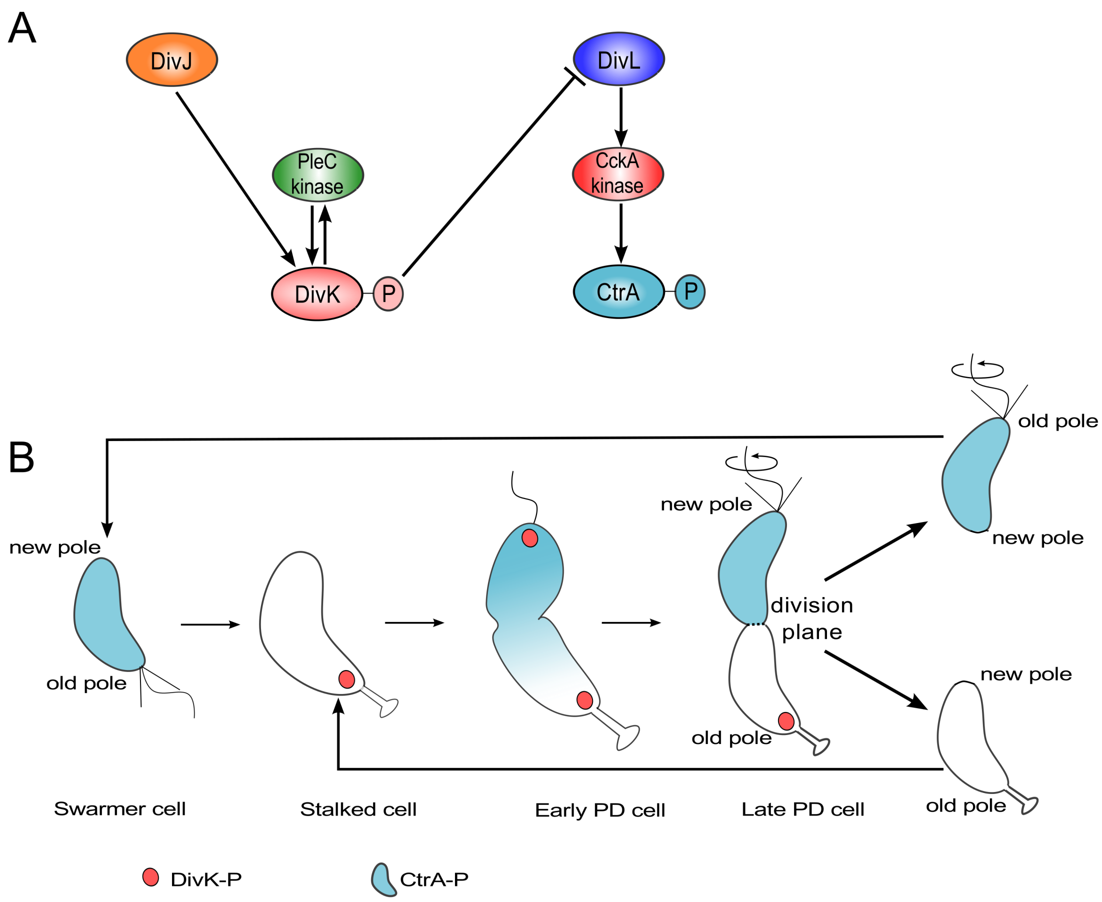

Figure 3.1: Both DivK and CtrA are phosphorylated during the predivisional stage of the *Caulobacter* cell cycle.

(A) Influence diagram of two signal transduction pathways in *C. crescentus*. Barbed arrows indicate activation, while the blunt-headed line indicates inhibition. (B) Spatiotemporal distributions of DivK~P (red) and CtrA~P (light blue).

The alternate view – that PleC is a phosphatase in predivisional cells [18] – is part of an informal model developed to explain reactivation of DivL and phosphorylation of CtrA in the predivisional stage [5]. As CtrA~P level falls in the stalked cell, its inhibition of DNA replication is lifted. Within the timeframe of the natural *Caulobacter* cell cycle, the single chromosome replicates only once to give two chromosomes. However, if cell division is blocked and the cell grows further, only the chromosomal origin proximal to the old pole begins a second round of replication to give a third chromosome [19]. This observation suggests a gradient of CtrA~P in the predivisional cell, with high concentration at the new pole (the incipient swarmer pole) and low concentration at the old pole (bearing the stalk). Mathematical modeling [6] has shown that such a phosphorylation gradient can only be established if CckA functions as a kinase at the new pole and a phosphatase at the old pole.

This scenario requires DivL to be active at the new pole, i.e., unbound to DivK~P. Intriguingly, DivK~P is found to co-localize with DivL and PleC at the new pole. How does DivL remain unbound and active (up-regulating CckA kinase) while in close-proximity to DivK~P? The suggested explanation is that predivisional PleC at the new pole is a phosphatase that is continuously working to dephosphorylate DivK~P and create an inhibition free 'protection zone' for DivL [5].

Of these informal models, the first (in support of PleC kinase) is necessary to explain stalk formation, while the second (in favor of PleC phosphatase) posits conditions that are to be satisfied for replicative asymmetry. While the first model lays out the evolution of PleC function during the course of the cell cycle, the second model only addresses the plausible function of PleC in the predivisional cell. Since PleC-dependent phosphorylation of PleD is required for the development of the stalk, it is fair to assume that PleC is a kinase in the stalked cell. Hence, the difference in the two models can be narrowed down to the suggested function of PleC at the new pole of the predivisional cell **(Figure 3.2)**.

One possible resolution of this conundrum is to assume that PleC becomes a kinase in the stalked stage and phosphorylates PleD, but later flips back to a phosphatase to revoke DivL inhibition. This explanation, however, raises the question of how PleC reverts back its phosphatase form before cytokinesis. On the other hand, if we assume that PleC is a kinase at the new pole, we are faced with explaining how DivL is protected from inhibition by DivK~P. In this paper, we propose a formal mathematical model of the DivJ-PleC-DivK and DivL-CckA-CtrA networks based on reaction-diffusion equations. Using this model, we first investigate conditions promoting PleC to function as a phosphatase or a kinase in the predivisional cell. Based on these simulation results, we favor the case where PleC is a kinase in the predivisional cell. Subsequently, we propose a mechanism by which DivL is reactivated in the predivisional cell in spite of co-localizing with PleC kinase and DivK~P.

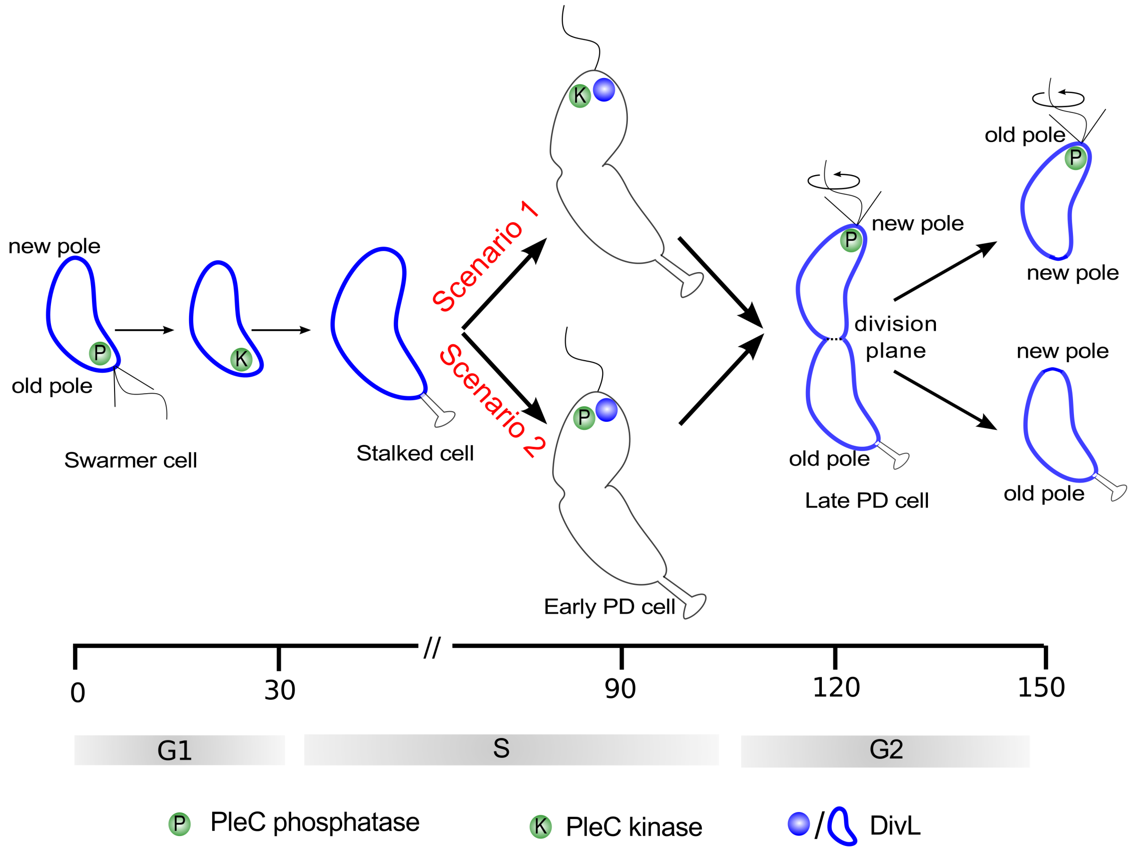

Figure 3.2: Two scenarios for the function of PleC (kinase or phosphatase) in the early predivisional (PD) cell.

Spatiotemporal dynamics of PleC (green) and DivL (dark blue) during the cell cycle under these two scenarios.

3.3 Methods

Modeling framework

Our reaction-diffusion model is based on the mechanism proposed in our earlier paper [32]. The proteins under investigation show non-homogeneous distributions along the long axis of a *Caulobacter* cell; hence, we consider it sufficient to formulate the model for one spatial dimension. The governing partial differential equation (PDE) for a generic chemical species takes the form:

$$\frac{\partial C}{\partial t} = \text{Reaction terms} + D \cdot \frac{\partial^2 C}{\partial x^2}$$

where $C(x,t)$ is the concentration of species C at location x and time t. The PDEs on which we base our explorations are provided in **Table B.1**. By discretizing the spatial dimension into n = 100 compartments of equal length $h = L/n$, where L is the total length of the *Caulobacter* cell and using a central difference scheme to approximate the Laplacian operator, we convert each PDE into a set of ordinary differential equations (ODEs). In our notation, C_i is the concentration of species C in compartment i ($1 \leq i \leq 100$) where

$$\frac{d\mathrm{C}_i}{dt} = \text{Reaction terms} \; + \; D \cdot \frac{\mathrm{C}_{i+1} - 2\mathrm{C}_i + \mathrm{C}_{i-1}}{h^2}$$

Because *Caulobacter* cells are elongating as a result of new cell wall material being added uniformly along the long axis [20], we assume that each compartment grows exponentially in time as

$$\frac{dh}{dt} = \; k_{\text{growth}} \cdot h$$

Since the molecules being investigated cannot diffuse across the cell wall, we implement no-flux boundary conditions at $x = 0$ and $x = L$ by adding two additional compartments, $i = 0$ and $i = 101$, and insisting at every time step that $C_0 = C_1$ and $C_{101} = C_{100}$. The reaction and diffusion rate constants for the wild-type and mutant cells are provided in **Tables B.2** and **B.3.**

A complete understanding of the mechanism behind localization of DivJ, PleC, DivL and CckA is lacking at this stage, and our model does not attempt to offer one. We enforce the localization of these four kinases based on experimentally observed distributions in wild-type and mutant cells [9,12,13,21,22]. We do this by defining rates of binding and unbinding of species C to docking proteins in compartment i as follows:

$$\frac{dC_i^b}{dt} = \; p_i \cdot k_{\text{binding}} \cdot C_i^f - k_{\text{unbinding}} \cdot C_i^b \; + \; \text{other terms}$$

where p_i is an indicator function that takes the value of 1 or 0, C_i^b is the concentration of the localized form and C_i^f is the concentration of the freely diffusing form of a generic protein in compartment i of the cell. The values of the indicator functions for DivJ, PleC, DivL and CckA are provided in **Table B.4**.

The full set of ODEs were simulated in MATLAB using the ode15s solver [23]. The spatiotemporal distribution plots in the figures were generated using the python library Matplotlib [24]. The colors indicate the concentration gradient from zero (blue) to the maximum value of protein concentration (red) during the cell cycle. A disadvantage of such a plot is that a shallow gradient can be interpreted as significant changes in protein activity and localization. On the other hand, a very steep gradient can result in underestimation of fluctuations in protein activity and localization occurring at the lower range of concentration values. To avoid these problems and to make comparison between wild-type and mutant simulations more convenient, the color bar for each simulation indicates the concentration gradient from zero (blue) to maximum wild-type concentration C^{wt_max} (red).

3.4 Results

3.4.1 Rapid diffusion of DivK indicates that PleC is a kinase in the predivisional cell

In swarmer cells, PleC is localized at the old pole and functions as a phosphatase [21,22]. During the swarmer-to-stalked transition, PleC becomes a kinase [2,15,16] before it is cleared from the old pole in mature stalked cells [22]. Later in the cell cycle, PleC localizes at the new pole (the incipient swarmer pole). In our model, the transition from newborn swarmer cell to compartmentalized predivisional cell takes 150 minutes. The cell is in the swarmer stage for the first 30 minutes, during which PleC is localized at the old pole (t = 0 – 30 min). Since PleC and DivJ are co-localized for a short duration in the developing stalked cell [15,16], we assume PleC is retained at the old pole for the first 20 minutes (t = 30 – 50 min) of the stalked stage (which comprises t = 30 – 90 min of the cell cycle). Although this 20-minute window may be on over-estimate, we chose it so that one can clearly see the transition of PleC to the kinase form before it is cleared from the stalked cell. (A shorter residency time does not qualitatively affect our simulation results; see **Figure B.1**). Between t = 50 – 90 min, PleC is delocalized before it relocates to the new pole to define the start of the predivisional stage of the cell cycle (t = 90 – 150 min). We enforce compartmentalization at t = 120 min by preventing the diffusion of proteins across the mid-cell line. To distinguish between pre- and post-compartmentalized stages, we refer to these two stages as early predivisional (t = 90 – 120 min) and late predivisional (t = 120 – 150 min).

To initiate the swarmer-to-stalked transition, we localize DivJ to the old pole at t = 30 min **(Figure 3.3 A)**. The surge in level of DivK~P results in up-regulation of the kinase form of PleC. In our simulations, when PleC translocates to the new pole, it continues to function as a kinase. Fluorescence-loss-in-photobleaching (FLIP) experiments show that DivK shuttles from pole to pole in about 5 seconds, indicating that $D_{\mathrm{DivK}} \cong 20 - 100 \mu\mathrm{m}^2\,\mathrm{min}^{-1}$ [18]. We assumed a diffusion coefficient of $100\,\mu\mathrm{m}^2\,\mathrm{min}^{-1}$ for DivK and DivK~P in our simulations. In the absence of cytokinesis, DivK diffuses freely between the new end of the cell, occupied by PleC, and the old end, containing DivJ. As a result, DivK phosphorylated by DivJ at the old pole is able to interact with new-pole PleC and induce it to become a kinase. We investigated whether a smaller value of D_{DivK} would permit PleC to be a phosphatase in predivisional cells. For PleC to be a kinase in an incipient stalked cell and regain phosphatase activity in the predivisional cell, D_{DivK} had to be 1000 fold smaller than estimated (**Figure B.2 A**; $D_{\mathrm{DivK}} = D_{\mathrm{DivKP}} = 0.1\ \mu\mathrm{m}^2\ \mathrm{min}^{-1}$). Our simulations support the notion that, provided D_{DivK} is sufficiently small, the phosphatase form of PleC can create a "protection zone" for DivL by dephosphorylating DivK in the vicinity of the new pole (**Figure B.2 B**), and, consequently, a gradient of CtrA~P is established to enforce replicative asymmetry (**Figure B.2 C**). However, unlike the distribution pattern observed in experiments [21], we find that DivK~P no longer localizes at the new pole of predivisional cells. This aberrant result combined with the fact that DivK~P has to diffuse significantly slower than estimated, leads us to conclude that new-pole PleC cannot be primarily a phosphatase.

3.4.2 PleC kinase can sequester inhibitor DivK~P from DivL

divL mutant cells that cannot localize DivL at the new pole in the predivisional stage also fail to localize and activate CckA [25]. In contrast, in the swarmer stage uniformly distributed DivL is actively up-regulating CckA. This lack of a causal relationship between localization and activation across two stages of the cell cycle indicates that new-pole localization itself is not essential for DivL activity. Rather, it appears that the act of localizing to the new pole protects DivL from inhibition by DivK~P in the predivisional cell. This may seem counter-intuitive at first, since DivL is positioned in close proximity to its inhibitor DivK~P in the early predivisional cell. Furthermore, as our simulations predict new-pole PleC to be a kinase in the early predivisional stage, we consider it unlikely that PleC dephosphorylates DivK~P in order to protect DivL. Hence, some other mechanism must maintain DivL in an active form.

Our simulation results show that in the process of up-regulation of the kinase form of PleC by its allosteric ligand, DivK~P, a significant fraction of PleC kinase is bound to DivK~P. In contrast, PleC phosphatase (that is prevalent in swarmer cells) does not form a complex with DivK (**Figure B.3**). Hence, PleC kinase may serve as a binding site for DivK~P at the new end of a predivisional cell. This simulation result is in agreement with FRET microscopy measurements that show interaction between DivK and PleC at the new pole [18]. In the predivisional cell, DivK~P is localized at both old and new poles [21]. Apart from PleC kinase, the only other recognized binding partners for DivK~P are DivJ and DivL [4]. DivJ accounts for old pole localization of DivK~P, but DivJ's absence from the new pole implies that it is not a binding factor for new-pole DivK~P. DivL is present at the new pole, but we require that DivL should not be bound to DivK~P, because DivL is actively up-regulating CckA kinase at the new pole. By ruling out DivJ and DivL and refraining from invoking an unidentified binding partner, we propose that new-pole DivK~P is bound to PleC kinase. Further, we hypothesize that PleC kinase outcompetes DivL for DivK~P binding. Instead of functioning as a phosphatase and dephosphorylating DivK~P, we predict that PleC is a kinase that sequesters DivK~P away from DivL. We speculate that DivK~P sequestration (rather than DivK~P dephosphorylation) may be the real reason for a "protection zone" for DivL at the new pole, so that it regains the ability to up-regulate CckA kinase there, prior to cytokinesis.

Using our model of the DivJ-PleC-DivK + DivL-CckA-CtrA network, we studied the plausibility of our "inhibitor sequestration" hypothesis. As in the case of PleC, there is limited information on the mechanism behind the dynamic localization of DivL. We force DivL to spread throughout the cell from $t = 0$ to $t = 90$ min, whereas, in the early predivisional stage ($t = 90 - 120$ min), DivL is forced to localize at the new pole. Our simulations show that DivL is in the free form in the swarmer stage (**Figure 3.3 B**). During the swarmer-to-stalked transition, the level of free DivL falls, due to binding with DivK~P. In the early predivisional stage, DivL is localized at the new pole and is in the unbound form even though DivK~P is present at the same location. As suggested in our hypothesis, co-localized PleC kinase sequesters DivK~P, allowing DivL to be reactivated in the early predivisional cell.

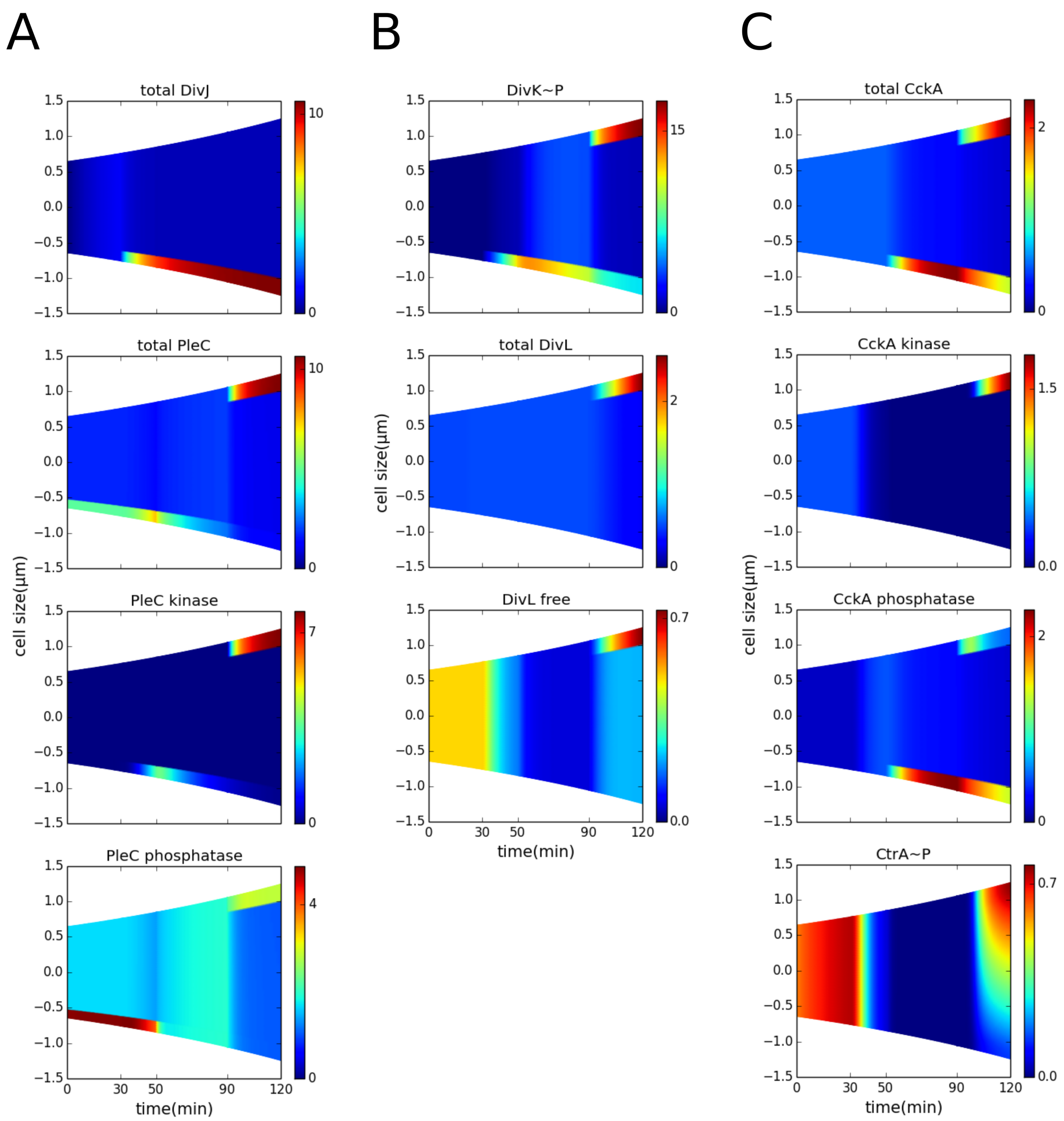

Figure 3.3: Co-localization of PleC kinase and DivL in the early predivisional cell is required for DivL reactivation.

Spatiotemporal distributions of proteins during the cell cycle (prior to cytokinesis). Color indicates concentration gradients from minimum (blue) to maximum (red). (A) DivJ is localized at the old pole (t = 30 – 120 min). The location of PleC is shifted from the old pole (t = 0 – 50 min) to the new pole of the predivisional cell (t = 90 – 150 min). Following DivJ localization, the function of PleC changes from a phosphatase to a kinase. (B) Upon phosphorylation, DivK localizes to the poles of the cell. Despite the presence of DivK~P at the new pole of the predivisional cell, DivL is present in the free form (unbound to DivK~P) because DivL co-localizes with PleC kinase and PleC kinase sequesters DivK~P, preventing it from binding to DivL. (C) CckA is uniformly distributed in the swarmer stage and localized at both poles in the predivisional stage. Reactivation of DivL at the new pole results in new-pole CckA becoming a kinase, while old-pole CckA remains a phosphatase. Consequently, the late predivisional cell establishes a gradient of CtrA~P along its length from high at the new pole to low at the old pole.

Why does inhibitor sequestration fail to protect DivL in the stalked cell during the time interval (t = 50 – 70 min), when PleC is transiently localized at the old pole as a kinase? We reason that the spatial separation of PleC kinase and DivL in the stalked cell stage means that a majority of DivL is outside the protection zone created by PleC-dependent inhibitor sequestration. Moreover, by spreading out over the entire length of the cell, DivL can be inhibited by a lower concentration of DivK~P per unit length of the cell. Our simulations demonstrate that *Caulobacter* cells can program different cell fates by regulating DivL inhibition through spatial reorganization of DivL and PleC.

3.4.3 The inhibitor-sequestration model reproduces replicative asymmetry in the early predivisional cell and swarmer pole development in the late predivisional cell

CckA localization is governed by both PopZ [26] and DivL [25]. Although the spatial distribution of CckA shows cell-to-cell variability, the consensus opinion is that CckA protein is spread uniformly throughout the cell in the swarmer stage, followed by old-pole localization in the stalked cell, followed by a bipolar distribution in the early predivisional stage [12,27]. The spatiotemporal distribution of CckA activity is a reflection of changes in local concentrations of free DivL. In the swarmer cell, when CckA is uniformly distributed, 70% of CckA is in the kinase conformation (**Figure 3.3 C** and **3.4 A**). In the stalked cell (t = 30 – 90 min), DivL inactivation results in an increase in the phosphatase fraction of CckA, even as total CckA localizes to the old pole. Finally in the early predivisional cell (t = 90 min), a second focus of CckA co-localizes as a kinase with reactivated DivL, while old-pole CckA remains in the phosphatase form (**Figure 3.3 C**). At the early predivisional stage, less than half (~36%) of total cellular CckA is in the kinase conformation (**Figure 3.4 A**). Importantly, however, this 36% is localized in the incipient swarmer half (new pole) of the early predivisional cell (**Figure 3.3 C**).

It has been suggested that replicative asymmetry is a result of differential phosphorylation and dephosphorylation of CtrA across the length of the predivisional cell [6]. Synthesis and degradation of CtrA has no bearing on the CtrA phosphorylation gradient. For these reasons, we do not account, in our model, for changes in the total amount of CtrA protein by means of transcriptional [28–30] and proteolytic [31–33] controls. We assume that CtrA is synthesized in the unphosphorylated form at a constant rate, while CtrA and CtrA~P are degraded at a rate proportional to their individual concentrations. Fluorescence-recovery-after-photobleaching (FRAP) experiments indicate that CtrA has a diffusion coefficient of 60 – 600 μm^2 min^{-1}, while modeling studies suggest that phosphorylation and dephosphorylation rate constants are faster than the inverse diffusive time scale ($k_{ctr\_phos} = k_{ctr\_kin} >> 2D/L^2$) in order to obtain a gradient [6]. In our model, we assume $D_{CtrA} = D_{CtrAP} =$ 100 μm^2 min^{-1} and $k_{ctr\_phos} = k_{ctr\_kin} = 600$ min^{-1}. Our simulations show that CtrA~P is dephosphorylated during the swarmer-to-stalked transition. Once CckA localizes as a kinase at the new pole, a gradient of phosphorylated CtrA is established across the cell body (**Figure 3.3 C**).

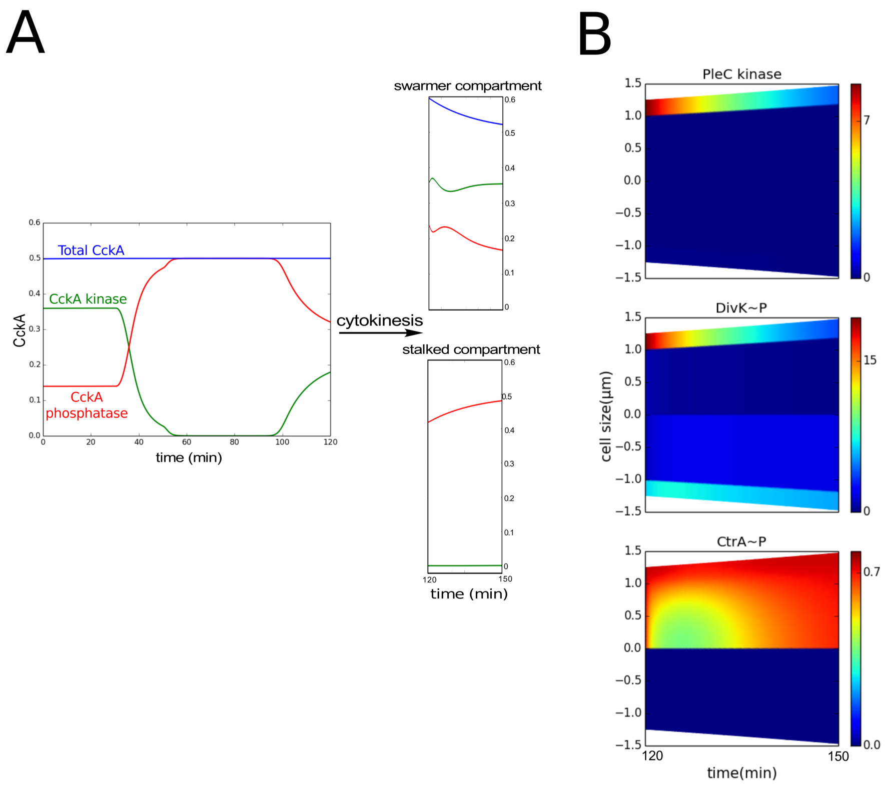

Figure 3.4: Following cytokinesis, PleC reverts to the phosphatase form.

(A) The total concentration of CckA (blue curve) remains constant during the cell cycle. However, the proportions of phosphatase (red curve) and kinase (green curve) forms of CckA change for each stage of the cell cycle. After cytokinesis (compartmentalization), the concentrations of kinase and phosphatase fraction of CckA in the swarmer and stalked compartments (t = 120 – 150 min) are similar to their concentration in the non-compartmentalized swarmer (t = 0 – 30 min) and stalked cell stages (t = 30 – 90 min) respectively. (B) Spatiotemporal distribution of PleC kinase, DivK~P and CtrA~P after compartmentalization (at t = 120 min). Color indicates concentration gradients from minimum (blue) to maximum (red).

In order to simulate compartmentalized predivisional cells (t = 120 – 150 min), we use end-point concentrations from the early predivisional stage (t = 120 min) as initial conditions in a simulation of a growing cell with a diffusion barrier at mid-cell. Since DivJ and PleC are in separate compartments, the level of new pole PleC kinase in the swarmer compartment begins to decline and DivK becomes unphosphorylated (**Figure 3.4 B**). The concentrations of the kinase and phosphatase forms of CckA in the swarmer and stalked compartments at t = 150 min are almost identical to their concentrations during the swarmer (t = 0 – 30 min) and stalked stages (t = 30 – 90 min), respectively (**Figure 3.4 A**). Finally, CtrA in the swarmer compartment of the late predivisional cell is phosphorylated, while stalked-compartment CtrA is unphosphorylated. While replicative asymmetry does not require cytokinesis, our simulations show that compartmentalization reinforces cell fate asymmetry by deactivating PleC kinase and dephosphorylating DivK~P in the swarmer compartments.

3.4.4 DivK overexpression negates inhibitor sequestration

The main assumption in our model is that PleC kinase and DivL compete for binding DivK~P. In the wild-type simulation, PleC kinase at the new pole in a predivisional cell outcompetes DivL for binding DivK~P, thus allowing DivL to remain in its active conformation. Overexpression of DivK should undermine this mechanism, since there will be sufficient DivK~P to bind both PleC kinase and DivL. Upon increasing DivK synthesis by 4-fold (k_{syn} = 0.2 min^{-1}), we see that the PleC kinase level in the stalked and predivisional cell increases compared to the wild type (**Figure 3.5 A**). Excess DivK~P in the cell binds to and inhibits DivL. Consequently, CckA localized at the new pole of predivisional cells does not convert to its kinase form, and CtrA does not get re-phosphorylated in the predivisional cell. Our simulations results are consistent with the observed decrease in CckA autophosphorylation and CtrA phosphorylation, which result in chromosome overreplication in cells overexpressing DivK [4,34].

In vitro experiments demonstrated that DivK need not be phosphorylated to up-regulate PleC kinase [2]. In our temporal model [35], we showed that the phosphatase-to-kinase transition of PleC is thermodynamically more favorable when DivK~P, not unphosphorylated DivK, is the allosteric ligand. We proposed that the concentration of DivK *in vivo* is within a range that requires DivK to be phosphorylated in order to induce the PleC kinase conformation. In this case, the swarmer-to-stalked transition is controlled by a bistable PleC switch that is flipped to the kinase state by the action of DivJ. However, when the rate of synthesis of DivK was increased 5–10 fold, our temporal model predicted that PleC kinase would be up-regulated even in the absence of DivJ-dependent phosphorylation of DivK. In this scenario, PleD would be phosphorylated throughout the cell cycle, thus committing the cell to obligate staked cell morphology.

In our current spatiotemporal model, a four-fold increase in the rate of DivK synthesis results in the cell being unable to enter the predivisional stage of the life cycle. However, because PleC is a phosphatase early (t = 0 – 50 min) and a kinase later (t = 50 – 120 min) in the simulation, the cell is predicted to retain distinct swarmer and stalked stages (**Figure 3.5 A**). Increasing the rate of synthesis of DivK by eight-fold (k_{syn} = 0.4 min^{-1}), we find (**Figure 3.5 B**) that PleC is a kinase even in the absence of DivJ (t = 0 – 30 min). DivK is phosphorylated and localized to the old pole, while the level of free and active DivL falls to a third of its wild-type concentration. Throughout the cell cycle, CckA is a phosphatase and CtrA is unphosphorylated.

Overall, our results show that an optimal level of DivK is required to maintain three distinct stages of the *Caulobacter* cell cycle. A four-fold increase in DivK sees the cell retain the swarmer-to-stalked transition but lose predivisional cell asymmetry. Further increase (eight-fold) restricts the cell to a stalked-only morphology. These predictions may be amenable to experimental verification by driving *divK* gene expression with a xylose promoter.

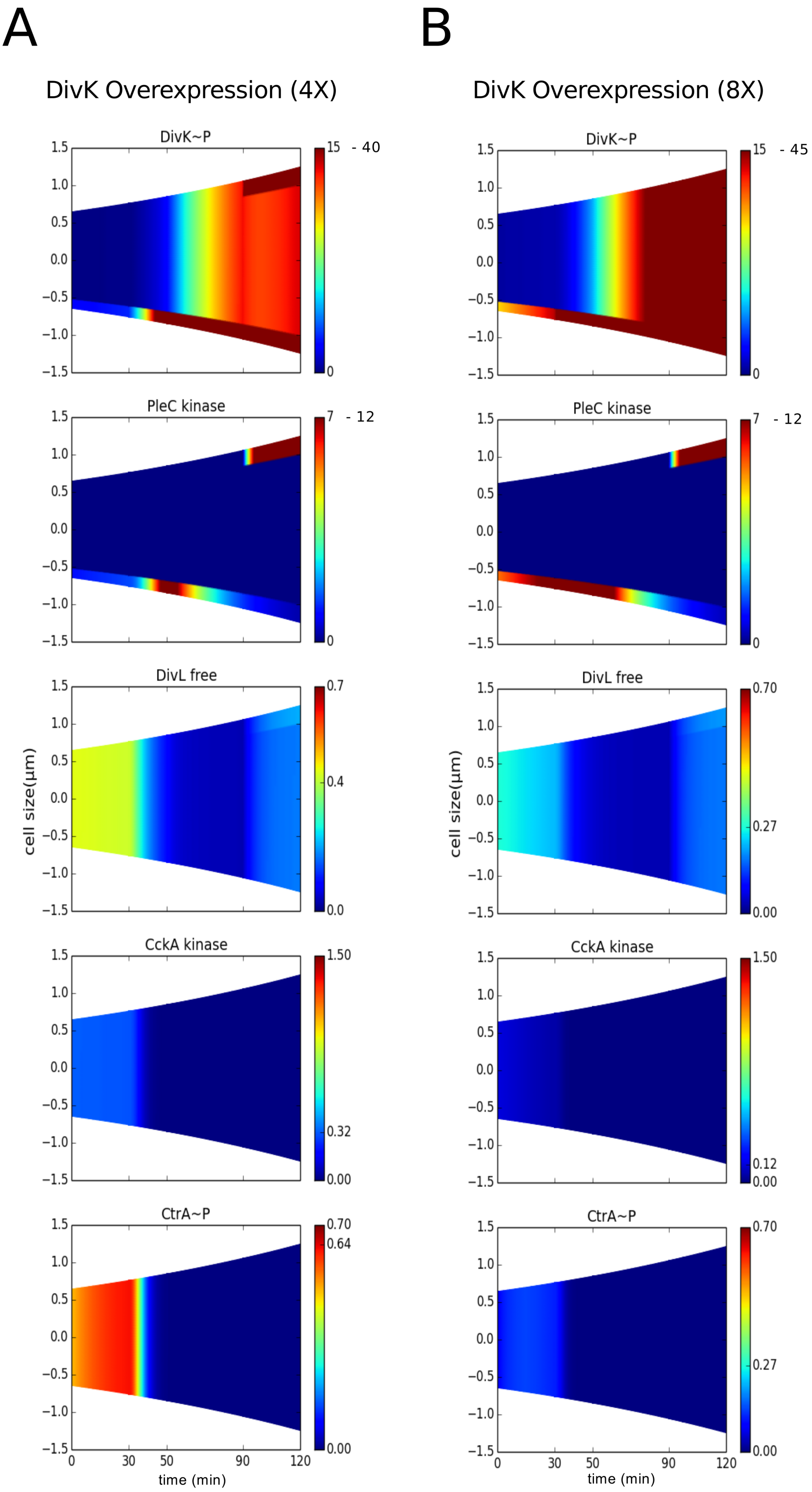

Figure 3.5: Overexpression of DivK may prevent the cell from progressing though different developmental

stages.

For better comparison of mutant and wild-type distributions, the colors indicate concentration gradients from zero (blue) to maximum wild-type concentration, C^{wt_max} (red). For $C^{wt\_max} < C^{mut\_max}$, the red color represents all concentrations from C^{wt_max} to C^{mut_max}. For $C^{wt\_max} > C^{mut\_max}$, an additional tick between 0 and C^{wt_max} indicates maximum concentration in the mutant. (A) A four-fold increase in DivK synthesis (k_{syn} = 0.2 min^{-1}) prevents competition between DivL and PleC kinase. DivL is not reactivated in the predivisional stage leading to the loss of CckA kinase and CtrA~P asymmetry in the early predivisional stage. (B) An eight-fold increase in DivK synthesis (k_{syn} = 0.4 min^{-1}) induces PleC to become a kinase independent of DivJ. Hence, the swarmer stage of the cell cycle is circumvented.

3.4.5 Co-localization of PleC and DivL is essential to DivL activity

We contend that the spatial segregation of PleC and DivL in stalked cells enables DivK~P to bind and inhibit DivL. In contrast, DivL is protected in predivisional cells by co-localized PleC kinase, which sequesters the inhibitor DivK~P. To test this hypothesis, we simulate a scenario where DivL and CckA are uniformly distributed (delocalized) throughout the cell cycle. Consistent with our reasoning, the simulations show (**Figure 3.6 A**) that free and active DivL is present only in the swarmer stage when no DivK~P is present. Despite the presence of PleC kinase at the new pole during the predivisional stage, DivK~P is able to inhibit DivL as it is diffusely spread over the entire cell. Consequently, new-pole CckA is a phosphatase, and a CtrA~P gradient is not established. Based on this simulation result, we propose that new-pole localization of DivL is not solely responsible for its activation. Instead, it is the co-localization of DivL and PleC kinase that enables DivL to up-regulate CckA kinase. The situation of delocalized DivL and CckA has been encountered in experiments where DNA replication is blocked, and, as in our simulations, these experiments reveal that CckA kinase activity and CtrA~P phosphorylation is prevented [13].

At the other extreme, we simulated a mutant in which DivL is always localized at one of the poles (**Figure 3.6 B**). In this mislocalization mutant, DivL is initially present at the old pole of swarmer and stalked cells (t = 0 – 90 min), and later relocates to the new pole in predivisional cells (t = 90 – 120 min). In comparison to the wild type case, the level of free DivL is higher for a further 20 minutes, from t = 0 to t = 50 min. This is also the duration of PleC localization at the old pole. While the PleC phosphatase-to-kinase transition occurs as usual (t = 30 min), DivL inactivation and the consequent dephosphorylation of CtrA is delayed by a period consistent with the co-localization of PleC kinase and DivL. Once PleC is delocalized (t = 50 min), DivL activity drops, CckA reverts back to a phosphatase, and CtrA is dephosphorylated. Essentially, the novel mutant is characterized by a delay in G1-to-S transition, which otherwise occurs concurrent to the swarmer-to-stalked transition. To further emphasize this point, we simulated the case where PleC and DivL are retained at the old pole throughout the stalked stage, before being redistributed to the new pole in the predivisional cell (**Figure 3.6 C**). PleC becomes a kinase in the stalked and predivisional cell. However, since DivL and PleC are always co-localized in this novel mutant, CckA remains a kinase while CtrA is phosphorylated during all stages of the cell cycle.

Overall, results from the localization mutants indicate that the cell exploits DivL and PleC localization to fashion two separate phosphorylation profiles for CtrA in stalked and predivisional stages of the cell cycle. Furthermore, a uniform distribution of DivL is essential to the temporal coupling of the swarmer-to-stalked transition with the G1-to-S transition.

3.4.6 Loss of asymmetry is a physiological consequence of mutations that alter the spatiotemporal profile of inhibitor sequestration

If the kinase form of PleC is required for inhibitor sequestration, then it follows that *pleC* mutants without kinase function would be ill-equipped to resolve the stalked and predivisional stages of the cell cycle. This class of mutants includes Δ*pleC,* *pleC*$_{\mathrm{H610A}}$, *pleC*$_{\mathrm{F778L}}$ and *divK*$_{\mathrm{D90G}}$. The first two mutations (Δ*pleC* and *pleC*$_{\mathrm{H610A}}$) produce non-motile, pili-less and stalk-less cells [21]. *pleC*$_{\mathrm{F778L}}$ mutants are similar to wild-type cells, except that they produce underdeveloped stalks [2]. On the other hand, *divK*$_{\mathrm{D90G}}$ mutant cells are arrested in G1 and lose morphological asymmetry [18]. We sought to explain the physiology of these mutants from the perspective of our inhibitor-sequestration hypothesis.

We simulated the Δ*pleC* mutant by setting the rate constant for PleC synthesis to zero (**Table B.3**). Our results show that the cell is able to complete the G1-to-S transition, but fails to progress any further (**Figure 3.7 A**). Devoid of PleC kinase, PleD will not be phosphorylated resulting in the stalk-less phenotype. In the predivisional cell, the kinase form of PleC is not available to sequester DivK~P. Early in the cell cycle, DivK~P localizes to the old pole by binding to DivJ, following which DivK shows moderate bipolar localization through binding to DivL at the new pole. Consequently, DivL remains inactive at the new pole of predivisional cells, thus preventing CtrA phosphorylation and loss of asymmetry.

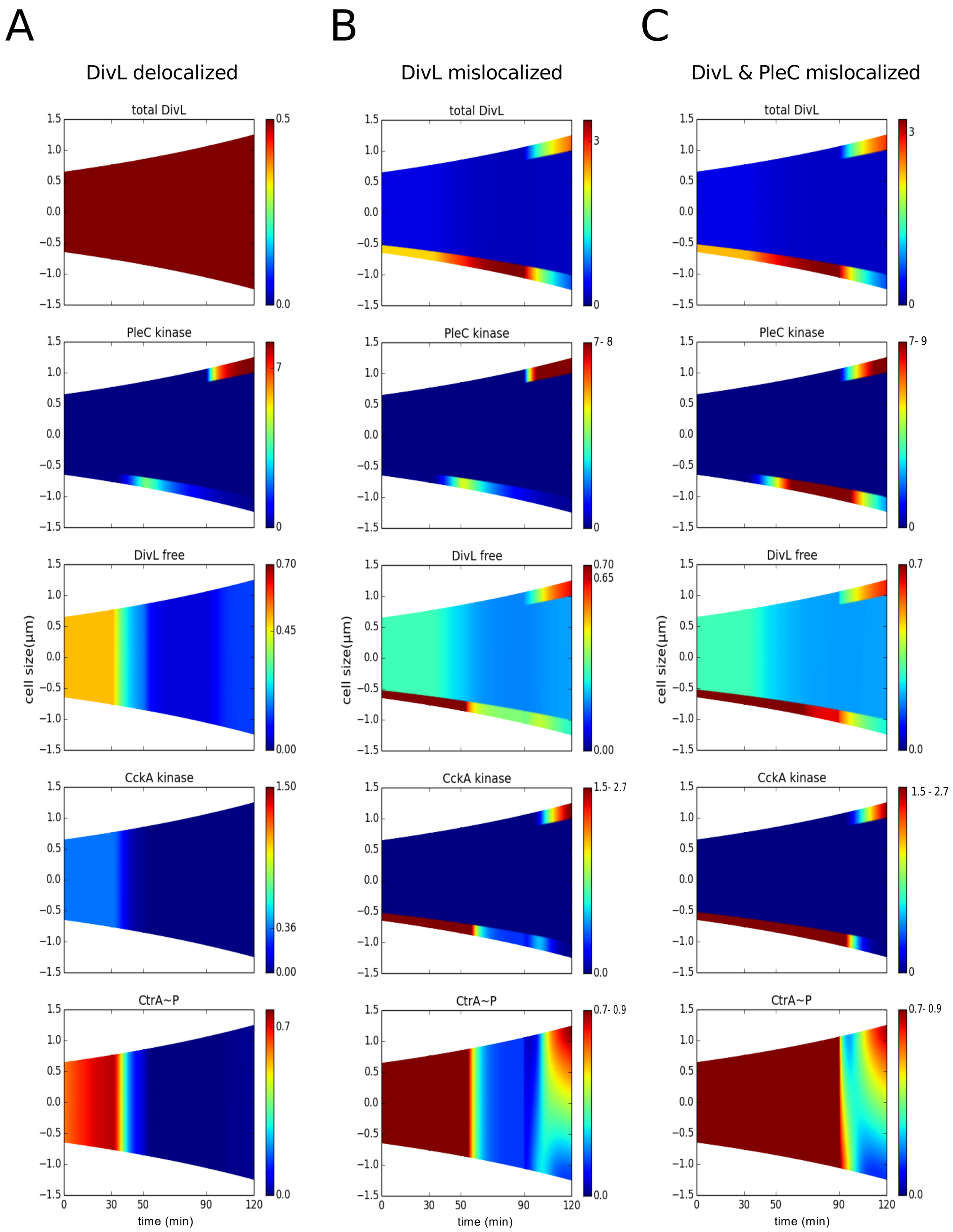

Figure 3.6: Swarmer-to-stalked transition is uncoupled from G1-to-S transition in DivL mislocalization mutants.

Concentration gradients are color coded as in Figure 3.5. (A) DivL is uniformly distributed at all times in the cell cycle. Even though PleC transitions to a kinase, DivL remains deactivated (bound to DivK~P) in the predivisional cell, resulting in no gradient of CtrA~P. (B) DivL (and CckA) are localized at the old pole (*t* =

0 – 90 min), before switching to the new pole in the predivisional cell (t = 90 – 120 min). Even after PleC transitions to a kinase, DivL is not deactivated in stalked cells, delaying the dephosphorylation of CtrA~P until PleC delocalizes from the old pole (at t = 50 min). (C) DivL and PleC are co-localized at one of the poles during all stages of the cell cycle. Hence, CtrA is phosphorylated through all stages of the cell cycle (G1-arrest).

$pleC_{H610A}$ is a mutant that is phosphatase-negative and kinase-negative (K^-P^-). For reasons unknown, PleC is not released from the old pole of stalked and predivisional cells [21]. Hence, we enforce the bipolar localization of PleC in our simulations (**Table B.4**). While the enzyme is incapable of auto-phosphorylation or phosphotransfer, it is unknown if $PleC_{H610A}$ retains its ability to undergo allosteric modification and become a kinase. We parameterize the $pleC_{H610A}$ mutant such that it is able to undergo allosteric modifications by DivK, but unable to auto-phosphorylate or change the phosphorylation status of DivK (**Table B.3**). Under such assumptions, our simulations show that PleC transitions from an inactive phosphatase form to an inactive kinase form during the swarmer-to-stalked transition (**Figure 3.7 B**). Although the inactive kinase form of PleC sequesters DivK~P (according to our assumptions), DivL is nonetheless inactivated. The reason why inhibitor sequestration fails in this case is the inability of $PleC_{H610A}$ to dephosphorylate DivK. As a result, the level of DivK~P is high in these mutant cells, and the excess DivK~P molecules bind and inactive DivL. The failure to dephosphorylate new pole DivK~P, which is characteristic of Δ*pleC* and $pleC_{H610A}$ mutants, is also reproduced in our simulations.

The two mutant alleles $pleC_{H610A}$ and $pleC_{F778L}$ are similar in all aspects, except that $PleC_{F778L}$ retains its phosphatase activity. Like $PleC_{H610A}$, new-pole $PleC_{F778L}$ can acquire the kinase conformation and sequester DivK~P. Unlike $PleC_{H610A}$ however, the ability of $PleC_{F778L}$ to dephosphorylate DivK means that the level of DivK~P is low enough to allow competition between DivL and PleC kinase. In this scenario, DivL remains active and up-regulates CckA kinase. Hence, even though $PleC_{F778L}$ kinase is unable to phosphorylate DivK, our simulations show that the inactive kinase form of PleC is present at the new pole and fulfilling the important role of DivK~P sequestration (**Figure 3.7 C**). Based on our results, we propose that the kinase form of PleC has two independent and important functions to ensure normal progression of the cell cycle. Firstly, the kinase activity of PleC is required to phosphorylate PleD and initiate stalk development. Secondly, the kinase conformation enables PleC to bind and sequester DivK~P, an effect that is essential for DivL activity and the replication-asymmetry of the predivisional cell.

The molecular level defects of the $divK_{D90G}$ allele are the inability of $DivK_{D90G}$ to up-regulate PleC kinase [2] and its reduced efficiency in binding or inhibiting DivL [5]. In our simulations, the PleC kinase level in the stalked and predivisional cell stages falls to a tenth of its wild-type maximum (**Figure B.4 A**). The experimentally observed unipolar localization of DivK in *divK*$_{D90G}$ mutant cells [18] is also reproduced in the simulations. Our results suggest that the lack of a new pole focus is in part due to ineffective binding of DivK$_{D90G}$ to DivL. The second binding partner, PleC, is also unable to bind DivK since PleC is in the phosphatase form. The unipolar localization of DivK in *divK*$_{D90G}$ cells further supports the notion that new-pole PleC in wild-type cells is in the kinase form. Even though PleC kinase is unavailable to sequester DivK$_{D90G}$~P, DivL retains much of its activity, since DivK$_{D90G}$ mutant protein is an ineffective inhibitor of DivL. DivL level remain high until t = 50 min, and only shows moderate decrease during the period when PleC is delocalized (t = 50 – 90 min). As a consequence, CtrA remains phosphorylated throughout the cell cycle, which explains the G1-arrest observed in experiments [31].

DNA replication does not occur in mutants that fail to dephosphorylate or degrade CtrA [36]. Under conditions of replication inhibition, CckA and DivL fail to localize at the new pole [13]. Hence, we enforce DivL and CckA to be delocalized in the predivisional cell of the *divK*$_{D90G}$ mutant, resulting in the loss of a CtrA~P gradient. Since *divK*$_{D53N}$ and Δ*divJ* mutants also display G1-arrest (**Figure B.4 B** and **B.4 C**), we keep DivL and CckA delocalized in these mutants as well (**Table B.4**). DivK$_{D53N}$ is a non-phosphorable form of DivK, while Δ*divJ* mutants cannot phosphorylate DivK. As our simulations show, the non-availability of DivK~P results in the failure to up-regulate PleC kinase or inactivate DivL. Subsequently, CtrA~P remains phosphorylated in the stalked stage of the cell cycle. We suggest that these mutants can be characterized by DivL and CckA delocalization resulting in a homogeneous distribution of CtrA~P in the predivisional cell.

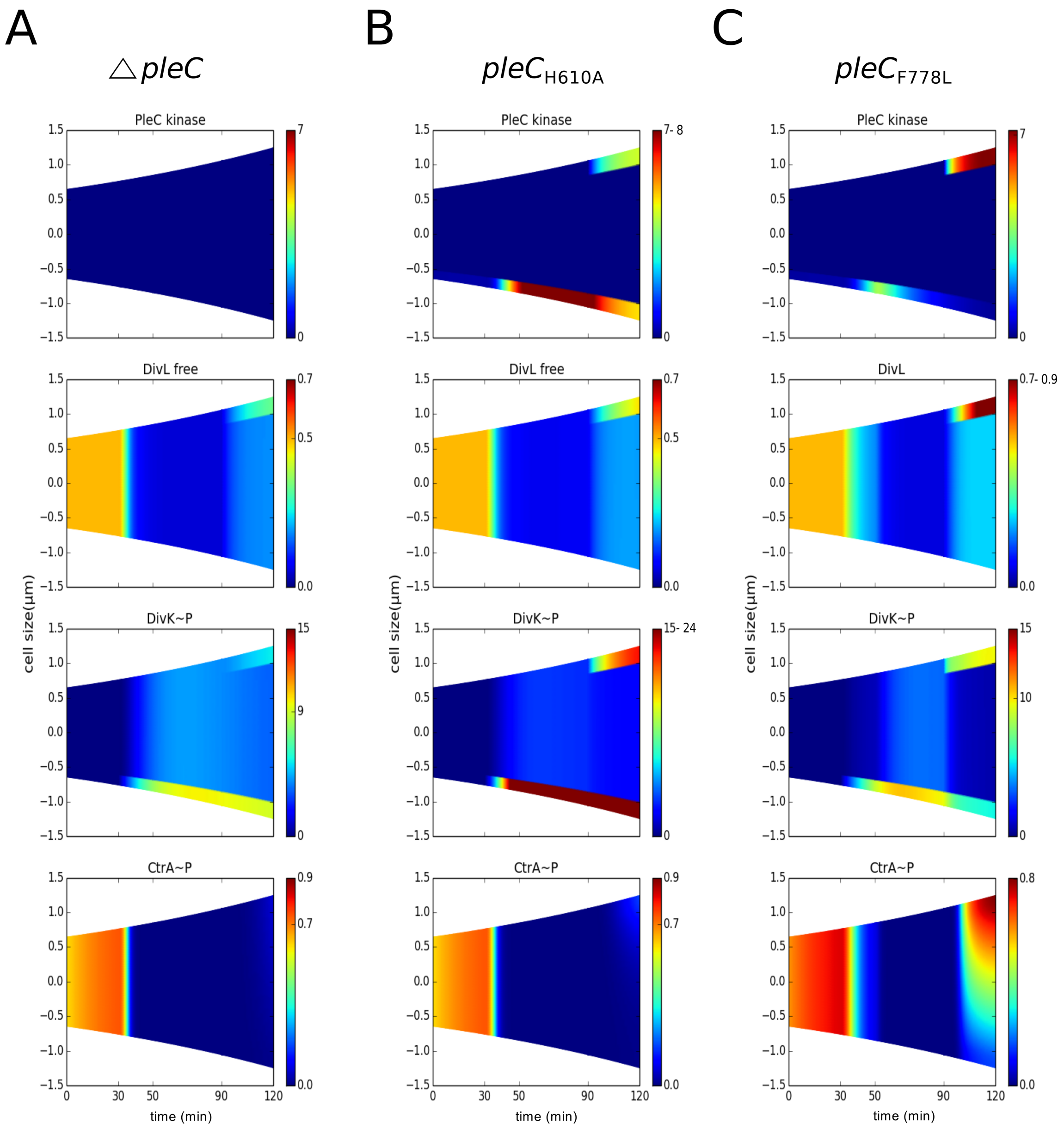

Figure 3.7: PleC kinase conformation is required to establish replicative asymmetry.

Concentration gradients are color coded as in Figure 3.5. (A) In the Δ*pleC* mutant, free active form of DivL is lower than in wild type, resulting in loss of predivisional cell CtrA~P. (B) In *pleC*$_{H610A}$ mutant cells (K^-P^-), an elevated level of DivK~P results in less active form of DivL and reduced CtrA~P. (C) In *pleC*$_{F778L}$ mutant cells (K^-P^+), inhibitor sequestration is retained, resulting in a normal CtrA~P gradient.

3.5 Discussion

3.5.1 A spatiotemporal model of cell cycle progression in *Caulobacter*

In earlier work, we proposed a mechanism for the DivK-dependent allosteric regulation of PleC kinase [35]. Our mathematical model of the proposed mechanism, based on elementary chemical reactions, showed that the transition of PleC activity from phosphatase to kinase might function as a bistable switch flipped by DivJ. We believe bistability of the PleC switch ensures a robust and irreversible transition from swarmer to stalked cell morphology. Based on our simulations of mutant phenotypes such as $divK_{\mathrm{D90G}}$ and $pleC_{\mathrm{F778L}}$, we predicted that the PleC kinase form is essential for stalked cell development. While the model itself was focused on understanding temporal dynamics during the window of the swarmer-to-stalked transition, we speculated that PleC at the new pole of predivisional cells is a kinase. Without an accurate spatiotemporal model however, we could not predict the effects that diffusion and localization might have on the behavior of the molecular switch or its physiological impact on the development of different stages of the asymmetric division cycle.

Spatiotemporal models focused solely on the DivJ-PleC-DivK [37] network or the CckA-CtrA [6] network have been developed. However, these models only simulated the predivisional stage of a non-growing *Caulobacter* cell. Hence, the mechanisms under investigation in these models could not be validated against the behavior of wild-type and mutant cells at other stages of the cell cycle. Unlike previous mathematical models of *Caulobacter* that capture only the temporal aspects of the cell cycle regulators [35,38,39], or spatiotemporal models restricted only to a specific stage of the cell cycle, the reaction-diffusion model described here captures spatiotemporal dynamics of the DivJ-PleC-DivK and DivL-CckA-CtrA networks in a *Caulobacter* cell that grows from swarmer to predivisional cell. A strength of our model is that we are able to successfully validate our "inhibitor sequestration" hypothesis against wild-type and mutant phenotypes at every stage of the cell cycle.

3.5.2 Inhibitor sequestration is a third function of the bifunctional histidine kinase PleC

We propose that PleC performs three distinct functions that are crucial to proper progression through the *Caulobacter* cell cycle. In the swarmer cell, PleC is a phosphatase that maintains DivK in its dephosphorylated state. In stalked cells, PleC is a kinase that phosphorylates PleD. Interestingly, the kinase conformation enables PleC to perform a third function – that of binding to DivK~P, which permits reactivation of DivL, activation of CckA at the new pole, and phosphorylation of CtrA in the swarmer-half of a predivisional cell.

Our model predicts the CtrA~P distribution pattern in predivisional cells of *pleC* and *divK* mutants (**Figure 3.8 A**). Each of these mutants can be defined in terms of the loss of one or more of the three distinct functions of PleC – namely, the auto-phosphorylation and phospho-transfer activities of the kinase form (K), the catalytic activity of the phosphatase form (P), and the DivK~P binding capability of the kinase form (B). A CtrA~P gradient from the new end (high) to the old end (low) is observed in wild-type cells ($K^+P^+B^+$) that have all three functions. Mutants that are defective only in the kinase activity ($K^-P^+B^+$) can establish CtrA~P gradients, as in the case of *pleC*$_{F778L}$. In this mutant, inhibitor sequestration is still operative, enabling DivL reactivation at the new pole of predivisional cells. In *pleC*$_{H610A}$ ($K^-P^-B^+$) mutant cells the phosphatase activity is impaired as well, resulting in an increased level of DivK~P, which binds both PleC and DivL. Therefore, a CtrA~P gradient cannot be established, despite the retention of DivK~P's binding function. In Δ*pleC* mutant cells, inhibitor sequestration is absent and DivK~P is also elevated, resulting in dephosphorylation of CtrA in the stalked and predivisional stages. We conclude that although auto-phosphorylation and phospho-transfer are dispensable, the phosphatase function of PleC and the DivK~P sequestration role of PleC kinase are required for replicative asymmetry.

3.5.3 Delocalized DivL couples the morphological transition with the G1-to-S transition

The morphological transition that occurs during stalked-cell development requires PleC to be active as a kinase, whereas the G1-to-S transition requires deactivation of DivL. The two processes are coupled because PleC kinase phosphorylates DivK and DivK~P binds and inactivates DivL. Our simulations show that mislocalizing PleC has no bearing on its functional change from phosphatase to kinase. On the other hand, co-localizing DivL with PleC kinase in the stalked cell does not allow DivK~P to inhibit DivL; hence, CtrA~P level stays high and DNA replication is inhibited. This simulation result prompts us to suggest that the G1-to-S transition requires DivL to be uniformly distributed in the cell membrane. We predict that the G1-to-S transition would be uncoupled from the morphological swarmer-to-stalked transition in a novel mutant where DivL always co-localizes with PleC.

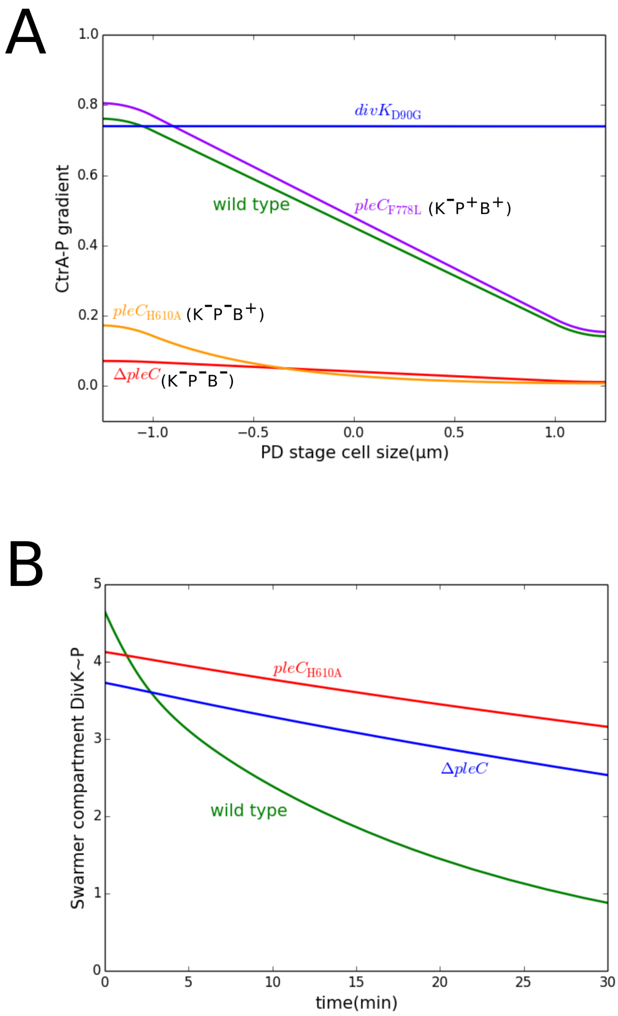

Figure 3.8: The model simulates distribution patterns of CtrA~P and DivK~P in mutant cells.

(A) Model simulations predict the concentration gradient of CtrA~P prior to cytokinesis (t = 120 min) in mutant cells: *pleC*$_{F778L}$ (purple), *divK*$_{D90G}$ (blue), Δ*pleC* (red) and *pleC*$_{H610A}$ (brown). The distribution for the wild-type cells (green) is plotted in green for reference. (B) The model reproduces the inadequate dephosphorylation of DivK~P observed in the swarmer compartment of post-compartmentalized cells in the Δ*pleC* (red) and *pleC*$_{H610A}$ (brown) mutant strains.

3.5.4 Reversion of PleC to phosphatase form is required for swarmer cell development

At cytokinesis, the cell must partition the phosphorylated forms of CtrA and DivK into separate compartments. This can be achieved only if PleC in the swarmer compartment switches back to the phosphatase form and dephosphorylates DivK~P. In earlier work, we demonstrated that the phosphatase-to-kinase transitions are robust to small changes in the level of DivJ [35]. Compartmentalization creates a situation where DivJ is completely absent in the PleC-containing swarmer compartment. Devoid of its signal kinase, PleC shows a decline in kinase level while DivK gets dephosphorylated. Our model is able to reproduce the defect in swarmer progeny development of Δ*pleC* and *pleC*$_{H610A}$ mutants (**Figure 3.8 B**). Given the absence of a functional phosphatase, DivK~P level remains high in the swarmer compartment of the mutant cells.

3.5.5 Proposed molecular mechanism to produce different developmental fates in *Caulobacter*

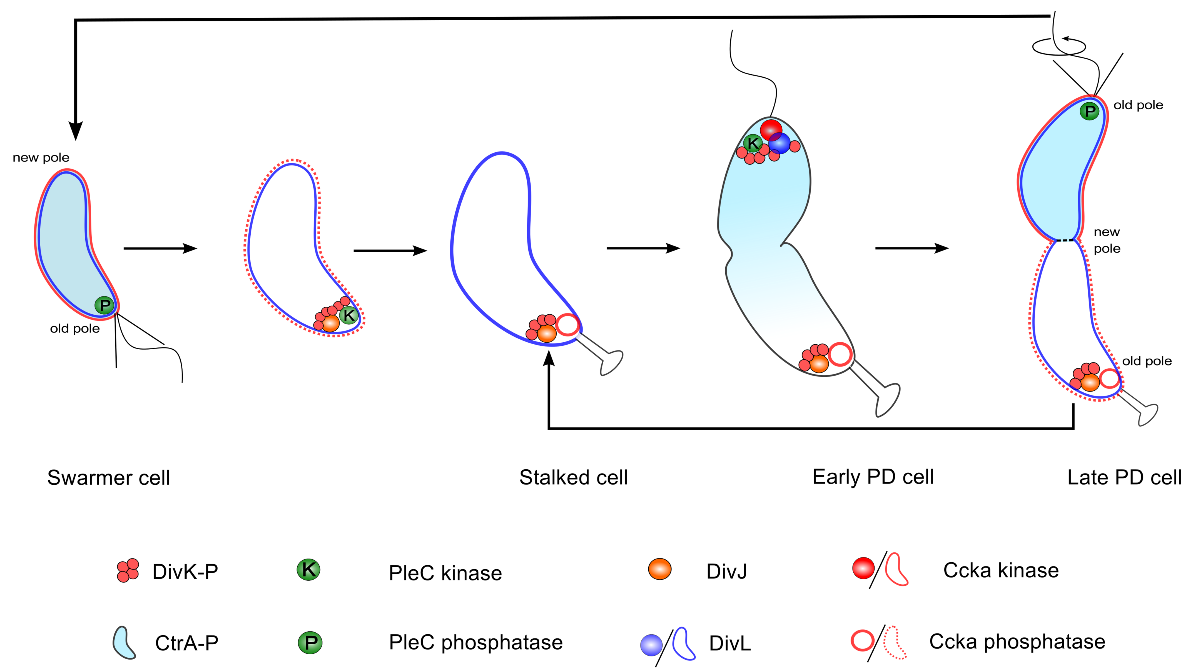

Figure 3.9: Localization and function of the DivK-PleC-DivK and DivL-CckA-CtrA signaling networks, as suggested by the model calculations reported here.

Figure 3.9 summarizes the localization and functional status of proteins, as proposed in our model. At the molecular level, the stalked cell is distinguished from the swarmer cell by the kinase DivJ, which localizes at the old pole and initiates the swarmer-to-stalked transition. Hence, DivJ can be considered as a cell fate determinant protein [40]. However, there is no counterpart for DivJ that initiates the transition from stalked to predivisional cell. Instead, the cell recycles the same components – namely, DivJ-PleC-DivK and DivL-CckA-CtrA – to program the predivisional stage of the cell cycle.

Based on our simulation results, we make the case that rapid diffusion of DivK~P does not permit PleC to be a phosphatase prior to cytokinesis. The co-localization of DivL and PleC kinase at the new pole of the predivisional cell enables the effective sequestration of DivK~P by PleC kinase, thus allowing both DivK and CtrA to be phosphorylated at the same stage of the cell cycle. Here, we use our mathematical model to offer further insight into how *Caulobacter crescentus* exploits spatial localization to temporally regulate the activity of DivL, ultimately giving rise to cell fate asymmetry.

3.6 References

1. Curtis PD, Brun Y V (2010) Getting in the Loop: Regulation of Development in *Caulobacter crescentus*. Microbiol Mol Biol Rev 74: 13–41. Available: http://mmbr.asm.org/cgi/content/abstract/74/1/13.

2. Paul R, Jaeger T, Abel S, Wiederkehr I, Folcher M, et al. (2008) Allosteric regulation of histidine kinases by their cognate response regulator determines cell fate. Cell 133: 452–461. Available: http://www.pubmedcentral.nih.gov/articlerender.fcgi?artid=2804905&tool=pmcentrez&rendertype=abstract.

3. Chen YE, Tsokos CG, Biondi EG, Perchuk BS, Laub MT (2009) Dynamics of two Phosphorelays controlling cell cycle progression in *Caulobacter crescentus*. J Bacteriol 191: 7417–7429. Available: http://www.pubmedcentral.nih.gov/articlerender.fcgi?artid=2786585&tool=pmcentrez&rendertype=abstract. Accessed 28 July 2011.

4. Reisinger SJ, Huntwork S, Viollier PH, Ryan KR (2007) DivL Performs Critical Cell Cycle Functions in *Caulobacter crescentus* Independent of Kinase Activity. J Bacteriol 189: 8308–8320. Available: http://www.pubmedcentral.nih.gov/articlerender.fcgi?artid=2168681&tool=pmcentrez&rendertype=abstract.

5. Tsokos CG, Perchuk BS, Laub MT (2011) A dynamic complex of signaling proteins uses polar localization to regulate cell fate asymmetry in *Caulobacter crescentus*. Dev Cell 20: 329–341.

6. Chen YE, Tropini C, Jonas K, Tsokos CG, Huang KC, et al. (2011) Spatial gradient of protein phosphorylation underlies replicative asymmetry in a bacterium. Proc Natl Acad Sci U S A 108: 1052–1057. Available: http://www.pubmedcentral.nih.gov/articlerender.fcgi?artid=298695&tool=pmcentrez&rendertype=abstract.

7. Quon KC, Yang B, Domian IJ, Shapiro L, Marczynski GT (1998) Negative control of bacterial DNA replication by a cell cycle regulatory protein that binds at the chromosome origin. Proc Natl Acad Sci U S A 95: 120–125. Available: http://www.ncbi.nlm.nih.gov/cgi-bin/Entrez/referer?http://www.pnas.org/cgi/content/full/95/1/120.

8. Siegal-Gaskins D, Crosson S (2008) Tightly Regulated and Heritable Division Control in Single Bacterial Cells. Biophys J 95: 2063–2072. Available: http://www.pubmedcentral.nih.gov/articlerender.fcgi?artid=2483777&tool=pmcentrez&rendertype=abstract.

9. Radhakrishnan SK, Thanbichler M, Viollier PH (2008) The dynamic interplay between a cell fate determinant and a lysozyme homolog drives the asymmetric division cycle of *Caulobacter crescentus*. Genes Dev 22: 212–225. Available: http://www.pubmedcentral.nih.gov/articlerender.fcgi?artid=2192755&tool=pmcentrez&rendertype=abstract.

10. Lin Y, Crosson S, Scherer NF (2010) Single-gene tuning of *Caulobacter* cell cycle period and noise, swarming motility, and surface adhesion. Mol Syst Biol 6: 445. Available: http://www.nature.com/doifinder/10.1038/msb.2010.95.

11. Jacobs C, Hung D, Shapiro L (2001) Dynamic localization of a cytoplasmic signal transduction response regulator controls morphogenesis during the *Caulobacter* cell cycle. Proc Natl Acad Sci U S A 98: 4095–4100. Available: http://www.pubmedcentral.nih.gov/articlerender.fcgi?artid=31185&tool=pmcentrez&rendertype=abstract.

12. Angelastro PS, Sliusarenko O, Jacobs-Wagner C (2010) Polar localization of the CckA histidine kinase and cell cycle periodicity of the essential master regulator CtrA in *Caulobacter crescentus*. J Bacteriol 192: 539–552. Available: http://www.pubmedcentral.nih.gov/articlerender.fcgi?artid=2805319&tool=pmcentrez&rendertype=abstract.

13. Iniesta AA, Hillson NJ, Shapiro L (2010) Polar Remodeling and Histidine Kinase Activation, Which Is Essential for *Caulobacter* Cell Cycle Progression, Are Dependent on DNA Replication Initiation. J Bacteriol 192: 3893–3902. Available: http://www.pubmedcentral.nih.gov/articlerender.fcgi?artid=2916389&tool=pmcentrez&rendertype=abstract.

14. Aldridge P, Paul R, Goymer P, Rainey P, Jenal U (2003) Role of the GGDEF regulator PleD in polar development of *Caulobacter crescentus*. Mol Microbiol 47: 1695–1708. Available: http://www.ncbi.nlm.nih.gov/pubmed/12622822.

15. Jenal U, Galperin MY (2009) Single domain response regulators: molecular switches with emerging roles in cell organization and dynamics. Curr Opin Microbiol 12: 152–160.

16. Thanbichler M (2009) Spatial regulation in *Caulobacter crescentus*. Curr Opin Microbiol 12: 715–721.

17. Thanbichler M (2010) Synchronization of chromosome dynamics and cell division in bacteria. Cold Spring Harb Perspect Biol 2: a000331.

18. Matroule J-Y, Lam H, Burnette DT, Jacobs-Wagner C (2004) Cytokinesis monitoring during development; rapid pole-to-pole shuttling of a signaling protein by localized kinase and phosphatase in *Caulobacter*. Cell 118: 579–590. Available: http://www.ncbi.nlm.nih.gov/pubmed/15339663.

19. Jonas K, Chen YE, Laub MT (2011) Modularity of the bacterial cell cycle enables independent spatial and temporal control of DNA replication. Curr Biol 21: 1092–1101.

20. Aaron M, Charbon G, Lam H, Schwarz H, Vollmer W, et al. (2007) The tubulin homologue FtsZ contributes to cell elongation by guiding cell wall precursor synthesis in *Caulobacter crescentus*. Mol Microbiol 64: 938–952. doi:10.1111/j.1365-2958.2007.05720.x.

21. Lam H, Matroule J-Y, Jacobs-Wagner C (2003) The asymmetric spatial distribution of bacterial signal transduction proteins coordinates cell cycle events. Dev Cell 5: 149–159. Available: http://www.ncbi.nlm.nih.gov/entrez/query.fcgi?cmd=Retrieve&db=PubMed&dopt=Citation&list_uids=12852859.

22. Wheeler RT, Shapiro L (1999) Differential localization of two histidine kinases controlling bacterial cell differentiation. Mol Cell 4: 683–694. Available: http://www.ncbi.nlm.nih.gov/pubmed/10619016.

23. Shampine LF, Reichelt MW (1997) The MATLAB ODE Suite. SIAM J Sci Comput 18: 1–22. doi:10.1137/S1064827594276424.

24. Hunter JD (2007) Matplotlib: A 2D Graphics Environment. Comput Sci Eng 9: 90–95. Available: http://ieeexplore.ieee.org/lpdocs/epic03/wrapper.htm?arnumber=4160265.

25. Iniesta AA, Hillson NJ, Shapiro L (2010) Cell pole-specific activation of a critical bacterial cell cycle kinase. Proc Natl Acad Sci U S A 107: 7012–7017. Available: http://www.pubmedcentral.nih.gov/articlerender.fcgi?artid=2872457&tool=pmcentrez&rendertype=abstract.

26. Ebersbach G, Briegel A, Jensen GJ, Jacobs-Wagner C (2008) A self-associating protein critical for chromosome attachment, division, and polar organization in *Caulobacter*. Cell 134: 956–968. Available: http://www.pubmedcentral.nih.gov/articlerender.fcgi?artid=2614312&tool=pmcentrez&rendertype=abstract.

27. Jacobs C, Domian IJ, Maddock JR, Shapiro L (1999) Cell cycle-dependent polar localization of an essential bacterial histidine kinase that controls DNA replication and cell division. Cell 97: 111–120. Available: http://www.ncbi.nlm.nih.gov/pubmed/10199407.

28. Domian IJ, Reisenauer A, Shapiro L (1999) Feedback control of a master bacterial cell-cycle regulator. Proc Natl Acad Sci U S A 96: 6648–6653. Available: http://www.pubmedcentral.nih.gov/articlerender.fcgi?artid=21969&tool=pmcentrez&rendertype=abstract.

29. Reisenauer A, Shapiro L (2002) DNA methylation affects the cell cycle transcription of the CtrA global regulator in *Caulobacter*. Eur Mol Biol Organ J 21: 4969–4977. Available: http://www.pubmedcentral.nih.gov/articlerender.fcgi?artid=126286&tool=pmcentrez&rendertype=abstract.

30. Spencer W, Siam R, Ouimet M-C, Bastedo DP, Marczynski GT (2009) CtrA, a global response regulator, uses a distinct second category of weak DNA binding sites for cell cycle

transcription control in *Caulobacter crescentus*. J Bacteriol 191: 5458–5470. Available: http://www.pubmedcentral.nih.gov/articlerender.fcgi?artid=2725627&tool=pmcentrez&rendertype=abstract.

31. Hung DY, Shapiro L (2002) A signal transduction protein cues proteolytic events critical to *Caulobacter* cell cycle progression. Proc Natl Acad Sci U S A 99: 13160–13165. Available: http://www.pubmedcentral.nih.gov/articlerender.fcgi?artid=130603&tool=pmcentrez&rendertype=abstract.

32. Iniesta AA, Shapiro L (2008) A bacterial control circuit integrates polar localization and proteolysis of key regulatory proteins with a phospho-signaling cascade. Proc Natl Acad Sci U S A 105: 16602–16607. Available: http://www.pubmedcentral.nih.gov/articlerender.fcgi?artid=2575466&tool=pmcentrez&rendertype=abstract.

33. Gorbatyuk B, Marczynski GT (2005) Regulated degradation of chromosome replication proteins DnaA and CtrA in *Caulobacter crescentus*. Mol Microbiol 55: 1233–1245. Available: http://www.ncbi.nlm.nih.gov/pubmed/15686567.

34. Biondi EG, Reisinger SJ, Skerker JM, Arif M, Perchuk BS, et al. (2006) Regulation of the bacterial cell cycle by an integrated genetic circuit. Nature 444: 899–904. Available: http://www.ncbi.nlm.nih.gov/pubmed/17136100.

35. Subramanian K, Paul MR, Tyson JJ (2013) Potential Role of a Bistable Histidine Kinase Switch in the Asymmetric Division Cycle of *Caulobacter crescentus*. PLoS Comput Biol 9.

36. Domian IJ, Quon KC, Shapiro L (1997) Cell type-specific phosphorylation and proteolysis of a transcriptional regulator controls the G1-to-S transition in a bacterial cell cycle. Cell 90: 415–424. Available: http://www.ncbi.nlm.nih.gov/pubmed/9150145.

37. Tropini C, Huang KC (2012) Interplay between the Localization and Kinetics of Phosphorylation in Flagellar Pole Development of the Bacterium *Caulobacter crescentus*. PLoS Comput Biol 8: e1002602. Available: http://www.pubmedcentral.nih.gov/articlerender.fcgi?artid=3410866&tool=pmcentrez&rendertype=abstract.

38. Li S, Brazhnik P, Sobral B, Tyson JJ (2008) A Quantitative Study of the Division Cycle of *Caulobacter crescentus* Stalked Cells. PLoS Comput Biol 4: 19. Available: http://www.pubmedcentral.nih.gov/articlerender.fcgi?artid=2217572&tool=pmcentrez&rendertype=abstract.

39. Li S, Brazhnik P, Sobral B, Tyson JJ (2009) Temporal Controls of the Asymmetric Cell Division Cycle in *Caulobacter crescentus*. PLoS Comput Biol 5: 15. Available: http://www.ncbi.nlm.nih.gov/pubmed/19680425.

40. Boutte CC, Henry JT, Crosson S (2012) ppGpp and polyphosphate modulate cell cycle progression in *Caulobacter crescentus*. J Bacteriol 194: 28–35. Available: http://www.ncbi.nlm.nih.gov/pubmed/22020649.

Chapter 4 *De novo* Production of Turing Activator Generates Polarity in Pattern Formation

Kartik Subramanian[1], Mark R. Paul[2] and John J. Tyson[3,4,*]

[1]Graduate Program in Genetics, Bioinformatics and Computational Biology, [2]Department of Mechanical Engineering, [3]Department of Biological Sciences, and [4]Virginia Bioinformatics Institute, Virginia Polytechnic Institute and State University, Blacksburg VA 24061

4.1 Abstract

Sixty years ago, Alan Turing showed that a system of reacting and diffusing chemicals could generate spontaneous, stable, stationary, spatial patterns of chemical concentrations. Since then "Turing patterns" have been used successfully to explain the development of patterns in both multicellular and unicellular organisms. In single-celled protists and bacteria, a common motif for spatial pattern formation is the autocatalytic production of filamentous protein polymers from globular protein subunits, which is an instance of the "activator-substrate depletion" (A-SD) mechanism of Turing patterning. A feature of A-SD models is that the peak of activator concentration tends to form at the center of the spatial domain rather than at the edges. Hence, a generic A-SD model cannot easily account for the generation of patterns with activator peaks at the poles of a cell. Here, we present a modified A-SD model that readily generates patterns with polar activator peaks. We explore the parameter combinations that determine whether the pattern has polar or central peaks. We propose that our mechanism may be used by living cells as a means to obtain polar localization of proteins.

4.2 Introduction

The impact of protein localization is evident at all levels of biological organization, from single cells to tissues, organs and whole organisms. Segregation of chromosomes during cell division, the positioning of flagella, and the specification of embryonic axes are some of the processes that depend on the timely placement of regulatory proteins at specific positions in the cell or organism. Advances in microscopy have dispelled the notion that protein localization is exclusive to the eukaryotic world. Bacteria such as *Escherichia coli*, *Bacillus subtilis* and *Caulobacter crescentus* all exhibit dynamic localization of specific proteins during the course of their cell division cycles [1–5]. In addition to modern methods to visualize and identify these localized proteins, many experiments have sought the mechanisms behind dynamic protein localization. In many cases, a particular protein is found to localize by binding to a previously localized protein (an "upstream factor"), ultimately leading to the identification of "landmark" proteins that appear at specific locations in the cell in the absence of an upstream factor. How do landmark proteins spontaneously self-organize in the cell? Not surprisingly, a Turing-type mechanism has been proposed in many cases to explain autonomous pattern formation of landmark proteins [6–10].

The essence of Turing's idea [11] was most clearly presented in a classical paper by Segel & Jackson [12], who showed that stable, stationary, spatial patterns can be generated in two-component reaction-diffusion systems under a few generic conditions: one component must be self-activating (autocatalytic) and slowly diffusing, and the other component—the fast-diffusing species—must inhibit the self-activation process in some way. In the Activator-Inhibitor Production (A-IP) mechanism, the activator produces an inhibitor that rapidly diffuses away from a zone of high activator concentration and restrains the self-activation process in surrounding regions. In the Activator-Substrate Depletion (A-SD) mechanism, the activator self-assembles from substrate molecules, which rapidly diffuse into the region of activator accumulation and thereby deplete the substrate from surrounding regions. In either case, the Turing instability generates patches of high activator concentration surrounded by regions of low activator concentration, either because inhibitor concentrations are high or substrate concentrations are low. A second activator patch can form only at some distance from the original patch, where inhibitor concentration is low enough or substrate concentration is high enough to allow for production of a new activator. This distance is the characteristic wavelength of the Turing pattern [13].

In this study we focus on pattern formation by A-SD models in growing domains of one spatial dimension (*i.e.*, a line segment, $0 \leq x \leq L(t)$, $\mathrm{d}L/\mathrm{d}t > 0$) to represent a growing, rod-shaped cell where x is the spatial coordinate and $L(t)$ is the length of the cell which varies with time t. A common feature of these patterns is that the first activator peaks forms at the center of the domain ($x = L/2$), and subsequent peaks bifurcate from previous peaks as the domain expands [14]. Hence, the AS-D model fails to explain patterns that have activator peaks at the boundaries (the poles of the cell). To generate patterns with activator peaks at the poles, we add an additional reaction—*de novo* synthesis of activator—to the classical Gierer-Meinhardt reaction-diffusion equations (RDEs). Simulations of the modified RDEs exhibit patterns with polar maxima that are reminiscent of landmark protein localization in rod-shaped bacteria.

4.3 Methods

We model Turing patterns in one spatial dimension, x, by RDEs (Eq. 1-2) for activator concentration $a(x,t)$ and substrate concentration $s(x,t)$:

$$\frac{\partial a}{\partial t} = k_{\text{aut}} \cdot a^2 \cdot s - k_{\text{deg}} \cdot a + k_{\text{dnv}} \cdot s - k_{\text{as}} \cdot a + D_{\text{a}} \cdot \frac{\partial^2 a}{\partial x^2} \qquad (1)$$

$$\frac{\partial s}{\partial t} = k_{\text{syn}} - k_{\text{deg}} \cdot s - k_{\text{dnv}} \cdot s - k_{\text{aut}} \cdot a^2 \cdot s + k_{\text{as}} \cdot a + D_{\text{s}} \cdot \frac{\partial^2 s}{\partial x^2} \qquad (2)$$

The "classical Geirer-Meinhardt" equations lack the terms $k_{\text{dnv}} \cdot s$ and $k_{\text{as}} \cdot a$, which correspond to *de novo* synthesis of activator (polymer) from substrate (monomer) and to dissociation of polymer into monomers. We solve the RDEs (1-2) in one spatial dimension, $0 \le x \le L$, by the method of lines [15] . That is, we discretize the spatial dimension into n compartments (n = 100) of length $h = L/n$, and approximate $\partial^2/\partial x^2$ by a central difference scheme (Eq. 3a). We implement no-flux boundary conditions as described in Eq. (3b,c). (In these equations, c_{i} represents the concentration of either activator or substrate in compartment *i.*)

$$\frac{\partial^2 c_i}{\partial x^2} = \frac{c_{i-1} - 2 \cdot c_i + c_{i+1}}{h^2} \qquad \textit{for } i = 2, \ldots, 99 \qquad (3a)$$

$$\frac{\partial^2 c_1}{\partial x^2} = \frac{c_2 - c_1}{h^2} \qquad (3b)$$

$$\frac{\partial^2 c_{100}}{\partial x^2} = \frac{c_{99} - c_{100}}{h^2} \qquad (3c)$$

In some cases we consider a growing spatial domain, $L = L(t)$, $\mathrm{d}L/\mathrm{d}t > 0$. In this case, we keep n fixed at 100 and let $h(t) = L(t)/n$ increase with growth

$$\frac{dh}{dt} = \mu \cdot h \qquad (4)$$

The resulting $2n$+1 ordinary differential equations are solved using MATLAB's ode15s solver. The parameter values used in our simulations are recorded in **Table 4.1**.

Table 4.1: Parameter set for the A-SD model

k_{syn} = 2 min^{-1}	k_{deg} = 0.25 min^{-1}	k_{aut} = 1.5 min^{-1}
k_{as} = 1 min^{-1}	D_{s} = 100 μm^2. min^{-1}	D_a = 0.01 μm^2. min^{-1}
μ = 0.005 min^{-1}		

* The values of the *de novo* polymerization constant, k_{dnv}, are defined in the text and figure captions.

4.4 Results

4.4.1 *De novo* conversion of substrate to activator supports activator peaks at cell poles

A Turing-type RDE generates periodic activator peaks with a characteristic wavelength, λ_0 that depends on parameter values. If $L \approx \lambda_0/2$, the domain is large enough to accommodate a half-wave, with the activator maximum pinned at one end of the cell and the minimum at the other end. If $L(t)$ increases to ~ λ_0, the domain can accommodate either two activator half-peaks at the poles with a minimum in the center (polar peaks) or an activator peak at the center with minima at the poles (polar troughs). As $L(t)$ increases further, additional activator peaks are generated, but the patterns can still be classified as either "polar peaks" or "polar troughs". In A-IP models, either pattern is possible [8]. In classical A-SD models, however, only polar trough patterns are observed.

In the classical A-SD model, Eq. (1-2) with $k_{\text{dnv}} = k_{\text{as}} = 0$, the only route to new activator production is the autocatalytic term, $k_{\text{aut}} \cdot a^2 \cdot s$. Hence, new activator tends to be produced where activator concentration is the highest, namely at the peak. However, the substrate necessary for activator production is more abundant at some distance from the peak. Hence, the activator peak tends to grow into the surrounding zone, where more substrate is available, and a depression tends to form in the center of the peak, where substrate concentration is lowest. When the activator peak reaches the center of the domain, substrate availability is equal on both sides of the peak, and the peak is anchored there. For this reason, classical A-SD models are unsuccessful in explaining patterns with polar peaks of landmark proteins.

To account for polar activator peaks, previous groups have modified the classical A-SD model in various ways. For the MinCD/DivIVA system in *B. subtilis*, Howard [1] proposed that increased curvature of the cell's boundary at the poles might account for polar localization. To explain growth zone formation in fission yeast, Csikasz-Nagy *et al*. [16] introduced a polarly localized nucleating factor that stimulates the autocatalytic production of activator from substrate at the poles. While these modifications are reasonable and yield appropriate results, they are case-specific. Examples of polar peaks in other biological systems would presumably need other case-specific explanations. We seek a more generic account of polar activator peaks in A-SD models.

Since the autocatalytic term biases A-SD models to produce central activator peaks, we conjectured that an alternative source of activator production might create a different pattern. Hence, we introduced the *de novo* activator production term, $k_{\text{dnv}} \cdot s$, into Eq. (1-2). This term, which implies that new activator can be produced from substrate independent of pre-existing activator, is reasonable both chemically and biologically. The *de novo* term describes the spontaneous production of polymers (activator) from a handful of monomers (substrates), while the autocatalytic term describes the extension of pre-existing polymers by the addition of new monomeric subunits. Our model also contains a term, $k_{\text{as}} \cdot a$ for the depolymerization of activator back to substrate monomers.

To test the impact of the *de novo* term, we simulated a cell of length $L \approx \lambda_0$, *i.e.*, long enough to accommodate either a central peak or central trough pattern. For the classical A-SD model, $k_{\text{dnv}} = k_{\text{as}} = 0$, we expected to find central peak patterns exclusively. By increasing the strength of *de novo* synthesis, we expected to find examples of spontaneous, stable polar peaks. We initialized the model with an excess of activator at one pole. When k_{dnv} is small, the activator peak moved towards the center (**Figure 4.1 A and B**). When we initialized the model with excess activator at the center, the peak stayed in place (**Figure 4.1 C**). Hence, for small values of k_{dnv}, our modified RDE behaves exactly as the classical A-SD model. For larger values of k_{dnv}, we saw that, for some initial conditions, the activator peak was no longer exclusively central. If the activator was initialized with a central bias, then the peak remained at the center (**Figure 4.2 C**). However, for simulations that were initialized with an excess of activator at one pole, we observed activator half-peaks not only at the end with the initial bias but also at the other end (**Figure 4.2 A and B**). While one of the half-peaks clearly arises from the initial bias, the other appears spontaneously, since the cell is long enough to hold two half-peaks at opposite poles.

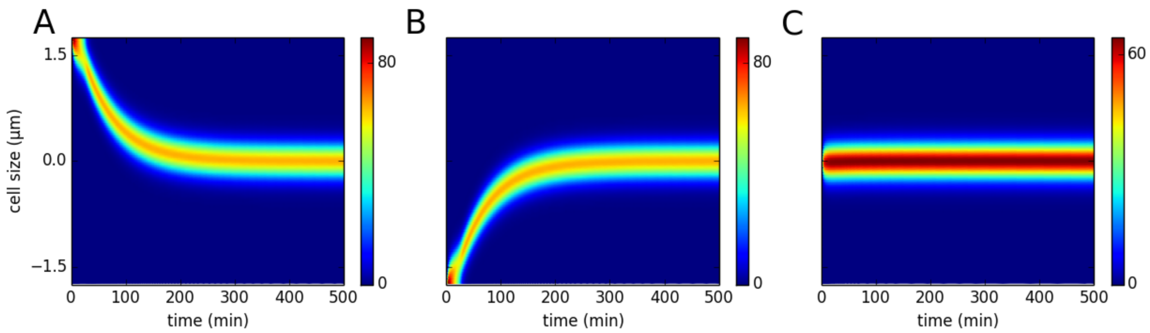

Figure 4.1: Space-time plot of activator concentration for varying initial conditions of the activator and k_{dnv} = 1 min^{-1}.

Initial activator bias is provided by setting activator concentration as 1 dimensionless unit in one compartment and 0 dimensionless units in all other compartments. Color indicates concentration gradients of the activator from minimum (blue) to maximum (red). (A) Initial activator bias at the left pole *i.e.* $a(1,0)$ = 1 dimensionless unit. (B) Initial activator bias at the right pole *i.e.* $a(100,0)$ = 1 dimensionless unit. (C) Initial activator bias in the middle *i.e.* $a(51,0)$ = 1 dimensionless unit.

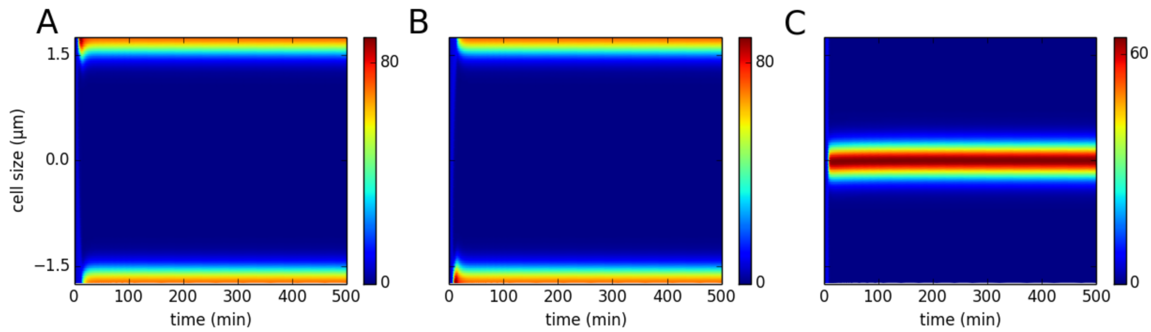

Figure 4.2: Space-time plot of activator concentration for varying initial conditions of the activator and k_{dnv} = 10 min^{-1}.

Initial activator bias is provided by setting activator concentration as 1 dimensionless unit in one compartment and 0 dimensionless units in all other compartments. Color indicates concentration gradients of the activator from minimum (blue) to maximum (red). (A) Initial activator bias at the left pole *i.e.* $a(1,0)$ = 1 dimensionless unit (B) Initial activator bias at the right pole *i.e.* $a(100,0)$ = 1 dimensionless unit. (C) Initial activator bias in the middle *i.e.* $a(51,0)$ = 1 unit.

4.4.2 Central and polar peaks are alternative attractors

Irrespective of the value of k_{dnv}, a central activator peak was obtained if the initial bias was at the center, suggesting that the location of the activator peak is sensitive to initial conditions. To determine the effects of initial conditions on pattern formation, we simulated our model with random sets of initial conditions. In **Figure 4.3 A**, we plot the final distribution of activator for 500 simulations, each initialized with different initial conditions selected randomly. For $k_{\mathrm{dnv}} = 0$, only 2 of 500 runs showed polar activator peaks. In these two cases, we suspect, both ends of the cell were initialized with nearly equal activator concentrations. When k_{dnv} was increased from 0 to 1 or 10, a significantly larger number of runs (≈ 40%) showed polar peaks (**Figure 4.3 B and C**). Further increase in the value of k_{dnv} showed moderate increase in polar peaks, indicating that central-peak patterns are dominant over polar-peak patterns. Importantly, both patterns are attractors, each with its own basin of attraction. The effect of increasing k_{dnv} is to increase the basin of attraction for the polar attractor, albeit only to a limited extent.

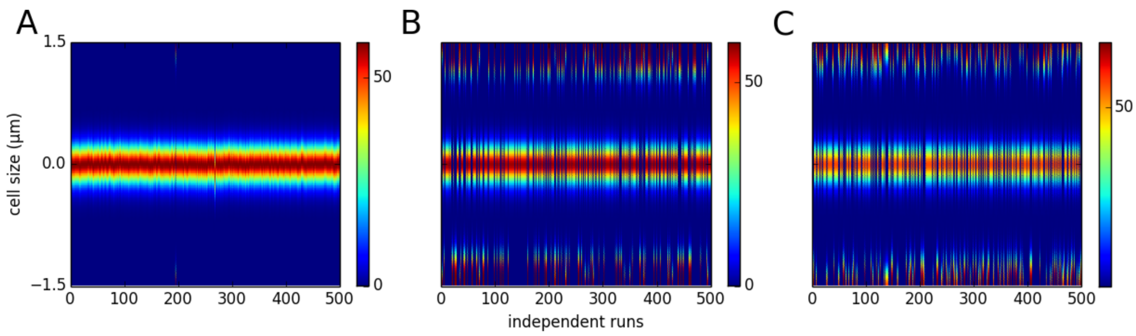

Figure 4.3: Final activator distribution (at t = 500 min) plotted for 500 independent runs.

Each run is initialized with random initial conditions (at t = 0) of activator and substrate, ranging from 0 to 1 dimensionless units. Color indicates concentration gradients of the activator from minimum (blue) to maximum (red). (A) $k_{\mathrm{dnv}} = 0\ \mathrm{min}^{-1}$. (B) $k_{\mathrm{dnv}} = 1\ \mathrm{min}^{-1}$. (C) $k_{\mathrm{dnv}} = 10\ \mathrm{min}^{-1}$.

4.4.3 Asymmetric pre-patterns lead to polar activator peaks above a critical value of $\mathbf{k_{dnv}}$

As our simulations show, varying initial conditions give rise to different final patterns. How then can the model explain robust polar localization of landmark proteins? In most cases, cells inherit a pre-pattern or asymmetric polarity from the parent cell. We therefore investigated if polar peaks are robustly inherited from asymmetric pre-patterns, *i.e.* from an initial pattern with a peak at one pole and a trough at the other. For varying values of k_{dnv}, we simulated our model starting with an initial polar bias at one end of the cell. **Figure 4.4 A** shows the final distribution of activator obtained for 1000 values of k_{dnv} ranging from 5.5 to 6.5. For each value of the parameter, the simulation was initialized with an initial activator peak at the right pole *i.e.* $a(100,0) = 1$ unit. Below a critical value of $k_{\mathrm{dnv},}$ the final distribution pattern shows a central peak, while above the critical value, two half-peaks are obtained at the poles. The results indicate that, given an asymmetric pre-pattern, polar activator peaks are robustly inherited above a critical value of $k_{\mathrm{dnv}} = 5.95$, On the other hand, if the pre-pattern is symmetric, then the corresponding final pattern is also symmetric, irrespective of the value of $k_{\mathrm{dnv}.}$ If the simulation is initialized with bias at both poles, then the corresponding final distribution pattern shows polar half-peaks for all values of k_{dnv} (**Figure 4.4 B**). If the pre-pattern at $t = 0$ min has a central bias, then the corresponding final pattern also show central peaks, even above critical value of k_{dnv} (**Figure 4.4 C**). Hence, above a critical rate of *de novo* activator synthesis, our model can account for the generation of polar peaks if the pre-pattern is asymmetric.

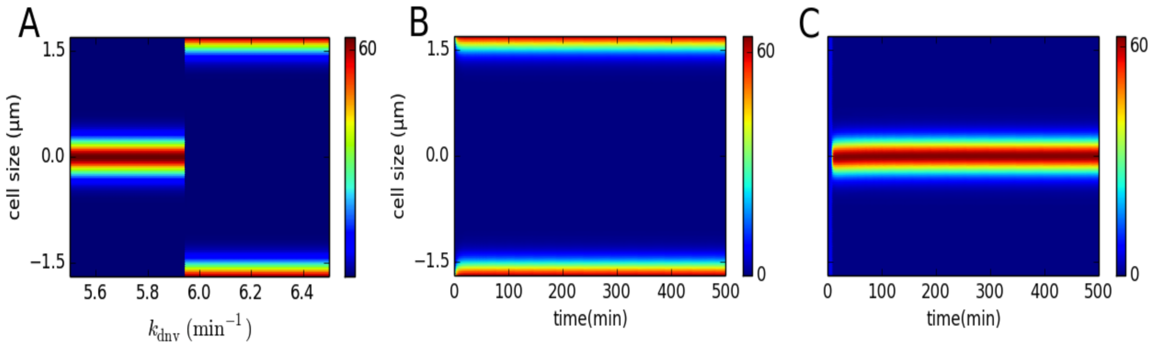

Figure 4.4: Final activator distribution plotted for 1000 values of k_{dnv} between 5.5 and 6.5 min^{-1}.

(A) The initial pattern is asymmetric, with an activator peak at one end and trough at the other *i.e.* $a(100,0) = 1$ dimensionless unit. (B) Space-time plot of activator distribution for $k_{\mathrm{dnv}} = 5.5$ min^{-1} and for an initial bias at both poles *i.e.* $a(1,0) = a(1,0) = 1$ dimensionless unit. (C) Space-time plot of activator distribution for $k_{\mathrm{dnv}} = 6.5$ min^{-1} and the initial bias is in the middle of the cell *i.e.* $a(51,0) = 1$ dimensionless unit. Color indicates concentration gradients of the activator from minimum (blue) to maximum (red).

The condition for an asymmetric polar pre-pattern is easily realized in the relevant biological context. Imagine a cell with activator peaks at both poles. Upon cell division, each daughter cell inherits one of the polar peaks and a trough at the other end, which was the central trough in the mother cell. Newly born daughter cells with such a pre-pattern will give rise to a second activator peak at the opposite pole when they grow long enough to accommodate a second peak. The cycle of small daughter cells with a single polar peak growing into predivisional cells with two polar peaks will continue in each generation.

4.4.4 In growing cells, new activator peaks appear spontaneously

Our simulations up to this point have been for cells of fixed size where L is a constant. In reality though, cells grow and divide over time and therefore $L = L(t)$. The effect of cell growth on pattern formation in a classical A-SD model was previously studied by Crampin *et al*. [14]. Additional activator peaks emerge when the size of the cell is a multiple of the characteristic wavelength of the Turing pattern. The transitions in the activator pattern have a characteristic feature: as cell size approaches a new multiple of λ_0, a pre-existent activator peak splits into additional activator peaks. Following this transition, the recently split activator peaks move away from each other as the cell continues to grow. This process of peak splitting occurs every time the cell becomes large enough to hold additional peaks, ultimately giving rise to a tree-like or branched activator pattern. For our set of equations, we found a similar branched pattern for low values ofk_{dnv} (**Figure 4.5 A**).

In sharp contrast, for larger values of the rate of *de novo* synthesis, we found that additional activator peaks appeared at locations where no peak existed previously (**Figure 4.5 B**). Transitions in the number of activator peaks also occurred when cell size crossed a multiple of a critical length. Another significant deviation from the branched pattern is the number of peaks that appear at each transition. For the branched pattern, a cell of length $L \approx \lambda_0/2$ holds one half-peak at a pole. When length $L \approx \lambda_0$, a single peak is found at the center of the cell. Thereafter, the number of peaks doubles in subsequent transitions, giving rise to 2, 4, 8 and 16 peaks respectively (**Figure 4.5 A**). For the case of *de novo* activator production in our model, the first transition, at $L \approx \lambda_0$, gives rise to two half-peaks at the poles. In the next transition, a third peak forms at the center. Subsequent transitions have 5, 9 and 17 peaks respectively. Hence, after the initial two transitions, the branched pattern shows an even number of peaks, while the *de novo* pattern shows an odd number of peaks. We propose that an odd number of activator peaks is a characteristic feature of an A-SD model with *de novo* synthesis of activator.

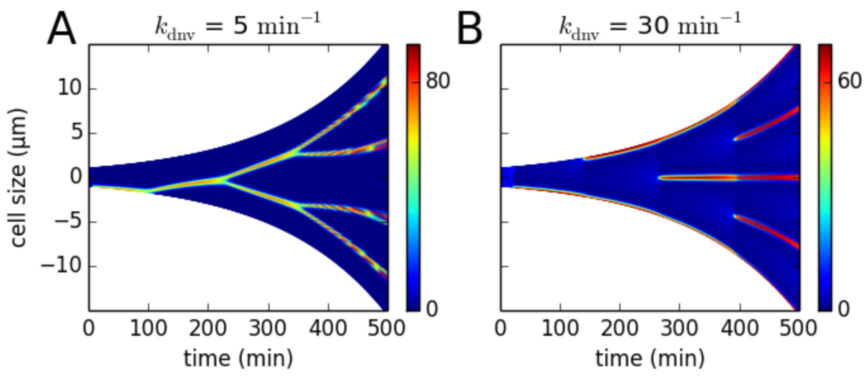

Figure 4.5: Space time plot of activator production in a growing cell.

$L(t = 0) = 1.3$ μm initialized with a bias of activator at the right pole *i.e.* $a(100,0) = 1$ dimensionless unit. Activator concentration in other compartments is set to 0 dimensionless units. Color indicates concentration gradients of the activator from minimum (blue) to maximum (red). (A) $k_{dnv} = 5$ min^{-1}. (B) $k_{dnv} = 30$ min^{-1}.

At $t = 500$ minutes, the cell length $L = 100$ μm and compartment size $h = 0.1$ μm. A concern at large L is that the discretization may not be smooth enough. We therefore discretized the domain into 200 compartments and repeated the simulations. We found that the activator patterns obtained from the two discretization schemes were comparable to each other.

4.5 Conclusions

The classical A-SD model, proposed years ago by Gierer and Meinhardt, exhibits activator peaks that localize away from the poles of a one-dimensional field. We present a modified set of RDEs that includes additional terms for *de novo* production of activator and conversion of activator back to substrate molecules. We show that our modified RDEs can account for patterns with activator peaks at the poles.

How does the addition of the *de novo* synthesis term account for the phase shift in the activator pattern? When the cell is small, production of new activator peaks is inhibited due the rapid diffusion of substrate molecules into the activator peak, depleting the surrounding region of substrate. Only when the cell grows sufficiently long may a second activator peak be formed. In the classical A-SD model, only the autocatalytic route produces activators. Hence, new peaks are obtained by splitting a pre-existing peak, resulting in a branched pattern. In contrast, the *de novo* synthesis term in our model allows the production of activators at any site. Therefore, as the cell grows, new activator peaks may be produced in between pre-existing peaks, where substrate concentration is largest. The autocatalytic and *de novo* terms compete for activator production. At low k_{dnv}, the autocatalytic term dominates, and we observe movement of the first peak towards the center of the cell, followed by peak splitting in subsequent transitions. When $k_{\mathrm{dnv}}$is large enough, *de novo* activator synthesis takes over, allowing the formation of new peaks between old ones. We propose that this mechanism, combining autocatalytic activator production with a *de novo* synthesis term, may be a means used by cells for polar localization of polymeric proteins.

4.6 References

1. Howard M (2004) A mechanism for polar protein localization in bacteria. J Mol Biol 335: 655–663.

2. Shapiro L, Losick R (1997) Protein localization and cell fate in bacteria. Science 276: 712–718. doi:10.1126/science.276.5313.712.

3. Johnson AS, van Horck S, Lewis PJ (2004) Dynamic localization of membrane proteins in Bacillus subtilis. Microbiology 150: 2815–2824. doi:10.1099/mic.0.27223-0.

4. Howard M, Kruse K (2005) Cellular organization by self-organization: mechanisms and models for Min protein dynamics. J Cell Biol 168: 533–536.

5. Hale CA, Meinhardt H, de Boer PA (2001) Dynamic localization cycle of the cell division regulator MinE in Escherichia coli. EMBO J 20: 1563–1572.

6. Kondo S, Miura T (2010) Reaction-diffusion model as a framework for understanding biological pattern formation. Science 329: 1616–1620. doi:10.1126/science.1179047.

7. Meinhardt H (1982) Models of biological pattern formation. Research Gate. pp. 1–10. doi:10.1016/S0070-2153(07)81001-5.

8. Meinhardt H (1982) Models of Biological Pattern Formation. Academic Press.

9. Meinhardt H, Gierer A (2000) Pattern formation by local self-activation and lateral inhibition. Bioessays 22: 753–760. doi:10.1002/1521-1878(200008)22:8<753::AID-BIES9>3.0.CO;2-Z.

10. Gierer A, Meinhardt H (1972) A theory of biological pattern formation. Kybernetik 12: 30–39. doi:10.1007/BF00289234.

11. Turing AM (1952) The Chemical Basis of Morphogenesis. Philos Trans R Soc B Biol Sci 237: 37–72. doi:10.1098/rstb.1952.0012.

12. Segel LA, Jackson JL (1972) Dissipative structure: an explanation and an ecological example. J Theor Biol 37: 545–559. Available: http://www.ncbi.nlm.nih.gov/pubmed/4645361.

13. Edelstein-Keshet L (2005) Mathematical Models in Biology. SIAM.

14. Crampin EJ, Hackborn WW, Maini PK (2002) Pattern formation in reaction-diffusion models with nonuniform domain growth. Bull Math Biol 64: 747–769.

15. Schiesser WE (1991) The Numerical method of lines. Academic Press.

16. Csikász-Nagy A, Gyorffy B, Alt W, Tyson JJ, Novák B (2008) Spatial controls for growth zone formation during the fission yeast cell cycle. Yeast 25: 59–69. doi:10.1002/yea.1571.

Chapter 5 Spatiotemporal Model of PopZ Localization in *Caulobacter crescentus*

Kartik Subramanian[1], Fei Li[2], Mark R. Paul[3], Yang Cao[2], and John J. Tyson[4,5,*]

[1]Graduate Program in Genetics, Bioinformatics and Computational Biology, [2]Department of Computer Science, [3]Department of Mechanical Engineering, [4]Department of Biological Sciences, and [5]Virginia Bioinformatics Institute, Virginia Polytechnic Institute and State University, Blacksburg VA 24061

5.1 Abstract

The asymmetric localization of proteins is crucial to the dimorphic life cycle of *Caulobacter crescentus.* The polymer PopZ is considered as a 'landmark' scaffolding protein as it is a localization determinant for key cell cycle regulators. In addition, PopZ plays a role in segregation and tethering of replicated chromosomes. However, the molecular mechanisms underlying the self-assembly of PopZ remain unclear, with competing models proposed to explain its dynamic and cell-cycle dependent localization profile. Here, we propose that an Activator Substrate-Depletion (A-SD) type Turing mechanism can explain localization of the PopZ polymer. We formulate a deterministic reaction-diffusion model to compare and resolve alternative hypotheses. Our simulation results demonstrate that the dependency of bipolar localization on chromosome segregation may be the result of limited dispersal of slow diffusing *popZ* mRNA, which makes it necessary for two *popZ* loci to be present close to the poles of the cell. We also develop a stochastic version of our model, and show that the observed variations in the time and cell length at which PopZ becomes bipolar can be accounted for by the biased random walk of the segregating chromosome.

5.2 Introduction

The list of proteins that localize at specific positions inside bacterial cells is growing steadily [1,2]. The landscape of the bacterial cytoplasm is not only organized in space but also changing in time, in a cell cycle-dependent manner [3]. Cell shape [4], chromosome segregation [5,6], chemotaxis [7], differentiation [8] and virulence [9] are some of the processes that depend on the localization of proteins. Advances in microscopy have allowed experimentalists to visualize the movement of single molecules [10] inside the bacterial cell, while genetic screens have revealed the functional importance of protein localization on cell physiology. What is not as clear is how the micron-sized cells are able to organize their components effectively in space and time.

The appearance of specific proteins at one or both poles of rod-shaped bacterial cells during their progression through the cell division cycle has prompted a number of proposals to explain these patterns [11]. For instance, polar bias may be attributable to the effects of membrane curvature at the poles of rod-shaped bacterial cells [12–15], but localized zones of protein accumulation have also been observed at periodic intervals along the axis of straight filamentous cells which lack curvature cues. Another explanation assumes that landmark proteins or scaffolds are present exclusively at the poles, and proteins that reach the poles (either by random diffusion or some targeting mechanism) are ensnared by these scaffolds and thereby fixed at the poles [16]. While such protein-protein interactions have often been observed, there remains the question of what prompted the landmark protein to reside at the poles in the first place. To add to the puzzle, the location of landmark proteins may change during the course of the cell cycle, indicating that such proteins can auto-regulate their localization. Hence, an understanding of the mechanisms that drive the spatial and temporal dynamics of landmark proteins is central to understanding certain fundamental properties of cell organization and morphology in bacteria.

5.2.1 Physiology of protein localization in the *Caulobacter* cell cycle

In *Caulobacter crescentus*, a model organism for the study of protein localization [17], the polymer PopZ has been identified as a potential landmark protein [18,19]. PopZ localizes to the old pole of newborn cells, and then attains a second zone of polymerization at the new pole in predivisional cells (see **Figure 5.1**). One function of PopZ is to bind with ParB molecules on the *parS*/ParB centromeric complex and act as a scaffold that tethers segregated chromosomes to the two poles of the cell [20]. As the chromosomes segregate to opposite poles of the cell, the cell division protein FtsZ (a tubulin homologue) polymerizes near the midpoint of the cell, at the future site of cell division. FtsZ polymerization at the correct time and place is a consequence of chromosome segregation. The moving chromosome front carries with it MipZ, a protein that promotes depolymerization of FtsZ [21,22]. As the replicated chromosomes segregate to opposite poles of the cell, the maximum concentration of MipZ localizes to the poles. Hence, the maximum concentration of FtsZ is found at the center of the cell, where MipZ concentration is lowest. Interestingly, the FtsZ peak is very sharp, much sharper than the drop off in MipZ would suggest.

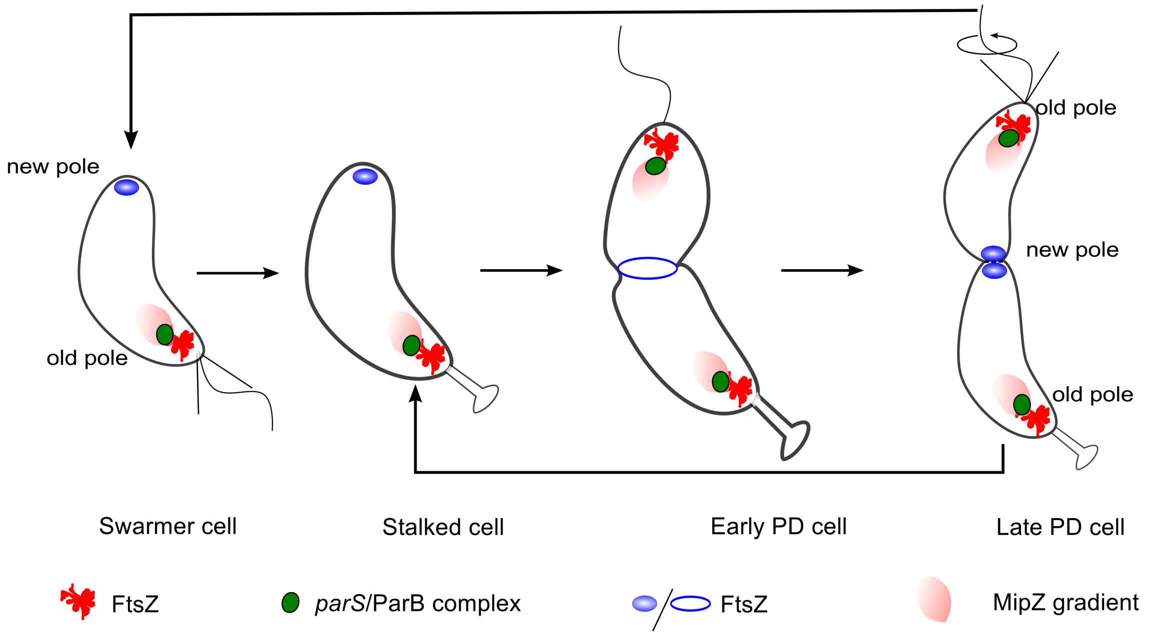

Figure 5.1: Schematic representation of the dynamic localization of poteins during the *Caulobacter crescentus* cell cycle.

PopZ polymer present at the old pole tethers the chromosome by docking the *parS*/ParB centromeric complex. Later in the cell cycle, PopZ polymer appears at the new pole, where it docks the newly replicated *parS/*ParB front. MipZ, which co-localizes with ParB, is a negative regulator of FtsZ polymerization. Hence, FtsZ, which promotes cell division, is always found to localize at the position in the cell that has the lowest concentration of MipZ.

While the dynamic localization of PopZ is clearly observed and its role in the cell cycle understood, the mechanism behind PopZ localization is still being investigated and debated. One hypothesis attributes new-pole localization of PopZ to the action of actin-like MreB filaments, because the MreB-inhibiting drug, A22, blocks polymerization of PopZ at the new pole [19]. Interestingly, MreB filaments lack global polarity [23], and hence should not have a preference for a specific pole. Furthermore, high doses of A22 retard cell growth [24]; whereas lower doses of A22, which inhibit MreB filament formation but do not interfere with cell growth, permit bipolar localization of PopZ [25]

A second hypothesis attributes new-pole localization of PopZ to DNA replication, because treating cells with novobiocin, an inhibitor of DNA gyrase, prevents PopZ polymerization at the new pole [20]. However, novobiocin treatment also retards growth and bipolar localization of PopZ is retained when milder doses of the drug are used [25], suggesting that unipolar localization of PopZ may be a consequence not of blocking DNA replication but of stunted cell growth. On the other hand, unipolar PopZ localization is still observed in cells depleted of DnaA, an initiator of DNA replication, which does not inhibit cell growth [25]. This observation suggests a third hypothesis, that the nucleoid region occludes PopZ polymerization, an idea based as well on the observation that DNA and PopZ localize in mutually exclusive regions [18].

More recently, chromosome translocation has been shown to be essential to the formation of new-pole PopZ [25]. As DNA replication proceeds, one of the replication origins is translocated from the old pole to the new pole, which is correlated with a retraction of ParA protein to the new end of the cell, suggesting to some that ParA is a nucleating factor for PopZ assembly [25].

Any one or a combination of these mechanisms may be responsible for new-pole localization of PopZ; or it may be that none of them play a definitive role in PopZ localization. In this paper we argue that PopZ localization may depend on a Turing-type mechanism [26,27] by comparing the predictions of a mathematical model to well established properties of PopZ patterns. We also propose that the sharp FtsZ band at the site of cell division is a consequence of a Turing-type mechanism of self-activating assembly and focusing. Our final model of the PopZ-MipZ-FtsZ interaction network will be formulated as a set of partial differential equations and solved using the Method of Lines (**Methods**). Simulations of the model reproduce experimentally observed spatiotemporal distributions of these proteins during the cell cycle of wild-type and mutant *Caulobacter* cells.

Unlike previous mathematical models of the *Caulobacter* cell cycle [28–30], which focus on the temporal dynamics of cell cycle regulators, the model described here captures the spatial dynamics of protein distributions as well. To accommodate the evolving hypothesis of a Turing mechanism behind protein localization in *Caulobacter*, our model has undergone several revisions, which we describe in turn, as they provide insights into how each modification contributes to the overall picture of protein localization in wild-type and mutant cells.

5.2.2 Spatiotemporal dynamics of Turing patterns

Turing models are best known for explaining patterns that are periodic in space [26,27], for example, the coat patterns of animals [31]. In bacterial systems, the spatiotemporal dynamics of the MinCD system has been explained using Turing's theory [32]. The theory of Turing patterns [33] predicts that stable, stationary patterns can be generated for a two-species system if two conditions are satisfied: one species must be self-activating and slow diffusing, while the other species must diffuse significantly faster and have an inhibitory effect on the self-activating species. In the Activator-Inhibitor Production (A-IP) version of Turing's mechanism, the initial patch of activator forms by chance, followed by local production of inhibitor molecules, which diffuse rapidly away from the activator patch and inhibit production of activator in the surrounding region [34–36]. At some distance away, the inhibitor concentration is low enough to permit a new zone of activator self-amplified accumulation. An alternative version of the scheme is the Activator-Substrate Depletion (A-SD) mechanism, where a substrate is converted to product by an autocatalytic reaction [35,36]. Local accumulation of the self-activating product depletes surrounding regions of the rapidly diffusing substrate. Only some distance away will substrate concentration be large enough to support a new zone of product accumulation. This critical distance between activator peaks (where inhibitor concentration is low enough or substrate concentration is high enough) is the characteristic wavelength, λ_0, of a Turing pattern **(Figure 5.2)**.

Indicative of a Turing-type pattern, PopZ polymers seem to exhibit a minimum distance between sites of aggregation [18]. Small cells of *Caulobacter* and *Escherichia coli* have only a single PopZ zone, and a second zone of PopZ polymerization appears as cells grow larger. Very long, filamentous forms of *Caulobacter* and *E. coli* have multiple sites of PopZ polymerization, more-or-less evenly spaced [18]. Furthermore, the biochemistry of PopZ polymerization is consistent with an A-SD mechanism of Turing pattern formation. PopZ forms branched polymers [19,37], which imply an autocatalytic growth process: the larger the polymer grows, the more branched arms it accumulates to take up more monomers. Clearly, PopZ polymers would diffuse substantially slower than monomeric PopZ subunits. Based on the specific nature of PopZ polymer formation and the observed pattern of PopZ localization in wild-type and mutant cells of *Caulobacter* and *E. coli*, we pursue the idea that an A-SD mechanism may be responsible for the observed distribution patterns of PopZ polymers.

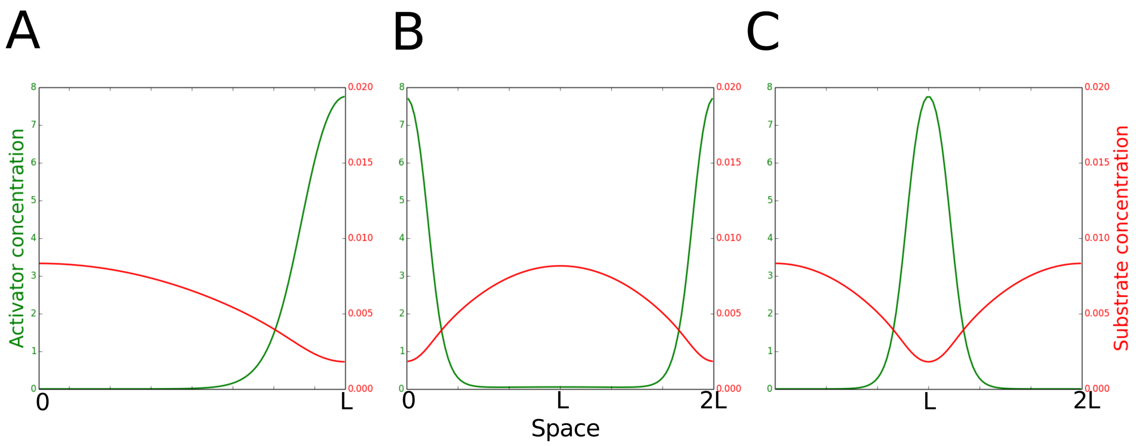

Figure 5.2: Spatial patterns in an A-SD Turing mechanism.

Substrate S is converted into product A by an autocatalytic reaction, and S diffuses more rapidly than A. When the length of the domain is $L \approx \lambda_0/2$, where λ_0 is the "Turing wavelength," a spatial pattern (**A**) arises spontaneously, with a half-peak of activator concentration at one end of the domain and a half-peak of substrate at the other end. When the length of the domain gets close to λ_0, the system may exhibit either a "bipolar" pattern (**B**), with a shallow peak of substrate at the center and half-peaks of activator at the poles, or a "bell-shaped" pattern (**C**), with a peak of activator at the center accompanied by a shallow trough of substrate.

In *Caulobacter*, newborn swarmer cells have a single polar focus of PopZ, while larger stalked and predivisional cells have two foci, one at each pole [18,19]. Hence, the characteristic wavelength of the Turing pattern (if such be the mechanism of PopZ localization) should be smaller than the size of a predivisional cell, but longer than the size of a cell at the swarmer-to-stalked transition. In this view, a swarmer cell should contain one-half of a Turing wave, with a peak of PopZ polymerization at one end (**Figure 5.2 A**), while the larger stalked cells should support a full wave with half-peaks at the poles and a trough mid-cell (**Figure 5.2 B**). However, classical A-SD models of Turing patterns tend to support a full wave that has troughs at the two boundaries and a peak at the center (**Figure 5.2 C**) [36]. In other words, a classical A-SD model would predict a PopZ focus that forms initially at one pole and then moves to the center of the larger stalked cell. To account for the observed bipolar pattern of PopZ polymerization, we propose some modifications to the classical A-SD equations and some constraints on the parameter values. We suggest that our modified A-SD model can serve as a generic template for self-assembly and polar localization of landmark proteins across bacterial species.

5.3 Methods

The proteins under investigation in this work are distributed heterogeneously along the long axis of a *Caulobacter* cell. Hence, it is sufficient to consider biochemical reactions and diffusion occurring in one spatial dimension, and to write the governing partial differential equation (PDE) for a generic chemical species C as:

$$\frac{\partial C}{\partial t} = \text{Reaction terms} + D \cdot \frac{\partial^2 C}{\partial x^2}$$

where $C(x,t)$ is the concentration of species C at location x and time t. The PDEs for our models are provided in **Tables C.1-C.3**. By discretizing the spatial dimension into n = 100 compartments of equal length $h = L/n$, where L is the total length of the *Caulobacter* cell and using a central difference scheme to approximate the Laplacian operator, we convert each PDE into a set of ODEs for C_i = concentration of species C in cell i ($1 \leq i \leq 100$)

$$\frac{d\mathrm{C}_i}{dt} = \text{Reaction terms} + D \cdot \frac{\mathrm{C}_{i+1} - 2\mathrm{C}_i + \mathrm{C}_{i-1}}{h^2}$$

Because *Caulobacter* cells are elongating as a result of new cell wall material being added uniformly along the long axis [38], we assume that each compartment grows exponentially in time:

$$\frac{dh}{dt} = k_{\text{growth}} \cdot h$$

Since molecules cannot diffuse across the cell wall, we implement no-flux boundary conditions at x = 0 and $x = L$ by adding two additional compartments, i = 0 and i = 101, and insisting at every time step that $C_0 = C_1$ and $C_{101} = C_{100}$.

The full set of ODEs were simulated in MATLAB using the ode15s solver. The spatiotemporal distribution plots in the figures were generated using the python library Matplotlib [39].

5.4 Results

5.4.1 Transient polar localization of a nucleating factor may generate bipolar PopZ patterns

One biologically relevant mechanism to ensure bipolar patterns in an A-SD model is to provide a nucleating factor at the poles, which promotes activator assembly there. An example of this case is found in fission yeast, where actin polymers promote polarized growth in the presence of the nucleating factor Tea1, while displaying mid-cell or T-shaped growth in *tea1Δ* mutants [40]. A mathematical model of actin polymerization in fission yeast based on a Turing mechanism reproduced the observed patterns of wild-type and mutant cells [41]. Within that mathematical model, an important distinction was made between autocatalytic polymer formation and *de novo* polymer formation. The differential equation for polymer production can have, in principle, two terms,

$$\frac{\mathrm{d[polymer]}}{\mathrm{d}t} = \cdots + k_{\mathrm{aut}}[\mathrm{monomer}][\mathrm{polymer}]^2 + k_{\mathrm{dnv}}[\mathrm{monomer}] + \ldots,$$

which describe, in order, the autocatalytic and *de novo* production of polymer from monomer. In the fission yeast model, bipolar patterns were generated only if the nucleating factor promoted autocatalytic self-assembly. If the nucleating factor promoted *de novo* polymer production instead, then bell-shaped patterns were retained.

Based on the fission yeast actin-Tea1 model, we formulated a PopZ model in which a nucleating factor promotes autocatalytic PopZ polymer formation (**Table C.1** and **C.4**). In the absence of nucleating factor at the poles, our simulations show a bell-shaped pattern that persists over the entire size range (1.3 to 3 μm) and time frame (150 min) of the *Caulobacter* cell cycle (**Figure 5.3 A, right panel**). When we introduced a nucleating component in five compartments at the extreme left and right ends of the domain, then the desired spatiotemporal pattern of PopZ distribution was obtained (**Figure 5.3 B, right panel**). In the first 80 min of the simulation, a single half-peak of PopZ was present at one pole, while a second half-peak spontaneously arose at the opposite pole at $t = 80$ min. It is important to note that, while the nucleating factor itself is always bipolar (**Figure 5.3 B, left panel**), the second focus of PopZ appears only after a critical cell size is crossed. Hence, the nucleating factor only ensures the correct placement of PopZ at the two poles; the time of appearance of PopZ at the new pole depends on cell growth and the characteristic wavelength of the Turing pattern.

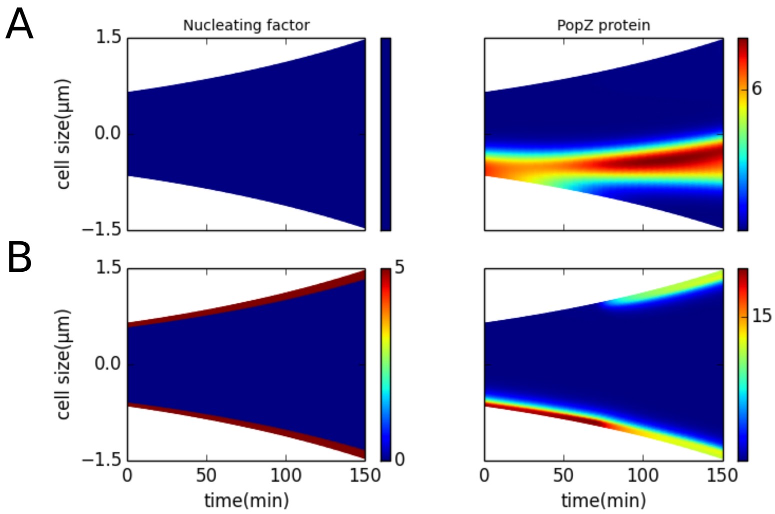

Figure 5.3: Presence of a nucleating factor at the poles can bias PopZ self-assembly at the poles.

Color indicates concentration gradients from minimum (blue) to maximum (red). (A) Nucleating factor is present uniformly across the length of the cell during the cell cycle. (B) Nucleating factor is present in five compartments at each pole during the course of the cell cycle.

At the time we developed this model, there was no evidence of a nucleating factor for PopZ. Even if there were such a nucleating factor, we would be faced with the task of understanding how the nucleating factor itself got to the poles. Recently however, it has been suggested that the partitioning protein ParA is a potential nucleating factor for bipolar localization of PopZ [25]. ParA itself shows dynamic localization during the course of the cell cycle [5,6]. Prior to DNA replication, a gradient of ParA extends across the length of the cell. During chromosome segregation, ParA retracts towards the new pole and binds TipN [5,6], resulting in an increase in concentration of ParA at the new pole. Localization of ParA to the new pole coincides with the appearance of PopZ at this site, indicating that ParA might be directly responsible for PopZ assembly. The new-pole localization of ParA is transient; it is redistributed across the length of the cell as the cell prepares for the next round of DNA replication and cell division.

It is possible that old-pole localization of PopZ is a result of spontaneous aggregation, while new-pole localization is driven by transient localization of ParA at the new pole. However, we considered it more likely that old-pole PopZ is inherited from PopZ localization in the previous cell cycle. Using our modeling framework, we asked if (1) transient polar localization of nucleation factor ParA can support PopZ production at a pole, and (2) the PopZ focus will remain at the pole even after the nucleating factor leaves the pole and redistributes throughout the cytoplasm. To initialize this model, the nucleating factor (ParA) was set to 1 CU (arbitrary concentration unit) in all compartments of a cell of fixed length 1.3 μm. As before, PopZ polymer concentration was biased towards the old pole. In this setting, PopZ polymer accumulated only at the old pole (not shown). The endpoint of this simulation was used as the initial condition for a simulation of PopZ redistribution in a growing cell with transient new-pole localization of ParA. At first, the concentration of ParA in five compartments at the new pole was increased to 5 CU from t = 75 to t = 125 min (**Figure 5.4 A, left panel**). As a result, PopZ polymerized at the new pole, but not until quite late, t = 140 min. Worse yet, the older focus of PopZ began to move to the center of the cell, in a manner typical of A-SD patterns (**Figure 5.4 A, right panel**). It appears that movement of the PopZ focus toward the center of the cell prevented formation of a second PopZ focus at the new pole at the expected time and cell size, and that the cell had to grow larger in order to accommodate two foci.

To prevent movement of old-pole PopZ to the center, we increased the cell size required to hold two foci by decreasing the synthesis rate of PopZ monomer (k_{syn} = 0.075 min^{-1}). With this alteration, polymeric PopZ remained in place at the old pole, and a second PopZ focus appeared at the new pole at t = 125 min (**Figure 5.4 B, right panel**). In order to advance the appearance of PopZ at the new pole (to accord better with observations), we advanced the transient localization of ParA at the new pole to 50–100 min (**Figure 5.4 C, left panel**). However, in this case PopZ did not polymerize at the new pole (**Figure 5.4 C, right panel**), because the cell was not large enough to hold two foci of PopZ at this earlier time interval. Hence, a shorter critical wavelength meant that old-pole PopZ moved to the center of the cell, while a longer critical wavelength meant that new-pole PopZ polymers appeared later than desired. PopZ bipolarity was also sensitive to the duration of ParA localization at the new pole, since new-pole PopZ failed to appear (**Figure 5.4 D, right panel**) when ParA was present there from t = 100 to t = 125 min (**Figure 5.4 D, left panel**).

Based on these results, we conclude that transient new-pole localization of a nucleating factor is sufficient to generate a bipolar PopZ pattern; however, new-pole localization of PopZ is sensitive to both the timing and the duration of localization of the nucleating factor at the new pole.

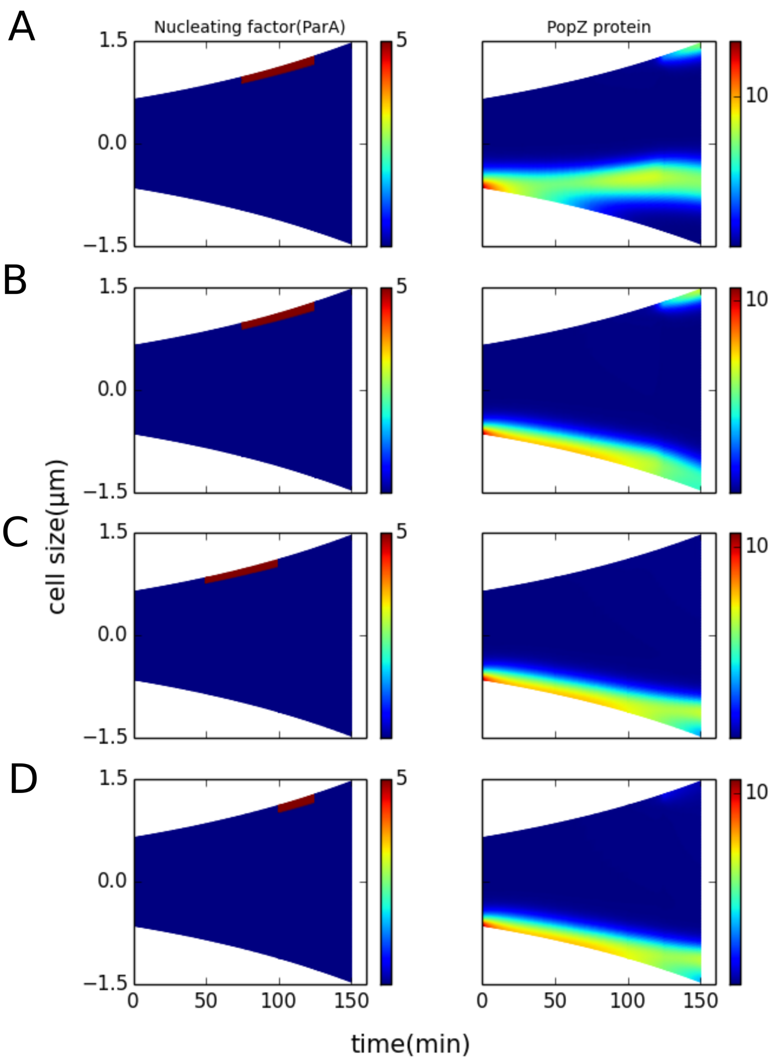

Figure 5.4**:** Bipolar localization of PopZ is sensitive to the timing and duration ParA localization at the new pole.

Color indicates concentration gradients from minimum (blue) to maximum (red). ParA is localized in the first five compartments of the new pole for various time intervals: **(A)** t = 75 - 125 min, $k_{syn\text{-}popz}$ = 0.1 min^{-1}; **(B)** t = 75 - 125 min, $k_{syn\text{-}popz}$ = 0.075 min^{-1}; **(C)** t = 50 - 100 min, $k_{syn\text{-}popz}$ = 0.075 min^{-1}; **(D)** t = 100 - 125 min, $k_{syn\text{-}popz}$ = 0.075 min^{-1}.

5.4.2 Bipolar patterns of PopZ can be generated in the absence of nucleating factors

As mentioned earlier, an inherent characteristic of classical A-SD models is that as a cell grows in length, beyond the characteristic wavelength of the Turing pattern, the activator peak migrates from the pole to the center of the cell. As the cell gets longer, the central activator peak splits into two peaks that also avoid the poles of the cell [42]. This pole-avoiding, branching pattern of activator peaks is a consequence of the assumption, in classical A-SD models, that the only source of activator production is the autocatalytic term $k_{\text{aut}} \cdot [\text{monomer}]\cdot[\text{polymer}]^2$. Because monomers are consumed in activator peaks, monomer concentration is low in peaks and in the local region surrounding each peak (see **Figure 5.2 and Figure C.1**). Monomer concentration increases further away from the activator peak. Therefore, as a small swarmer cell grows, the focus of PopZ polymer at the old pole moves away from the pole in the direction of higher PopZ monomer concentration. When the focus reaches the center of the cell, the concentration of PopZ monomer is equal on either side of the polymer focus, resulting in no net movement in either direction. When the cell grows larger, a combination of high PopZ polymer concentration in the peak area and higher PopZ monomer concentration outside of the peak area results in two new polymer peaks arising by splitting of the original peak. The new peaks migrate away from each other in the direction of higher monomer concentrations, all the time staying away from the poles of the cell (**Figure C.1 D**).

Our model differs from the classical Gierer-Meinhardt A-SD model [34–36] in that it contains a *de novo* polymerization term that allows PopZ to polymerize from PopZ monomers without prior existence of polymer. In addition, our equations also include a depolymerization term that allows breakdown of the polymer into monomer units. In the simulations discussed thus far, a nucleation factor was required to position PopZ polymers at the poles. There is no evidence for the constant presence of a nucleating factor in *Caulobacter*, while our simulations showed that transient localization of ParA as a nucleating factor resulted in bipolar PopZ polymerization only when certain strict conditions are met. We therefore investigated the possibility of obtaining bipolar PopZ patterns in the absence of a nucleating factor (**Table C.2**).

Since the autocatalytic term is responsible for pole-avoiding polymerization, we conjectured that an additional *de novo* term of activator production might favor a different pattern. The *de novo* term, which implies that new activator molecules (PopZ polymers) can be produced from substrate (PopZ monomers) in the absence of pre-existing activator molecules, is plausible both biologically and chemically. We proceeded to tune the *de novo* rate constant in our model with the aim of generating spontaneous assembly of PopZ polymer at the new pole (**Table C.4**). For the value of k_{dnv} used in earlier simulations (k_{dnv} = 1 min^{-1}), the PopZ peak moved to the center of the predivisional cell (**Figure 5.5 A, left panel**). In sharp contrast, when the value of k_{dnv} was increased to 12 min^{-1}, the PopZ focus was retained at the old pole during the course of the simulation, and second half-peak emerged spontaneously at the new pole at t = 100 min and remained there until the end of the cell cycle, at t = 150 min (**Figure 5. 5 A, right panel**). Hence, a sufficiently large value of the *de novo* polymerization rate can account for a bipolar PopZ pattern, even in the absence of a nucleating factor.

When the simulation was run for longer time, corresponding to a non-dividing, filamentous cell (**Figure 5.5 B)**, additional activator peaks emerged as cell length crossed multiples of the critical wavelength. For the low rate of *de novo* polymerization **(Figure 5.5 B, left panel)**, the new peaks formed by splitting of old peaks; whereas for the high rate of *de novo* polymerization (**Figure 5.5 B, right panel)**, the new peaks formed spontaneously at locations where no previous activator was present. Importantly, the PopZ foci in the elongated cell appear evenly spaced, reminiscent of multiple PopZ foci observed in filamentous *E. coli* and *Caulobacter* cells.

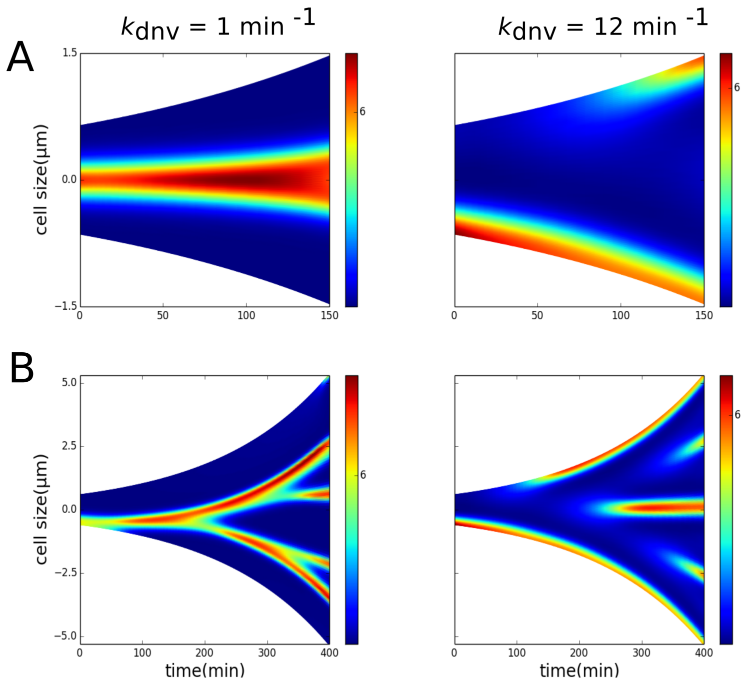

Figure 5.5: Unipolar to bipolar transitions in PopZ localization can be realized in the absence of nucleating factors.

Color indicates concentration gradients from minimum (blue) to maximum (red). (A) One division cycle (150 min). Left panel: k_{dnv} = 1 min^{-1}; a single PopZ focus forms at the center of the cell. Right panel: k_{dnv} = 12 min^{-1}; a PopZ focus forms at the old end of the cell, and a second focus forms at the new end at t = 100 min. (B) A non-dividing (filamentous) cell. Left panel: k_{dnv} = 1 min^{-1}; PopZ polymers undergo splitting to form a branched pattern as the cell grows. Right panel: k_{dnv} = 12 min^{-1}; new PopZ foci arise *de novo* as the cell grows.

The distribution of multiple foci of PopZ polymers in filamentous cells has been attributed to a tendency of PopZ to self-assemble in chromosome- and ribosome-free regions [20], and a mathematical model based on this notion successfully recreated the observed distribution patterns [43,44]. However, in Δ*popZ* mutants, ribosomes extrude into the space otherwise occupied by PopZ [20], while the *parS*/ParB front is pushed further into the cytoplasm when PopZ is overexpressed [18]. These experiments suggest to us that it is PopZ that exerts an influence on chromosome and ribosome organization, rather than *vice versa*.

Although our model does not distinguish among the various alternative hypotheses, it does show that a modified A-SD Turing model can generate observed PopZ patterns independent of membrane curvature, nucleating factors or chromosome-driven exclusion.

5.4.3 Localization of slow diffusing *popZ* mRNA suggests that bipolarity requires the presence of two *popZ* genes

Although our deterministic model of PopZ localization gives promising results, we must consider the effects of random molecular fluctuations on PopZ reactions and diffusion. A prominent source of noise in gene expression is fluctuations in the number of mRNA transcripts in a cell [45]. On average, only a small number of mRNA copies of a gene are present in a bacterial cell at any given time [46]. Each mRNA transcript is used as template to synthesize hundreds of proteins. Hence, small variations in mRNA number are translated into large fluctuations at the protein level. A stochastic model, therefore, must include *popZ* mRNA as an additional diffusing species. The deterministic models of PopZ localization described thus far assume uniform production of PopZ proteins throughout the cell cytoplasm. In reality, however, *popZ* mRNA is transcribed at one or two locations in the cell cytoplasm, depending on the number and location of *popZ* genes at the current stage of the cell cycle.

To recreate this scenario, we allowed mRNA to be produced from a single randomly chosen compartment of our domain. If we assume a liberal diffusion coefficient for mRNA (D_{mRNA} = 100 μm^2 min^{-1}), the resultant patterns are in agreement with PopZ polymer localization observed in experiments and in our deterministic simulations. However, mRNA diffusion may be orders of magnitudes slower than previously believed; a study of dispersion of *Caulobacter* mRNA species places the apparent diffusion coefficients in the range 0.01–0.05 μm^2 min^{-1} [47]. In this case, mRNA molecules are unable to move far from their site of production within the timeframe (tens of minutes) of cell cycle events. If we set D_{mRNA} = 0.05 μm^2 min^{-1} and allow mRNA to be produced only from a single compartment, then we obtain only a single peak of PopZ polymer close to the region of mRNA production (**Figure 5.6**). Because of the high rate of autocatalytic polymerization, PopZ monomers (in spite of their large diffusion constant) are unable to move far from their site of production before they are incorporated into slow moving PopZ polymers. Other regions of the bacterial cytoplasm can neither produce their own monomers nor obtain a sufficient supply of monomers from the single site of monomer production. Hence, PopZ polymer is formed only at the location of the *popZ* gene.

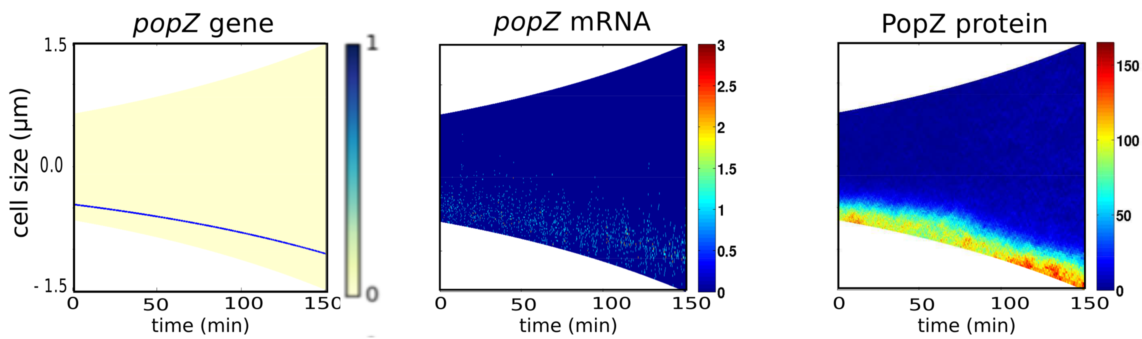

Figure 5.6 Stochastic simulations show that limited dispersal of mRNA produced from a single gene results in unipolar PopZ patterns.

One *popZ* gene is present throughout the cell cycle at a distance of $0.2 \cdot L(t)$ from the old pole producing mRNA with a diffusion coefficient of 0.05 μm^2 min^{-1}. For *popZ* gene, color indicates presence (blue) or absence (yellow) of the gene. For *popZ* mRNA and PopZ protein, color indicates concentration gradients from minimum (blue) to maximum (red).

If the dispersion of mRNA in *Caulobacter* is as limited as suggested, how do PopZ polymers attain bipolar localization in predivisional cells and multiple foci observed in filamentous cells? It has been shown that stalling DNA replication results in unipolar PopZ localization [20]. This observation, although now disputed [25], suggests to us that two *popZ* genes in different locations may be required for two foci of PopZ to form. In the swarmer cell stage, a single copy of *popZ* gene is associated with unipolar localization of PopZ at the old pole. After the *popZ* gene is replicated, the second copy segregates to the opposite pole; we propose that upon arrival, the new *popZ* gene drives production of PopZ monomers that self-assemble into polymers at the new pole. We tested our hypothesis first with a deterministic model (**Table C.3 and S5**) that contained *popZ* genes and mRNA as additional variables. In the first case, we placed *popZ* genes in the extreme end compartments of our discretized domain (**Figure 5.7 A, panel 1**), where they produced slowly diffusing *popZ* mRNA molecules

(D_{mRNA} = 0.05 μm^2 min^{-1}) at a rate k_{syn_popZ} = 1.25 min^{-1} (larger than before, in order to maintain a comparable amount of PopZ protein in the cell). On simulating this system, we found that mRNA is produced at both poles, but PopZ protein exhibited the correct distribution (first monopolar and later bipolar) (**Figure 5.7 A, panels 2 and 3**). This simulation suggests that, while a new pole-proximal gene may be essential for the localization of the second PopZ focus at the new pole, the timing of the new focus is determined by a Turing instability.

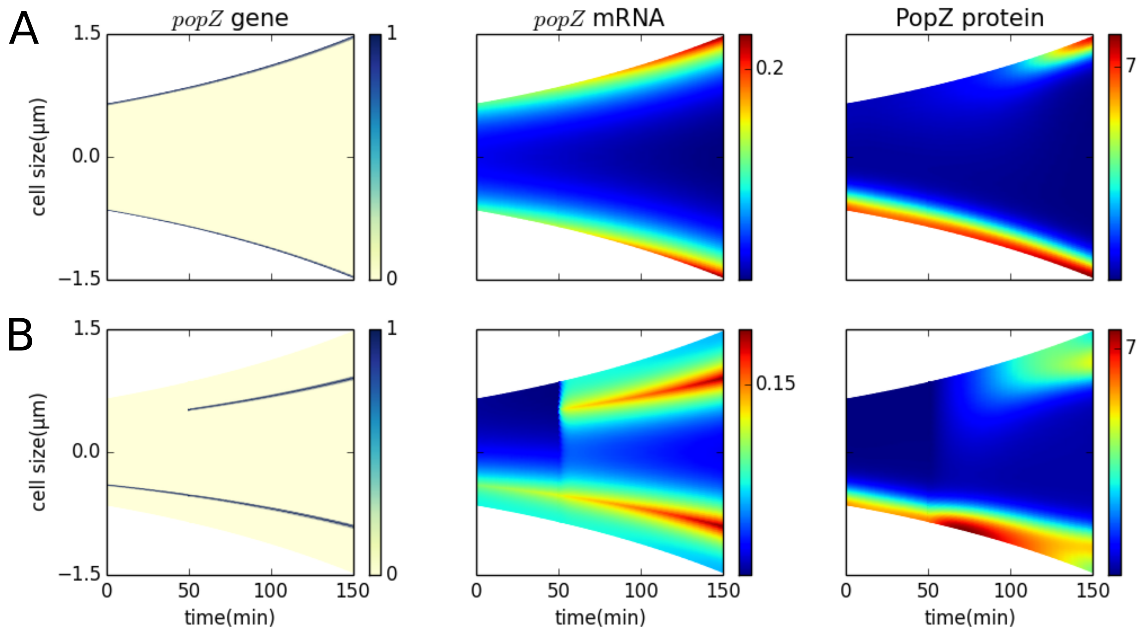

Figure 5.7 Limited dispersal of *popZ* mRNA warrants the need for two *popZ* genes to obtain bipolar PopZ localization.

For *popZ* gene, color indicates presence (blue) or absence (yellow) of the gene. For *popZ* mRNA and PopZ protein, color indicates concentration gradients from minimum (blue) to maximum (red). (A) *popZ* genes are located in the extreme end compartments throughout the cell cycle; k_{syn} = 1 min^{-1}. (B) One *popZ* gene is present throughout the cell cycle at a distance of $0.2 \cdot L(t)$ from the old pole while the other gene appears at t = 50 min at a distance of $0.2 \cdot L(t)$ from the new pole; k_{syn} = 1.5 min^{-1}.

Although this simulation recreates the observed pattern of PopZ polymerization, the number and position of the *popZ* genes is not correct: the number of *popZ* genes changes from one to two at the swarmer-to-stalked cell transition, and the *popZ* genes should be positioned further into the cytoplasm (not at the extreme ends). In **Figure 5.7 B (panel 1)** we assume that, early in the cell cycle, a single *popZ* gene occupied one compartment near the old end of the domain, and later in the cell cycle (t = 50 min) a second copy of the *popZ* gene appeared in a second compartment near the new end of the domain. In this case as well, PopZ shows the correct bipolar distribution in space and time (**Figure 5.7 B, panel 3**).

What limits on the spatial location of the *popZ* genes are consistent with a bipolar pattern of PopZ polymerization? We address this question in the Supplementary Material (**Figure C.2**). In summary of these results, we find that, if the two *popZ* genes (of a stalked cell) are located close to the center of the cell, then a single PopZ focus appears at the center; but if the two genes are located close to the poles (within ~0.2 L from either end of a cell of length L), then the bipolar pattern is established. If the locations of the genes from the poles are shifted further inward, then the zones of PopZ polymerization also shift further inward, away from the poles (**Figure C.3**). Bipolarity is not a result of increased concentration of PopZ associated with the increase in gene copy number, as demonstrated in **Figure C.4**, where PopZ monomers were expressed from a single overexpressing *popZ* gene. In this case, the PopZ polymer distribution increased in magnitude but remained unipolar. This simulation result is consistent with experiments showing that increased expression of PopZ affects the size of the PopZ foci [18] but not their number [20].

Cells show variability in the time required to completely segregate the replicated genome, and this variability is reflected in the time and cell length at which PopZ becomes bipolar [25]. To determine the effects of erratic translocation of the newly replicated *popZ* gene, we developed the following stochastic model (**Figure 5.8**). The old-pole proximal gene was fixed in place, while a second gene, introduced at t = 50 min, was allowed to translocate. Advection and diffusion terms in the translocation process resulted in a biased random walk of the new gene towards the new pole of the cell (**Figure 5.8 A, panel 1**). *popZ* mRNA is being produced at a constant probability per unit time, for the entire time the genes are in existence; hence, *popZ* mRNA is distributed in a pattern that mimics the locations of the genes (**Figure 5.8 A, panel 2**). Nonetheless, PopZ polymerizes only at the cell poles (**Figure 5.8 A, panel 3**). On average, the second *popZ* gene arrives at the new pole at t = 63 min, and PopZ becomes bipolar at t = 92 min, which corresponds to a cell length of 2.5 μm (**Figure 5.8 B**). (We considered PopZ to be bipolar when at least 20% of the total PopZ molecules were present in the new pole-proximal 20 compartments.) Although experiments, using MipZ as a proxy for the chromosome front, show that completion of segregation is concurrent with new-pole localization of PopZ, our simulations show a delay of ~30 min. In our simulations, PopZ polymers begin to accumulate at the new pole immediately after gene translocation, and the delay is due to the threshold we assume for scoring PopZ polymerization at the new pole.

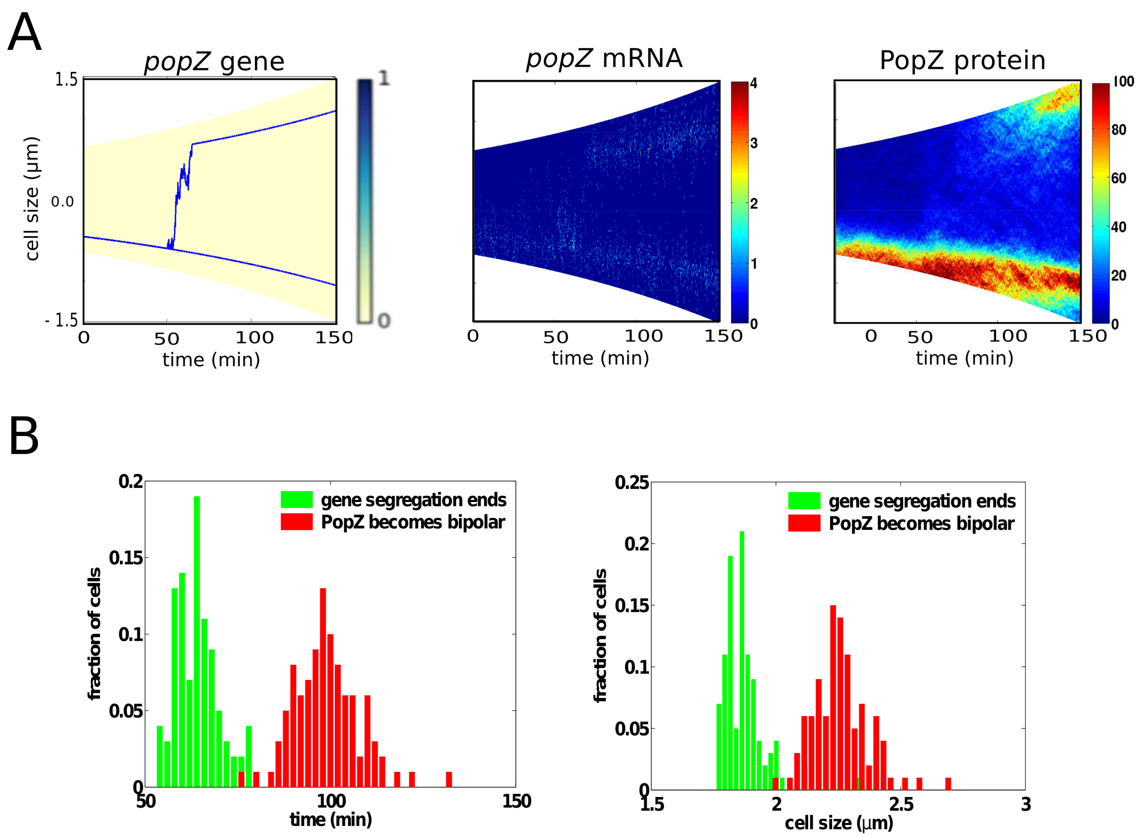

Figure 5.8: Stochastic simulation of the two-gene model.

(A) One *popZ* gene (red) is constantly present at a distance of $0.2 \cdot L(t)$ from the old pole, while a second popZ gene (blue) is introduced at $t = 50$ min. The second *popZ* gene is translocated across the cell until it reaches a distance of $0.2 \cdot L(t)$ from the new pole. *popZ* mRNA ($D_{\mathrm{mRNA}} = 0.05$ μm^2 min^{-1}) is produced by both genes. PopZ polymer shows a unipolar-to-bipolar transition at $t = 92$ min. For *popZ* gene, color indicates presence (blue) or absence (yellow) of the gene. For *popZ* mRNA and PopZ protein, color indicates concentration gradients from minimum (blue) to maximum (red). (B) Distribution of the time (left panel) and cell size (right panel) at which *popZ* gene segregation is completed (green bars) and PopZ becomes bipolar (red bars).

5.4.4 The two-gene model of PopZ localization recreates distribution patterns observed in mutant cells

Our two-gene model of PopZ localization is based on experiments showing that bipolar PopZ localization is lost when DNA replication is blocked, for example, by depletion of the DNA replication initiator, DnaA [20,25], or by treating cells with the DNA gyrase inhibitor, novobiocin [20]. It should be noted that an increasing fraction of cells retained bipolarity when treated with less toxic levels of novobiocin [25]. In addition, Laloux and Jacobs-Wagner [25] observed bipolar PopZ in cells where a single unreplicated chromosome was translocated from the old to the new pole.

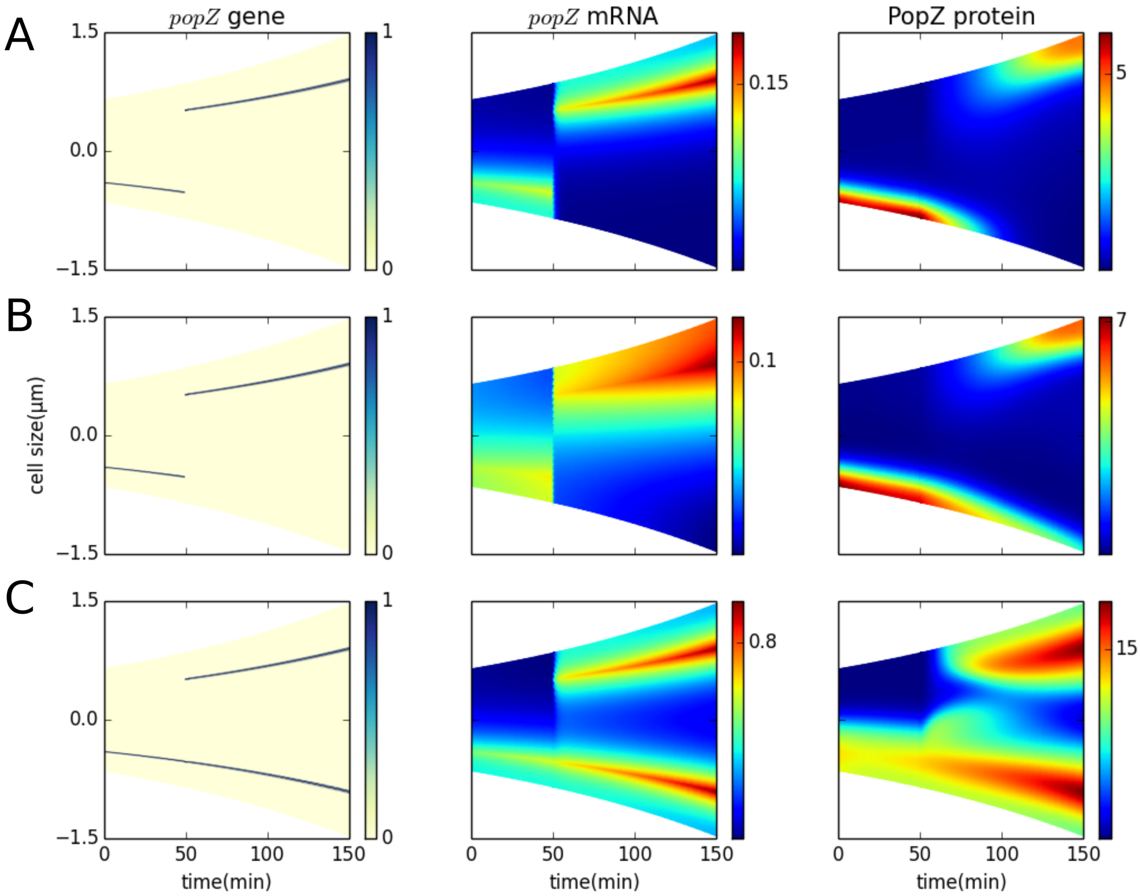

Figure 5.9**:** The two-gene model can also account for observed PopZ distribution patterns in mutant cells.

For *popZ* gene, color indicates presence (blue) or absence (yellow) of the gene. For *popZ* mRNA and PopZ protein, color indicates concentration gradients from minimum (blue) to maximum (red). (A) Shifting the position of a single *popZ* gene from the old pole to the new pole results in a corresponding shift in the polar localization of PopZ polymer ($k_{syn\text{-}mRNA} = 2$ min^{-1}, $D_{mRNA} = 0.05$ μm^2 min^{-1}). (B) Transient bipolar localization of PopZ is observed under mild-overproduction ($k_{syn\text{-}mRNA} = 3$ min^{-1}) and faster diffusion of mRNA ($D_{mRNA} = 0.5$ μm^2 min^{-1}). (C) Overexpression ($k_{syn\text{-}mRNA} = 10$ min^{-1}) results in PopZ polymerizing further into the cytoplasm.

Using our mathematical model, we investigated whether a shift in the position of the *popZ* gene could result in bipolar PopZ polymerization. Our first simulations showed that switching the position of the *popZ* gene simply shifted the PopZ peak from the old pole to the new pole (**Figure 5.9A**). Transient bipolar localization could be achieved (**Figure 5.9 B**) by mildly overproducing the mRNA and assuming that it diffused 10-fold faster (D_{mRNA} = 0.5 $\mu m^2\, min^{-1}$). (This mRNA diffusion constant is still small in absolute terms.)

Elongated *Caulobacter* cells show multiple PopZ foci that are fairly evenly distributed in the cell cytoplasm, which we observed in a version of the model without mRNA or genes (**Figure 5.3 B**). To reproduce this distribution in the model with genes and mRNA, we model the scenario where the filamentous *Caulobacter* cell possesses multiple copies of the chromosome. Simulating this case, we find that PopZ polymerizes at multiple foci if multiple copies of the *popZ* gene are present (**Figure C.5**).

Finally we simulated the distribution pattern when PopZ is overexpressed (**Figure 5.9 C**). As observed in experiments, PopZ overproduction leads to an extension of the scaffold into the cytoplasm [18]. However, our model does not account for (or explain) the filamentation that results from PopZ overproduction.

5.4.5 A Turing pattern may also account for the dynamic localization of division protein FtsZ

The FtsZ ring is a polymer assembled from tubulin-like subunits. While a single but shifting focus of FtsZ is present in wild-type cells of *Caulobacter*, multiple foci of FtsZ form in filamentous cells devoid of MipZ regulator. The number of foci increases with increasing length of the cell [21], characteristic of a Turing pattern. We speculated that FtsZ also shows a mechanism of self- assembly governed by a Turing pattern, with the added fact that MipZ influences FtsZ depolymerization. The ParB-embedded chromosome front binds to and translocates MipZ. Since the chromosome front ultimately docks with PopZ, the MipZ distribution pattern resembles that of PopZ. Our model does not include a moving chromosome front as a variable. Hence, we made the simplifying assumption that MipZ binds to PopZ directly and co-localized with it. We contend that this simplification, although untrue, is acceptable since our purpose is not to understand MipZ dynamics but to probe its downstream effects on FtsZ. The equations governing FtsZ and MipZ dynamics are defined in **Table C.3, Eq. (4-7**), with parameter values given in **Table C.5**. Upon simulating the system, we observed that, in a small swarmer cell, MipZ colocalized with PopZ at the old pole while FtsZ self-assembles at the new pole with no intervention/bias introduced on our part. When the cell grows and forms bipolar MipZ foci FtsZ rapidly shifts to the mid-cell (**Figure 5.10 A**), the point of lowest MipZ concentration. Lack of MipZ in filamentous cells results in multiple foci of FtsZ (**Figure 5.10B**), as observed. As the cell gets longer, the number of FtsZ foci increases, but they are rarely seen at the poles. This pattern is reminiscent of the classical A-SD Turing pattern, and is reflected in our simulations as well. Because our Turing-type model of FtsZ localization recreates the FtsZ distributions observed in wild-type and mutant cells, we contend that Turing's mechanism is biologically relevant and a plausible explanation of FtsZ dynamics in *Caulobacter*.

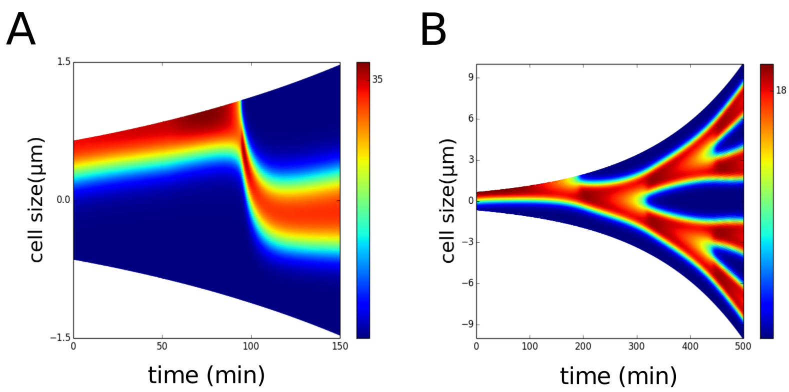

Figure 5.10: Turing mechanism may also explain dynamic FtsZ localization during the cell cycle.

Colors indicate concentration gradients from minimum (blue) to maximum (red). Spatiotemporal distribution of FtsZ polymer in (A) wild type cell and (B) Δ*mipZ* mutant cell, growing without division to become filamentous.

5.5 Discussion

The asymmetric division cycle of the free-living aquatic bacterium, *Caulobacter crescentus*, is driven in large part by the time-dependent, asymmetric accumulation of proteins at the morphologically distinct poles of the cell (the "old" pole carries the stalk, and the "new" pole is the site of flagellum biosynthesis in the predivisional cell). The polymeric protein PopZ is a potential landmark protein, which accumulates first at the old pole and later at the new pole, where it binds distinct sets of proteins that determine the fate of each pole. PopZ also tethers chromosomes to the poles by binding to their centromeric regions.

Exactly how PopZ localizes in the cell is a subject of ongoing debate. Correct spatial and temporal localization of PopZ in *Caulobacter* has been attributed to many cellular processes, such as DNA replication, chromosomal segregation, chromosome occlusion, and ParA-dependent nucleation. Although chromosome occlusion is a particularly plausible explanation of PopZ localization, it is equally likely that PopZ is organizing the chromosomes in the cell as *vice versa*. In the absence of a clear distinction between cause and effect, we have chosen to study the elegant and appealing notion that PopZ drives its own spatiotemporal distribution by a process of self-assembly. We propose that a mathematical model of PopZ self-assembly can be useful for investigating the potential roles of each regulatory process within the framework of a single mechanism of PopZ self-assembly. In this article, we show that an Activator-Substrate Depletion (A-SD) type of Turing mechanism can generate the unipolar-to-bipolar PopZ patterns observed during the course of the *Caulobacter* cell cycle.

Turing patterns are stable, spatially periodic distributions of chemical species, exhibiting a characteristic wavelength, λ_0. Consequently, the number of foci of a Turing 'activator' increases as a cell grows through integral multiples of λ_0. Given the observed distribution pattern of PopZ in swarmer, stalked and filamentous cells, Turing's mechanism emerges as a natural choice to explain PopZ localization. Although an A-SD type Turing mechanism readily describes the biochemical properties of PopZ self-assembly, the classical A-SD model does not predict the formation of PopZ foci at the poles, unless a nucleating factor is provided at the poles. In this paper, we formulate a modified A-SD model that robustly generates polar PopZ foci in the absence of a pre-patterned nucleating factor and that is consistent with the phenotypes of PopZ polymerization in a variety of mutant *Caulobacter* cells. The model is generic and can serve as a template for polar distributions of polymers or scaffolds in any organism.

Unlike earlier models of Turing-type pattern formation, our model takes into account the crucial role played by chromosome replication and segregation in *Caulobacter* cells and the slow rate of diffusion of mRNA molecules. If *popZ* mRNA is synthesized in only a single compartment of the spatial domain, then PopZ protein polymerizes only at the site of mRNA synthesis; i.e., bipolarity is lost. We therefore propose that bipolarity requires the presence of two *popZ* genes in opposite halves of the predivisional cell, an assumption that is consistent with the observed dependence of bipolarity on DNA replication and chromosome segregation. Multiple foci of PopZ in filamentous cells would depend, consequently, on multiple chromosomes distributed along the cell.

In our model, the location of foci of PopZ polymer is highly dependent on the spatial location of *popZ* genes, as a result of limited mRNA dispersal. This effect may allow *Caulobacter* cells to tune the timing of new-pole PopZ polymerization to the completion of chromosome segregation. A caveat of our two-gene model is that proper localization of PopZ in a predivisional cell requires that the *popZ* genes be located within a certain restricted distance (~20%) of the poles.

Our model does not take into account chromosome occlusion, nor does its one-dimensional domain allow a study of the effects of membrane curvature. It is possible that PopZ localization is a result of a combination of many such factors. Nonetheless, we have presented adequate theoretical evidence that an activator-substrate depletion model of Turing patterns must be given serious consideration in future investigations and discussions of the spatiotemporal distribution of PopZ in *Caulobacter* cells.

5.6 References

1. Bardy SL, Maddock JR (2007) Polar explorations. Recent insights into the polarity of bacterial proteins. Curr Opin Microbiol 10: 617–623.

2. Werner JN, Chen EY, Guberman JM, Zippilli AR, Irgon JJ, et al. (2009) Quantitative genome-scale analysis of protein localization in an asymmetric bacterium. Proc Natl Acad Sci U S A 106: 7858–7863.

3. Collier J, Shapiro L (2007) Spatial complexity and control of a bacterial cell cycle. Curr Opin Biotechnol 18: 333–340.

4. Charbon G, Cabeen MT, Jacobs-Wagner C (2009) Bacterial intermediate filaments: in vivo assembly, organization, and dynamics of crescentin. Genes Dev 23: 1131–1144.

5. Ptacin JL, Lee SF, Garner EC, Toro E, Eckart M, et al. (2010) A spindle-like apparatus guides bacterial chromosome segregation. Nat Cell Biol 12: 791–798. Available: http://www.ncbi.nlm.nih.gov/pubmed/20657594.

6. Schofield WB, Lim HC, Jacobs-Wagner C (2010) Cell cycle coordination and regulation of bacterial chromosome segregation dynamics by polarly localized proteins. Eur Mol Biol Organ J 29: 3068–3081. Available: http://www.ncbi.nlm.nih.gov/pubmed/20802464.

7. Wadhams GH, Armitage JP (2004) Making sense of it all: bacterial chemotaxis. Nat Rev Mol Cell Biol 5: 1024–1037. doi:10.1038/nrm1524.

8. Kobayashi H, De Nisco NJ, Chien P, Simmons LA, Walker GC (2009) Sinorhizobium meliloti CpdR1 is critical for co-ordinating cell cycle progression and the symbiotic chronic infection. Mol Microbiol 73: 586–600.

9. Shapiro L, McAdams HH, Losick R (2002) Generating and exploiting polarity in bacteria. Science 298: 1942–1946. doi:10.1126/science.1072163.

10. Gahlmann A, Moerner WE (2013) Exploring bacterial cell biology with single-molecule tracking and super-resolution imaging. Nat Rev Microbiol 12: 9–22. Available: http://www.ncbi.nlm.nih.gov/pubmed/24336182.

11. Laloux G, Jacobs-Wagner C (2014) How do bacteria localize proteins to the cell pole? J Cell Sci 127: 11–19. Available: http://www.ncbi.nlm.nih.gov/pubmed/24345373.

12. Bowman GR, Lyuksyutova AI, Shapiro L (2011) Bacterial polarity. Curr Opin Cell Biol 23: 71–77.

13. Huang KC, Mukhopadhyay R, Wingreen NS (2006) A curvature-mediated mechanism for localization of lipids to bacterial poles. PLoS Comput Biol 2: 1357–1364.

14. Ramamurthi KS, Losick R (2009) Negative membrane curvature as a cue for subcellular localization of a bacterial protein. Proc Natl Acad Sci U S A 106: 13541–13545.

15. Howard M (2004) A mechanism for polar protein localization in bacteria. J Mol Biol 335: 655–663.

16. Rudner DZ, Losick R (2010) Protein subcellular localization in bacteria. Cold Spring Harb Perspect Biol 2: a000307. doi:10.1101/cshperspect.a000307.

17. Goley ED, Iniesta AA, Shapiro L (2007) Cell cycle regulation in *Caulobacter*: location, location, location. J Cell Sci 120: 3501–3507. doi:10.1242/jcs.005967.

18. Ebersbach G, Briegel A, Jensen GJ, Jacobs-Wagner C (2008) A self-associating protein critical for chromosome attachment, division, and polar organization in *Caulobacter*. Cell 134: 956–968. Available: http://www.pubmedcentral.nih.gov/articlerender.fcgi?artid=2614312&tool=pmcentrez&rendertype=abstract.

19. Bowman GR, Comolli LR, Zhu J, Eckart M, Koenig M, et al. (2008) A polymeric protein anchors the chromosomal origin/ParB complex at a bacterial cell pole. Cell 134: 945–955. Available: http://www.ncbi.nlm.nih.gov/pubmed/18805088.

20. Bowman GR, Comolli LR, Gaietta GM, Fero M, Hong S-H, et al. (2010) *Caulobacter* PopZ forms a polar subdomain dictating sequential changes in pole composition and function. Mol Microbiol 76: 173–189. Available:

http://www.pubmedcentral.nih.gov/articlerender.fcgi?artid=2935252&tool=pmcentrez&rendertype=abstract.

21. Thanbichler M, Shapiro L (2006) MipZ, a spatial regulator coordinating chromosome segregation with cell division in *Caulobacter*. Cell 126: 147–162. Available: http://www.ncbi.nlm.nih.gov/pubmed/16839883.

22. Kiekebusch D, Michie KA, Essen LO, Löwe J, Thanbichler M (2012) Localized Dimerization and Nucleoid Binding Drive Gradient Formation by the Bacterial Cell Division Inhibitor MipZ. Mol Cell 46: 245–259.

23. Kim SY, Gitai Z, Kinkhabwala A, Shapiro L, Moerner WE (2006) Single molecules of the bacterial actin MreB undergo directed treadmilling motion in *Caulobacter crescentus*. Proc Natl Acad Sci U S A 103: 10929–10934.

24. Sliusarenko O, Heinritz J, Emonet T, Jacobs-Wagner C (2011) High-throughput, subpixel precision analysis of bacterial morphogenesis and intracellular spatio-temporal dynamics. Mol Microbiol 80: 612–627.

25. Laloux G, Jacobs-Wagner C (2013) Spatiotemporal control of PopZ localization through cell cycle-coupled multimerization. J Cell Biol 201: 827–841. Available: http://www.mendeley.com/research/spatiotemporal-control-popz-localization-through-cell-cyclecoupled-multimerization/. Accessed 17 October 2013.

26. Turing AM (1952) The Chemical Basis of Morphogenesis. Philos Trans R Soc B Biol Sci 237: 37–72. doi:10.1098/rstb.1952.0012.

27. Kondo S, Miura T (2010) Reaction-diffusion model as a framework for understanding biological pattern formation. Science 329: 1616–1620. doi:10.1126/science.1179047.

28. Li S, Brazhnik P, Sobral B, Tyson JJ (2008) A Quantitative Study of the Division Cycle of *Caulobacter crescentus* Stalked Cells. PLoS Comput Biol 4: 19. Available: http://www.pubmedcentral.nih.gov/articlerender.fcgi?artid=2217572&tool=pmcentrez&rendertype=abstract.

29. Li S, Brazhnik P, Sobral B, Tyson JJ (2009) Temporal Controls of the Asymmetric Cell Division Cycle in *Caulobacter crescentus*. PLoS Comput Biol 5: 15. Available: http://www.ncbi.nlm.nih.gov/pubmed/19680425.

30. Subramanian K, Paul M., Tyson J. (2012) Bistable Histidine Kinase Switches in *Caulobacter crescentus*.

31. Murray JD (1988) How the Leopard Gets its Spots. Sci Am 258: 80–87. doi:10.1038/scientificamerican0388-80.

32. Meinhardt H, de Boer PA (2001) Pattern formation in Escherichia coli: a model for the pole-to-pole oscillations of Min proteins and the localization of the division site. Proc Natl Acad Sci U S A 98: 14202–14207.

33. Segel LA, Jackson JL (1972) Dissipative structure: an explanation and an ecological example. J Theor Biol 37: 545–559. Available: http://www.ncbi.nlm.nih.gov/pubmed/4645361.

34. Gierer A, Meinhardt H (1972) A theory of biological pattern formation. Kybernetik 12: 30–39. doi:10.1007/BF00289234.

35. Meinhardt H, Gierer A (2000) Pattern formation by local self-activation and lateral inhibition. Bioessays 22: 753–760. doi:10.1002/1521-1878(200008)22:8<753::AID-BIES9>3.0.CO;2-Z.

36. Meinhardt H (1982) Models of biological pattern formation. Research Gate. pp. 1–10. doi:10.1016/S0070-2153(07)81001-5.

37. Bowman GR, Perez AM, Ptacin JL, Ighodaro E, Folta-Stogniew E, et al. (2013) Oligomerization and higher-order assembly contribute to sub-cellular localization of a bacterial scaffold. Mol Microbiol 90: 776–795. Available: http://www.ncbi.nlm.nih.gov/pubmed/24102805.

38. Aaron M, Charbon G, Lam H, Schwarz H, Vollmer W, et al. (2007) The tubulin homologue FtsZ contributes to cell elongation by guiding cell wall precursor synthesis in *Caulobacter crescentus*. Mol Microbiol 64: 938–952. doi:10.1111/j.1365-2958.2007.05720.x.

39. Hunter JD (2007) Matplotlib: A 2D Graphics Environment. Comput Sci Eng 9: 90–95. Available: http://ieeexplore.ieee.org/lpdocs/epic03/wrapper.htm?arnumber=4160265.

40. Mata J, Nurse P (1997) tea1 and the microtubular cytoskeleton are important for generating global spatial order within the fission yeast cell. Cell 89: 939–949. doi:10.1016/S0092-8674(00)80279-2.

41. Csikász-Nagy A, Gyorffy B, Alt W, Tyson JJ, Novák B (2008) Spatial controls for growth zone formation during the fission yeast cell cycle. Yeast 25: 59–69. Available: http://www.ncbi.nlm.nih.gov/entrez/query.fcgi?cmd=Retrieve&db=PubMed&dopt=Citation&list_uids=17957823.

42. Crampin EJ, Hackborn WW, Maini PK (2002) Pattern formation in reaction-diffusion models with nonuniform domain growth. Bull Math Biol 64: 747–769.

43. Saberi S, Emberly E (2010) Chromosome Driven Spatial Patterning of Proteins in Bacteria. PLoS Comput Biol 6: 10. Available: http://www.ncbi.nlm.nih.gov/pubmed/21085680.

44. Saberi S, Emberly E (2013) Non-Equilibrium Polar Localization of Proteins in Bacterial Cells. PLoS One 8.

45. Swain PS, Elowitz MB, Siggia ED (2002) Intrinsic and extrinsic contributions to stochasticity in gene expression. Proc Natl Acad Sci U S A 99: 12795–12800. Available: http://www.pubmedcentral.nih.gov/articlerender.fcgi?artid=130539&tool=pmcentrez&rendertype=abstract.

46. Passalacqua KD, Varadarajan A, Ondov BD, Okou DT, Zwick ME, et al. (2009) Structure and complexity of a bacterial transcriptome. J Bacteriol 191: 3203–3211.

47. Montero Llopis P, Jackson AF, Sliusarenko O, Surovtsev I, Heinritz J, et al. (2010) Spatial organization of the flow of genetic information in bacteria. Nature 466: 77–81.

Chapter 6 Spatiotemporal Model of Chromosome Segregation in *Caulobacter crescentus*

6.1 Abstract

In the bacterium *Caulobacter crescentus*, the processes of protein localization, differentiation and cell division are dependent on the faithful separation of replicated chromosomes to the two halves of the cell. Chromosome segregation in *Caulobacter* is mediated by the ParABS system in concert with the proteins PopZ and TipN. It is unclear how ParA, PopZ and TipN regulate the speed of translocation. Here we formulate a deterministic reaction-diffusion-advection model that reproduces the variations observed in segregation time and ParA localization patterns among wild-type and mutant cells. Our simulations support the hypothesis that TipN is required for the establishment of an asymmetric gradient of ParA. We find that proper chromosome segregation requires the interaction of PopZ with only the dimeric form of ParA but not with ParA monomers. Based on our results, we propose that PopZ is needed to sequester excess ParA dimers so as to maintain an optimal concentration of nucleoid-bound ParA dimers.

6.2 Introduction

It is now an accepted notion that chromosome segregation in bacteria is an active process orchestrated by a dedicated set of partitioning proteins: ParA and ParB [1–8]. These proteins, along with a DNA sequence called *parS* [9], are highly conserved across bacteria and are collectively referred to as the ParABS system. Genetic studies have revealed that each component of this partitioning system is required for the proper segregation of chromosomes [10,11]. However, a mechanistic understanding of how these components combine to generate robust and directed chromosomal movement is still being investigated.

In recent years, ParABS-mediated chromosomal segregation has been frequently studied in the bacterium *Caulobacter crescentus* [1,2,9,12–14]. The *parS* locus is located 8 kb away from the origin of replication [15], which in turn is oriented towards the old (stalked) pole of the *Caulobacter* cell. The ParB protein binds specifically to the *parS* sequence forming a centromere-like complex. Chromosome replication results in two copies of the *parS/*ParB complex. While the old copy is retained at the old pole, the new centromeric complex or 'chromosome front' is translocated to the opposite pole in a matter of minutes [1,12,14]. Fluorescence microscopy experiments demonstrate that the *parS/*ParB complex follows a retracting cloud of ParA towards the new pole [1,2], suggesting that ParA participates in the segregation of the replicated bacterial chromosome (**Figure 6.1**).

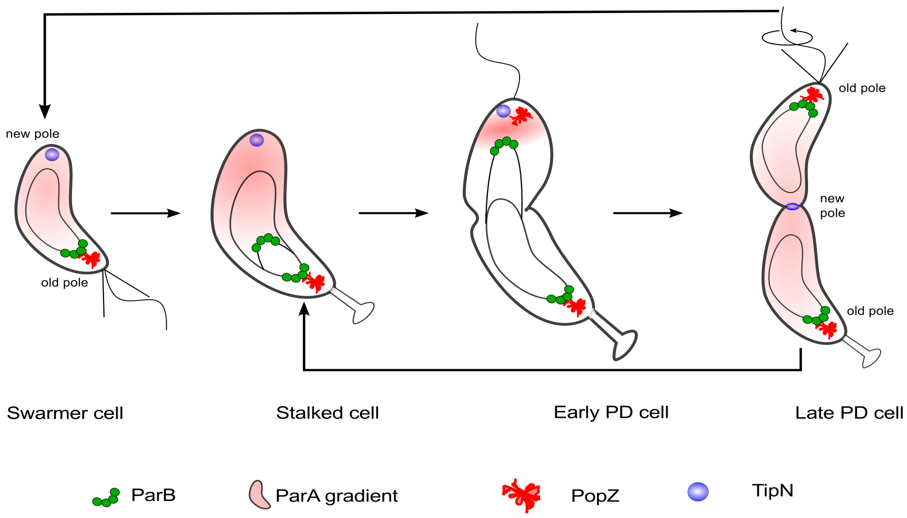

Figure 6.1: Schematic illustration of the consensus model of chromosome segregation in *Caulobacter crescentus*.

In the swarmer cell, a ParA concentration gradient (pink) extends from a maximum at the new pole to a minimum at the old pole. The *parS*/ParB chromosome front (green circles) is tethered to the single focus of PopZ (red). Once DNA replication is initiated in the stalked cell, a second copy of the *parS*/ParB chromosome front translocates behind the receding ParA structure. Concurrent with the completion of segregation in the early predivisional cell, a new focus of PopZ is formed at the new pole to tether the newly replicated chromosome front. TipN (blue circle) is localized at the new pole in the early stages of the cell cycle before being repositioned at mid-cell in the late predivisional stage.

In its active, ATP-bound conformation, ParA forms dimers that can bind to DNA non-specifically. Although a weak ATPase, biochemical studies have shown that binding with ParB results in the up-regulation of ParA's ATPase activity [16]. This results in the breakdown of the ParA into monomers and its subsequent release from DNA. This understanding of the ParA biochemical pathway has motivated the formulation of verbal models to explain the mechanism of chromosome segregation. One model suggests that ParA-mediated chromosome segregation is mechanistically similar to chromosome segregation during the metaphase stage in eukaryotes [1,17]. According to this model, ParA activated by ATP forms a polymer along the length of the cell. The kinetochore analogue ParB is bound to the *parS* centromere. As the *parS*/ParB chromosome front comes in contact with ParA polymers, it binds to and up-regulates ParA ATPase activity, thereby generating a force to 'pull' the *parS*/ParB chromosome front. The mechanistic explanation that has been offered for both chromosome and plasmid segregation is the 'burnt-bridge Brownian ratchet model' [2,18]. According to this model, the *parS/*ParB complex releases ParA molecules from the end of a ParA filament even as it remains attached to the receding structure. An alternative to the filament-based pulling mechanism is the 'DNA-relay mechanism', in which the ParA dimer-DNA complex itself exhibits limited elastic movement around a mean position. This model suggests that translocation is a result of the timely release and subsequent relay of the *parS/*ParB complex from one DNA-bound ParA dimer to the next [12]. Further investigation is required to establish which of these proposed mechanisms, if any, is responsible for ParA-mediated movement of the chromosome front.

Whereas these proposed mechanisms differ in their details, an aspect that unifies them is the requirement for a ParA gradient to ensure uni-directional chromosome segregation. The TipN protein is suggested to help form the ParA gradient. TipN, which itself is localized at the new pole [19,20], binds only to the monomeric form of ParA [2]. In Δ*tipN* mutants, the *parS/*ParB front moves with frequent reversals in direction, prompting suggestions that new-pole TipN may serve as a sink for 'burnt' ParA monomers. According to the consensus model, the TipN-dependent sequestration of ParA monomers prevents them from reorganizing into DNA-bound dimers behind the moving chromosome front. Instead, they bind TipN at the new pole, resulting in the formation of an asymmetric gradient of ParA that extends from its maximum concentration at the new pole to a minimum at the location of the *parS/*ParB complex. However, the chromosome front manages to reach the opposite pole even in Δ*tipN* mutants, albeit belatedly and in an erratic fashion [21]. This observation led us to speculate that TipN is not essential for the uni-directional movement. Instead, it may enable robust and efficient segregation.

In addition to the chromosome sequence *parS*, ParB also has strong affinity for the polymeric protein PopZ [13]. These affinities enable the chromosome front to dock at the poles after the completion of segregation. In addition to its role in tethering the chromosome to the poles, PopZ may also play a role in establishing the ParA gradient [22]. Unlike TipN, PopZ can bind both monomeric and dimeric forms of PopZ. A $\mathrm{ParA_{G16V}}$ mutant that cannot dimerize localizes at both poles in Δ*tipN* background; but is spread diffusely over the cell in Δ*popZ* background. Compared to Δ*tipN* cells, chromosome movement is significantly more erratic in cells containing a PopZ variant that cannot bind ParA. These experiments have led to the suggestion that PopZ may be more important than TipN in executing the directional movement of the chromosome [13]. We found this result surprising for two reasons. Unlike TipN, which localizes only to the new pole, PopZ shows bipolar localization. How can a protein that binds ParA at both ends promote the formation of ParA gradient only towards the new pole? One possibility is that the new-pole focus of PopZ is functionally different from the old-pole focus. This suggestion has been made previously to explain the differential tethering of the chromosome at the old and new poles [22]. However, a more significant contradiction is that PopZ does not appear at the new pole until after the chromosome front has completed segregation. PopZ requires chromosome segregation for bipolarity, making it unlikely for new pole PopZ to regulate the preceding translocation of the newly replicated chromosome. The dependency of PopZ localization on chromosome segregation has been observed experimentally [21] and also predicted by our mathematical model of PopZ localization (Chapter 4). These paradoxical results warrant a closer examination of the consensus model of *parS* segregation in the context of *tipN* and *popZ* mutants.

Here, we formulate a preliminary reaction-diffusion-advection model of *parS* segregation that takes into account the ParA-ParB-DNA interaction pathway. It is important to note that this study does not seek to offer any mechanistic insight into how ParB-dependent release of ParA monomers results in chromosome translocation. Such studies have already been performed [12,23,24]. While the earlier studies used molecular dynamic simulations [12, 24] or stochastic differential equations [23] to model chromosome segregation, we have formulated a deterministic model of the ParABS system. Additionally, the earlier studies did not include details of the ParA biochemical pathway. Here, we seek to reproduce the observed variation in ParA localization and chromosome translocation time between wild-type and mutant cells that are unable to complete distinct steps of the ParA biochemical pathway.

Another important contribution of the ParABS segregation system is the role it plays in positioning of division protein FtsZ by transporting MipZ proteins along with the chromosome front. MipZ promotes the depolymerization of FtsZ. In the nascent swarmer cell, MipZ is bound to the only copy of *parS/*ParB present at the old pole. As a result, FtsZ is found in the opposite end, *i.e.* at the new pole. Additional MipZ molecules bind to the newly replicated *parS* sequence and hitchhike across the length of the cell from the old to the new pole. Subsequently, FtsZ leaves the new pole and re-polymerizes at the center of the cell, where MipZ concentration is lowest [25]. Thus, the departure of FtsZ from the new pole is dependent upon *parS/*ParB/MipZ translocation. In Δ*tipN* mutants, release of FtsZ from the new pole is significantly delayed, in keeping with the late arrival of *parS*/ParB/MipZ. Late in the cell cycle, TipN leaves the new pole and localizes to mid-cell. In doing so, the old-new pole labels are reassigned for subsequent rounds of the cell cycle. In this manner, the cross talk between the segregation machinery and PopZ, MipZ and FtsZ proteins ensure that *parS* segregation occurs in a reproducible and robust fashion in every round of the cell cycle. We validate our model by simulating the localization of MipZ, FtsZ and PopZ as observed in wild-type and Δ*tipN* cells. Additionally, we use the model to predict the localization of FtsZ and PopZ in *parA* mutants as well.

6.3 Methods

A detailed description of the modeling framework is provided below.

Spatial discretization. The proteins under investigation in this work are distributed heterogeneously along the long axis of a *Caulobacter* cell. Hence, it is sufficient to consider biochemical reactions and diffusion occurring in one spatial dimension, and to write the governing partial differential equation (PDE) for a generic chemical species C as:

$$\frac{\partial C}{\partial t} = \text{Reaction terms} + D \cdot \frac{\partial^2 C}{\partial x^2}$$

where $C(x,t)$ is the concentration of species C at location $0 \leq x \leq L$ and time $t \geq 0$. The PDEs for our models are provided in **Tables D.1**. By discretizing the spatial dimension into $n = 100$ compartments of equal length $h = L/n$, where L is the total length of the *Caulobacter* cell and using a central difference scheme to approximate the Laplacian operator, we convert each PDE into a set of ODEs for C_i = concentration of species C in cell i ($1 \leq i \leq 100$)

$$\frac{d\mathrm{C}_i}{dt} = \text{Reaction terms} \;+\; D \cdot \frac{\mathrm{C}_{i+1} - 2\mathrm{C}_i + \mathrm{C}_{i-1}}{h^2}$$

In *Caulobacter*, elongation is a result of new cell wall material being added uniformly along the long axis [26]. Hence, we assume that each compartment grows exponentially in time:

$$\frac{dh}{dt} = k_{\text{growth}} \cdot h$$

Since molecules cannot diffuse across the cell wall, we implement no-flux boundary conditions at $x = 0$ and $x = L$ by adding two additional compartments, $i = 0$ and $i = 101$, and insisting at every time step that $C_0 = C_1$ and $C_{101} = C_{100}$.

The full set of ODEs were simulated in MATLAB using the ode15s solver [27]. The spatiotemporal distribution plots in the figures were generated using the python library Matplotlib [28].

***parS*/ParB segregation.** All variables in our differential equation model have units of concentration. There can be only one or two *parS* sequences at any given stage of the cell cycle; hence, defining *parS* in terms of a real number variable *S(x,t)* is not accessible to our model. Instead, we treat the chromosome sequence *parS* and the protein ParB as a single polymeric entity (abbreviated SB_p in the **Table D.1, Eq. 8**). Furthermore, for microscopy experiments reported in literature, ParB is tagged and used as a proxy for *parS* movement in the cell. Hence, representing the two as single entity reflects the protocol of the experimental observations we are trying to replicate in simulation.

The detailed equation for the *parS*/ParB polymer (SB_p) is provided in **Table D.1**. The reaction and diffusion terms for the *parS*/ParB polymer are *ad hoc* and do not represent the physical reality of how DNA polymers are formed or diffuse in the cell. The terms and reaction constants used allow us to generate a sharp focus of polymer, as expected of ParB molecules bound to the *parS* sequence. Of importance to this study is the advection term, which represents the translocation of *parS*/ParB from the old to the new pole. Translocation of the *parS/* ParB chromosome front requires hydrolysis of DNA-bound ParA-ATP dimers into freely diffusing ParA monomers. We formulated the advection term to be proportional to the fraction of ParA that is not present as dimers. Therefore, the higher the ratio of $ParA_d/ParA_{total}$, the slower the advection of the *parS*/ParB polymer. This phenomenological description of the advection term implies that in our simulations, the chromosome front will translocate even in the absence of ParA dimers; a result that is inconsistent with the observed dependency of chromosome segregation on a ParA nucleoprotein bridge. Hence, this preliminary model can be used to correctly simulate only merodiploid *parA* mutant strains that contain both the wild-type and mutated *parA* allele.

Once the *parS*/ParB front reaches the poles of the cell, it is held in place by docking with polymeric PopZ. By defining the advection term to also be dependent on the fraction of PopZ present in the polymeric form, we are able to simulate the limited movement of the chromosome front in the region the PopZ polymer scaffold is present.

$$\frac{\partial[\mathrm{SB_p}]}{\partial t} = \text{Reaction terms} \quad + \quad \text{Diffusion} \; + \; v \cdot \frac{\partial[S\mathrm{B_p}]}{\partial x} \cdot \left(1 - \frac{[\mathrm{ParA_d}]}{[\mathrm{ParA_{tot}}]}\right) \cdot \left(1 - \frac{[\mathrm{PopZ_{pol}}]}{[\mathrm{PopZ_{tot}}]}\right)$$

$$[\mathrm{ParA_d}] = [\mathrm{ParA_{dim}}] + [\mathrm{ParA_{DNA}}] + [\mathrm{ParA_{ParB}}]$$

$$[\mathrm{ParA_{tot}}] = [\mathrm{ParA_{dim}}] + [\mathrm{ParA_{DNA}}] + [\mathrm{ParA_{ParB}}] + [\mathrm{ParA_{2\_PopZ}}] + [\mathrm{ParA_{PopZ}}] + [\mathrm{ParA_f}] + [\mathrm{ParA_{tn}}]$$

ParA biochemical pathway. Since we desire to investigate *parS* segregation in both ParA wild-type and mutant backgrounds, a description of ParA's interactions with ParB, DNA and other ParA molecules is important. **Figure 6.2** shows the biochemical reactions that form the bases for the equations (**Table D.1**) in our model. The numbers of ParA molecules present in the cell are not sufficient to make up a polymer filament that is long enough to span the long axis of the *Caulobacter* cell, making it unlikely for the chromosome to be segregated by a ParA filament [12]. Hence, we do not include the ParA polymer species in our model. We desired to simulate three important ParA mutants in our model, namely (i) $ParA_{G16V}$, which is a dimerization-negative mutant, (ii) $ParA_{R195E}$, which is deficient in DNA binding, and (iii) $ParA_{D44A}$, in which the ATPase activity is blocked. For each of these mutants, the rate constant for the corresponding reaction is set to zero (**Table D.3**).

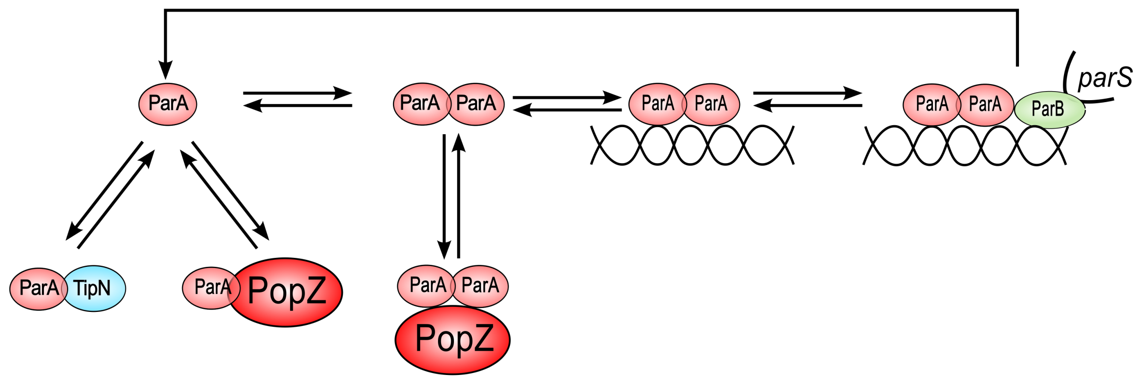

Figure 6.2: Proposed ParA biochemical cycle

ParA monomers (pink) can bind TipN (blue), PopZ (red), or form dimers. ParA dimers bind non-specifically to DNA. The *parS*/ParB chromosome front (green) has high affinity for DNA-bound ParA dimers. ParB up-regulates the ATPase activity of ParA, resulting in the release of ParA in the form of free monomers.

FtsZ, TipN and MipZ localization dynamics. In our model, MipZ is present in a freely diffusing monomeric form and a *parS*-bound form that cannot diffuse. FtsZ is represented in both monomeric and polymeric forms. Polymer formation occurs by *de novo* and autocatalytic growth, as explained in Chapter 4. The rate of FtsZ depolymerization is a function of total MipZ. The localization of TipN depends indirectly on FtsZ [29]. For simplicity however, we assume TipN directly binds to and co-localizes with FtsZ.

PopZ. *In vivo*, the PopZ protein assembles into polymeric aggregates that localize at the old pole in swarmer cells and later assumes bipolar distribution [30,31]. New pole localization of PopZ requires DNA replication [22] and chromosome segregation [21]. In earlier work, we formulated a model to show that PopZ localization pattern can be explained based on a Turing mechanism (Chapter 4). Further, we proposed that slow diffusion of *popZ* mRNA makes it necessary for the *popZ* gene to be present close to both poles for bipolar PopZ localization. The current model does not include *popZ* genes or mRNA. In this preliminary model, we set the rate of PopZ monomer production to be dependent on the concentration of the *parS*/ParB focus. As a result, the emergence of a PopZ focus at the new pole coincides with the completion of chromosome segregation.

6.4 Results

6.4.1 The model is able to reproduce the wild type distribution of ParA, *parS*/ParB, PopZ and FtsZ.

We initialized our simulation by having a single *parS*/ParB focus fixed to the old pole of the cell. In response, a gradient of ParA is established with the maximum concentration at the old pole and minimum concentration at the new pole. At t = 20 minutes, we introduce the second *parS*/ParB chromosome front at the old-pole proximal end. Unlike the old pole focus, the new *parS*/ParB focus is allowed to convect towards the new pole at a speed dependent on the local fraction of ParA monomers (**Table D.1, Eq. 8**). The segregating chromosome reaches the distal pole after ~20 minutes, at t = 40 minutes (**Figure 6.3 A, left panel**). The time duration for chromosome translocation is within the intervals observed in fluorescence microscopy experiments [1,12,14]. It is important to note that, *in vivo*, chromosome movement is erratic, frequently reversing its direction [1,2,14]. Such movements cannot be modeled with a deterministic representation of chromosome movement. A stochastic model, which we plan to reserve for later versions of the model, would be able to capture the erratic movement.

Since MipZ co-localizes with the *parS*/ParB focus, the concentration of MipZ during the early stage of the cell cycle is highest at the old pole. As a result, the FtsZ polymer focus is localized at the opposite, new pole of the cell. Once *parS*/ParB (and therefore MipZ) acquires bipolar localization, our model shows that FtsZ shifts to mid-cell position (**Figure 6.4 A, left panel**). Under physiological conditions, the release of TipN from the new pole is delayed until late in the predivisional cell. The localization pattern of TipN mirrors the FtsZ distribution in our simulations, since we assume direct interaction between the two proteins. Hence, TipN is released prematurely from the new pole in our model.

The simulation also shows that the concentration of ParA builds up in front of the translocating chromosome, reaching peak ParA concentration at the new pole upon completion of translocation (**Figure 6.3 A, right panel**). Therefore, as has been observed experimentally, ParA appears to recede in front of the segregating *parS*/ParB complex. The receding ParA structure shows new-pole localization on account of binding to TipN. The delocalization of new-pole ParA at t = ~ 70 min is a consequence of the migration of TipN from the new pole to a mid-cell position. However, instead of

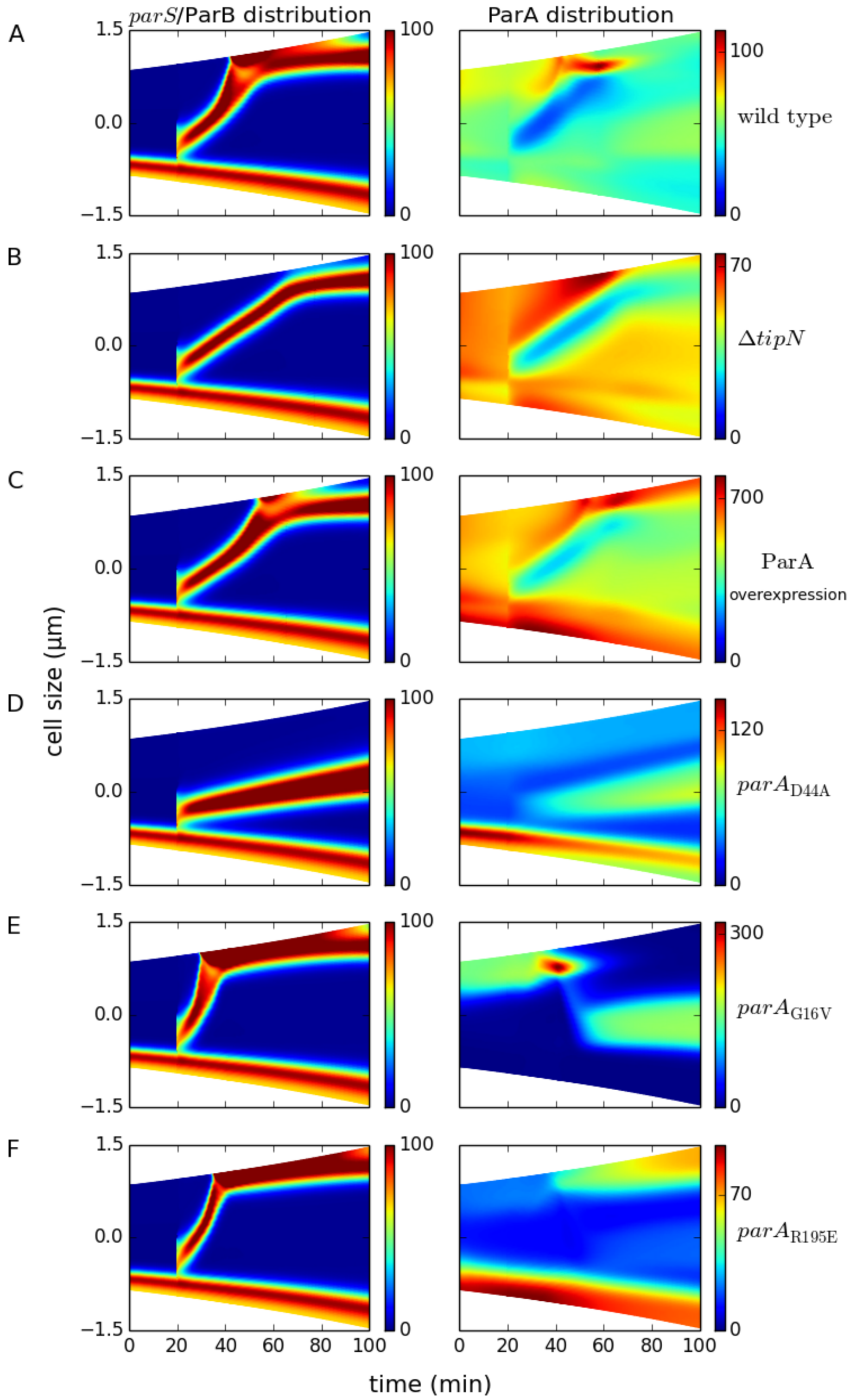

Figure 6.3: Spatiotemporal distribution of ParA (right panel) and *parS*/ParB chromosome fronts in wild-type and mutant cells.

Colors indicate concentration gradients from minimum (blue) to maximum (red). (A) Wild type, (B) Δ*tipN,* and (C) ParA overexpression. (D) *parA*$_{D44A}$ mutants express ParA$_{D44A}$ proteins that cannot be hydrolyzed by ParB.

(E) *parA*$_{G16V}$ mutants express ParA$_{G16V}$ proteins that cannot form dimers. (F) *parA*$_{R195E}$ mutants express ParA$_{R195E}$ proteins that cannot bind DNA.

co-localizing with TipN at mid-cell, ParA once again assumes uniform distribution along the cell (**Figure 6.3 A**, t = 70 – 100 min). This occurs because ParA is once again free to dimerize and bind non-specifically to DNA. This simulation result is in agreement with experimental observations of ParA and TipN distributions in predivisional *Caulobacter* cells [1]. Initially, the PopZ polymer is present as a single focus only at the old pole of our simulated cell. Approximately 5 minutes after the completion of *parS*/ParB segregation, a second focus of PopZ appears at the new pole as well (t = ~ 45 min) (**Figure 6.4 A, right panel**).

6.4.2 The model reproduces delays in chromosome segregation and FtsZ mid-cell localization in Δ*tipN* and ParA overexpression background

Δ*tipN* cells show slow chromosome segregation [1,2,21], diffuse ParA localization [1] and delayed release of cell division protein FtsZ [21]. Based on the stalling and frequent reversals observed in the direction of *parS*/ParB translocation, one study concludes that TipN may be a directionality factor [2]. Other studies report that chromosomes complete segregation, albeit in a delayed and erratic manner in Δ*tipN* background [1,21]. Irrespective of the severity of the defect, TipN appears to play an important role in ensuring that the predivisional cells can segregate their chromosomes and prepare for cell division in a timely manner. In our simulation of the Δ*tipN* mutant, the rate constant governing TipN synthesis is set to zero (k_{syn_tn} = 0 min^{-1}, **Table D.3**). The three experimentally observed defects of Δ*tipN* mutants were observed in our simulation results. The new-pole localization of ParA is diminished, and a significant concentration of ParA is observed in either direction of the moving *parS*/ParB focus **(Figure 6.3 B, right panel)**. The *parS*/ParB focus reaches the new pole at t = 65 minutes **(Figure 6.3 B, left panel)**, which is 20 minutes longer than the time taken to complete segregation in wild type **(Figure 6.3 A, left panel)**. Consequently, a corresponding delay is also observed in the release of FtsZ from the new pole to the mid-cell **(Figure 6.4 B, left panel).** Finally, our simulations also reproduce the late appearance of new pole PopZ observed in Δ*tipN* mutants **(Figure 6.4 B, right panel)**.

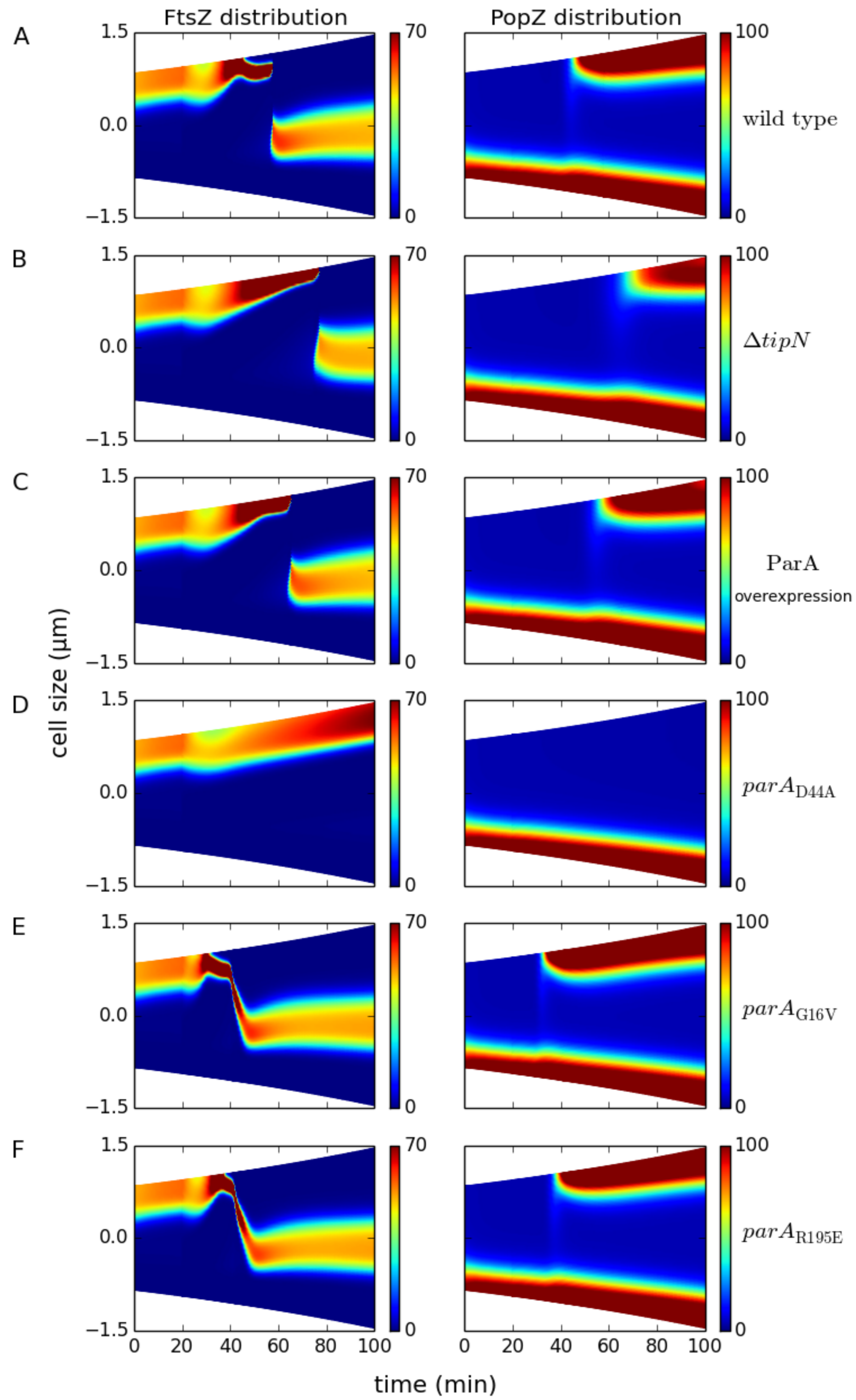

Figure 6.4: Spatiotemporal distribution of FtsZ (left panel) and PopZ (right panel) in wild-type and mutant cells.

Colors indicate concentration gradients from minimum (blue) to maximum (red). (A) Wild type, (B) Δ*tipN,* and (C) ParA overexpression. (D) *parA*$_{\mathrm{D44A}}$ mutants express ParA$_{\mathrm{D44A}}$ proteins that cannot be hydrolyzed by ParB. (E) $parA_{\mathrm{G16V}}$ mutants express $\mathrm{ParA}_{\mathrm{G16V}}$ proteins that cannot form dimers. (F) $parA_{\mathrm{R195E}}$ mutants express $\mathrm{ParA}_{\mathrm{R195E}}$ proteins that cannot bind DNA.

One explanation for the slow movement of the *parS*/ParB focus is the time lost due to the erratic back-and-forth movement of the chromosome front. As mentioned earlier though, our deterministic modeling framework is not suitable for capturing the erratic movement of the chromosome. Hence, the delayed segregation time in our model is a direct result of the decrease in ParA monomer fraction in the region of the segregating *parS*/ParB complex.

We also simulated ParA overexpression in $tipN^{+}$ background by setting ParA expression rate to be ten times higher than wild type ($k_{\mathrm{syn\_pra}} = 2\ \mathrm{min}^{-1}$). Our simulation shows the *parS*/ParB complex taking an additional ten minutes to reach the new pole (**Figure 6.3 C, left panel**). The delay in our simulations is less pronounced than what has been observed experimentally [1]. Additionally, pole-to-pole oscillations of ParA focus have been observed in experiments [1]. Our simulations are unable to capture these oscillations, instead showing polar accumulation at both poles (**Figure 6.3 C, right panel**). Further, the repositioning of the FtsZ polymer and the new pole localization of PopZ in our simulations show a moderate delay compared to the wild-type simulations (**Figure 6.4 C**).

6.4.3 The model reproduces aberrant localization of ParA mutants

We further validated our model by reproducing the mislocalization of mutant ParA proteins in $parA_{\mathrm{D44A}}$, $parA_{\mathrm{G16V}}$, and $parA_{\mathrm{R195E}}$ strains. In the published experiments, localization of mutant ParA proteins were observed in strains that retained the wild-type copy of ParA in addition to possessing YFP-fused ParA mutant proteins expressed from a separate locus on the chromosome [1,2]. To simulate the merodiploid condition of these mutant strains, we expanded our model by including an additional set of equations to represent the mutant ParA proteins. The advection rate for chromosome segregation was correspondingly altered to be dependent on the free fraction of both wild-type and mutant ParA proteins.

In $parA_{\mathrm{D44A}}$ mutants, the newly replicated chromosome manages to translocate only partially towards the new pole [1,2]. The mutant ParA molecules also colocalize with the moving *parS/*ParB complex. $\mathrm{ParA}_{\mathrm{D44A}}$ is defective in ATP hydrolysis, so the rate constant governing ATP hydrolysis was set to zero ($k_{\mathrm{hyd}} = 0\ \mathrm{min}^{-1}$). In other words, ParB-bound ParA dimers cannot be broken down to ParA monomers. Strikingly, our simulations show that the *parS*/ParB complex manages to reach only the middle of the cell at $t = 100$ minutes (**Figure 6.3 D, left panel**), while ParA colocalizes with the two *parS*/ParB complexes (**Figure 6.3 D, right panel**). $ParA_{D44A}$ mutant proteins retain their ability to form dimers and bind the nucleoid. However, the dimers cannot be hydrolyzed after they form complexes with the chromosome front. Hence, we reason that the initial ParA monomer fraction is high enough to allow moderate speed of translocation. As the ParB:$ParA_{D44A}$ complexes bind and accumulate on the moving chromosome front, the ParA monomer fraction reduces thereby stalling further segregation. Further, we predict that PopZ remains unipolar in $parA_{D44A}$ mutants, while the release of FtsZ from the new pole is delayed (**Figure 6.4 D**).

To model the $parA_{G16V}$ mutant, the forward rate constant governing ParA dimerization was set to zero (k_{dimf} = 0 min^{-1}; **Table D.3**). Our simulation shows that the chromosome front traverses the cell length in ~20 minutes (**Figure 6.3 E, left panel**), similar to the time taken in our wild type simulations (**Figure 6.3 A, left panel**). Localization of $ParA_{G16V}$ itself shows exclusive new pole localization prior to, and during chromosome segregation. After segregation, $ParA_{G16V}$ is relocated to the center of the cell (**Figure 6.3 B, left panel**), as it co-localizes wuth TipN. *In vivo*, $ParA_{G16V}$ stays at the pole for a longer duration after chromosome segregation. The premature release is an artifact of our model, as TipN is also release prematurely in our simulations. $ParA_{R195E}$ proteins form dimers that cannot bind DNA but retain their ability to bind PopZ. For the $parA_{R195E}$ mutant, we set the rate constant governing DNA binding to zero (k_{a_ad} = 0 min^{-1}; **Table D.3**). As observed in experiments, our results show the localization of $ParA_{R195E}$ (**Figure 6.3 F, left panel**) coincides with that of the PopZ polymer; unipolar localization in the swarmer cell followed by bipolar localization after chromosome segregation. The timing of PopZ localization and FtsZ release in $parA_{G16V}$ and $parA_{R195E}$ mutants is similar to wild-type phenotype (**Figure 6.4 E & F**).

6.4.4 PopZ may regulate chromosome segregation via binding ParA dimers instead of ParA monomers.

Until recently, it was considered that the primary role of PopZ in chromosome segregation was to bind the *parS*/ParB complex, terminate segregation and prevent reversals in chromosome orientation [1,2,22,30,31]. However, the chromosome still segregated and appeared to bind loosely to the poles in strains containing PopZ mutant proteins (PopZ-KE) that could not bind ParB. In contrast, mutant strains containing PopZ proteins (PopZ-SP) that are deficient in ParA binding show erratic chromosome movement with frequent reversals [13]. We simulated the *popZ*-SP mutant by setting the rate constants pertaining to PopZ–ParA interaction to zero. Our results show that segregation is delayed compared to wild type, resulting in PopZ being present only at the old pole. Since chromosome segregation precedes new pole PopZ localization in wild-type and mutant cells alike, we reason that a new pole PopZ focus is not required to bind ParA monomers and generate the new pole-proximal ParA gradient. Instead, we speculate that defective segregation might be a result of PopZ being unable to bind the dimeric form of ParA. To distinguish between the two cases, we simulated two version of the *popZ*-SP mutant; one defective in binding ParA monomers (*popZ*-SP1), and the other defective in binding ParA dimers (*popZ*-SP2). Our simulations show that *parS*/ParB segregation and ParA localization in wild-type and mutant *popZ*-SP1 is comparable to the wild type (**Figure 6.5 A & B**). In contrast, simulations of the *popZ*-SP2 mutant shows that the *parS*/ParB chromosome front reaches the new pole 20 minutes later than wild type (**Figure 6.5 C)**, supporting our hypothesis that interaction of PopZ with the dimeric form of ParA, and not with ParA monomers, is important for proper segregation of the chromosome.

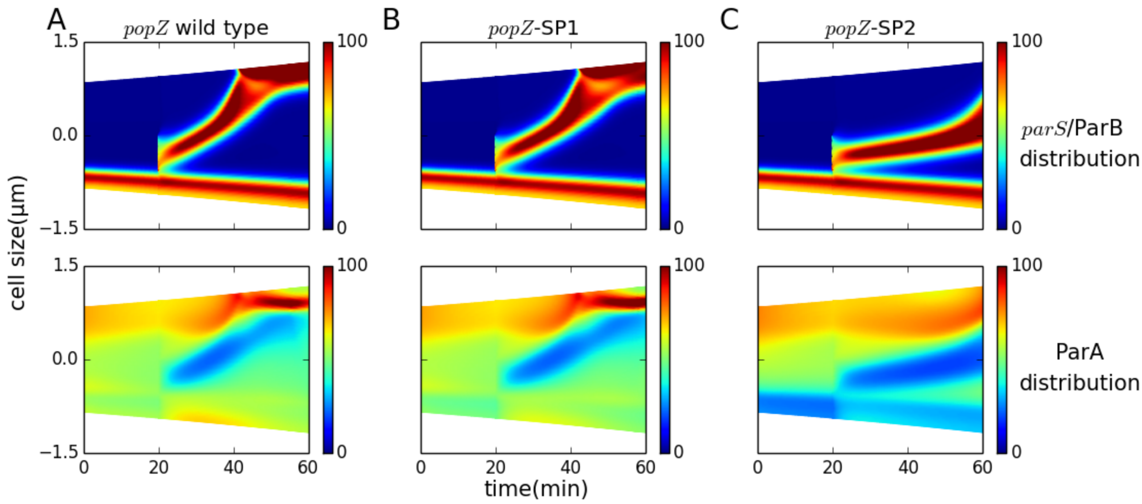

Figure 6.5: Centromere segregation requires PopZ to interact with the dimeric form of ParA.

Colors indicate concentration gradients from minimum (blue) to maximum (red). The time taken for translocating the *parS*/ParB chromosome front (upper panel), and the ParA distribution profile (lower panel) are comparable between simulations of the (A) wild type strain, and (B) a mutant strain containing a PopZ variant that cannot bind ParA monomer (*popZ*-SP1). (C) Simulations of a strain containing a PopZ variant that cannot bind ParA dimers (*popZ*-SP2) shows that the *parS*/ParB segregation is delayed.

Since a similar delay in segregation times is also observed when ParA is overexpressed, we reasoned that the ParA segregation machinery needs to be within a critical concentration range to prevent erratic segregation. We propose that the PopZ scaffold sequesters ParA dimers so as to maintain nucleoid-bound ParA dimers at an optimal level. Under normal physiological conditions, PopZ may be a sink for excess ParA dimers, thus making the system robust to fluctuations in the level of ParA.

In the absence of PopZ, additional ParA dimers bind the nucleoid. As a result, the chromosome front will interact with more nucleoid-bound ParA dimers, thereby stalling or delaying progress of the *parS*/ParB chromosome front.

6.5 Discussion

This study was motivated by the observation that PopZ localization and FtsZ repositioning requires the completion of chromosome segregation. We formulated a deterministic reaction-diffusion-advection model to reproduce or predict the varying translocation speeds of the chromosome front in wild-type and mutant cells. Our simulations support the hypothesis that TipN is required to generate a ParA gradient extending from the new pole to the newly replicated chromosome front. Our simulations are not in agreement with the suggestion that PopZ binds inactive ParA monomers in order to create an asymmetric ParA gradient [13]. Instead, or simulations indicate that it is the interaction between PopZ and the dimeric form of ParA that promotes robust and efficient chromosome segregation. We propose that the concentration of nucleoid-bound ParA dimers in the cell cytoplasm is maintained at the optimum level by the PopZ-dependent sequestration of excess ParA dimers.

The deterministic model described here enabled us to perform a preliminary investigation of the roles of ParA, TipN and PopZ in chromosome segregation. While the equations describing ParA and TipN dynamics are reasonable, the equations defining the formation and segregation of the *parS*/ParB chromosome front (and therefore the distribution of PopZ polymer) are *ad hoc*. Recent experimental evidence also shows that the nucleoid is not static, but diffuses around a mean position, thereby enabling the relay of the chromosome front across the cytoplasm [12]. Furthermore, advances in experimental techniques have enabled measurement of the number of ParA molecules present as dimers in the cell. Given the shortcomings of our deterministic model, we are in the process of formulating a detailed stochastic model that will (a) correctly represent the *parS* chromosome front, (b) include diffusion of the translocating chromosome front and nucleoid-bound ParA dimers, (c) integrate our stochastic model of PopZ localization, and (d) utilize experimental data available on numbers of molecules to guide parameter optimization. We seek to use our stochastic model to address the two important aspects of ParABS-mediated chromosome segregation *i.e.* the mechanistic details of how the chromosome front is moved, and whether a ParA gradient can ensure uni-directional movement of the chromosome towards the new pole.

6.6 References

1. Schofield WB, Lim HC, Jacobs-Wagner C (2010) Cell cycle coordination and regulation of bacterial chromosome segregation dynamics by polarly localized proteins. Eur Mol Biol Organ J 29: 3068–3081. Available: http://www.ncbi.nlm.nih.gov/pubmed/20802464.

2. Ptacin JL, Lee SF, Garner EC, Toro E, Eckart M, et al. (2010) A spindle-like apparatus guides bacterial chromosome segregation. Nat Cell Biol 12: 791–798. Available: http://www.ncbi.nlm.nih.gov/pubmed/20657594.

3. Godfrin-Estevenon AM, Pasta F, Lane D (2002) The parAB gene products of Pseudomonas putida exhibit partition activity in both P. putida and Escherichia coli. Mol Microbiol 43: 39–49.

4. Donovan C, Schwaiger A, Krämer R, Bramkamp M (2010) Subcellular localization and characterization of the ParAB system from Corynebacterium glutamicum. J Bacteriol 192: 3441–3451.

5. Kim HJ, Calcutt MJ, Schmidt FJ, Chater KF (2000) Partitioning of the linear chromosome during sporulation of Streptomyces coelicolor A3(2) involves an oriC-linked parAB locus. J Bacteriol 182: 1313–1320.

6. Iniesta A a (2014) ParABS system in chromosome partitioning in the bacterium Myxococcus xanthus. PLoS One 9: e86897. Available: http://www.pubmedcentral.nih.gov/articlerender.fcgi?artid=3899335&tool=pmcentrez&rendertype=abstract.

7. Mierzejewska J, Jagura-Burdzy G (2012) Prokaryotic ParA-ParB-parS system links bacterial chromosome segregation with the cell cycle. Plasmid 67: 1–14.

8. Viollier PH, Thanbichler M, McGrath PT, West L, Meewan M, et al. (2004) Rapid and sequential movement of individual chromosomal loci to specific subcellular locations during bacterial DNA replication. Proc Natl Acad Sci U S A 101: 9257–9262.

9. Toro E, Hong S-H, McAdams HH, Shapiro L (2008) *Caulobacter* requires a dedicated mechanism to initiate chromosome segregation. Proc Natl Acad Sci U S A 105: 15435–15440. Available:

http://www.pubmedcentral.nih.gov/articlerender.fcgi?artid=2563096&tool=pmcentrez&rendertype=abstract.

10. Mohl DA, Gober JW (1997) Cell Cycle–Dependent Polar Localization of Chromosome Partitioning Proteins in *Caulobacter crescentus*. Cell 88: 675–684. Available: http://www.mendeley.com/research/cell-cycledependent-polar-localization-chromosome-partitioning-proteins-*Caulobacter*-*crescentus*/. Accessed 17 October 2013.

11. Mohl DA, Easter J, Gober JW (2001) The chromosome partitioning protein, ParB, is required for cytokinesis in *Caulobacter crescentus*. Mol Microbiol 42: 741–755. Available: http://www.mendeley.com/research/chromosome-partitioning-protein-parb-required-cytokinesis-*Caulobacter*-*crescentus*/. Accessed 17 October 2013.

12. Lim HC, Surovtsev VI, Beltran BG, HUang F, Bewesdorf Jorg, et al. (2014) Evidence for a DNA-relay mechanism in ParABS-mediated chromosome segregation. Elife 3.

13. Ptacin JL, Gahlmann A, Bowman GR, Perez AM, von Diezmann ARS, et al. (2014) Bacterial scaffold directs pole-specific centromere segregation. Proc Natl Acad Sci U S A. Available: http://www.ncbi.nlm.nih.gov/pubmed/24778223.

14. Shebelut CW, Guberman JM, Van Teeffelen S, Yakhnina AA, Gitai Z (2010) *Caulobacter* chromosome segregation is an ordered multistep process. Proc Natl Acad Sci U S A 107: 14194–14198. Available: http://www.ncbi.nlm.nih.gov/pubmed/20660743.

15. Hong S-H, McAdams HH (2011) Compaction and transport properties of newly replicated *Caulobacter crescentus* DNA. Mol Microbiol 82: 1349–1358. Available: http://www.mendeley.com/catalog/compaction-transport-properties-newly-replicated-*Caulobacter*-*crescentus*-dna/. Accessed 17 October 2013.

16. Easter J, Gober JW (2002) ParB-Stimulated Nucleotide Exchange Regulates a Switch in Functionally Distinct ParA Activities. Mol Cell 10: 427–434. Available: http://www.mendeley.com/research/parbstimulated-nucleotide-exchange-regulates-switch-functionally-distinct-para-activities/. Accessed 17 October 2013.

17. Fogel MA, Waldor MK (2006) A dynamic, mitotic-like mechanism for bacterial chromosome segregation. Genes Dev 20: 3269–3282. Available:

http://www.mendeley.com/catalog/dynamic-mitoticlike-mechanism-bacterial-chromosome-segregation/. Accessed 17 October 2013.

18. Vecchiarelli AG, Hwang LC, Mizuuchi K (2013) Cell-free study of F plasmid partition provides evidence for cargo transport by a diffusion-ratchet mechanism. Proc Natl Acad Sci U S A 2013: E1390–7. Available: http://www.pubmedcentral.nih.gov/articlerender.fcgi?artid=3625265&tool=pmcentrez&rendertype=abstract\nhttp://www.ncbi.nlm.nih.gov/pubmed/23479605.

19. Lam H, Schofield WB, Jacobs-Wagner C (2006) A landmark protein essential for establishing and perpetuating the polarity of a bacterial cell. Cell 124: 1011–1023. Available: http://www.ncbi.nlm.nih.gov/pubmed/16530047.

20. Huitema E, Pritchard S, Matteson D, Radhakrishnan SK, Viollier PH (2006) Bacterial birth scar proteins mark future flagellum assembly site. Cell 124: 1025–1037.

21. Laloux G, Jacobs-Wagner C (2013) Spatiotemporal control of PopZ localization through cell cycle-coupled multimerization. J Cell Biol 201: 827–841. Available: http://www.mendeley.com/research/spatiotemporal-control-popz-localization-through-cell-cyclecoupled-multimerization/. Accessed 17 October 2013.

22. Bowman GR, Comolli LR, Gaietta GM, Fero M, Hong S-H, et al. (2010) *Caulobacter* PopZ forms a polar subdomain dictating sequential changes in pole composition and function. Mol Microbiol 76: 173–189. Available: http://www.pubmedcentral.nih.gov/articlerender.fcgi?artid=2935252&tool=pmcentrez&rendertype=abstract.

23. Shtylla B, Keener JP (2012) A mathematical model of ParA filament-mediated chromosome movement in *Caulobacter crescentus*. J Theor Biol 307: 82–95. Available: http://www.mendeley.com/catalog/mathematical-model-para-filamentmediated-chromosome-movement-*Caulobacter*-*crescentus*/. Accessed 17 October 2013.

24. Liu AJ, Banigan EJ, Gelbart MA, Gitai Z, Wingreen NS (2011) Filament Depolymerization Can Explain Chromosome Pulling during Bacterial Mitosis. PLoS Comput Biol 7: e1002145. doi:10.1371/journal.pcbi.1002145.

25. Thanbichler M, Shapiro L (2006) MipZ, a spatial regulator coordinating chromosome segregation with cell division in *Caulobacter*. Cell 126: 147–162. Available: http://www.ncbi.nlm.nih.gov/pubmed/16839883.

26. Aaron M, Charbon G, Lam H, Schwarz H, Vollmer W, et al. (2007) The tubulin homologue FtsZ contributes to cell elongation by guiding cell wall precursor synthesis in *Caulobacter crescentus*. Mol Microbiol 64: 938–952. doi:10.1111/j.1365-2958.2007.05720.x.

27. Shampine LF, Reichelt MW (1997) The MATLAB ODE Suite. SIAM J Sci Comput 18: 1–22. doi:10.1137/S1064827594276424.

28. Hunter JD (2007) Matplotlib: A 2D Graphics Environment. Comput Sci Eng 9: 90–95. Available: http://ieeexplore.ieee.org/lpdocs/epic03/wrapper.htm?arnumber=4160265.

29. Yeh Y-C, Comolli LR, Downing KH, Shapiro L, McAdams HH (2010) The *Caulobacter* Tol-Pal complex is essential for outer membrane integrity and the positioning of a polar localization factor. J Bacteriol 192: 4847–4858. Available: http://www.pubmedcentral.nih.gov/articlerender.fcgi?artid=2944545&tool=pmcentrez&rendertype=abstract.

30. Ebersbach G, Briegel A, Jensen GJ, Jacobs-Wagner C (2008) A self-associating protein critical for chromosome attachment, division, and polar organization in *Caulobacter*. Cell 134: 956–968. Available: http://www.pubmedcentral.nih.gov/articlerender.fcgi?artid=2614312&tool=pmcentrez&rendertype=abstract.

31. Bowman GR, Comolli LR, Zhu J, Eckart M, Koenig M, et al. (2008) A polymeric protein anchors the chromosomal origin/ParB complex at a bacterial cell pole. Cell 134: 945–955. Available: http://www.ncbi.nlm.nih.gov/pubmed/18805088.

Chapter 7 Towards a Comprehensive Model of the Asymmetric Division Cycle of *Caulobacter crescentus*: Ongoing and Future Research Interests

The modules described in each chapter offer additional insight on how proteins localize at the poles, how dynamic localization of proteins is regulated, and finally, how the cell exploits localization in order to fashion separate cell-fates. A goal of our modeling efforts is to integrate these distinct modules into a comprehensive model of the *Caulobacter* cell cycle. This effort, although ongoing, is impeded by gaps in our understanding of localization and interactions of some of the regulatory molecules. **Figure 7.1** is a schematic representation of the cell cycle regulatory network that summarizes the modules we have built, along with depicting ongoing work and missing information.

1. Regulation of SpmX synthesis

The cell-fate determinant DivJ is a kinase that initiates swarmer-to-stalked transition by binding to SpmX at the old pole. SpmX in turn is localized at the old pole by binding the PopZ polymer scaffold in the swarmer cells. However, when PopZ becomes bipolar later in the cell cycle, SpmX retains its old-pole specific unipolar localization pattern. Subsequently, DivJ is present only in one compartment, allowing the predivisional cell to divide in an asymmetric manner. A reason for the lack of correlation between the localization patterns of PopZ and SpmX in predivisional cells is that *spmX* mRNA is not transcribed in the predivisional cells, thus precluding the production of new molecules of SpmX proteins that could potentially bind new-pole PopZ [1]. The regulatory pathway that limits the transcription of *spmX* mRNA only to the swarmer cell stage is not understood. Hence, we were unable to integrate the DivJ-DivK-PleC module (Chapters 2 and 3) with the PopZ module (Chapter 5). For the moment, the localization pattern of DivJ is artificially enforced in our model.

2. Localization of DivL, CckA and PleC

In addition to DivJ, the localization patterns of DivL, CckA and PleC are also artificially enforced in our model. Co-localization of DivL with PleC kinase is important for the development of asymmetry in the predivisional cell, as it enables PleC kinase to effectively sequester DivK~P away from DivL. It has been shown that inhibiting DNA replication prevents the new-pole specific localization of DivL [2]. A polarly localized protein PodJ is required for new-pole localization of DivL [3]. However, PodJ and DivL only co-localize during the predivisional stage of the cell cycle, suggesting that additional localization determinants are yet to be accounted for.

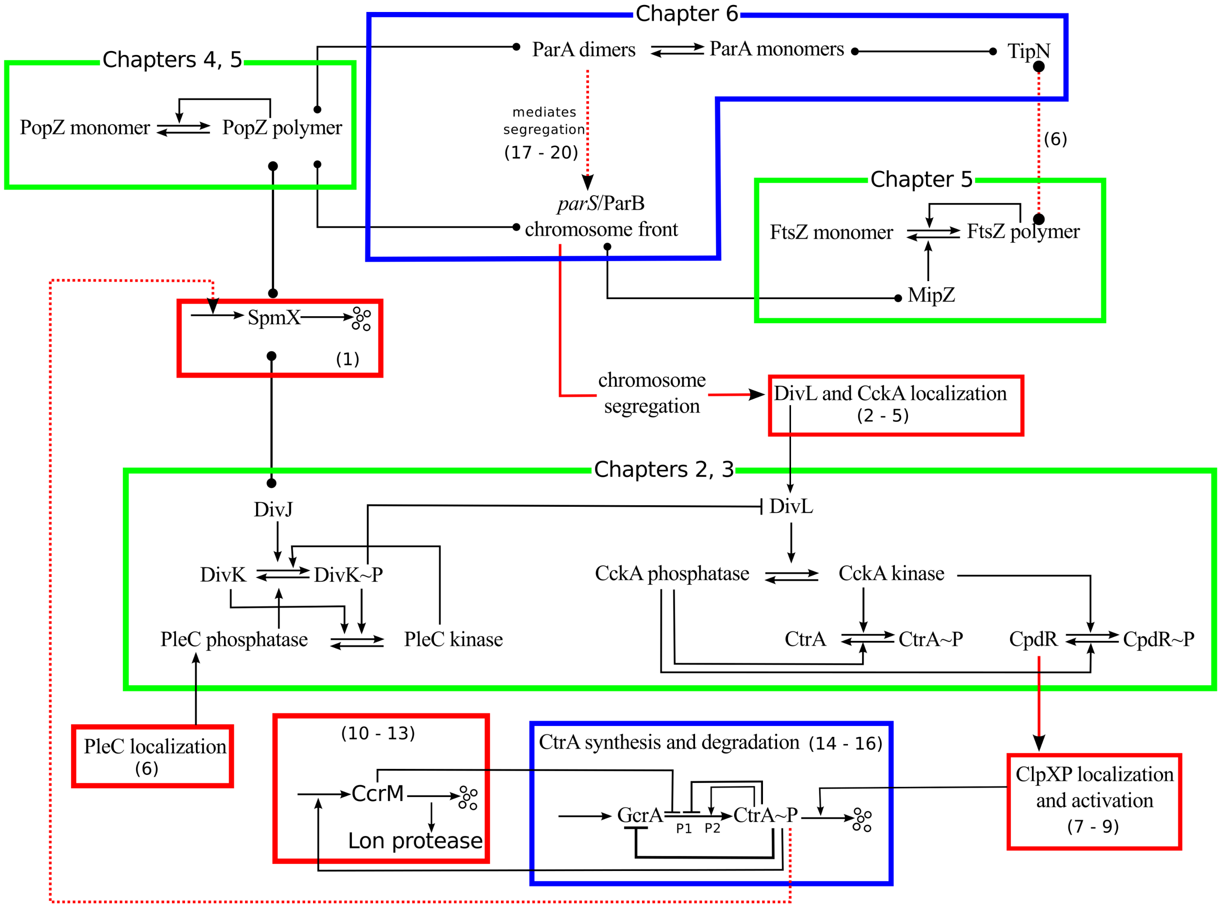

Figure 7.1: Schematic representation of the regulatory network controlling the asymmetric division cycle of *Caulobacter crescentus*

Portions of the wiring diagram enclosed in boxes represent how the regulatory network was divided into modules. Green boxes represent modules that have been modeled satisfactorily as per current state of knowledge (Chapters 2 – 5). Blue boxes represent modules that will be the focus of immediate attention. Modules enclosed in red boxes are those for which there is insufficient experimental data or hypotheses to attempt formulating a mathematic model at present. Lines ending in arrows represent activation, lines ending with a perpendicular dash represent inhibitory signals, and lines with closed circles at both ends indicates a binding reaction resulting in complex formation. Lines in red indicate interactions that are not included in the model because of insufficient information. Dashed lines indicate indirect interaction. Numbers in brackets are citations to important articles pertaining to the modules.

The downstream bifunctional enzyme CckA also requires DNA replication for new-pole localization. CckA is uniformly distributed in swarmer cells, and then acquires old-pole specific unipolar localization, before attaining bipolar distribution in predivisional cells [4]. PopZ [5] and DivL [2] have been shown as important for CckA localization, but the localization patterns of these three proteins are dissimilar.

PleC is present at the old pole of swarmer cells. Soon after the cells transition to the stalked stage, PleC is delocalized from the old pole and repositioned at the new pole of predivisional cells. PodJ, a protein with a similar localization pattern is required for PleC localization. TipN is also predicted to influence PleC localization [6]. However, the mechanics of PodJ and TipN localization are also obscure. Until further experimental data emerge, a detailed description of the localization of DivL, CckA, PleC, and PodJ cannot be included in our mathematical model.

3. Regulation of ClpXP activation and localization

The G1-to-S transition requires that the DNA replication inhibitor CtrA~P be dephosphorylated. The model described in Chapters 2 and 3 provides a detailed account of the regulatory pathway that controls the phosphorylation status of CtrA. However, this pathway also branches -via the response regulator CpdR- into a proteolytic pathway that ensures CtrA is not only dephosphorylated but also degraded by the protease ClpXP during the stalked stage of the cell cycle [7,8]. Recent experimental efforts have revealed that a complex signaling pathway is responsible for ClpXP activation, which includes accessory proteins like RcdA, PopA, and cyclic di-GMP [9]. While progress is being made to uncover the mechanism for the cell cycle-dependent activation of ClpXP, even less is known about how ClpXP is dynamically localized during the cell cycle. Hence, a spatiotemporal model of the ClpXP proteolytic pathway is reserved for future versions of our model.

4. Dynamics of CcrM and Lon protease

CcrM is a hemimethyl transferase that works to methylate promoters of several cell cycle genes, such as *dnaA*, *gcrA*, *and ctrA* [10], during the S- and G2-phases of the cell cycle. The temporal dynamics of CcrM have been included in earlier versions of the *Caulobacter* cell cycle model [11,12]. CcrM is rapidly degraded by Lon protease, the activity of which peaks during the predivisional stage. Little is known about the temporal regulation of Lon protease [13]. CcrM dynamics will be included in future versions as more information emerges regarding regulation of Lon protease.

5. Synthesis and degradation of CtrA

For the models described in Chapter 2 and 3, we assume CtrA is synthesized constitutively. This simplification is sufficient when the aim is to understand changes in the phosphorylation status of CtrA. In reality though, GcrA, CcrM, and CtrA itself control transcription of *ctrA* mRNA via interactions with two promoters P1 and P2 [10,14–16]. Earlier versions of our model have included details regarding control of CtrA synthesis. Once our model is successful in explaining activation and localization of the protease ClpXP, we can move towards including the temporal dynamics of CtrA activation and proteolysis in the model.

6. Mechanistic details of ParABS segregation machinery and TipN localization

As described in the discussion to Chapter 6, the mechanism of ParA-dependent segregation of the *parS*/ParB chromosome front is still unclear [17–20]. Our current description of the segregation of the chromosome front is phenomenological, and a clearer mechanistic description would be desirable. A stochastic version of our model is also required to capture the erratic movement of the chromosome front, as well as capturing variations in translocation times for completion of chromosome segregation. Furthermore, we make the simplifying assumption that TipN and FtsZ bind directly with each other. Experimental observations show that TipN does not immediately follow FtsZ as it relocates from new pole to mid-cell. This delay may be due to the requirement of intermediate binding partners such as the Tol-Pal complex [6]. More experimental data will be needed before we can proceed with formulating an accurate model for TipN localization.

References

1. Radhakrishnan SK, Thanbichler M, Viollier PH (2008) The dynamic interplay between a cell fate determinant and a lysozyme homolog drives the asymmetric division cycle of Caulobacter crescentus. Genes Dev 22: 212–225. Available: http://www.pubmedcentral.nih.gov/articlerender.fcgi?artid=2192755&tool=pmcentrez&rendertype=abstract.

2. Iniesta AA, Hillson NJ, Shapiro L (2010) Polar Remodeling and Histidine Kinase Activation, Which Is Essential for Caulobacter Cell Cycle Progression, Are Dependent on DNA Replication Initiation. J Bacteriol 192: 3893–3902. Available: http://www.pubmedcentral.nih.gov/articlerender.fcgi?artid=2916389&tool=pmcentrez&rendertype=abstract.

3. Curtis PD, Quardokus EM, Lawler ML, Guo X, Klein D, et al. (2012) The scaffolding and signalling functions of a localization factor impact polar development. Mol Microbiol 84: 1–24. Available: http://www.ncbi.nlm.nih.gov/pubmed/22512778.

4. Ausmees N, Jacobs-Wagner C (2003) Spatial and temporal control of differentiation and cell cycle progression in Caulobacter crescentus. Annu Rev Microbiol 57: 225–247. Available: http://www.ncbi.nlm.nih.gov/pubmed/14527278.

5. Ebersbach G, Briegel A, Jensen GJ, Jacobs-Wagner C (2008) A self-associating protein critical for chromosome attachment, division, and polar organization in caulobacter. Cell 134: 956–968. Available: http://www.pubmedcentral.nih.gov/articlerender.fcgi?artid=2614312&tool=pmcentrez&rendertype=abstract.

6. Yeh Y-C, Comolli LR, Downing KH, Shapiro L, McAdams HH (2010) The caulobacter Tol-Pal complex is essential for outer membrane integrity and the positioning of a polar localization factor. J Bacteriol 192: 4847–4858. Available: http://www.pubmedcentral.nih.gov/articlerender.fcgi?artid=2944545&tool=pmcentrez&rendertype=abstract.

7. Chen YE, Tsokos CG, Biondi EG, Perchuk BS, Laub MT (2009) Dynamics of two Phosphorelays controlling cell cycle progression in Caulobacter crescentus. J Bacteriol 191: 7417–7429. Available: http://www.pubmedcentral.nih.gov/articlerender.fcgi?artid=2786585&tool=pmcentrez&rendertype=abstract. Accessed 28 July 2011.

8. Iniesta AA, Shapiro L (2008) A bacterial control circuit integrates polar localization and proteolysis of key regulatory proteins with a phospho-signaling cascade. Proc Natl Acad Sci U S A 105: 16602–16607. Available: http://www.pubmedcentral.nih.gov/articlerender.fcgi?artid=2575466&tool=pmcentrez&rendertype=abstract.

9. Abel S, Chien P, Wassmann P, Schirmer T, Kaever V, et al. (2011) Regulatory Cohesion of Cell Cycle and Cell Differentiation through Interlinked Phosphorylation and Second Messenger Networks. Mol Cell 43: 550–560.

10. Collier J, McAdams HH, Shapiro L (2007) A DNA methylation ratchet governs progression through a bacterial cell cycle. Proc Natl Acad Sci U S A 104: 17111–17116. Available: http://www.pubmedcentral.nih.gov/articlerender.fcgi?artid=2040471&tool=pmcentrez&rendertype=abstract.

11. Li S, Brazhnik P, Sobral B, Tyson JJ (2008) A Quantitative Study of the Division Cycle of Caulobacter crescentus Stalked Cells. PLoS Comput Biol 4: 19. Available: http://www.pubmedcentral.nih.gov/articlerender.fcgi?artid=2217572&tool=pmcentrez&rendertype=abstract.

12. Li S, Brazhnik P, Sobral B, Tyson JJ (2009) Temporal Controls of the Asymmetric Cell Division Cycle in Caulobacter crescentus. PLoS Comput Biol 5: 15. Available: http://www.ncbi.nlm.nih.gov/pubmed/19680425.

13. Gora KG, Cantin A, Wohlever M, Joshi KK, Perchuk BS, et al. (2013) Regulated proteolysis of a transcription factor complex is critical to cell cycle progression in Caulobacter crescentus. Mol Microbiol 87: 1277–1289.

14. Domian IJ, Reisenauer A, Shapiro L (1999) Feedback control of a master bacterial cell-cycle regulator. Proc Natl Acad Sci U S A 96: 6648–6653. Available: http://www.pubmedcentral.nih.gov/articlerender.fcgi?artid=21969&tool=pmcentrez&rendertype=abstract.

15. Spencer W, Siam R, Ouimet M-C, Bastedo DP, Marczynski GT (2009) CtrA, a global response regulator, uses a distinct second category of weak DNA binding sites for cell cycle transcription control in Caulobacter crescentus. J Bacteriol 191: 5458–5470. Available: http://www.pubmedcentral.nih.gov/articlerender.fcgi?artid=2725627&tool=pmcentrez&rendertype=abstract.

16. Holtzendorff J, Hung D, Brende P, Reisenauer A, Viollier PH, et al. (2004) Oscillating global regulators control the genetic circuit driving a bacterial cell cycle. Science (80-) 304: 983–987. Available: http://www.ncbi.nlm.nih.gov/pubmed/15087506.

17. Ptacin JL, Lee SF, Garner EC, Toro E, Eckart M, et al. (2010) A spindle-like apparatus guides bacterial chromosome segregation. Nat Cell Biol 12: 791–798. Available: http://www.ncbi.nlm.nih.gov/pubmed/20657594.

18. Schofield WB, Lim HC, Jacobs-Wagner C (2010) Cell cycle coordination and regulation of bacterial chromosome segregation dynamics by polarly localized proteins. Eur Mol Biol Organ J 29: 3068–3081. Available: http://www.ncbi.nlm.nih.gov/pubmed/20802464.

19. Ptacin JL, Gahlmann A, Bowman GR, Perez AM, von Diezmann ARS, et al. (2014) Bacterial scaffold directs pole-specific centromere segregation. Proc Natl Acad Sci U S A. Available: http://www.ncbi.nlm.nih.gov/pubmed/24778223.

20. Lim HC, Surovtsev VI, Beltran BG, HUang F, Bewesdorf Jorg, et al. (2014) Evidence for a DNA-relay mechanism in ParABS-mediated chromosome segregation. Elife 3.

Appendix A Supplementary information for Chapter 2

A.1 Supplementary text

In **Figure A.1** we propose a set of molecular interactions governing the PleC phosphatase-to-kinase transition. Each step in the mechanism is an elementary chemical reaction governed by mass-action kinetics. To each species in the mechanism we assign a standard Gibbs free energy that is consistent with our estimate of the standard Gibbs free energy change for the reaction, ΔG^0. To each reaction we then assign forward and reverse rate constants that are consistent with the equilibrium constant of the reaction, $K_{\mathrm{eq}} = e^{-\Delta G^0/RT}$. In this way, we can be sure that our reaction mechanism satisfies the principle of detailed balance around every closed loop of chemical reactions.

In the following sections, we (A) review some basic concepts of histidine kinases and allosteric enzymes, (B) assign free energies to the chemical species and estimate the standard free energy change for all the reactions in **Figure A.1**, (C) explain our rationale for assigning rate constants to all reactions, and (D) propose a simplified reaction mechanism that retains the crucial feature of bistability.

A.1.1 Histidine kinases and allosteric enzymes

Histidine kinases in two-component systems

A common signaling motif in microbes is the ‘two-component system’ comprised of a histidine kinase (HK) and a response regulator (RR). The HK component, typically a homodimer located in the bacterial membrane, responds to environmental stimuli by autophosphorylating a histidine residue and then transfering the phosphoryl group to an aspartate residue of the RR. HKs are bifunctional, in that they can serve as either a kinase or a phosphatase to a given RR. In keeping with this complexity, HKs have an elaborate and modular design. Each monomer has three subdomains: a membrane-bound sensor domain, a dimerization domain containing the phospho-accepting His residue, and a catalytic domain containing an ATP binding site [1]. It is believed that an HK, in response to sensory input via its sensor domain, changes its conformation to act as either a kinase or a phosphatase. This view of two-component systems is a generalization, and no two are alike. There are variations of the general scheme both in terms of architecture and activity. Some two-component systems have more than two components, forming a chain of alternating His and Asp containing domains [2]. Each domain may be on a distinct protein, or some of the domains may be parts of a single protein [3]. The exact details of how the change between kinase and phosphatase forms is achieved also vary, and different mechanisms have been suggested [1].

PleC, an HK in *Caulobacter*, has its own unique traits. Although it is bifunctional, its function is not regulated by ligand binding to a sensor domain. Instead, its RR (DivK) up-regulates the kinase form of PleC [4]. DivK binds to only one site on PleC [5] and, interestingly, PleC's sensor domain is not essential to its role in cell cycle progression [6]. These observations suggest that, when DivK binds to PleC, it acts as substrate/product and allosteric modulator concurrently. These dual roles of DivK (and DivK~P) are central to our model (**Figure A.1**).

MWC model of allosteric regulation

Allosteric regulation can be explained using either the Monod-Wyman-Changeux (MWC) model [7] or the Koshland-Némethy-Filmer (KNF) model [8]. The main difference between the two is that KNF allows monomers within a single protein complex to exist in different states while MWC does not. As a result, the MWC 'dose-response' curve is more sigmoidal, and hence in our opinion, more suited to explain the switch-like transition from swarmer cell to stalked cell in the *Caulobacter* cell cycle. **Figure A.2** illustrates the general idea behind the MWC model. The allosteric protein can exist in either an inactive form (R for 'relaxed') or an active form (T for 'tensed'). In the absence of ligand binding, the R form is more stable than the T form. However, ligand binding stabilizes the T form to a greater extent than it does the R form (i.e., the TL intermediate has a lower free energy than the RL intermediate). In short, in the absence of ligand, equilibrium favors an excess of R over T, while in the presence of the ligand, the TL form is in excess [9].

A.1.2 Thermodynamic considerations

Free energy change of a chemical reaction and definition of 'standard state'

The free energy change of a chemical reaction, A + B → C + D, is

$$\Delta G = \Delta G^0 + RT\ln\left(\frac{a_{\mathrm{C}}a_{\mathrm{D}}}{a_{\mathrm{A}}a_{\mathrm{B}}}\right)$$

where ΔG^0 is the standard free energy change of the reaction, and a_{A} etc. are the 'activities' of the reactants and products. For an ideal solution (a reasonable approximation for our purposes), $a_{\mathrm{A}} = [\mathrm{A}]/[\mathrm{A}]^0$, where $[\mathrm{A}]^0$ is the 'standard' concentration of species A. (Clearly, ΔG^0 is the free energy change of the reaction when all participating species are present at their standard concentrations; i.e., $a_A = 1$, etc.) In physical chemistry textbooks, it is conventional to define the standard concentration of all chemical species to be 1 M, but this definition is neither necessary nor desirable. Even physical chemists define the standard concentration of H_2O to be 55.5 M (the unchanging concentration of water in dilute aqueous solutions), and biochemists find it convenient to define the standard concentration of H^+ to be 10^{-7} M (i.e., neutral pH, characteristic of living cells). We will define the standard states of the chemical species in our reaction mechanism to make thermodynamic calculations and kinetic simulations as simple as possible.

The kinetic rate constants for a chemical reaction are related to ΔG^0 for the reaction through the equilibrium constant, $K_{eq} = e^{-\Delta G^0/RT}$, where R = gas constant and T = absolute temperature (RT = 2.48 kJ/mole at 298 K) and K_{eq} is the mass-action quotient at equilibrium:

$$K_{eq} = \frac{a_{C,eq} a_{D,eq}}{a_{A,eq} a_{B,eq}}$$

For an elementary chemical reaction (described by mass-action kinetics), the rates of the forward and reverse reactions are

$$k_f \cdot a_A \cdot a_B, \quad k_r \cdot a_C \cdot a_D,$$

respectively. At equilibrium, the rates of the forward and reverse reactions are equal; hence, $K_{eq} = k_f/k_r$.

For numerical simulations of a chemical reaction system, it is convenient to scale the concentrations of all time-dependent intermediates so that $a_A(t) \approx 1$, etc. Hence, to connect our thermodynamics estimates of ΔG^0 and K_{eq} to our kinetic simulations, we must choose the 'standard' concentrations of our species to be the typical intracellular concentrations used to scale the kinetic rate equations.

As an example of these ideas, consider the hydrolysis of ATP in *Caulobacter* cells. It is reasonable to assume that the concentrations of ATP, ADP and P_i are constant in the cell (say, [ATP] = 13 mM, [ADP] = 2 mM, [P_i] = 2 mM). We take these intracellular concentrations as our 'standard' concentrations for ATP, ADP and Pi, so that $a_{ATP} = a_{ADP} = a_{Pi} = 1$ at all times. With this choice, the concentrations of ATP, ADP and P_i drop out of all our equilibrium calculations and kinetic rate laws, because their activities are always ≡ 1 (in the same way that [H_2O] drops out of all such calculations because the standard concentration of water is defined to be 55.5 M). With this definition of standard state, we have

$$\text{ATP} + H_2O \rightarrow \text{ADP} + P_i, \quad \Delta G^0 = -50 \text{ kJ/mole}$$

for ATP hydrolysis under these (standard) conditions inside the cell.

Assigning standard free energy changes to the generic reactions in our model

In **Table A.2** we catalog the generic reactions in our model (**Figure A.1**), starting with the phosphorylation of ADP to ATP (reaction R1).

To estimate ΔG^0 for the auto-phosphorylation of PleC, we observe that HKs auto-phosphorylate on a histidine residue, resulting in a phosphoramidate bond. Unlike phosphorylation on serine, threonine or tyrosine residues that give rise to stable phosphoesters, phosphoramidates are high-energy bonds [10,11]. As a result, HK auto-phosphorylation may have $\Delta G^0 \approx 0$. To estimate ΔG^0 for PleC auto-phosphorylation (for which there are no data), we refer to the case of CheA, a more well studied HK. In the presence of ATP alone, CheA auto-phosphorylation is reported to be highly endergonic (ΔG^0 = +12.3 kJ/mole [12] and ΔG^0 = + 4.8 kJ/mole [13].) However, in the presence of CheW and Tar receptors, CheA shows a 300-fold increase in kinase activity [14] and a 10- to 100-fold increase in autokinase activity [15]. Hence, under favorable conditions, CheA auto-phosphorylation is close to equilibrium, if not exergonic. Therefore, it is reasonable to assume that, when bound to DivK or DivK~P, PleC auto-phosphorylation is close to equilibrium under typical intracellular conditions:

$\mathrm{PleC_{kin}} + \mathrm{ATP} \rightarrow \mathrm{PleC_{kin}{\sim}P} + \mathrm{ADP}$, $\Delta G^0 = 0$, $K_{eq} = 1$

From this assumption and ΔG^0 for ATP hydrolysis, we calculate ΔG^0 for the phosphorylation of $\mathrm{PleC_{kin}}$ (reaction R2 in **Table A.2**). Loosely speaking, we may say that $\mathrm{PleC_{kin}{\sim}P}$ is 50 kJ/mole higher in Gibbs free energy than $\mathrm{PleC_{kin}}$.

HK~P binds to its cognate RR and transfers its phosphate group to an aspartate residue on the RR. The resultant acyl phosphate (RR-Asp~P) is also a high-energy bond, suggesting that the phospho-transfer reaction is reversible [11]. However, RR-Asp~P is thought to undergo a conformational change that makes it more stable [16], so that the free energy of hydrolysis of RR~P is not as negative as that of ATP (−50 kJ/mole) (**Figure A.3 A**). Here again, in the absence of any data on the free energy of hydrolysis of DivK~P, we assume that

$$\mathrm{DivK{\sim}P} + H_2O \rightarrow \mathrm{DivK} + P_i,\ \ \Delta G^0 = -30 \text{ kJ/mole}$$

under (standard) conditions inside the cell. Loosely speaking, we may say that DivK~P is 30 kJ/mole higher in free energy than DivK (reaction R3 in **Table A.2**).

Next, consider the $R_0 \rightarrow T_0$ reaction in our MWC representation of the PleC kinase-to-phosphatase transition. Given that PleC is a phosphatase by default and requires DivK to become a kinase, we choose PleC phosphatase to be the R form and PleC kinase to be the T form. We assume

$PleC_{kin}$ is higher in free energy by 8.55 kJ/mole (reaction R4 in **Table A.2**). Taking into account that PleC is a dimer, we have, for the phosphatase-to-kinase transition in the absence of DivK,

$(PleC_{pho})_2 \rightarrow (PleC_{kin})_2$, $\Delta G^0 = 17.1$ kJ/mole, $K_{eq} = 10^{-3}$.

There is a change in free energy with the binding of successive molecules of DivK to each PleC monomer (reactions R5-R8 in **Table A.2**). We propose that each ΔG^0 should be a sum of the individual changes associated with DivK's role as a substrate or product and as an allosteric ligand. **Table A.3** lists the ΔG^0 values we assume for each effect. Formation of an enzyme-substrate complex, being a favorable reaction, has been assigned $\Delta G^0 \leq 0$. Enzyme-product complexes presumably dissociate, and hence have been assigned $\Delta G^0 > 0$. The free energy change when ligand binds to the R form ($PleC_{pho}$) has to be smaller than when it binds to the T form ($PleC_{kin}$). For the sake of simplicity, we set the drop in free energy associated with formation of RL_1 and RL_2 complexes to be 0. For the formation of TL_1 and TL_2 complexes, we assume that $\Delta G^0_{KL} = -14.25$ kJ/mole. Based on the ΔG^0 values in **Table A.3**, we assign free energy changes for the typical ligand binding reactions (R5-R8) in **Table A.2**.

Next, we use R5-R8 to calculate ΔG^0 values for all the binding reactions in our wiring diagram. For example, to calculate ΔG^0 for the reaction $(PleC_{pho}:DivK)_2 \rightarrow (PleC_{kin}:DivK)_2$, we notice that this reaction is equivalent to 2(R4 + R8 − R6), so ΔG^0 for the overall reaction is 2(8.55 – 19.95 − 11.4) = −45.6 kJ/mole. Similarly, we express $DivK{\sim}P:PleC_{pho}:PleC_{pho}:DivK \rightarrow DivK{\sim}P:PleC_{kin}:PleC_{kin}:DivK$ as the sum −R5 − R6 + 2R4 + R7 + R8, so ΔG^0 for the overall reaction is 0 – 11.4 + 17.1 – 8.55 – 19.95 = −22.8 kJ/mole. In like manner, ΔG^0 for the reaction $(PleC_{pho}:DivK{\sim}P)_2 \rightarrow (PleC_{kin}:DivK{\sim}P)_2$ is 0. All other binding reactions are treated the same way.

To make these ΔG^0 calculations easier, we can assign 'baseline' free energies to species ($\Delta G^\#_A$) such that $\Delta G^0 = \Delta G^\#_C + \Delta G^\#_D - \Delta G^\#_A - \Delta G^\#_B$. For example, if we assign a baseline free energy of 0 to $(PleC_{pho})_2$ and to DivK, then (see **Figure A.1**)

$\Delta G^\# = 17.1$ kJ/mole for $(PleC_{kin})_2$

$\Delta G^\# = 30$ kJ/mole for DivK~P

$\Delta G^\# = 11.4$ kJ/mole for $PleC_{pho}:PleC_{pho}:DivK$

$\Delta G^\# = 30$ kJ/mole for $PleC_{pho}:PleC_{pho}:DivK{\sim}P$

$\Delta G^\# = 41.4$ kJ/mole for $DivK:PleC_{pho}:PleC_{pho}:DivK{\sim}P$

From these free energies, we can calculate ΔG^0 for the phosphatase reaction (R9)

$PleC_{pho}$:$PleC_{pho}$:DivK~P + H_2O → $PleC_{pho}$:$PleC_{pho}$:DivK + P_i,

$\Delta G^0 = -18.6$ kJ/mole, $K_{eq} = 1.8\times10^3$.

In like manner, we assign baseline free energies to all the species in **Figure 2.1**.

To estimate ΔG^0 for phosphotransfer from $PleC_{kin}$~P to DivK (R10 in **Table A.2**), we consider the reaction cycle in **Figure A.3 B**. The net reaction of this cycle is

DivK + ATP → DivK~P + ADP, $\Delta G^0 = -20$ kJ/mole, $K_{eq} = 3.2\times10^3$.

At equilibrium (recalling that $a_{ATP} = a_{ADP} = 1$):

$$K_{eq} = \frac{k_{pk3-pk4}}{k_{pk4-pk3}} \cdot \frac{k_{pk4-pt4}}{k_{pt4-pk4}} \cdot \frac{k_{pt4-pk3h}}{k_{pk3h-pt4}} \cdot \frac{k_{pk3h-pk3}}{k_{pk3-pk3h}} = \frac{[\text{DivK}\sim\text{P}]}{[\text{DivK}]} = e^{20/2.48} \approx 3.2\times10^3$$

Using K_{eq} values from **Table A.2**,

$$3.2\times10^3 = (3162) \cdot \frac{k_{pt4\text{-}pk3h}}{k_{pk3h\text{-}pt4}} \cdot \left(\frac{1}{31.62}\right) \cdot (1),$$

we calculate the equilibrium constant for the phosphotransfer reaction to be

$PleC_{kin}$~P:DivK → $PleC_{kin}$:DivK~P, $K_{pt} = \frac{k_{pt4\text{-}pk3h}}{k_{pk3h\text{-}pt4}} = 32$, $\Delta G^0_{pt} = -8.6$ kJ/mole.

Finally, HK molecules undergo auto-dephosphorylation (R11 in **Table A.2**) in which the high-energy phosphoryl group (+50 kJ/mole) is hydrolyzed to give inorganic phosphate. In our model we set this to be an irreversible reaction because of the large free energy change accompanying the reaction.

We assume that PleD and PleD~P have similar baseline free energies as DivK and DivK~ P, respectively. Hence, the equilibrium constant for the phosphotransfer reaction is the same for PleD as for DivK:

$\Delta G^{\#} = 0$ kJ/mole for PleD

$\Delta G^{\#} = 30$ kJ/mole for PleD~P

$PleC_{kin}$~P:PleD → $PleC_{kin}$:PleD~P, $K_{pt} = 32$, $\Delta G^0_{pt} = -8.6$ kJ/mole.

A.1.3 Kinetic parameters used in the model.

The choice of parameter values is constrained by the fact that the ratio of the forward and reverse rate constants for any reaction is equal to its computed equilibrium constant. As a first approximation, for the main part of **Figure A.1**, we set the rate constant in the spontaneous direction to be 5 min^{-1}, and then set the rate constant in the reverse direction so that the ratio of rate constants = K_{eq}. This simple choice immediately generated bistability in the output of the HK switch (see **Figure 2.3** in the main text)

In order to get sufficient phosphorylation of PleD by $PleC_{kin}$, we made the PleD-associated rate constants 2 fold faster than the DivK-associated rate constants (see the lower part of **Figure A.1**).

Table A.4 and **A.5** lists the equations and parameters used in the model.

A.1.4 Model reduction

Our model of the DivJ-PleC-DivK system is comprised of 30 differential equations and 83 rate constants (**Table A.4** Eq.1-30). It contains necessary details regarding the three roles of PleC histidine kinase in autophosphorylation, phosphotransfer and phosphatase reactions. It incorporates a general understanding of enzyme-substrate reactions, allosteric theory and detailed balance, in order to formulate a reaction scheme that is consistent with both *in vivo* and *in vitro* experimental observations. Ultimately though, we admit that the full model is unwieldy, especially if it has to be integrated into a larger model describing other components of the gene/protein regulatory network controlling the asymmetric division cycle of *Caulobacter*. Therefore, we propose a reduced model (**Figure A.4**), based on the following reasonable assumptions. In **Figure A.5** we plot one-parameter bifurcation diagrams for the reduced model in order to show that its behavior is comparable to the full model.

Assumption 1. We have eliminated those components of the full model (namely, $PleC_{kin}$, $PleC_{pt3h}$ and $PleC_{kin}$:DivK) that are present at concentrations below 0.01.

Assumption 2. We assumed that other components ($PleC_{ph1p}$ and $PleC_{ph2p}$) are always at steady state values:

$$[\mathrm{PleC_{ph1p}}]_{ss} = \frac{k_{\mathrm{pk1p-ph1p}} \cdot [\mathrm{PleC_{kin1p}}]}{k_{\mathrm{ph1p-pc}} + k_{\mathrm{ph1p-pk1p}}} \text{ and } [\mathrm{PleC_{ph2p}}]_{ss} = \frac{k_{\mathrm{pk2p-h2p}} \cdot [\mathrm{PleC_{kin1p}}]}{k_{\mathrm{ph2p-pc}} + k_{\mathrm{ph2p-pk2p}}}$$

Substituting these relationships into Eqs. 21 and 22 of **Table A.4** gives the following modified equations and parameters (see also **Tables A.6** and **A.7**):

$$\frac{d[\mathrm{PleC_{kin1p}}]}{dt} = -k_{\mathrm{pk1p-pc}} \cdot [\mathrm{PleC_{kin1p}}] + \textit{other terms} \qquad k_{\mathrm{pk1p-pc}} = \frac{k_{\mathrm{pk1p-ph1p}} + k_{\mathrm{ph1p-pc}}}{k_{\mathrm{ph1p-pk1p}}}$$

$$\frac{d[\mathrm{PleC_{kin2p}}]}{dt} = -k_{\mathrm{pk2p-pc}} \cdot [\mathrm{PleC_{kin2p}}] + \textit{other terms} \qquad k_{\mathrm{pk2p-pc}} = \frac{k_{\mathrm{pk2p-ph2p}} + k_{\mathrm{ph2p-pc}}}{k_{\mathrm{ph2p-pk2p}}}$$

Assumption 3. The reaction $\mathrm{PleC_{ph11}} \leftrightarrow \mathrm{PleC_{kin11}}$ is at equilibrium, so we combined the two variables into a single modified variable $\mathrm{PleC_{kin11}}$. The modified differential equation and parameters for $\mathrm{PleC_{kin11}}$ is given in **Table A.6** and **A.7**.

Assumption 4. $\mathrm{PleC_{ph22}}$ was also assumed to be at steady state:

$$[\mathrm{PleC_{ph22}}]_{ss} = \frac{k_{\mathrm{ph2-ph22}} \cdot [\mathrm{PleC_{ph2}}] \cdot [\mathrm{DivK}] + k_{\mathrm{pk22-ph22}} \cdot [\mathrm{PleC_{kin22}}]}{k_{\mathrm{ph22-ph2}} + k_{\mathrm{ph22-pk22}}}$$

Substituting this expression into Equations 2, 5 & 11 of **Table A.4** gives the following modified equations and parameters (see also **Table A.6** and **A.7**):

$$\frac{d[\mathrm{PleC_{ph2}}]}{dt} = -k_{\mathrm{ph2-pk22}} \cdot [\mathrm{PleC_{ph2}}] \cdot [\mathrm{DivK}] + k_{\mathrm{pk22-ph2}} \cdot [\mathrm{PleC_{kin22}}] + \textit{other terms}$$

$$\frac{d[\mathrm{PleC_{kin22}}]}{dt} = k_{\mathrm{ph2-pk22}} \cdot [\mathrm{PleC_{ph2}}] \cdot [\mathrm{DivK}] - k_{\mathrm{pk22-ph2}} \cdot [\mathrm{PleC_{kin22}}] + \textit{other terms}$$

$$\frac{d[\mathrm{DivK}]}{dt} = -k_{\mathrm{ph2-pk22}} \cdot [\mathrm{PleC_{ph2}}] \cdot [\mathrm{DivK}] + k_{\mathrm{pk22-ph2}} \cdot [\mathrm{PleC_{kin22}}] + \textit{other terms}$$

$$k_{\mathrm{ph2-pk22}} = \frac{k_{\mathrm{ph2-ph22}} \cdot k_{\mathrm{ph22-pk22}}}{k_{\mathrm{ph22-ph2}} + k_{\mathrm{ph22-pk22}}} \qquad k_{\mathrm{pk22-ph2}} = \frac{k_{\mathrm{pk22-ph22}} \cdot k_{\mathrm{ph22-ph2}}}{k_{\mathrm{ph22-ph2}} + k_{\mathrm{ph22-pk22}}}$$

Assumption 5. In a similar fashion, we made a steady-state approximation for $\mathrm{PleC_{ph12}}$:

$$[\mathrm{PleC_{ph12}}]_{ss} = \frac{k_{\mathrm{ph2-ph12}} \cdot [\mathrm{PleC_{ph2}}] \cdot [\mathrm{DivK{\sim}P}] + k_{\mathrm{ph1-ph12}} \cdot [\mathrm{PleC_{ph1}}] \cdot [\mathrm{DivK}] + k_{\mathrm{pk12-ph12}} \cdot [\mathrm{PleC_{kin22}}]}{k_{\mathrm{ph12-ph2}} + k_{\mathrm{ph12-pk12}} + k_{\mathrm{ph12-ph2}}}$$

$$k_{\mathrm{ph1-pk12}} = \frac{k_{\mathrm{ph1-ph12}} \cdot k_{\mathrm{ph12-pk12}}}{k_{\mathrm{ph12-ph1}} + k_{\mathrm{ph12-ph2}} + k_{\mathrm{ph12-pk12}}} \qquad k_{\mathrm{pk12-ph1}} = \frac{k_{\mathrm{pk12-ph12}} \cdot k_{\mathrm{ph12-ph1}}}{k_{\mathrm{ph12-ph1}} + k_{\mathrm{ph12-ph2}} + k_{\mathrm{ph12-pk12}}}$$

$$k_{\mathrm{ph2-pk12}} = \frac{k_{\mathrm{ph2-ph12}} \cdot k_{\mathrm{ph12-pk12}}}{k_{\mathrm{ph12-ph1}} + k_{\mathrm{ph12-ph2}} + k_{\mathrm{ph12-pk12}}} \qquad k_{\mathrm{pk12-pk12}} = \frac{k_{\mathrm{pk12-ph12}} \cdot k_{\mathrm{ph12-ph2}}}{k_{\mathrm{ph12-ph1}} + k_{\mathrm{ph12-ph2}} + k_{\mathrm{ph12-pk12}}}$$

$$k_{\mathrm{h1-h2}} = \frac{k_{\mathrm{ph1-ph12}} \cdot k_{\mathrm{ph12-ph2}}}{k_{\mathrm{ph12-ph1}} + k_{\mathrm{ph12-ph2}} + k_{\mathrm{ph12-pk12}}} \qquad k_{\mathrm{h2-h1}} = \frac{k_{\mathrm{ph2-ph12}} \cdot k_{\mathrm{ph12-ph1}}}{k_{\mathrm{ph12-ph1}} + k_{\mathrm{ph12-ph2}} + k_{\mathrm{ph12-pk12}}}$$

These changes propagate to the differential equations for $PleC_{kin12}$, $PleC_{ph2}$, $PleC_{ph1}$, DivK and DivK~P, as documented in **Table A.6**.

A.2 References

1. Stewart RC (2010) Protein histidine kinases: assembly of active sites and their regulation in signaling pathways. Current Opinion in Microbiology 13: 133–141. Available: http://www.pubmedcentral.nih.gov/articlerender.fcgi?artid=2847664&tool=pmcentrez&rendertype=abstract.

2. Perego M, Hoch JA (1996) Protein aspartate phosphatases control the output of two-component signal transduction systems. Trends in Genetics 12: 97–101. Available: http://www.ncbi.nlm.nih.gov/pubmed/8868347.

3. Georgellis D, Kwon O, De Wulf P, Lin EC (1998) Signal decay through a reverse phosphorelay in the Arc two-component signal transduction system. The Journal of Biological Chemistry 273: 32864–32869. Available: http://www.ncbi.nlm.nih.gov/pubmed/9830034.

4. Paul R, Jaeger T, Abel S, Wiederkehr I, Folcher M, et al. (2008) Allosteric regulation of histidine kinases by their cognate response regulator determines cell fate. Cell 133: 452–461. Available: http://www.pubmedcentral.nih.gov/articlerender.fcgi?artid=2804905&tool=pmcentrez&rendertype=abstract.

5. Ohta N, Newton A (2003) The Core Dimerization Domains of Histidine Kinases Contain Recognition Specificity for the Cognate Response Regulator. Journal of bacteriology 185: 4424–4431. Available: http://jb.asm.org/content/185/15/4424.abstract

6. Wang SP, Sharma PL, Schoenlein P V, Ely B (1993) A histidine protein kinase is involved in polar organelle development in *Caulobacter crescentus*. Proceedings of the National Academy of Sciences of the United States of America 90: 630–634. Available: http://www.pubmedcentral.nih.gov/articlerender.fcgi?artid=45717&tool=pmcentrez&rendertype=abstract.

7. Rubin MM, Changeux JP (1966) On the nature of allosteric transitions: implications of non-exclusive ligand binding. Journal of Molecular Biology 21: 265–274. Available: http://www.ncbi.nlm.nih.gov/pubmed/5972463.

8. Koshland DE Jr, Nemethy G, FIlmer D: Comparison of experimental binding data and theoretical models in protein containing subunits. (1965) Biochemistry 5: 365–385. Available: http://pubs.acs.org/doi/abs/10.1021/bi00865a047

9. Changeux J-P (2011) Allostery and the Monod-Wyman-Changeux Model After 50 Years. Annual review of biophysics 41: 103–133. Available: http://www.ncbi.nlm.nih.gov/pubmed/22224598.

10. Stock AM, Robinson VL, Goudreau PN (2000) Two-component signal transduction. Annual Review of Biochemistry 69: 183–215. Available: http://www.ncbi.nlm.nih.gov/pubmed/10966457.

11. Perry J, Koteva K, Wright G (2011) Receptor domains of two-component signal transduction systems. Molecular Biosystems 7: 1388–1398. Available: http://www.ncbi.nlm.nih.gov/pubmed/21347487.

12. Wylie D, Stock A, Wong CY, Stock J (1988) Sensory transduction in bacterial chemotaxis involves phosphotransfer between Che proteins. Biochemical and Biophysical Research Communications 151: 891–896. Available: http://linkinghub.elsevier.com/retrieve/pii/S0006291X88803656.

13. Tawa P, Stewart RC (1994) Kinetics of CheA autophosphorylation and dephosphorylation reactions. Biochemistry 33: 7917–7924. Available: http://www.ncbi.nlm.nih.gov/pubmed/8011654.

14. Borkovich KA, Kaplan N, Hess JF, Simon MI (1989) Transmembrane signal transduction in bacterial chemotaxis involves ligand-dependent activation of phosphate group transfer. Proceedings of the National Academy of Sciences of the United States of America 86: 1208–1212. Available: http://www.pubmedcentral.nih.gov/articlerender.fcgi?artid=286655&tool=pmcentrez&rendertype=abstract.

15. Levit MN, Liu Y, Stock JB (1999) Mechanism of CheA protein kinase activation in receptor signaling complexes. Biochemistry 38: 6651–6658. Available: http://www.ncbi.nlm.nih.gov/pubmed/10350484.

16. Stock J, Da Re S (2000) Signal transduction: response regulators on and off. Current Biology 10: R420–R424. Available: http://www.ncbi.nlm.nih.gov/pubmed/10837243

A.3 Supplementary Figures

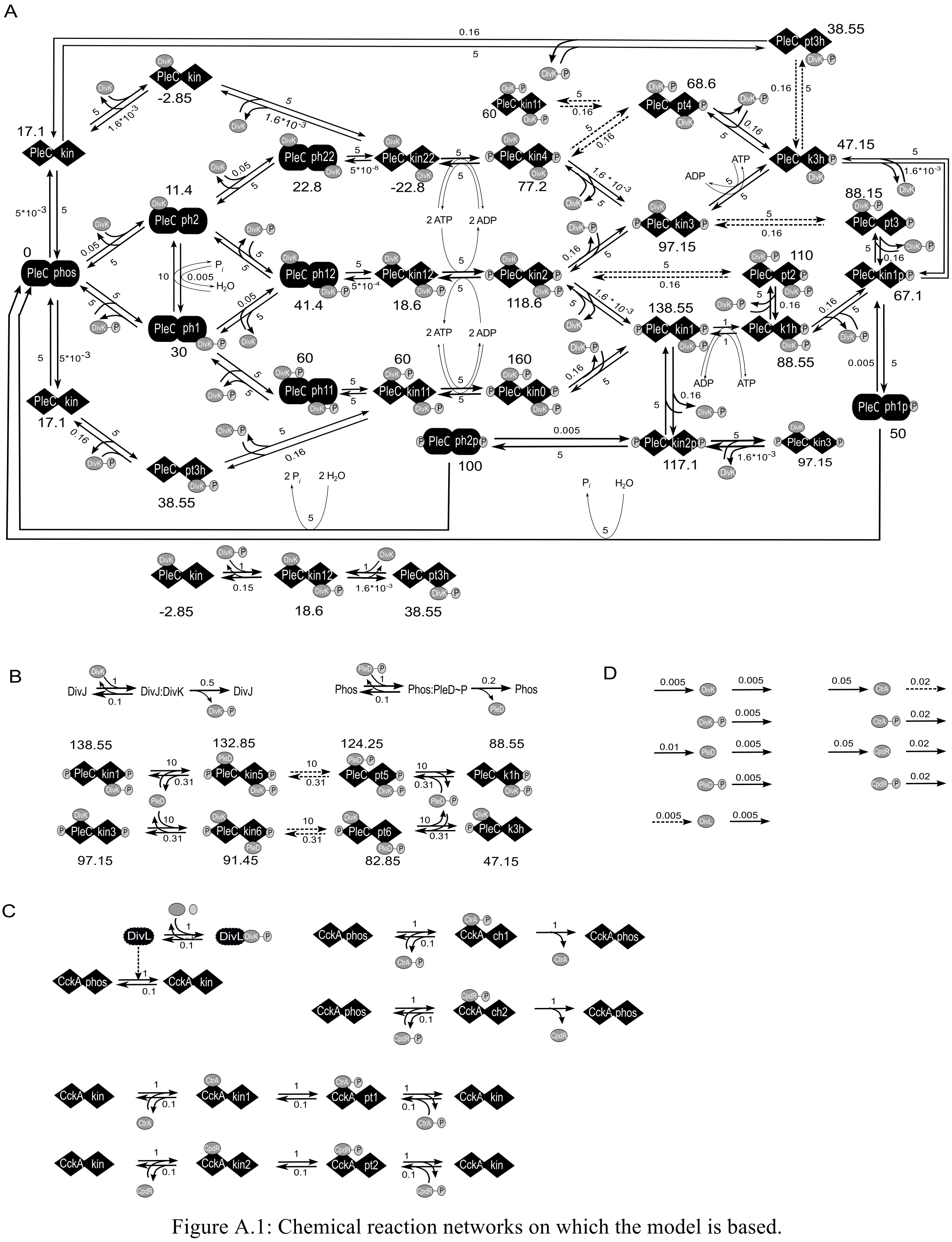

Figure A.1: Chemical reaction networks on which the model is based.

(A) PleC-DivK system. (B) DivJ-DivK and PleC-PleD system. (C) DivL-CckA-CtrA-CpdR system. (D) Synthesis and degradation of proteins. See Table A.1 for definitions of the protein complexes appearing in these figures.

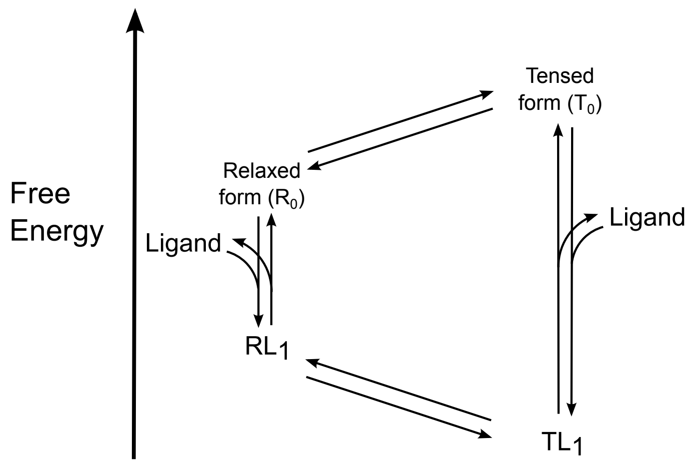

Figure A.2: Schematic diagram of the free energy differences between the relaxed and tensed states of the free and ligand-bound enzyme.

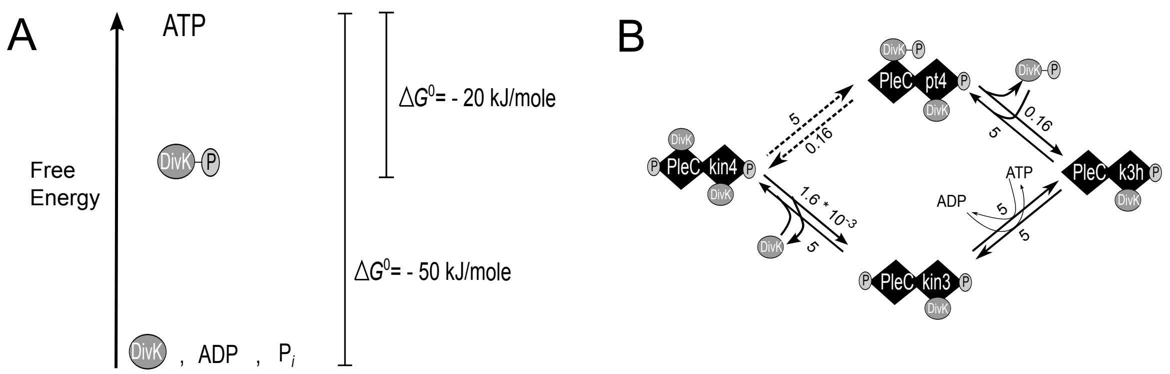

Figure A.3: (A) Baseline free energies assigned to intermediates in our model. (B) The common motif for all phospho-transfer reactions in our model.

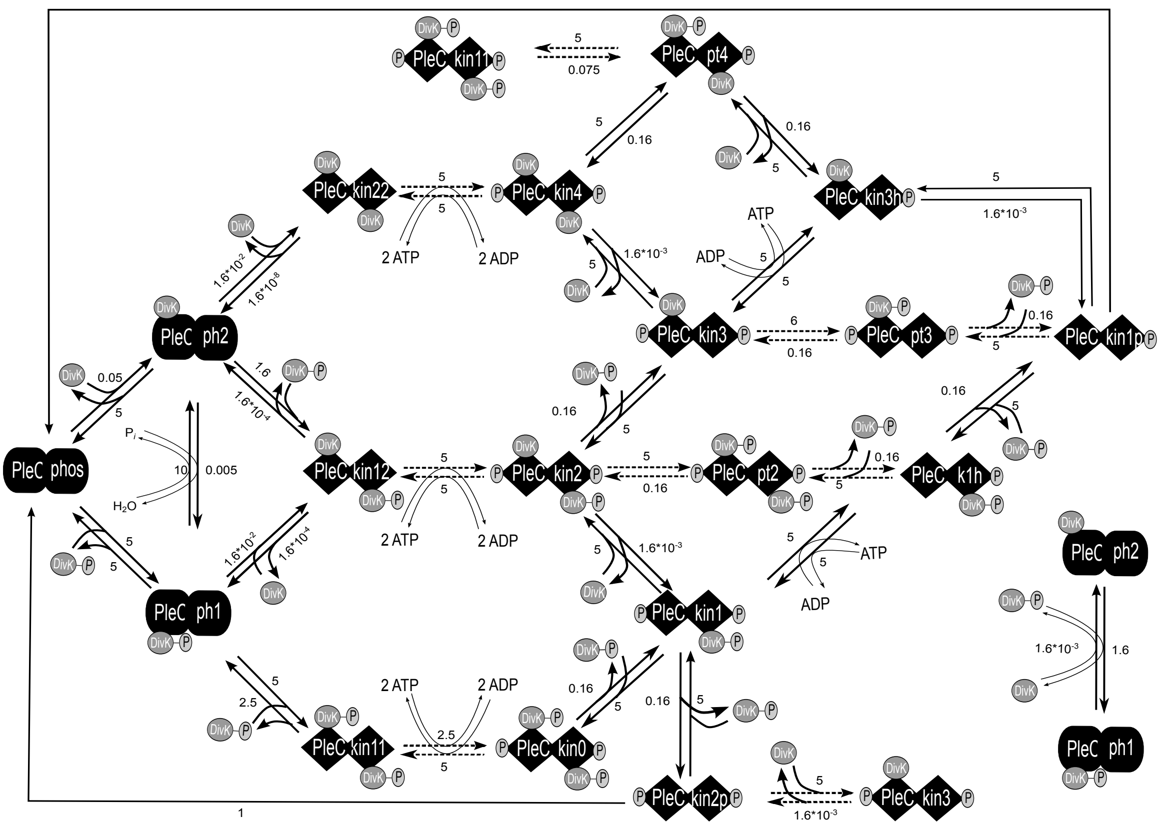

Figure A.4: Wiring diagram illustrating the elementary chemical reactions in the reduced model.

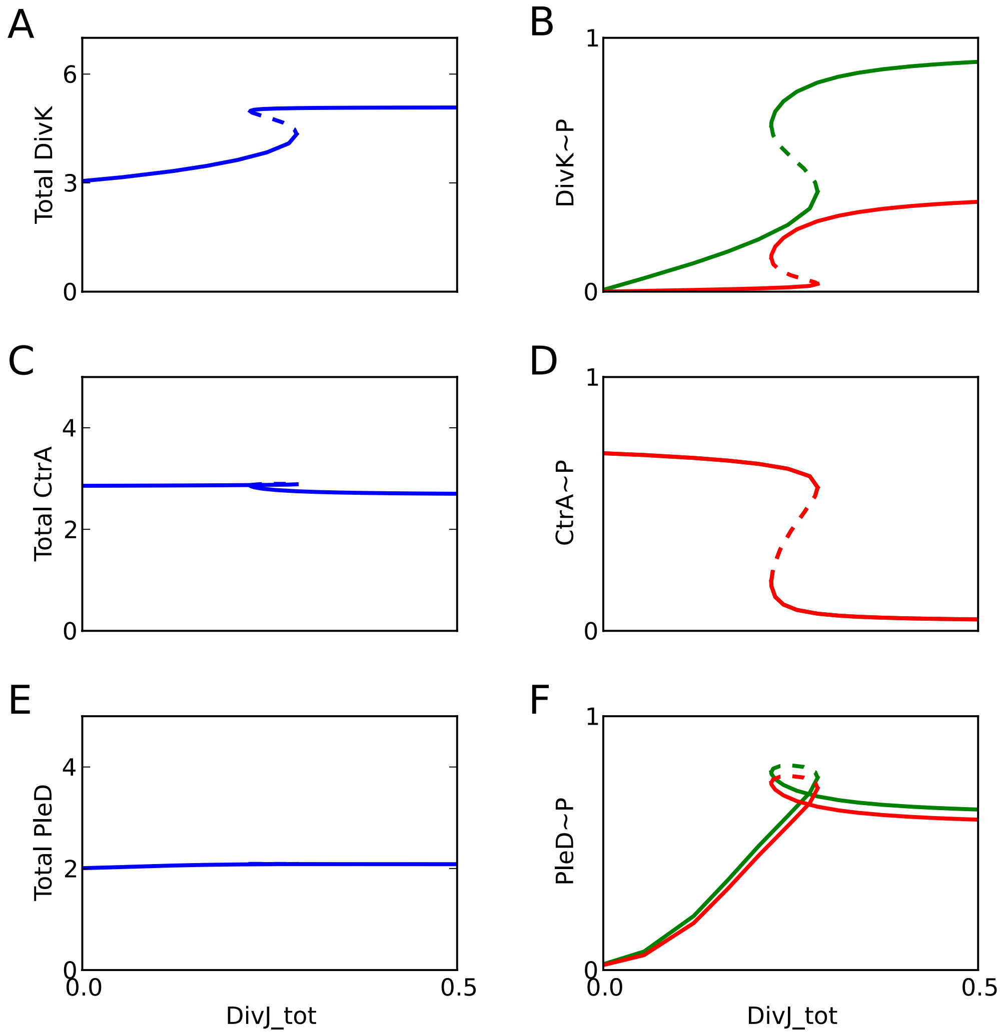

Figure A.5: Bistability properties of the reduced version of the DivJ-PleC-DivK model are similar to the full-sized model.

The one-parameter bifurcation diagrams compare the steady state values of (A) PleC kinase, (B) DivK~P, and (C) PleD~P between the full-sized (blue line) and reduced (green line) versions of the model.

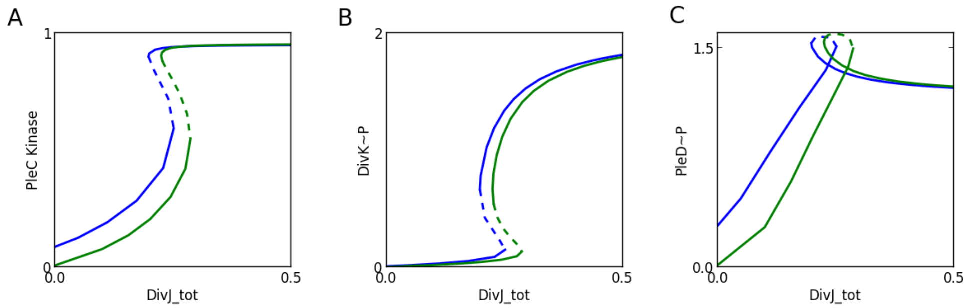

Figure A.6: The swarmer-to-stalked transition is accompanied by modest changes to the total concentrations of regulatory proteins but significant changes to their phosphorylation states.

The one-parameter bifurcation diagrams on the left show the total concentration of (A) DivK, (C) CtrA, and (E) PleD as functions of total DivJ. On the right, the one-parameter bifurcation diagrams show the phosphorylated fraction of the total concentration for (B) DivK, (D) CtrA, and (F) PleD. Red line, fraction that is phosphorylated and free; green line, phosphorylated fraction both free and bound.

A.4 Supplementary Tables

Table A.1**:** Description of species in the model with their abbreviated names.

Figure abbreviations	Complete description	Parameter abbreviation
DivK~P		dk
DivK		dkp
PleC	PleC:PleC	pc
$PleC_{ph1}$	PleC:PleC:DivK~P	ph1
$PleC_{ph2}$	PleC:PleC:DivK	ph2
$PleC_{ph11}$	DivK~P:PleC:PleC:DivK~P (phosphatase)	ph11
$PleC_{ph12}$	DivK:PleC:PleC:DivK~P (phosphatase)	ph12
$PleC_{ph22}$	DivK:PleC:PleC:DivK (phosphatase)	ph22
$PleC_{kin11}$	DivK~P: PleC:PleC: DivK~P (kinase)	pk11
$PleC_{kin12}$	DivK: PleC:PleC: DivK~P (kinase)	pk12
$PleC_{kin22}$	DivK:PleC: PleC: DivK (kinase)	pk22
$PleC_{kin0}$	DivK~P: PleC~P:PleC~P: DivK~P	pk0
$PleC_{kin2}$	DivK: PleC~P:PleC~P: DivK~P	pk2
$PleC_{kin4}$	DivK: PleC~P:PleC~P: DivK	pk4
$PleC_{kin1}$	PleC~P:PleC~P: DivK~P	pk1
$PleC_{kin3}$	PleC~P:PleC~P: DivK	pk3
$PleC_{pt2}$	DivK~P: PleC:PleC~P: DivK~P	pt2
$PleC_{pt3}$	PleC~P:PleC: DivK~P	pt3
$PleC_{pt4}$	DivK:PleC~P:PleC: DivK~P	pt4
$PleC_{k1h}$	PleC:PleC~P: DivK~P	pk1h
$PleC_{k3h}$	DivK:PleC~P:PleC	pk3h
$PleC_{pt3h}$	DivK~P:PleC:PleC	pt3h
$PleC_{kin1p}$	PleC:PleC~P (kinase form)	pk1p
$PleC_{kin2p}$	PleC~P:PleC~P (kinase form)	pk2p
$PleC_{ph1p}$	PleC:PleC~P (phosphatase form)	ph1p
$PleC_{ph2p}$	PleC~P:PleC~P (phosphatase form)	ph2p
$PleC_{kin}$	PleC:PleC (kinase)	pck

$PleC_{pkdk}$	PleC:PleC:DivK	pkdk
PleD		pld
PleD~P		pldp
$PleC_{kin5}$	DivK~P:PleC~P:PleC~P:PleD	pk5
$PleC_{kin6}$	DivK:PleC~P:PleC~P:PleD	pk6
$PleC_{pt5}$	DivK~P:PleC~P:PleC:PleD~P	pt5
$PleC_{pt6}$	DivK:PleC~P:PleC:PleD~P	pt6
DivJ		dj
DivK:DivK		jk
DivL		dl
DivL:DivK~P	DivL:DivK~P	dldk
CtrA		ctr
CtrA~P		ctrp
CpdR		cpd
CpdR~P		cpdp
$CckA_{kin}$		ck
$CckA_{phos}$		cp
$CckA_{kin1}$	CckA~P:CtrA	ck1
$CckA_{kin2}$	CckA~P:CpdR	ck2
$CckA_{ct1}$	CckA:CtrA~P (kinase)	ct1
$CckA_{ct2}$	CckA:CpdR~P (kinase)	ct2
$CckA_{ph1}$	CckA:CtrA~P (phosphatase)	ch1
$CckA_{ph2}$	CckA:CpdR~P (phosphatase)	ch2

Table A.2: Representative reactions in the model.

Phosphorylation reactions			
$ADP + P_i \rightarrow ATP + H_2O$	$\Delta G^0_{ATP} = +50$ kJ/mole		(R1)
$PleC_{kin} + P_i \rightarrow PleC_{kin}{\sim}P + H_2O$	$\Delta G^0_{PleC\sim P} = +50$ kJ/mole		(R2)
$DivK + P_i \rightarrow DivK{\sim}P + H_2O$	$\Delta G^0_{DivK\sim P} = +30$ kJ/mole		(R3)
$R_0 \rightarrow T_0$ reaction			
$PleC_{pho} \rightarrow PleC_{kin}$	$\Delta G^0_{RT} = +8.55$ kJ/mole	$K_{eq} = 0.0316$	(R4)
Typical ligand binding reactions			
$PleC_{pho} + DivK{\sim}P \rightarrow PleC_{pho}: DivK{\sim}P$	$\Delta G^0_{HS} + \Delta G^0_{HL} = 0$ kJ/mole	$K_{eq} = 1$	(R5)
$PleC_{pho} + DivK \rightarrow PleC_{pho}: DivK$	$\Delta G^0_{HP} + \Delta G^0_{HL} = +11.4$ kJ/mole	$K_{eq} = 0.01$	(R6)
$PleC_{kin} + DivK{\sim}P \rightarrow PleC_{kin}: DivK{\sim}P$	$\Delta G^0_{KP} + \Delta G^0_{KL} = -8.55$ kJ/mole	$K_{eq} = 31.6$	(R7)
$PleC_{kin} + DivK \rightarrow PleC_{kin}: DivK$	$\Delta G^0_{KS} + \Delta G^0_{KL} = -19.95$ kJ/mole	$K_{eq} = 3160$	(R8)
Phosphatase reaction			
$PleC_{pho}: DivK{\sim}P + H_2O \rightarrow PleC_{pho}: DivK + P_i$	$\Delta G^0_{ph} = -18.6$ kJ/mole	$K_{eq} = 1830$	(R9)
Phosphotransfer reaction			
$PleC_{kin}{\sim}P: DivK \rightarrow PleC_{kin}: DivK{\sim}P$	$\Delta G^0_{pt} = -8.6$ kJ/mole	$K_{eq} = 32$	(R10)
Auto-dephosphorylation reaction			
$PleC_{pho}{\sim}P + H_2O \rightarrow PleC_{pho} + P_i$	$\Delta G^0_{ad} = -50$ kJ/mole	irreversible	(R11)

Table A.3: Gibbs free energy change for DivK binding to PleC.

Formation of phosphatase-substrate complex	$\Delta G^0_{\mathrm{HS}} = 0$ kJ/mole	$K_{\mathrm{eq}} = 1$
Formation of kinase-substrate complex	$\Delta G^0_{\mathrm{KS}} = -5.7$ kJ/mole	$K_{\mathrm{eq}} = 10$
Formation of phosphatase-product complex	$\Delta G^0_{\mathrm{HP}} = +11.4$ kJ/mole	$K_{\mathrm{eq}} = 0.01$
Formation of kinase-product complex	$\Delta G^0_{\mathrm{KP}} = +5.7$ kJ/mole	$K_{\mathrm{eq}} = 0.1$
Ligand binding to phosphatase (relaxed form)	$\Delta G^0_{\mathrm{HL}} = 0$ kJ/mole	$K_{\mathrm{eq}} = 1$
Ligand binding to kinase (tensed form)	$\Delta G^0_{\mathrm{KL}} = -14.25$ kJ/mole	$K_{\mathrm{eq}} = 316$

Table A.4**:** Equations governing the full model*.

$$
\begin{aligned}
\frac{\mathrm{d}[\mathrm{DivK{\sim}P}]}{\mathrm{d}t} = & -k_{\mathrm{deg-dkp}} \cdot [\mathrm{DivK{\sim}P}] - k_{\mathrm{pc-ph1}} \cdot [\mathrm{PleC}] \cdot [\mathrm{DivK{\sim}P}] + k_{\mathrm{ph1-pc}} \cdot [\mathrm{PleC_{ph1}}] \\
& - k_{\mathrm{ph1-ph11}} \cdot [\mathrm{PleC_{ph1}}] \cdot [\mathrm{DivK{\sim}P}] + k_{\mathrm{ph11-ph1}} \cdot [\mathrm{PleC_{ph11}}] \\
& - k_{\mathrm{ph2-ph12}} \cdot [\mathrm{PleC_{ph2}}] \cdot [\mathrm{DivK{\sim}P}] + k_{\mathrm{ph12-ph2}} \cdot [\mathrm{PleC_{ph12}}] \\
& - k_{\mathrm{pk1-pk0}} \cdot [\mathrm{PleC_{kin1}}] \cdot [\mathrm{DivK{\sim}P}] + k_{\mathrm{pk0-pk1}} \cdot [\mathrm{PleC_{kin0}}] \\
& - k_{\mathrm{pk3-pk2}} \cdot [\mathrm{PleC_{kin3}}] \cdot [\mathrm{DivK{\sim}P}] + k_{\mathrm{pk2-pk3}} \cdot [\mathrm{PleC_{kin2}}] \\
& + k_{\mathrm{pt2-pk1h}} \cdot [\mathrm{PleC_{pt2}}] - k_{\mathrm{pk1h-pt2}} \cdot [\mathrm{PleC_{kin1h}}] \cdot [\mathrm{DivK{\sim}P}] \\
& - k_{\mathrm{pk2p-pk1}} \cdot [\mathrm{PleC_{kin2p}}] \cdot [\mathrm{DivK{\sim}P}] + k_{\mathrm{pk1-pk2p}} \cdot [\mathrm{PleC_{kin1}}] \\
& - k_{\mathrm{pk1p-1h}} \cdot [\mathrm{PleC_{kin1p}}] \cdot [\mathrm{DivK{\sim}P}] + k_{\mathrm{1h-pk1p}} \cdot [\mathrm{PleC_{kin1h}}] \\
& + k_{\mathrm{pt3-pk1p}} \cdot [\mathrm{PleC_{pt3}}] - k_{\mathrm{pk1p-pt3}} \cdot [\mathrm{PleC_{kin1p}}] \cdot [\mathrm{DivK{\sim}P}] \\
& + k_{\mathrm{e-jk}} \cdot [\mathrm{DivJ{:}\,DivK}] - k_{\mathrm{pck-pt3h}} \cdot [\mathrm{PleC_{kin}}] \cdot [\mathrm{DivK{\sim}P}] \\
& + k_{\mathrm{pt3h-pck}} \cdot [\mathrm{PleC_{pt3h}}] - k_{\mathrm{pkdk-pk12}} \cdot [\mathrm{PleC_{pkdk}}] \cdot [\mathrm{DivK{\sim}P}] \\
& + k_{\mathrm{pk12-pkdk}} \cdot [\mathrm{PleC_{kin12}}] - k_{\mathrm{pt3h-pk11}} \cdot [\mathrm{PleC_{pt3h}}] \cdot [\mathrm{DivK{\sim}P}] \\
& + k_{\mathrm{pk11-pt3h}} \cdot [\mathrm{PleC_{kin11}}] - k_{\mathrm{pk3h-pt4}} \cdot [\mathrm{PleC_{kin3h}}] \cdot [\mathrm{DivK{\sim}P}] \\
& + k_{\mathrm{pt4-pk3h}} \cdot [\mathrm{PleC_{pt4}}] - k_{\mathrm{dl-dldk}} \cdot [\mathrm{DivL}] \cdot [\mathrm{DivK{\sim}P}] \\
& + k_{\mathrm{dldk-dl}} \cdot [\mathrm{DivL{:}\,DivK{\sim}P}] \qquad (1)
\end{aligned}
$$

$$\frac{d[\mathrm{DivK}]}{dt} = k_{syn-\mathrm{dk}} - k_{\mathrm{deg-dk}} \cdot [\mathrm{DivK}] - k_{\mathrm{pc-ph2}} \cdot [\mathrm{PleC}] \cdot [\mathrm{DivK}] + k_{\mathrm{ph2-pc}} \cdot [\mathrm{PleC_{ph2}}]$$
$$- k_{\mathrm{ph2-ph22}} \cdot [\mathrm{PleC_{ph2}}] \cdot [\mathrm{DivK}] + k_{\mathrm{ph22-ph2}} \cdot [\mathrm{PleC_{ph22}}]$$
$$- k_{\mathrm{ph1-ph12}} \cdot [\mathrm{PleC_{h1}}] \cdot [\mathrm{DivK}] + k_{\mathrm{ph12-ph1}} \cdot [\mathrm{PleC_{ph12}}]$$
$$- k_{\mathrm{pk1-pk2}} \cdot [\mathrm{PleC_{kin1}}] \cdot [\mathrm{DivK}] + k_{\mathrm{pk2-pk1}} \cdot [\mathrm{PleC_{kin2}}]$$
$$- k_{\mathrm{pk3-pk4}} \cdot [\mathrm{PleC_{kin3}}] \cdot [\mathrm{DivK}] + k_{\mathrm{pk4-pk3}} \cdot [\mathrm{PleC_{kin4}}]$$
$$- k_{\mathrm{pk2p-pk3}} \cdot [\mathrm{PleC_{pk2p}}] \cdot [\mathrm{DivK}] + k_{\mathrm{pk3-pk2p}} \cdot [\mathrm{PleC_{kin3}}]$$
$$- k_{\mathrm{j-jk}} \cdot [\mathrm{DivJ}] \cdot [\mathrm{DivK}] + k_{\mathrm{jk-j}} \cdot [\mathrm{DivJ:DivK}] - k_{\mathrm{pk1p-pk3h}} \cdot [\mathrm{PleC_{kin1p}}] \cdot [\mathrm{DivK}]$$
$$+ k_{\mathrm{pk3h-1p}} \cdot [\mathrm{PleC_{kin3h}}] - k_{\mathrm{pkdk-pk22}} \cdot [\mathrm{PleC_{pkdk}}] \cdot [\mathrm{DivK}]$$
$$+ k_{\mathrm{pk22-pkdk}} \cdot [\mathrm{PleC_{kin22}}] - k_{\mathrm{pck-pkdk}} \cdot [\mathrm{PleC_{kin}}] \cdot [\mathrm{DivK}]$$
$$+ k_{\mathrm{pkdk-pck}} \cdot [\mathrm{PleC_{pkdk}}] - k_{\mathrm{pt3h-pk12}} \cdot [\mathrm{PleC_{pt3h}}] \cdot [\mathrm{DivK}]$$
$$+ k_{\mathrm{pk12-pt3h}} \cdot [\mathrm{PleC_{kin12}}] \tag{2}$$

$$\frac{d[\mathrm{PleC}]}{dt} = - k_{\mathrm{pc-ph2}} \cdot [\mathrm{PleC}] \cdot [\mathrm{DivK}] + k_{\mathrm{ph2-pc}} \cdot [\mathrm{PleC_{ph2}}] - k_{\mathrm{pc-ph1}} \cdot [\mathrm{PleC}] \cdot [\mathrm{DivK{\sim}P}]$$
$$+ k_{\mathrm{ph1-pc}} \cdot [\mathrm{PleC_{ph1}}] + k_{\mathrm{ph2p-pc}} \cdot [\mathrm{PleC_{ph2p}}] + k_{\mathrm{ph1p-pc}} \cdot [\mathrm{PleC_{ph1p}}]$$
$$- k_{\mathrm{pch-pck}} \cdot [\mathrm{PleC}] + k_{\mathrm{pck-pch}} \cdot [\mathrm{PleC_{kin}}] \tag{3}$$

$$\frac{d[\mathrm{PleC_{ph1}}]}{dt} = k_{\mathrm{pc-ph1}} \cdot [\mathrm{PleC}] \cdot [\mathrm{DivK{\sim}P}] - k_{\mathrm{ph1-pc}} \cdot [\mathrm{PleC_{h1}}] - k_{\mathrm{ph1-ph11}} \cdot [\mathrm{PleC_{h1}}] \cdot [\mathrm{DivK{\sim}P}]$$
$$+ k_{\mathrm{ph11-ph1}} \cdot [\mathrm{PleC_{h11}}] - k_{\mathrm{ph1-ph12}} \cdot [\mathrm{PleC_{ph1}}] \cdot [\mathrm{DivK}] + k_{\mathrm{ph12-ph1}} \cdot [\mathrm{PleC_{ph12}}]$$
$$- k_{\mathrm{ph1-ph2}} \cdot [\mathrm{PleC_{h1}}] + k_{\mathrm{ph2-ph1}} \cdot [\mathrm{PleC_{ph2}}] \tag{4}$$

$$\frac{d[\mathrm{PleC_{ph2}}]}{dt} = k_{\mathrm{pc-ph2}} \cdot [\mathrm{PleC}] \cdot [\mathrm{DivK}] - k_{\mathrm{ph2-pc}} \cdot [\mathrm{PleC_{ph2}}] - k_{\mathrm{ph2-ph22}} \cdot [\mathrm{PleC_{ph2}}] \cdot [\mathrm{DivK}]$$
$$+ k_{\mathrm{ph22-ph2}} \cdot [\mathrm{PleC_{h22}}] - k_{\mathrm{ph2-ph12}} \cdot [\mathrm{PleC_{ph2}}] \cdot [\mathrm{DivK{\sim}P}]$$
$$+ k_{\mathrm{ph12-ph2}} \cdot [\mathrm{PleC_{ph12}}] + k_{\mathrm{ph1-ph2}} \cdot [\mathrm{PleC_{ph1}}] - k_{\mathrm{ph2-ph1}} \cdot [\mathrm{PleC_{ph2}}] \tag{5}$$

$$\frac{d[\mathrm{PleC_{ph11}}]}{dt} = k_{\mathrm{ph1-ph11}} \cdot [\mathrm{PleC_{ph1}}] \cdot [\mathrm{DivK{\sim}P}] - k_{\mathrm{ph11-ph1}} \cdot [\mathrm{PleC_{ph11}}]$$
$$- k_{\mathrm{ph1-pk11}} \cdot [\mathrm{PleC_{ph11}}] + k_{\mathrm{pk11-ph11}} \cdot [\mathrm{PleC_{kin11}}] \tag{6}$$

$$\frac{d[\mathrm{PleC_{ph12}}]}{dt} = k_{\mathrm{ph1-ph12}} \cdot [\mathrm{PleC_{ph1}}] \cdot [\mathrm{DivK}] - k_{\mathrm{ph12-ph1}} \cdot [\mathrm{PleC_{ph12}}]$$
$$+ k_{\mathrm{ph2-ph12}} \cdot [\mathrm{PleC_{ph2}}] \cdot [\mathrm{DivK{\sim}P}] - k_{\mathrm{ph12-ph2}} \cdot [\mathrm{PleC_{ph12}}]$$
$$- k_{\mathrm{ph12-pk12}} \cdot [\mathrm{PleC_{ph12}}] + k_{\mathrm{pk12-ph12}} \cdot [\mathrm{PleC_{kin12}}] \tag{7}$$

$$\frac{\mathrm{d}[\mathrm{PleC_{ph22}}]}{\mathrm{d}t} = k_{\mathrm{ph2-ph22}} \cdot [\mathrm{PleC_{ph2}}] \cdot [\mathrm{DivK}] - k_{\mathrm{ph22-ph2}} \cdot [\mathrm{PleC_{ph22}}] - k_{\mathrm{ph22-pk22}} \cdot [\mathrm{PleC_{ph22}}] + k_{\mathrm{pk22-ph22}} \cdot [\mathrm{PleC_{kin22}}] \quad (8)$$

$$\frac{\mathrm{d}[\mathrm{PleC_{kin11}}]}{\mathrm{d}t} = k_{\mathrm{ph1-pk11}} \cdot [\mathrm{PleC_{ph11}}] - k_{\mathrm{pk11-ph11}} \cdot [\mathrm{PleC_{kin11}}] - k_{\mathrm{pk11-pk0}} \cdot [\mathrm{PleC_{kin11}}] + k_{\mathrm{pk0-pk11}} \cdot [\mathrm{PleC_{kin0}}] - k_{\mathrm{pk11-pt4}} \cdot [\mathrm{PleC_{kin11}}] + k_{\mathrm{pt4-pk11}} \cdot [\mathrm{PleC_{pt4}}] + k_{\mathrm{pt3h-pk11}} \cdot [\mathrm{PleC_{pt3h}}] \cdot [\mathrm{DivK{\sim}P}] - k_{\mathrm{pk11-pt3h}} \cdot [\mathrm{PleC_{kin11}}] \quad (9)$$

$$\frac{\mathrm{d}[\mathrm{PleC_{kin12}}]}{\mathrm{d}t} = k_{\mathrm{ph12-pk12}} \cdot [\mathrm{PleC_{ph12}}] - k_{\mathrm{pk12-ph12}} \cdot [\mathrm{PleC_{kin12}}] - k_{\mathrm{pk12-pk2}} \cdot [\mathrm{PleC_{kin12}}] + k_{\mathrm{pk2-pk12}} \cdot [\mathrm{PleC_{kin2}}] + k_{\mathrm{pkdk-pk12}} \cdot [\mathrm{PleC_{pkdk}}] \cdot [\mathrm{DivK{\sim}P}] - k_{\mathrm{pk12-pkdk}} \cdot [\mathrm{PleC_{kin12}}] + k_{\mathrm{pt3h-pk12}} \cdot [\mathrm{PleC_{pt3h}}] \cdot [\mathrm{DivK}] - k_{\mathrm{pk12-pt3h}} \cdot [\mathrm{PleC_{kin12}}] \quad (10)$$

$$\frac{\mathrm{d}[\mathrm{PleC_{kin22}}]}{\mathrm{d}t} = k_{\mathrm{ph22-pk22}} \cdot [\mathrm{PleC_{ph22}}] - k_{\mathrm{pk22-ph22}} \cdot [\mathrm{PleC_{kin22}}] - k_{\mathrm{pk22-pk4}} \cdot [\mathrm{PleC_{kin22}}] + k_{\mathrm{pk4-pk22}} \cdot [\mathrm{PleC_{kin4}}] + k_{\mathrm{pkdk-k22}} \cdot [\mathrm{PleC_{pkdk}}] \cdot [\mathrm{DivK}] - k_{\mathrm{pk22-pkdk}} \cdot [\mathrm{PleC_{kin22}}] \quad (11)$$

$$\frac{\mathrm{d}[\mathrm{PleC_{kin0}}]}{\mathrm{d}t} = k_{\mathrm{pk11-pk0}} \cdot [\mathrm{PleC_{kin11}}] - k_{\mathrm{pk0-pk11}} \cdot [\mathrm{PleC_{kin0}}] - k_{\mathrm{pk0-pk1}} \cdot [\mathrm{PleC_{kin0}}] + k_{\mathrm{pk1-pk0}} \cdot [\mathrm{PleC_{kin1}}] \cdot [\mathrm{DivK{\sim}P}] \quad (12)$$

$$\frac{\mathrm{d}[\mathrm{PleC_{kin2}}]}{\mathrm{d}t} = k_{\mathrm{pk12-pk2}} \cdot [\mathrm{PleC_{kin12}}] - k_{\mathrm{pk2-pk12}} \cdot [\mathrm{PleC_{kin2}}] - k_{\mathrm{pk2-pk1}} \cdot [\mathrm{PleC_{kin2}}] + k_{\mathrm{pk1-pk2}} \cdot [\mathrm{PleC_{kin1}}] \cdot [\mathrm{DivK}] - k_{\mathrm{pk2-pk3}} \cdot [\mathrm{PleC_{kin2}}] + k_{\mathrm{pk3-pk2}} \cdot [\mathrm{PleC_{kin3}}] \cdot [\mathrm{DivK{\sim}P}] + k_{\mathrm{pt2-pk2}} \cdot [\mathrm{PleC_{pt2}}] - k_{\mathrm{pk2-pt2}} \cdot [\mathrm{PleC_{kin2}}] \quad (13)$$

$$\frac{\mathrm{d}[\mathrm{PleC_{kin4}}]}{\mathrm{d}t} = k_{\mathrm{pk22-pk4}} \cdot [\mathrm{PleC_{kin22}}] - k_{\mathrm{pk4-pk22}} \cdot [\mathrm{PleC_{kin4}}] - k_{\mathrm{pk4-pk3}} \cdot [\mathrm{PleC_{kin4}}] + k_{\mathrm{pk3-pk4}} \cdot [\mathrm{PleC_{kin3}}] \cdot [\mathrm{DivK}] - k_{\mathrm{pk4-pt4}} \cdot [\mathrm{PleC_{kin4}}] + k_{\mathrm{pt4-pk4}} \cdot [\mathrm{PleC_{pt4}}] \quad (14)$$

$$\frac{\mathrm{d}[\mathrm{PleC_{kin1}}]}{\mathrm{d}t} = -k_{\mathrm{pk1-pk0}} \cdot [\mathrm{PleC_{kin1}}] \cdot [\mathrm{DivK{\sim}P}] + k_{\mathrm{pk0-pk1}} \cdot [\mathrm{PleC_{kin0}}] - k_{\mathrm{pk1-pk2}} \cdot [\mathrm{PleC_{kin1}}] \cdot [\mathrm{DivK}] + k_{\mathrm{pk2-pk1}} \cdot [\mathrm{PleC_{kin2}}] + k_{\mathrm{pk2p-pk1}} \cdot [\mathrm{PleC_{kin2p}}] \cdot [\mathrm{DivK{\sim}P}] - k_{\mathrm{pk1-pk2p}} \cdot [\mathrm{PleC_{kin1}}] + k_{\mathrm{pk1h-pk1}} \cdot [\mathrm{PleC_{kin1h}}] - k_{\mathrm{pk1-pk1h}} \cdot [\mathrm{PleC_{kin1}}] - k_{\mathrm{pk1-pk5}} \cdot [\mathrm{PleC_{kin1}}] \cdot [\mathrm{PleD}] + k_{\mathrm{pk5-pk1}} \cdot [\mathrm{PleC_{kin5}}] \quad (15)$$

$$\frac{d[\mathrm{PleC_{kin3}}]}{dt} = -k_{\mathrm{pk3-pk2}} \cdot [\mathrm{PleC_{kin3}}] \cdot [\mathrm{DivK{\sim}P}] + k_{\mathrm{pk2-pk3}} \cdot [\mathrm{PleC_{kin2}}] - k_{\mathrm{pk3-pk4}} \cdot [\mathrm{PleC_{kin3}}] \cdot [\mathrm{DivK}] + k_{\mathrm{pk4-pk3}} \cdot [\mathrm{PleC_{kin4}}] + k_{\mathrm{pk2p-pk3}} \cdot [\mathrm{PleC_{kin2p}}] \cdot [\mathrm{DivK}] - k_{\mathrm{pk3-pk2p}} \cdot [\mathrm{PleC_{kin3}}] + k_{\mathrm{pk3h-pk3}} \cdot [\mathrm{PleC_{kin3h}}] - k_{\mathrm{pk3-pk3h}} \cdot [\mathrm{PleC_{kin3}}] + k_{\mathrm{pt3-pk3}} \cdot [\mathrm{PleC_{pt3}}] - k_{\mathrm{pk3-pt3}} \cdot [\mathrm{PleC_{kin3}}] - k_{\mathrm{pk3-pk6}} \cdot [\mathrm{PleC_{kin3}}] \cdot [\mathrm{PleD}] + k_{\mathrm{pk6-pk3}} \cdot [\mathrm{PleC_{kin6}}] \tag{16}$$

$$\frac{d[\mathrm{PleC_{pt2}}]}{dt} = k_{\mathrm{pk1h-pt2}} \cdot [\mathrm{PleC_{kin1h}}] \cdot [\mathrm{DivK{\sim}P}] - k_{\mathrm{pt2-pk1h}} \cdot [\mathrm{PleC_{pt2}}] - k_{\mathrm{pt2-pk2}} \cdot [\mathrm{PleC_{pt2}}] + k_{\mathrm{pk2-pt2}} \cdot [\mathrm{PleC_{kin2}}] \tag{17}$$

$$\frac{d[\mathrm{PleC_{pt3}}]}{dt} = k_{\mathrm{pk1p-pt3}} \cdot [\mathrm{PleC_{kin1p}}] \cdot [\mathrm{DivK{\sim}P}] - k_{\mathrm{pt3-pk1p}} \cdot [\mathrm{PleC_{pt3}}] - k_{\mathrm{pt3-pk3}} \cdot [\mathrm{PleC_{pt3}}] + k_{\mathrm{pk3-pt3}} \cdot [\mathrm{PleC_{kin3}}] \tag{18}$$

$$\frac{d[\mathrm{PleC_{pt4}}]}{dt} = k_{\mathrm{pk3h-pt4}} \cdot [\mathrm{PleC_{kin3h}}] \cdot [\mathrm{DivK{\sim}P}] - k_{\mathrm{pt4-pk3h}} \cdot [\mathrm{PleC_{pt4}}] - k_{\mathrm{pt4-pk4}} \cdot [\mathrm{PleC_{pt4}}] + k_{\mathrm{pk4-pt4}} \cdot [\mathrm{PleC_{kin4}}] - k_{\mathrm{pt4-pk11}} \cdot [\mathrm{PleC_{pt4}}] + k_{\mathrm{pk11-pt4}} \cdot [\mathrm{PleC_{kin11}}] \tag{19}$$

$$\frac{d[\mathrm{PleC_{kin1h}}]}{dt} = -k_{\mathrm{pk1h-pt2}} \cdot [\mathrm{PleC_{kin1h}}] \cdot [\mathrm{DivK{\sim}P}] + k_{\mathrm{pt2-pk1h}} \cdot [\mathrm{PleC_{pt2}}] - k_{\mathrm{pk1h-pk1}} \cdot [\mathrm{PleC_{kin1h}}] + k_{\mathrm{pk1-pk1h}} \cdot [\mathrm{PleC_{kin1}}] + k_{\mathrm{pk1p-pk1h}} \cdot [\mathrm{PleC_{kin1p}}] \cdot [\mathrm{DivK{\sim}P}] - k_{\mathrm{pk1h-pk1p}} \cdot [\mathrm{PleC_{kin1h}}] - k_{\mathrm{pk1h-pt5}} \cdot [\mathrm{PleC_{kin1h}}] \cdot [\mathrm{PleD{\sim}P}] + k_{\mathrm{pt5-pk1h}} \cdot [\mathrm{PleC_{pt5}}] \tag{20}$$

$$\frac{d[\mathrm{PleC_{kin3h}}]}{dt} = -k_{\mathrm{pk3h-pk3}} \cdot [\mathrm{PleC_{kin3h}}] + k_{\mathrm{pk3-pk3h}} \cdot [\mathrm{PleC_{kin3}}] + k_{\mathrm{pk1p-pk3h}} \cdot [\mathrm{PleC_{kin1p}}] \cdot [\mathrm{DivK}] - k_{\mathrm{pk3h-pk1p}} \cdot [\mathrm{PleC_{kin3h}}] - k_{\mathrm{pk3h-pt4}} \cdot [\mathrm{PleC_{kin3h}}] \cdot [\mathrm{DivK{\sim}P}] + k_{\mathrm{pt4-pk3h}} \cdot [\mathrm{PleC_{pt4}}] - k_{\mathrm{pk3h-pt6}} \cdot [\mathrm{PleC_{kin3h}}] \cdot [\mathrm{PleD{\sim}P}] + k_{\mathrm{pt6-pk3h}} \cdot [\mathrm{PleC_{pt6}}] + k_{\mathrm{pt3h-p3h}} \cdot [\mathrm{PleC_{pt3h}}] - k_{\mathrm{pk3h-pt3h}} \cdot [\mathrm{PleC_{kin3h}}] \tag{21}$$

$$\frac{d[\mathrm{PleC_{kin2p}}]}{dt} = -k_{\mathrm{pk2p-pk1}} \cdot [\mathrm{PleC_{kin2p}}] \cdot [\mathrm{DivK{\sim}P}] + k_{\mathrm{pk1-pk2p}} \cdot [\mathrm{PleC_{kin1}}] - k_{\mathrm{pk2p-pk3}} \cdot [\mathrm{PleC_{pk2p}}] \cdot [\mathrm{DivK}] + k_{\mathrm{pk3-pk2p}} \cdot [\mathrm{PleC_{kin3}}] - k_{\mathrm{pk2p-ph2p}} \cdot [\mathrm{PleC_{kin2p}}] + k_{\mathrm{ph2p-pk2p}} \cdot [\mathrm{PleC_{ph2p}}] \tag{22}$$

$$\frac{\mathrm{d}[\mathrm{PleC_{kin1p}}]}{\mathrm{d}t} = -k_{\mathrm{pk1p-pk1h}} \cdot [\mathrm{PleC_{kin1p}}] \cdot [\mathrm{DivK{\sim}P}] + k_{\mathrm{pk1h-pk1p}} \cdot [\mathrm{PleC_{kin1h}}] - k_{\mathrm{pk1p-pt3}} \cdot [\mathrm{PleC_{pk1p}}] \cdot [\mathrm{DivK}] + k_{\mathrm{pt3-pk1p}} \cdot [\mathrm{PleC_{pt3}}] - k_{\mathrm{pk1p-ph1p}} \cdot [\mathrm{PleC_{kin1p}}] + k_{\mathrm{h1p-pk1p}} \cdot [\mathrm{PleC_{ph1p}}] - k_{\mathrm{pk1p-pk3h}} \cdot [\mathrm{PleC_{kin1p}}] \cdot [\mathrm{DivK}] + k_{\mathrm{pk3h-pk1p}} \cdot [\mathrm{PleC_{kin3h}}] \quad 23$$

$$\frac{\mathrm{d}[\mathrm{PleC_{ph2p}}]}{\mathrm{d}t} = k_{\mathrm{pk2p-ph2p}} \cdot [\mathrm{PleC_{kin2p}}] - k_{\mathrm{ph2p-pk2p}} \cdot [\mathrm{PleC_{ph2p}}] - k_{\mathrm{ph2p-pc}} \cdot [\mathrm{PleC_{ph2p}}] \quad 24$$

$$\frac{\mathrm{d}[\mathrm{PleC_{ph1p}}]}{\mathrm{d}t} = k_{\mathrm{pk1p-ph1p}} \cdot [\mathrm{PleC_{kin1p}}] - k_{\mathrm{ph1p-pk1p}} \cdot [\mathrm{PleC_{ph1p}}] - k_{\mathrm{ph1p-pc}} \cdot [\mathrm{PleC_{ph1p}}] \quad 25$$

$$\frac{\mathrm{d}[\mathrm{PleC_{kin}}]}{\mathrm{d}t} = k_{\mathrm{pch-pck}} \cdot [\mathrm{PleC}] - k_{\mathrm{pck-pch}} \cdot [\mathrm{PleC_{kin}}] - k_{\mathrm{pck-pkdk}} \cdot [\mathrm{PleC_{kin}}] \cdot [\mathrm{DivK}] + k_{\mathrm{pkdk-pck}} \cdot [\mathrm{PleC_{pkdk}}] - k_{\mathrm{pck-pt3h}} \cdot [\mathrm{PleC_{kin}}] \cdot [\mathrm{DivK{\sim}P}] + k_{\mathrm{pt3h-pck}} \cdot [\mathrm{PleC_{pt3h}}] \quad 26$$

$$\frac{\mathrm{d}[\mathrm{PleC_{pkdk}}]}{\mathrm{d}t} = k_{\mathrm{pck-pkdk}} \cdot [\mathrm{PleC_{ki}}] \cdot [\mathrm{DivK}] - k_{\mathrm{pkdk-pck}} \cdot [\mathrm{PleC_{pkdk}}] - k_{\mathrm{pkdk-k22}} \cdot [\mathrm{PleC_{pkdk}}] \cdot [\mathrm{DivK}] + k_{\mathrm{pk22-pkdk}} \cdot [\mathrm{PleC_{kin22}}] - k_{\mathrm{pkdk-k12}} \cdot [\mathrm{PleC_{pkdk}}] \cdot [\mathrm{DivK{\sim}P}] + k_{\mathrm{pk12-pkdk}} \cdot [\mathrm{PleC_{kin12}}] \quad 27$$

$$\frac{\mathrm{d}[\mathrm{PleC_{pt3h}}]}{\mathrm{d}t} = k_{\mathrm{pck-pt3h}} \cdot [\mathrm{PleC_{kin}}] \cdot [\mathrm{DivK{\sim}P}] - k_{\mathrm{pt3h-pck}} \cdot [\mathrm{PleC_{pt3h}}] - k_{\mathrm{pt3h-pk11}} \cdot [\mathrm{PleC_{pt3h}}] \cdot [\mathrm{DivK{\sim}P}] + k_{\mathrm{pk11-pt3h}} \cdot [\mathrm{PleC_{kin11}}] - k_{\mathrm{pt3h-pk12}} \cdot [\mathrm{PleC_{pt3h}}] \cdot [\mathrm{DivK}] + k_{\mathrm{pk12-pt3h}} \cdot [\mathrm{PleC_{kin12}}] - k_{\mathrm{pt3h-pk3h}} \cdot [\mathrm{PleC_{pt3h}}] + k_{\mathrm{pk3h-pt3h}} \cdot [\mathrm{PleC_{kin3h}}] \quad 28$$

$$\frac{\mathrm{d}[\mathrm{DivJ}]}{\mathrm{d}t} = -k_{\mathrm{j-jk}} \cdot [\mathrm{DivJ}] \cdot [\mathrm{DivK}] + k_{\mathrm{jk-j}} \cdot [\mathrm{DivJ{:}\,DivK}] + k_{\mathrm{e-jk}} \cdot [\mathrm{DivJ{:}\,DivK}] \quad 29$$

$$\frac{\mathrm{d}[\mathrm{DivJ{:}\,DivK}]}{\mathrm{d}t} = k_{\mathrm{j-jk}} \cdot [\mathrm{DivJ}] \cdot [\mathrm{DivK}] - k_{\mathrm{jk-j}} \cdot [\mathrm{DivJ{:}\,DivK}] - k_{\mathrm{e-jk}} \cdot [\mathrm{DivJ{:}\,DivK}] \quad 30$$

$$\frac{\mathrm{d}[\mathrm{PleD}]}{\mathrm{d}t} = k_{\mathrm{syn-pld}} - k_{\mathrm{deg-pld}} \cdot [\mathrm{PleD}] - k_{\mathrm{pk1-pk5}} \cdot [\mathrm{PleC_{kin1}}] \cdot [\mathrm{PleD}] + k_{\mathrm{pk5-pk1}} \cdot [\mathrm{PleC_{kin5}}] - k_{\mathrm{pk3-pk6}} \cdot [\mathrm{PleC_{kin3}}] \cdot [\mathrm{PleD}] + k_{\mathrm{pk6-pk3}} \cdot [\mathrm{PleC_{kin6}}] + k_{\mathrm{e-ph3}} \cdot [\mathrm{Phos{:}\,PleD{\sim}P}] \quad 31$$

$$\frac{d[\mathrm{PleD{\sim}P}]}{dt} = -k_{\mathrm{deg-pldp}} \cdot [\mathrm{PleD{\sim}P}] - k_{\mathrm{pk1h-pt5}} \cdot [\mathrm{PleC_{kin1h}}] \cdot [\mathrm{PleD{\sim}P}] + k_{\mathrm{pt5-pk1h}} \cdot [\mathrm{PleC_{pt5}}] - k_{\mathrm{pk3h-pt6}} \cdot [\mathrm{PleC_{kin3h}}] \cdot [\mathrm{PleD{\sim}P}] + k_{\mathrm{pt6-pk3h}} \cdot [\mathrm{PleC_{pt6}}] - k_{\mathrm{phos-ph3}} \cdot [\mathrm{Phos}] \cdot [\mathrm{PleD{\sim}P}] + k_{\mathrm{ph3-phos}} \cdot [\mathrm{Phos{:}\,PleD{\sim}P}] \tag{32}$$

$$\frac{d[\mathrm{PleC_{kin5}}]}{dt} = k_{\mathrm{pk1-pk5}} \cdot [\mathrm{PleC_{kin1}}] \cdot [\mathrm{PleD}] - k_{\mathrm{pk5-pk1}} \cdot [\mathrm{PleC_{kin5}}] - k_{\mathrm{pk5-pt5}} \cdot [\mathrm{PleC_{kin5}}] + k_{\mathrm{pt5-pk5}} \cdot [\mathrm{PleC_{pt5}}] \tag{33}$$

$$\frac{d[\mathrm{PleC_{kin6}}]}{dt} = k_{\mathrm{pk3-pk6}} \cdot [\mathrm{PleC_{kin3}}] \cdot [\mathrm{PleD}] - k_{\mathrm{pk6-pk3}} \cdot [\mathrm{PleC_{kin6}}] - k_{\mathrm{pk6-pt6}} \cdot [\mathrm{PleC_{kin6}}] + k_{\mathrm{pt6-pk6}} \cdot [\mathrm{PleC_{pt6}}] \tag{34}$$

$$\frac{d[\mathrm{PleC_{pt5}}]}{dt} = k_{\mathrm{pk5-pt5}} \cdot [\mathrm{PleC_{kin5}}] - k_{\mathrm{pt5-pk5}} \cdot [\mathrm{PleC_{pt5}}] + k_{\mathrm{pk1h-pt5}} \cdot [\mathrm{PleC_{kin1h}}] \cdot [\mathrm{PleD{\sim}P}] - k_{\mathrm{pt5-pk1h}} \cdot [\mathrm{PleC_{pt5}}] \tag{35}$$

$$\frac{d[\mathrm{PleC_{pt6}}]}{dt} = k_{\mathrm{pk6-pt6}} \cdot [\mathrm{PleC_{kin6}}] - k_{\mathrm{pt6-pk6}} \cdot [\mathrm{PleC_{pt6}}] + k_{\mathrm{pk3h-pt6}} \cdot [\mathrm{PleC_{kin3h}}] \cdot [\mathrm{PleD{\sim}P}] - k_{\mathrm{pt6-pk3h}} \cdot [\mathrm{PleC_{pt6}}] \tag{36}$$

$$\frac{d[\mathrm{Phos}]}{dt} = -k_{\mathrm{phos-ph3}} \cdot [\mathrm{Phos}] \cdot [\mathrm{PleD{\sim}P}] + k_{\mathrm{ph3-phos}} \cdot [\mathrm{Phos{:}\,PleD{\sim}P}] + k_{\mathrm{e-ph3}} \cdot [\mathrm{Phos{:}\,PleD{\sim}P}] \tag{37}$$

$$\frac{d[\mathrm{Phos{:}\,PleD{\sim}P}]}{dt} = k_{\mathrm{phos-ph3}} \cdot [\mathrm{Phos}] \cdot [\mathrm{PleD{\sim}P}] - k_{\mathrm{ph3-phos}} \cdot [\mathrm{Phos{:}\,PleD{\sim}P}] - k_{\mathrm{e-ph3}} \cdot [\mathrm{Phos{:}\,PleD{\sim}P}] \tag{38}$$

$$\frac{d[\mathrm{DivL}]}{dt} = k_{\mathrm{syndl}} - k_{\mathrm{degdl}} \cdot [\mathrm{DivL}] - k_{\mathrm{dl-dldk}} \cdot [\mathrm{DivL}] \cdot [\mathrm{DivK{\sim}P}] + k_{\mathrm{dldk-dl}} \cdot [\mathrm{DivL{:}\,DivK{\sim}P}] \tag{39}$$

$$\frac{d[\mathrm{DivL{:}\,DivK{\sim}P}]}{dt} = k_{\mathrm{dl-dldk}} \cdot [\mathrm{DivL}] \cdot [\mathrm{DivK{\sim}P}] - k_{\mathrm{dldk-dl}} \cdot [\mathrm{DivL{:}\,DivK{\sim}P}] \tag{40}$$

$$\frac{d[\mathrm{CtrA}]}{dt} = k_{\mathrm{syn-ctr}} - k_{\mathrm{deg-ctr}} \cdot [\mathrm{CtrA}] - k_{\mathrm{ck-ck1}} \cdot [\mathrm{CckA_{kin}}] \cdot [\mathrm{CtrA}] + k_{\mathrm{ck1-ck}} \cdot [\mathrm{CckA_{kin1}}] + k_{\mathrm{e-ch1}} \cdot [\mathrm{CckA_{h1}}] \tag{41}$$

$$\frac{d[\mathrm{CtrA{\sim}P}]}{dt} = -k_{\mathrm{deg-ctr}} \cdot [\mathrm{CtrA{\sim}P}] + k_{\mathrm{ct1-ck}} \cdot [\mathrm{CckA_{ct1}}] - k_{\mathrm{ck-ct1}} \cdot [\mathrm{CckA_{kin}}] \cdot [\mathrm{CtrA{\sim}P}] - k_{\mathrm{cp-ch1}} \cdot [\mathrm{CckA_{phos}}] \cdot [\mathrm{CtrA{\sim}P}] + k_{\mathrm{ch1-cp}} \cdot [\mathrm{CckA_{h1}}] \tag{42}$$

$$\frac{d[\mathrm{CpdR}]}{dt} = k_{\mathrm{syn-cpd}} - k_{\mathrm{deg-cpd}} \cdot [\mathrm{CpdR}] - k_{\mathrm{ck-ck2}} \cdot [\mathrm{CckA_{kin}}] \cdot [\mathrm{CpdR}] + k_{\mathrm{ck2-ck}} \cdot [\mathrm{CckA_{kin2}}] + k_{\mathrm{e-ch2}} \cdot [\mathrm{CckA_{h2}}] \quad 43$$

$$\frac{d[\mathrm{CpdR{\sim}P}]}{dt} = -k_{\mathrm{deg-cpd}} \cdot [\mathrm{CpdR{\sim}P}] + k_{\mathrm{ct2-ck}} \cdot [\mathrm{CckA_{ct1}}] - k_{\mathrm{ck-ct2}} \cdot [\mathrm{CckA_{kin}}] \cdot [\mathrm{CpdR{\sim}P}] - k_{\mathrm{cp-ch2}} \cdot [\mathrm{CckA_{phos}}] \cdot [\mathrm{CpdR{\sim}P}] + k_{\mathrm{ch2-cp}} \cdot [\mathrm{CckA_{h2}}] \quad 44$$

$$\frac{d[\mathrm{CckA_{phos}}]}{dt} = -k_{\mathrm{cp-ch1}} \cdot [\mathrm{CckA_{phos}}] \cdot [\mathrm{CtrA{\sim}P}] + k_{\mathrm{ch1-cp}} \cdot [\mathrm{CckA_{h1}}] - k_{\mathrm{cp-ch2}} \cdot [\mathrm{CckA_{phos}}] \cdot [\mathrm{CpdR{\sim}P}] + k_{\mathrm{ch2-cp}} \cdot [\mathrm{CckA_{h2}}] - k_{\mathrm{cp-ck}} \cdot [\mathrm{CckA_{phos}}] \cdot \frac{[\mathrm{DivL}]^2}{K_{\mathrm{dl}}^2 + [\mathrm{DivL}]^2} + k_{\mathrm{ck-cp}} \cdot [\mathrm{CckA_{kin}}] + k_{\mathrm{e-ch1}} \cdot [\mathrm{CckA_{h1}}] + k_{\mathrm{e-ch2}} \cdot [\mathrm{CckA_{h2}}] \quad 45$$

$$\frac{d[\mathrm{CckA_{kin}}]}{dt} = k_{\mathrm{cp-ck}} \cdot [\mathrm{CckA_{phos}}] \cdot \frac{[\mathrm{DivL}]^2}{K_{\mathrm{dl}}^2 + [\mathrm{DivL}]^2} - k_{\mathrm{ck-cp}} \cdot [\mathrm{CckA_{kin}}] - k_{\mathrm{ck-ck1}} \cdot [\mathrm{CckA_{kin}}] \cdot [\mathrm{CtrA}] + k_{\mathrm{ck1-ck}} \cdot [\mathrm{CckA_{kin1}}] - k_{\mathrm{ck-ck2}} \cdot [\mathrm{CckA_{kin}}] \cdot [\mathrm{CpdR}] + k_{\mathrm{ck2-ck}} \cdot [\mathrm{CckA_{kin2}}] + k_{\mathrm{ct1-ck}} \cdot [\mathrm{CckA_{ct1}}] - k_{\mathrm{ck-ct1}} \cdot [\mathrm{CckA_{kin}}] \cdot [\mathrm{CtrA{\sim}P}] + k_{\mathrm{ct2-ck}} \cdot [\mathrm{CckA_{ct2}}] - k_{\mathrm{ck-ct2}} \cdot [\mathrm{CckA_{kin}}] \cdot [\mathrm{CpdR{\sim}P}] \quad 46$$

$$\frac{d[\mathrm{CckA_{kin1}}]}{dt} = k_{\mathrm{ck-ck1}} \cdot [\mathrm{CckA_{kin}}] \cdot [\mathrm{CtrA}] - k_{\mathrm{ck1-ck}} \cdot [\mathrm{CckA_{kin1}}] - k_{\mathrm{ck1-ct1}} \cdot [\mathrm{CckA_{kin1}}] + k_{\mathrm{ct1-ck1}} \cdot [\mathrm{CckA_{ct1}}] \quad 47$$

$$\frac{d[\mathrm{CckA_{kin2}}]}{dt} = k_{\mathrm{ck-ck2}} \cdot [\mathrm{CckA_{kin}}] \cdot [\mathrm{CpdR}] - k_{\mathrm{ck2-ck}} \cdot [\mathrm{CckA_{kin2}}] - k_{\mathrm{ck2-ct2}} \cdot [\mathrm{CckA_{kin2}}] + k_{\mathrm{ct2-ck2}} \cdot [\mathrm{CckA_{ct2}}] \quad 48$$

$$\frac{d[\mathrm{CckA_{ct1}}]}{dt} = k_{\mathrm{ck1-ct1}} \cdot [\mathrm{CckA_{kin1}}] - k_{\mathrm{ct1-ck1}} \cdot [\mathrm{CckA_{ct1}}] - k_{\mathrm{ct1-ck}} \cdot [\mathrm{CckA_{ct1}}] + k_{\mathrm{ck-ct1}} \cdot [\mathrm{CckA_{kin}}] \cdot [\mathrm{CtrA{\sim}P}] \quad 49$$

$$\frac{d[\mathrm{CckA_{ct2}}]}{dt} = k_{\mathrm{ck2-ct2}} \cdot [\mathrm{CckA_{kin2}}] - k_{\mathrm{ct2-ck2}} \cdot [\mathrm{CckA_{ct2}}] - k_{\mathrm{ct2-ck}} \cdot [\mathrm{CckA_{ct2}}] + k_{\mathrm{ck-ct2}} \cdot [\mathrm{CckA_{kin}}] \cdot [\mathrm{CpdR{\sim}P}] \quad 50$$

$$\frac{d[\mathrm{CckA_{h1}}]}{dt} = k_{\mathrm{cp-ch1}} \cdot [\mathrm{CckA_{phos}}] \cdot [\mathrm{CtrA{\sim}P}] - k_{\mathrm{ch1-cp}} \cdot [\mathrm{CckA_{h1}}] - k_{\mathrm{e-ch1}} \cdot [\mathrm{CckA_{h1}}] \quad 51$$

$$\frac{d[\mathrm{CckA_{h2}}]}{dt} = k_{\mathrm{cp-ch2}} \cdot [\mathrm{CckA_{phos}}] \cdot [\mathrm{CpdR{\sim}P}] - k_{\mathrm{ch2-cp}} \cdot [\mathrm{CckA_{h2}}] - k_{\mathrm{e-ch2}} \cdot [\mathrm{CckA_{h2}}] \quad 52$$

* Equations are ordered as the corresponding variables appear from left to right in Figure A.1.

Table A.5: Basal parameter values used in the full model*.

$k_{ph1-ph11}$	5	$k_{ph11-ph1}$	5	$k_{ph11-pk11}$	5	$k_{pk11-ph11}$	5
$k_{pk11-pk0}$	5	$k_{pk0-pk11}$	5	$k_{pk0-pk1}$	0.16	$k_{pk1-pk0}$	5
$k_{pk1-pk2}$	5	$k_{pk2-pk1}$	0.0016	$k_{pk1-pk1h}$	5	$k_{pk1h-pk1}$	5
$k_{pk1-pk2p}$	0.16	$k_{pk2p-pk1}$	5	$k_{pk2-pt2}$	5	$k_{pt2-pk2}$	0.16
$k_{pt2-pk1h}$	0.16	$k_{pk1h-pt2}$	5	$k_{pk2p-ph2p}$	5	$k_{ph2p-pk2p}$	0.005
$k_{ph2p-pc}$	5	$k_{ph1p-pc}$	5	$k_{pk3-pk2p}$	0.0016	$k_{pk2p-pk3}$	5
$k_{pk2-pk3}$	0.16	$k_{pk3-pk2}$	5	$k_{pk3-pt3}$	5	$k_{pt3-pk3}$	0.16
$k_{pt3-pk1p}$	0.16	$k_{pk1p-pt3}$	5	$k_{pk1p-pk1h}$	5	$k_{pk1h-pk1p}$	0.16
$k_{pk3-pk4}$	5	$k_{pk4-pk3}$	0.0016	$k_{pk4-pt4}$	5	$k_{pt4-pk4}$	0.16
$k_{pt4-pk11}$	5	$k_{pk11-pt4}$	0.16	k_{pc-ph2}	0.05	k_{ph2-pc}	5
$k_{ph2-ph22}$	0.05	$k_{ph22-ph2}$	5	$k_{ph22-pk22}$	5	$k_{pk22-ph22}$	5e-08
$k_{pk22-pk4}$	5	$k_{pk4-pk22}$	5	$k_{ph2-ph12}$	5	$k_{ph12-ph2}$	5
$k_{ph1-ph12}$	0.05	$k_{ph12-ph1}$	5	$k_{ph12-pk12}$	5	$k_{pk12-ph12}$	5e-04
$k_{pk12-pk2}$	5	$k_{pk2-pk12}$	5	$k_{pch-pck}$	0.005	$k_{pck-pch}$	5
$k_{pck-pkdp}$	5	$k_{pkdk-pck}$	0.0016	$k_{pkdk-pk22}$	5	$k_{pk22-pkdk}$	0.0016
$k_{pkdk-pk12}$	5	$k_{pk12-pkdk}$	0.16	$k_{pck-pt3h}$	5	$k_{pt3h-pck}$	0.16
$k_{pt3h-pk11}$	5	$k_{pk11-pt3h}$	0.16	$k_{pt3h-pk12}$	5	$k_{pk12-pt3h}$	0.0016
$k_{pt4-pk3h}$	0.16	$k_{pk3h-pt4}$	5	$k_{pk3-pk3h}$	5	$k_{pk3h-pk3}$	5
$k_{pk1p-pk3h}$	5	$k_{pk3h-pk1p}$	0.0016	$k_{pk3h-pt3h}$	5	$k_{pt3h-pk3h}$	0.16
$k_{pk1p-ph1p}$	5	$k_{ph1p-pk1p}$	0.005	k_{syn-dk}	0.015	k_{deg-dk}	0.005
$k_{deg-dkp}$	0.005	k_{j-jk}	1	k_{jk-j}	0.1	$k_{ph1-ph2}$	10
$k_{ph2-ph1}$	5e-03	k_{pc-ph1}	5	k_{ph1-pc}	5	$k_{syn-pld}$	0.01

$k_{\text{deg-pld}}$	0.005	$k_{\text{deg-pldp}}$	0.005	$k_{\text{phos-ph3}}$	1	$k_{\text{ph3-phos}}$	0.1
$k_{\text{pk1-pk5}}$	10	$k_{\text{pk5-pk1}}$	0.31	$k_{\text{pk5-pt5}}$	10	$k_{\text{pt5-pk5}}$	0.31
$k_{\text{pt5-pk1h}}$	10	$k_{\text{pk1h-pt5}}$	0.31	$k_{\text{pk3-pk6}}$	10	$k_{\text{pk6-pk3}}$	0.31
$k_{\text{pk6-pt6}}$	10	$k_{\text{pt6-pk6}}$	0.31	$k_{\text{pt6-pk3h}}$	10	$k_{\text{pk3h-pt6}}$	0.31
$k_{\text{e-ph3}}$	0.2						
$k_{\text{dl-dldk}}$	1	$k_{\text{dldk-dl}}$	0.1	k_{syndl}	0.005	k_{degdl}	0.005
$k_{\text{cp-ck}}$	1	$k_{\text{cp-ck}}$	0.1	$k_{\text{cp-ch2}}$	1	$k_{\text{ch2-cp}}$	0.1
$k_{\text{syn-ctra}}$	0.05	$k_{\text{deg-ctr}}$	0.02	$k_{\text{deg-ctrp}}$	0.02	$k_{\text{syn-cpdr}}$	0.05
$k_{\text{deg-cpdr}}$	0.02	$k_{\text{deg-cpdp}}$	0.02	$k_{\text{ck-ck1}}$	1	$k_{\text{ck1-ck}}$	0.1
$k_{\text{ck1-ct1}}$	1	$k_{\text{ct1-ck1}}$	0.1	$k_{\text{ct1-ck}}$	1	$k_{\text{ck-ct1}}$	0.1
$k_{\text{cp-ch1}}$	1	$k_{\text{ch1-cp}}$	0.1	$k_{\text{e-ch1}}$	1	$k_{\text{ck-ck2}}$	1
$k_{\text{ck2-ck}}$	0.1	$k_{\text{ck2-ct2}}$	1	$k_{\text{ct2-ck2}}$	0.1	$k_{\text{ct2-ck}}$	1
$k_{\text{ck-ct2}}$	0.1	$k_{\text{e-ch2}}$	1				
DivJ_tot	0.5	PleC_tot	1	CckA_tot	1	Phos_tot	0.1
K_{dl}	0.75						

*For each reaction of the form X → Y, the parameters $k_{\text{x-y}}$ and $k_{\text{y-x}}$ are the forward and reverse rate constants (min^{-1}). DivJ_tot, PleC_tot, CckA_tot, Phos_tot and K_{dl} are dimensionless constants representing concentrations.

Table A.6: Equations governing the reduced model*.

$$\begin{aligned}\frac{\mathrm{d[DivK{\sim}P]}}{\mathrm{d}t} = & -k_{\mathrm{deg-dkp}}\cdot[\mathrm{DivK{\sim}P}] - k_{\mathrm{pc-ph1}}\cdot[\mathrm{PleC}]\cdot[\mathrm{DivK{\sim}P}] + k_{\mathrm{ph1-pc}}\cdot[\mathrm{PleC_{h1}}]\\
& - k_{\mathrm{ph1-pk11}}\cdot[\mathrm{PleC_{ph1}}]\cdot[\mathrm{DivK{\sim}P}] + k_{\mathrm{pk11-ph1}}\cdot[\mathrm{PleC_{kin11}}]\\
& - k_{\mathrm{ph2-pk12}}\cdot[\mathrm{PleC_{ph2}}]\cdot[\mathrm{DivK{\sim}P}] + k_{\mathrm{pk12-ph2}}\cdot[\mathrm{PleC_{kin12}}]\\
& - k_{\mathrm{pk1-pk0}}\cdot[\mathrm{PleC_{kin1}}]\cdot[\mathrm{DivK{\sim}P}] + k_{\mathrm{pk0-pk1}}\cdot[\mathrm{PleC_{kin0}}]\\
& - k_{\mathrm{pk3-pk2}}\cdot[\mathrm{PleC_{kin3}}]\cdot[\mathrm{DivK{\sim}P}] + k_{\mathrm{pk2-pk3}}\cdot[\mathrm{PleC_{kin2}}]\\
& + k_{\mathrm{pt2-pk1h}}\cdot[\mathrm{PleC_{pt2}}] - k_{\mathrm{pk1h-pt2}}\cdot[\mathrm{PleC_{kin1h}}]\cdot[\mathrm{DivK{\sim}P}]\\
& - k_{\mathrm{pk2p-pk1}}\cdot[\mathrm{PleC_{kin2p}}]\cdot[\mathrm{DivK{\sim}P}] + k_{\mathrm{pk1-pk2p}}\cdot[\mathrm{PleC_{kin1}}]\\
& - k_{\mathrm{pk1p-pk1h}}\cdot[\mathrm{PleC_{kin1p}}]\cdot[\mathrm{DivK{\sim}P}] + k_{\mathrm{pk1h-pk1p}}\cdot[\mathrm{PleC_{kin1h}}]\\
& + k_{\mathrm{pt3-pk1p}}\cdot[\mathrm{PleC_{pt3}}] - k_{\mathrm{pk1p-pt3}}\cdot[\mathrm{PleC_{kin1p}}]\cdot[\mathrm{DivK{\sim}P}]\\
& + k_{\mathrm{e-jk}}\cdot[\mathrm{DivJ{:}\,DivK}] - k_{\mathrm{pk3h-pt4}}\cdot[\mathrm{PleC_{kin3h}}]\cdot[\mathrm{DivK{\sim}P}]\\
& + k_{\mathrm{pt4-pk3h}}\cdot[\mathrm{PleC_{pt4}}] + k_{\mathrm{h1-h2}}\cdot[\mathrm{PleC_{ph1}}]\cdot[\mathrm{DivK}]\\
& - k_{\mathrm{h2-h1}}\cdot[\mathrm{PleC_{ph2}}]\cdot[\mathrm{DivK{\sim}P}] - k_{\mathrm{dl-dldk}}\cdot[\mathrm{DivL}]\cdot[\mathrm{DivK{\sim}P}]\\
& + k_{\mathrm{dldk-dl}}\cdot[\mathrm{DivL{:}\,DivK{\sim}P}]\end{aligned} \tag{1}$$

$$\begin{aligned}\frac{\mathrm{d[DivK]}}{\mathrm{d}t} = & \; k_{\mathrm{syn-dk}} - k_{\mathrm{deg-dk}}\cdot[\mathrm{DivK}] - k_{\mathrm{pc-ph2}}\cdot[\mathrm{PleC}]\cdot[\mathrm{DivK}] + k_{\mathrm{ph2-pc}}\cdot[\mathrm{PleC_{h2}}]\\
& - k_{\mathrm{ph2-pk22}}\cdot[\mathrm{PleC_{ph2}}]\cdot[\mathrm{DivK}] + k_{\mathrm{pk22-ph2}}\cdot[\mathrm{PleC_{kin22}}]\\
& - k_{\mathrm{ph1-pk12}}\cdot[\mathrm{PleC_{ph1}}]\cdot[\mathrm{DivK}] + k_{\mathrm{pk12-ph1}}\cdot[\mathrm{PleC_{kin12}}]\\
& - k_{\mathrm{pk1-pk2}}\cdot[\mathrm{PleC_{kin1}}]\cdot[\mathrm{DivK}] + k_{\mathrm{pk2-pk1}}\cdot[\mathrm{PleC_{kin2}}]\\
& - k_{\mathrm{pk3-pk4}}\cdot[\mathrm{PleC_{kin3}}]\cdot[\mathrm{DivK}] + k_{\mathrm{pk4-pk3}}\cdot[\mathrm{PleC_{kin4}}]\\
& - k_{\mathrm{pk2p-pk3}}\cdot[\mathrm{PleC_{pk2p}}]\cdot[\mathrm{DivK}] + k_{\mathrm{pk3-pk2p}}\cdot[\mathrm{PleC_{kin3}}]\\
& - k_{\mathrm{j-jk}}\cdot[\mathrm{DivJ}]\cdot[\mathrm{DivK}] + k_{\mathrm{jk-j}}\cdot[\mathrm{DivJ{:}\,DivK}] - k_{\mathrm{ph1-pk12}}\cdot[\mathrm{PleC_{h1}}]\cdot[\mathrm{DivK}]\\
& + k_{\mathrm{pk12-ph1}}\cdot[\mathrm{PleC_{kin12}}] - k_{\mathrm{pk1p-pk3h}}\cdot[\mathrm{PleC_{kin1p}}]\cdot[\mathrm{DivK}]\\
& + k_{\mathrm{pk3h-pk1p}}\cdot[\mathrm{PleC_{kin3h}}] - k_{\mathrm{h1-h2}}\cdot[\mathrm{PleC_{ph1}}]\cdot[\mathrm{DivK}]\\
& + k_{\mathrm{h2-h1}}\cdot[\mathrm{PleC_{ph2}}]\cdot[\mathrm{DivK{\sim}P}]\end{aligned} \tag{2}$$

$$\begin{aligned}\frac{\mathrm{d[PleC]}}{\mathrm{d}t} = & - k_{\mathrm{pc-ph2}}\cdot[\mathrm{PleC}]\cdot[\mathrm{DivK}] + k_{\mathrm{ph2-pc}}\cdot[\mathrm{PleC_{h2}}] - k_{\mathrm{pc-ph1}}\cdot[\mathrm{PleC}]\cdot[\mathrm{DivK{\sim}P}]\\
& + k_{\mathrm{ph1-pc}}\cdot[\mathrm{PleC_{h1}}] + k_{\mathrm{ph2p-pc}}\cdot[\mathrm{PleC_{h2p}}] + k_{\mathrm{ph1p-pc}}\cdot[\mathrm{PleC_{h1p}}]\end{aligned} \tag{3}$$

$$\frac{\mathrm{d}[\mathrm{PleC_{ph1}}]}{\mathrm{d}t} = k_{\mathrm{pc-ph1}} \cdot [\mathrm{PleC}] \cdot [\mathrm{DivK{\sim}P}] - k_{\mathrm{ph1-pc}} \cdot [\mathrm{PleC_{h1}}] - k_{\mathrm{ph1-pk11}} \cdot [\mathrm{PleC_{ph1}}] \cdot [\mathrm{DivK{\sim}P}] + k_{\mathrm{pk11-ph1}} \cdot [\mathrm{PleC_{kin11}}] - k_{\mathrm{ph1-pk12}} \cdot [\mathrm{PleC_{ph1}}] \cdot [\mathrm{DivK}] + k_{\mathrm{pk12-ph1}} \cdot [\mathrm{PleC_{kin12}}] - k_{\mathrm{h1-h2}} \cdot [\mathrm{PleC_{ph1}}] \cdot [\mathrm{DivK}] + k_{\mathrm{h2-h1}} \cdot [\mathrm{PleC_{ph2}}] \cdot [\mathrm{DivK{\sim}P}] - k_{\mathrm{ph1-ph2}} \cdot [\mathrm{PleC_{ph1}}] + k_{\mathrm{ph2-ph1}} \cdot [\mathrm{PleC_{ph2}}] \tag{4}$$

$$\frac{\mathrm{d}[\mathrm{PleC_{ph2}}]}{\mathrm{d}t} = k_{\mathrm{pc-ph2}} \cdot [\mathrm{PleC}] \cdot [\mathrm{DivK}] - k_{\mathrm{ph2-pc}} \cdot [\mathrm{PleC_{ph2}}] - k_{\mathrm{ph2-pk22}} \cdot [\mathrm{PleC_{ph2}}] \cdot [\mathrm{DivK}] + k_{\mathrm{pk22-ph2}} \cdot [\mathrm{PleC_{kin22}}] - k_{\mathrm{ph2-pk12}} \cdot [\mathrm{PleC_{ph2}}] \cdot [\mathrm{DivK{\sim}P}] + k_{\mathrm{pk12-ph2}} \cdot [\mathrm{PleC_{kin12}}] + k_{\mathrm{h1-h2}} \cdot [\mathrm{PleC_{ph1}}] \cdot [\mathrm{DivK}] - k_{\mathrm{h2-h1}} \cdot [\mathrm{PleC_{ph2}}] \cdot [\mathrm{DivK{\sim}P}] + k_{\mathrm{ph1-ph2}} \cdot [\mathrm{PleC_{ph1}}] - k_{\mathrm{ph2-ph1}} \cdot [\mathrm{PleC_{ph2}}] \tag{5}$$

$$\frac{\mathrm{d}[\mathrm{PleC_{kin11}}]}{\mathrm{d}t} = k_{\mathrm{ph1-p11}} \cdot [\mathrm{PleC_{ph1}}] \cdot [\mathrm{DivK{\sim}P}] - k_{\mathrm{pk11-ph1}} \cdot [\mathrm{PleC_{kin11}}] - k_{\mathrm{pk11-pk0}} \cdot [\mathrm{PleC_{kin11}}] + k_{\mathrm{pk0-pk11}} \cdot [\mathrm{PleC_{kin0}}] + k_{\mathrm{pt4-pk11}} \cdot [\mathrm{PleC_{pt4}}] - k_{\mathrm{pk11-pt4}} \cdot [\mathrm{PleC_{kin11}}] \tag{6}$$

$$\frac{\mathrm{d}[\mathrm{PleC_{kin12}}]}{\mathrm{d}t} = k_{\mathrm{ph2-pk12}} \cdot [\mathrm{PleC_{ph2}}] \cdot [\mathrm{DivK{\sim}P}] - k_{\mathrm{pk12-ph2}} \cdot [\mathrm{PleC_{kin12}}] + k_{\mathrm{ph1-pk12}} \cdot [\mathrm{PleC_{ph1}}] \cdot [\mathrm{DivK}] - k_{\mathrm{pk12-ph1}} \cdot [\mathrm{PleC_{kin12}}] - k_{\mathrm{pk22-pk2}} \cdot [\mathrm{PleC_{kin22}}] + k_{\mathrm{pk2-pk22}} \cdot [\mathrm{PleC_{kin2}}] \tag{7}$$

$$\frac{\mathrm{d}[\mathrm{PleC_{kin22}}]}{\mathrm{d}t} = k_{\mathrm{ph2-pk22}} \cdot [\mathrm{PleC_{h2}}] \cdot [\mathrm{DivK}] - k_{\mathrm{pk22-ph2}} \cdot [\mathrm{PleC_{kin22}}] - k_{\mathrm{p22-pk4}} \cdot [\mathrm{PleC_{kin22}}] + k_{\mathrm{pk4-pk22}} \cdot [\mathrm{PleC_{kin4}}] \tag{8}$$

$$\frac{\mathrm{d}[\mathrm{PleC_{kin0}}]}{\mathrm{d}t} = k_{\mathrm{pk11-pk0}} \cdot [\mathrm{PleC_{kin11}}] - k_{\mathrm{pk0-pk11}} \cdot [\mathrm{PleC_{kin0}}] - k_{\mathrm{pk0-pk1}} \cdot [\mathrm{PleC_{kin0}}] + k_{\mathrm{pk1-pk0}} \cdot [\mathrm{PleC_{kin1}}] \cdot [\mathrm{DivK{\sim}P}] \tag{9}$$

$$\frac{\mathrm{d}[\mathrm{PleC_{kin2}}]}{\mathrm{d}t} = k_{\mathrm{pk12-pk2}} \cdot [\mathrm{PleC_{kin12}}] - k_{\mathrm{pk2-pk11}} \cdot [\mathrm{PleC_{kin2}}] - k_{\mathrm{pk2-pk1}} \cdot [\mathrm{PleC_{kin2}}] + k_{\mathrm{pk1-pk2}} \cdot [\mathrm{PleC_{kin1}}] \cdot [\mathrm{DivK}] - k_{\mathrm{pk2-pk3}} \cdot [\mathrm{PleC_{kin2}}] + k_{\mathrm{pk3-pk2}} \cdot [\mathrm{PleC_{kin3}}] \cdot [\mathrm{DivK{\sim}P}] + k_{\mathrm{pt2-pk2}} \cdot [\mathrm{PleC_{pt2}}] - k_{\mathrm{pk2-pt2}} \cdot [\mathrm{PleC_{kin2}}] \tag{10}$$

$$\frac{\mathrm{d}[\mathrm{PleC_{kin4}}]}{\mathrm{d}t} = k_{\mathrm{pk22-pk4}} \cdot [\mathrm{PleC_{kin22}}] - k_{\mathrm{pk4-pk22}} \cdot [\mathrm{PleC_{kin4}}] - k_{\mathrm{pk4-pk3}} \cdot [\mathrm{PleC_{kin4}}] + k_{\mathrm{pk3-pk4}} \cdot [\mathrm{PleC_{kin3}}] \cdot [\mathrm{DivK}] + k_{\mathrm{pt4-pk4}} \cdot [\mathrm{PleC_{pt4}}] - k_{\mathrm{pk4-pt4}} \cdot [\mathrm{PleC_{kin4}}] \tag{11}$$

$$\frac{d[\mathrm{PleC_{kin1}}]}{dt} = -k_{\mathrm{pk1-pk0}} \cdot [\mathrm{PleC_{kin1}}] \cdot [\mathrm{DivK{\sim}P}] + k_{\mathrm{pk0-pk1}} \cdot [\mathrm{PleC_{kin0}}] - k_{\mathrm{pk1-pk2}} \cdot [\mathrm{PleC_{kin1}}] \cdot [\mathrm{DivK}] + k_{\mathrm{pk2-pk1}} \cdot [\mathrm{PleC_{kin2}}] + k_{\mathrm{pk2p-pk1}} \cdot [\mathrm{PleC_{kin2p}}] \cdot [\mathrm{DivK{\sim}P}] - k_{\mathrm{pk1-pk2p}} \cdot [\mathrm{PleC_{kin1}}] + k_{\mathrm{pk1h-pk1}} \cdot [\mathrm{PleC_{kin1h}}] - k_{\mathrm{pk1-pk1h}} \cdot [\mathrm{PleC_{kin1}}] - k_{\mathrm{pk1-pk5}} \cdot [\mathrm{PleC_{kin1}}] \cdot [\mathrm{PleD}] + k_{\mathrm{pk5-pk1}} \cdot [\mathrm{PleC_{kin5}}] \quad (12)$$

$$\frac{d[\mathrm{PleC_{kin3}}]}{dt} = -k_{\mathrm{pk3-pk2}} \cdot [\mathrm{PleC_{kin3}}] \cdot [\mathrm{DivK{\sim}P}] + k_{\mathrm{pk2-pk3}} \cdot [\mathrm{PleC_{kin2}}] - k_{\mathrm{pk3-pk4}} \cdot [\mathrm{PleC_{kin3}}] \cdot [\mathrm{DivK}] + k_{\mathrm{pk4-pk3}} \cdot [\mathrm{PleC_{kin4}}] + k_{\mathrm{pk2p-pk3}} \cdot [\mathrm{PleC_{kin2p}}] \cdot [\mathrm{DivK}] - k_{\mathrm{pk3-pk2p}} \cdot [\mathrm{PleC_{kin3}}] + k_{\mathrm{pk3h-pk3}} \cdot [\mathrm{PleC_{kin3h}}] - k_{\mathrm{pk3-pk3h}} \cdot [\mathrm{PleC_{kin3}}] + k_{\mathrm{pt3-pk3}} \cdot [\mathrm{PleC_{pt3}}] - k_{\mathrm{pk3-pt3}} \cdot [\mathrm{PleC_{kin3}}] - k_{\mathrm{pk3-pk6}} \cdot [\mathrm{PleC_{kin3}}] \cdot [\mathrm{PleD}] + k_{\mathrm{pk6-pk3}} \cdot [\mathrm{PleC_{kin6}}] \quad (13)$$

$$\frac{d[\mathrm{PleC_{pt2}}]}{dt} = k_{\mathrm{pk1h-pt2}} \cdot [\mathrm{PleC_{kin1h}}] \cdot [\mathrm{DivK{\sim}P}] - k_{\mathrm{pt2-pk1h}} \cdot [\mathrm{PleC_{pt2}}] - k_{\mathrm{pt2-pk2}} \cdot [\mathrm{PleC_{pt2}}] + k_{\mathrm{pk2-pt2}} \cdot [\mathrm{PleC_{kin2}}] \quad (14)$$

$$\frac{d[\mathrm{PleC_{pt3}}]}{dt} = k_{\mathrm{pk1p-pt3}} \cdot [\mathrm{PleC_{kin1p}}] \cdot [\mathrm{DivK{\sim}P}] - k_{\mathrm{pt3-pk1p}} \cdot [\mathrm{PleC_{pt3}}] - k_{\mathrm{pt3-pk3}} \cdot [\mathrm{PleC_{pt3}}] + k_{\mathrm{pk3-pt3}} \cdot [\mathrm{PleC_{kin3}}] \quad (15)$$

$$\frac{d[\mathrm{PleC_{pt4}}]}{dt} = k_{\mathrm{pk3h-pt4}} \cdot [\mathrm{PleC_{kin3h}}] \cdot [\mathrm{DivK{\sim}P}] - k_{\mathrm{pt4-pk3h}} \cdot [\mathrm{PleC_{pt4}}] - k_{\mathrm{pt4-pk4}} \cdot [\mathrm{PleC_{pt4}}] + k_{\mathrm{pk4-pt4}} \cdot [\mathrm{PleC_{kin4}}] - k_{\mathrm{pt4-p11}} \cdot [\mathrm{PleC_{pt4}}] + k_{\mathrm{p11-pt4}} \cdot [\mathrm{PleC_{kin11}}] \quad (16)$$

$$\frac{d[\mathrm{PleC_{kin1h}}]}{dt} = -k_{\mathrm{pk1h-pt2}} \cdot [\mathrm{PleC_{kin1h}}] \cdot [\mathrm{DivK{\sim}P}] + k_{\mathrm{pt2-pk1h}} \cdot [\mathrm{PleC_{pt2}}] - k_{\mathrm{pk1h-pk1}} \cdot [\mathrm{PleC_{kin1h}}] + k_{\mathrm{pk1-pk1h}} \cdot [\mathrm{PleC_{kin1}}] + k_{\mathrm{pk1p-pk1h}} \cdot [\mathrm{PleC_{kin1p}}] \cdot [\mathrm{DivK{\sim}P}] - k_{\mathrm{pk1h-pk1p}} \cdot [\mathrm{PleC_{kin1h}}] - k_{\mathrm{pk1h-pt5}} \cdot [\mathrm{PleC_{kin1h}}] \cdot [\mathrm{PleD{\sim}P}] + k_{\mathrm{pt5-pk1h}} \cdot [\mathrm{PleC_{pt5}}] \quad (17)$$

$$\frac{d[\mathrm{PleC_{kin3h}}]}{dt} = -k_{\mathrm{pk3h-pk3}} \cdot [\mathrm{PleC_{kin3h}}] + k_{\mathrm{pk3-pk3h}} \cdot [\mathrm{PleC_{kin3}}] + k_{\mathrm{pk1p-pk3h}} \cdot [\mathrm{PleC_{kin1p}}] \cdot [\mathrm{DivK}] - k_{\mathrm{pk3h-pk1p}} \cdot [\mathrm{PleC_{kin3h}}] - k_{\mathrm{pk3h-pt4}} \cdot [\mathrm{PleC_{kin3h}}] \cdot [\mathrm{DivK{\sim}P}] + k_{\mathrm{pt4-pk3h}} \cdot [\mathrm{PleC_{pt4}}] - k_{\mathrm{pk3h-pt6}} \cdot [\mathrm{PleC_{kin3h}}] \cdot [\mathrm{PleD{\sim}P}] + k_{\mathrm{pt6-pk3h}} \cdot [\mathrm{PleC_{pt6}}] \quad (18)$$

$$\frac{d[\mathrm{PleC_{kin2p}}]}{dt} = -k_{\mathrm{pk2p-pk1}} \cdot [\mathrm{PleC_{kin2p}}] \cdot [\mathrm{DivK{\sim}P}] + k_{\mathrm{pk1-pk2p}} \cdot [\mathrm{PleC_{kin1}}] - k_{\mathrm{pk2p-pk3}} \cdot [\mathrm{PleC_{pk2p}}] \cdot [\mathrm{DivK}] + k_{\mathrm{pk3-pk2p}} \cdot [\mathrm{PleC_{kin3}}] - k_{\mathrm{pk2p-pc}} \cdot [\mathrm{PleC_{kin2p}}] \tag{19}$$

$$\frac{d[\mathrm{PleC_{kin1p}}]}{dt} = -k_{\mathrm{pk1p-pk1h}} \cdot [\mathrm{PleC_{kin1p}}] \cdot [\mathrm{DivK{\sim}P}] + k_{\mathrm{pk1h-pk1p}} \cdot [\mathrm{PleC_{kin1h}}] - k_{\mathrm{pk1p-pt3}} \cdot [\mathrm{PleC_{pk1p}}] \cdot [\mathrm{DivK}] + k_{\mathrm{pt3-pk1p}} \cdot [\mathrm{PleC_{pt3}}] - k_{\mathrm{pk1p-pc}} \cdot [\mathrm{PleC_{kin1p}}] - k_{\mathrm{pk1p-pk3h}} \cdot [\mathrm{PleC_{kin1p}}] \cdot [\mathrm{DivK}] + k_{\mathrm{pk3h-pk1p}} \cdot [\mathrm{PleC_{kin3h}}] \tag{20}$$

$$\frac{d[\mathrm{DivJ}]}{dt} = -k_{\mathrm{j-jk}} \cdot [\mathrm{DivJ}] \cdot [\mathrm{DivK}] + k_{\mathrm{jk-j}} \cdot [\mathrm{DivJ{:}\,DivK}] + k_{\mathrm{e-jk}} \cdot [\mathrm{DivJ{:}\,DivK}] \tag{21}$$

$$\frac{d[\mathrm{DivJ{:}\,DivK}]}{dt} = k_{\mathrm{j-jk}} \cdot [\mathrm{DivJ}] \cdot [\mathrm{DivK}] - k_{\mathrm{jk-j}} \cdot [\mathrm{DivJ{:}\,DivK}] - k_{\mathrm{e-jk}} \cdot [\mathrm{DivJ{:}\,DivK}] \tag{22}$$

$$\frac{d[\mathrm{PleD}]}{dt} = k_{\mathrm{syn-pld}} - k_{\mathrm{deg-pld}} \cdot [\mathrm{PleD}] - k_{\mathrm{pk1-pk5}} \cdot [\mathrm{PleC_{kin1}}] \cdot [\mathrm{PleD}] + k_{\mathrm{pk5-pk1}} \cdot [\mathrm{PleC_{kin5}}] - k_{\mathrm{pk3-pk6}} \cdot [\mathrm{PleC_{kin3}}] \cdot [\mathrm{PleD}] + k_{\mathrm{pk6-pk3}} \cdot [\mathrm{PleC_{kin6}}] + k_{\mathrm{e-ph3}} \cdot [\mathrm{Phos{:}\,PleD{\sim}P}] \tag{23}$$

$$\frac{d[\mathrm{PleD{\sim}P}]}{dt} = -k_{\mathrm{deg-pldp}} \cdot [\mathrm{PleD{\sim}P}] - k_{\mathrm{pk1h-pt5}} \cdot [\mathrm{PleC_{kin1h}}] \cdot [\mathrm{PleD{\sim}P}] + k_{\mathrm{pt5-pk1h}} \cdot [\mathrm{PleC_{pt5}}] - k_{\mathrm{pk3h-pt6}} \cdot [\mathrm{PleC_{kin3h}}] \cdot [\mathrm{PleD{\sim}P}] + k_{\mathrm{pt6-pk3h}} \cdot [\mathrm{PleC_{pt6}}] - k_{\mathrm{phos-ph3}} \cdot [\mathrm{Phos}] \cdot [\mathrm{PleD{\sim}P}] + k_{\mathrm{ph3-phos}} \cdot [\mathrm{Phos{:}\,PleD{\sim}P}] \tag{24}$$

$$\frac{d[\mathrm{PleC_{kin5}}]}{dt} = k_{\mathrm{pk1-pk5}} \cdot [\mathrm{PleC_{kin1}}] \cdot [\mathrm{PleD}] - k_{\mathrm{pk5-pk1}} \cdot [\mathrm{PleC_{kin5}}] - k_{\mathrm{pk5-pt5}} \cdot [\mathrm{PleC_{kin5}}] + k_{\mathrm{pt5-pk5}} \cdot [\mathrm{PleC_{pt5}}] \tag{25}$$

$$\frac{d[\mathrm{PleC_{kin6}}]}{dt} = k_{\mathrm{pk3-pk6}} \cdot [\mathrm{PleC_{kin3}}] \cdot [\mathrm{PleD}] - k_{\mathrm{pk6-pk3}} \cdot [\mathrm{PleC_{kin6}}] - k_{\mathrm{pk6-pt6}} \cdot [\mathrm{PleC_{kin6}}] + k_{\mathrm{pt6-pk6}} \cdot [\mathrm{PleC_{pt6}}] \tag{26}$$

$$\frac{d[\mathrm{PleC_{pt5}}]}{dt} = k_{\mathrm{pk5-pt5}} \cdot [\mathrm{PleC_{kin5}}] - k_{\mathrm{pt5-pk5}} \cdot [\mathrm{PleC_{pt5}}] + k_{\mathrm{pk1h-pt5}} \cdot [\mathrm{PleC_{kin1h}}] \cdot [\mathrm{PleD{\sim}P}] - k_{\mathrm{pt5-pk1h}} \cdot [\mathrm{PleC_{pt5}}] \tag{27}$$

$$\frac{d[\mathrm{PleC_{pt6}}]}{dt} = k_{\mathrm{pk6-pt6}} \cdot [\mathrm{PleC_{kin6}}] - k_{\mathrm{pt6-pk6}} \cdot [\mathrm{PleC_{pt6}}] + k_{\mathrm{pk3h-pt6}} \cdot [\mathrm{PleC_{kin3h}}] \cdot [\mathrm{PleD{\sim}P}] - k_{\mathrm{pt6-pk3h}} \cdot [\mathrm{PleC_{pt6}}] \tag{28}$$

$$\frac{d[\mathrm{Phos}]}{dt} = -k_{\mathrm{phos-ph3}} \cdot [\mathrm{Phos}] \cdot [\mathrm{PleD{\sim}P}] + k_{\mathrm{ph3-phos}} \cdot [\mathrm{Phos{:}PleD{\sim}P}] + k_{\mathrm{e-ph3}} \cdot [\mathrm{Phos{:}PleD{\sim}P}] \quad (29)$$

$$\frac{d[\mathrm{Phos{:}PleD{\sim}P}]}{dt} = k_{\mathrm{phos-ph3}} \cdot [\mathrm{Phos}] \cdot [\mathrm{PleD{\sim}P}] - k_{\mathrm{ph3-phos}} \cdot [\mathrm{Phos{:}PleD{\sim}P}] - k_{\mathrm{e-ph3}} \cdot [\mathrm{Phos{:}PleD{\sim}P}] \quad (30)$$

$$\frac{d[\mathrm{DivL}]}{dt} = k_{\mathrm{syndl}} - k_{\mathrm{degdl}} \cdot [\mathrm{DivL}] - k_{\mathrm{dl-dldk}} \cdot [\mathrm{DivL}] \cdot [\mathrm{DivK{\sim}P}] + k_{\mathrm{dldk-dl}} \cdot [\mathrm{DivL{:}DivK{\sim}P}] \quad (31)$$

$$\frac{d[\mathrm{DivL{:}DivK{\sim}P}]}{dt} = k_{\mathrm{dl-dldk}} \cdot [\mathrm{DivL}] \cdot [\mathrm{DivK{\sim}P}] - k_{\mathrm{dldk-dl}} \cdot [\mathrm{DivL{:}DivK{\sim}P}] \quad (32)$$

$$\frac{d[\mathrm{CtrA}]}{dt} = k_{\mathrm{syn-ctr}} - k_{\mathrm{deg-ctr}} \cdot [\mathrm{CtrA}] - k_{\mathrm{ck-ck1}} \cdot [\mathrm{CckA_{kin}}] \cdot [\mathrm{CtrA}] + k_{\mathrm{ck1-ck}} \cdot [\mathrm{CckA_{kin1}}] + k_{\mathrm{e-ch1}} \cdot [\mathrm{CckA_{h1}}] \quad (33)$$

$$\frac{d[\mathrm{CtrA{\sim}P}]}{dt} = -k_{\mathrm{deg-ctr}} \cdot [\mathrm{CtrA{\sim}P}] + k_{\mathrm{ct1-ck}} \cdot [\mathrm{CckA_{ct1}}] - k_{\mathrm{ck-ct1}} \cdot [\mathrm{CckA_{kin}}] \cdot [\mathrm{CtrA{\sim}P}] - k_{\mathrm{cp-ch1}} \cdot [\mathrm{CckA_{phos}}] \cdot [\mathrm{CtrA{\sim}P}] + k_{\mathrm{ch1-cp}} \cdot [\mathrm{CckA_{h1}}] \quad (34)$$

$$\frac{d[\mathrm{CpdR}]}{dt} = k_{\mathrm{syn-cpd}} - k_{\mathrm{deg-cpd}} \cdot [\mathrm{CpdR}] - k_{\mathrm{ck-ck2}} \cdot [\mathrm{CckA_{kin}}] \cdot [\mathrm{CpdR}] + k_{\mathrm{ck2-ck}} \cdot [\mathrm{CckA_{kin2}}] + k_{\mathrm{e-ch2}} \cdot [\mathrm{CckA_{h2}}] \quad (35)$$

$$\frac{d[\mathrm{CpdR{\sim}P}]}{dt} = -k_{\mathrm{deg-cpd}} \cdot [\mathrm{CpdR{\sim}P}] + k_{\mathrm{ct2-ck}} \cdot [\mathrm{CckA_{ct1}}] - k_{\mathrm{ck-ct2}} \cdot [\mathrm{CckA_{kin}}] \cdot [\mathrm{CpdR{\sim}P}] - k_{\mathrm{cp-ch2}} \cdot [\mathrm{CckA_{phos}}] \cdot [\mathrm{CpdR{\sim}P}] + k_{\mathrm{ch2-cp}} \cdot [\mathrm{CckA_{h2}}] \quad (36)$$

$$\frac{d[\mathrm{CckA_{phos}}]}{dt} = -k_{\mathrm{cp-ch1}} \cdot [\mathrm{CckA_{phos}}] \cdot [\mathrm{CtrA{\sim}P}] + k_{\mathrm{ch1-cp}} \cdot [\mathrm{CckA_{h1}}] - k_{\mathrm{cp-ch2}} \cdot [\mathrm{CckA_{phos}}] \cdot [\mathrm{CpdR{\sim}P}] + k_{\mathrm{ch2-cp}} \cdot [\mathrm{CckA_{h2}}] - k_{\mathrm{cp-ck}} \cdot [\mathrm{CckA_{phos}}] \cdot \frac{[\mathrm{DivL}]^2}{K_{\mathrm{dl}}^2 + [\mathrm{DivL}]^2} + k_{\mathrm{ck-cp}} \cdot [\mathrm{CckA_{kin}}] + k_{\mathrm{e-ch1}} \cdot [\mathrm{CckA_{h1}}] + k_{\mathrm{e-ch2}} \cdot [\mathrm{CckA_{h2}}] \quad (37)$$

$$\frac{d[\mathrm{CckA_{kin}}]}{dt} = k_{\mathrm{cp-ck}} \cdot [\mathrm{CckA_{phos}}] \cdot \frac{[\mathrm{DivL}]^2}{K_{\mathrm{dl}}^2 + [\mathrm{DivL}]^2} - k_{\mathrm{ck-cp}} \cdot [\mathrm{CckA_{kin}}] - k_{\mathrm{ck-ck1}} \cdot [\mathrm{CckA_{kin}}] \cdot [\mathrm{CtrA}] + k_{\mathrm{ck1-ck}} \cdot [\mathrm{CckA_{kin1}}] - k_{\mathrm{ck-ck2}} \cdot [\mathrm{CckA_{kin}}] \cdot [\mathrm{CpdR}] + k_{\mathrm{ck2-ck}} \cdot [\mathrm{CckA_{kin2}}] + k_{\mathrm{ct1-ck}} \cdot [\mathrm{CckA_{ct1}}] - k_{\mathrm{ck-ct1}} \cdot [\mathrm{CckA_{kin}}] \cdot [\mathrm{CtrA{\sim}P}] + k_{\mathrm{ct2-ck}} \cdot [\mathrm{CckA_{ct2}}] - k_{\mathrm{ck-ct2}} \cdot [\mathrm{CckA_{kin}}] \cdot [\mathrm{CpdR{\sim}P}] \quad (38)$$

$$\frac{\mathrm{d}[\mathrm{CckA_{kin1}}]}{\mathrm{d}t} = k_{\mathrm{ck-ck1}} \cdot [\mathrm{CckA_{kin}}] \cdot [\mathrm{CtrA}] - k_{\mathrm{ck1-ck}} \cdot [\mathrm{CckA_{kin1}}] - k_{\mathrm{ck1-ct1}} \cdot [\mathrm{CckA_{kin1}}] + k_{\mathrm{ct1-ck1}} \cdot [\mathrm{CckA_{ct1}}] \quad 39$$

$$\frac{\mathrm{d}[\mathrm{CckA_{kin2}}]}{\mathrm{d}t} = k_{\mathrm{ck-ck2}} \cdot [\mathrm{CckA_{kin}}] \cdot [\mathrm{CpdR}] - k_{\mathrm{ck2-ck}} \cdot [\mathrm{CckA_{kin2}}] - k_{\mathrm{ck2-ct2}} \cdot [\mathrm{CckA_{kin2}}] + k_{\mathrm{ct2-ck2}} \cdot [\mathrm{CckA_{ct2}}] \quad 40$$

$$\frac{\mathrm{d}[\mathrm{CckA_{ct1}}]}{\mathrm{d}t} = k_{\mathrm{ck1-ct1}} \cdot [\mathrm{CckA_{kin1}}] - k_{\mathrm{ct1-ck1}} \cdot [\mathrm{CckA_{ct1}}] - k_{\mathrm{ct1-ck}} \cdot [\mathrm{CckA_{ct1}}] + k_{\mathrm{ck-ct1}} \cdot [\mathrm{CckA_{kin}}] \cdot [\mathrm{CtrA{\sim}P}] \quad 41$$

$$\frac{\mathrm{d}[\mathrm{CckA_{ct2}}]}{\mathrm{d}t} = k_{\mathrm{ck2-ct2}} \cdot [\mathrm{CckA_{kin2}}] - k_{\mathrm{ct2-ck2}} \cdot [\mathrm{CckA_{ct2}}] - k_{\mathrm{ct2-ck}} \cdot [\mathrm{CckA_{ct2}}] + k_{\mathrm{ck-ct2}} \cdot [\mathrm{CckA_{kin}}] \cdot [\mathrm{CpdR{\sim}P}] \quad 42$$

$$\frac{\mathrm{d}[\mathrm{CckA_{h1}}]}{\mathrm{d}t} = k_{\mathrm{cp-ch1}} \cdot [\mathrm{CckA_{phos}}] \cdot [\mathrm{CtrA{\sim}P}] - k_{\mathrm{ch1-cp}} \cdot [\mathrm{CckA_{h1}}] - k_{\mathrm{e-ch1}} \cdot [\mathrm{CckA_{h1}}] \quad 43$$

$$\frac{\mathrm{d}[\mathrm{CckA_{h2}}]}{\mathrm{d}t} = k_{\mathrm{cp-ch2}} \cdot [\mathrm{CckA_{phos}}] \cdot [\mathrm{CpdR{\sim}P}] - k_{\mathrm{ch2-cp}} \cdot [\mathrm{CckA_{h2}}] - k_{\mathrm{e-ch2}} \cdot [\mathrm{CckA_{h2}}] \quad 44$$

Table A.7: Basal parameter values used in the reduced model*.

$k_{\text{pc-ph1}}$	5	$k_{\text{ph1-pc}}$	5	$k_{\text{j-jk}}$	1	$k_{\text{jk-j}}$	0.1
$k_{\text{ph1-pk11}}$	5	$k_{\text{pk11-ph1}}$	2.5	$k_{\text{pk0-pk1}}$	0.16	$k_{\text{pk1-pk0}}$	5
$k_{\text{pk1-pk2}}$	5	$k_{\text{pk2-pk1}}$	0.0016	$k_{\text{pk1-pk1h}}$	5	$k_{\text{pk1h-pk1}}$	5
$k_{\text{pk1-pk2p}}$	0.16	$k_{\text{pk2p-pk1}}$	5	$k_{\text{pk2-pt2}}$	5	$k_{\text{pt2-pk2}}$	0.16
$k_{\text{pt2-pk1h}}$	0.16	$k_{\text{pk1h-pt2}}$	5	$k_{\text{pk2p-pc}}$	5	$k_{\text{pk1p-pc}}$	5
$k_{\text{pk2-pk3}}$	0.16	$k_{\text{pk3-pk2}}$	5	$k_{\text{pk3-pk2p}}$	0.0016	$k_{\text{pk2p-pk3}}$	5
$k_{\text{pk3-pt3}}$	5	$k_{\text{pt3-pk3}}$	0.16	$k_{\text{pt3-pk1p}}$	0.16	$k_{\text{pk1p-pt3}}$	5
$k_{\text{pk1p-pk1h}}$	5	$k_{\text{pk1h-pk1p}}$	0.16	$k_{\text{ph2-pk22}}$	0.016	$k_{\text{pk22-ph2}}$	1.6-08
$k_{\text{pk3-pk4}}$	5	$k_{\text{pk4-pk3}}$	0.0016	$k_{\text{pk4-pt4}}$	5	$k_{\text{pt4-pk4}}$	0.16
$k_{\text{pt4-pk11}}$	5	$k_{\text{pk11-pt4}}$	0.0775	$k_{\text{pc-ph2}}$	0.5	$k_{\text{ph2-pc}}$	5

$k_{\text{ph2-pk12}}$	1.6	$k_{\text{pk12-ph2}}$	1.6e-04	$k_{\text{ph1-pk12}}$	1.6e-02	$k_{\text{pk12-ph1}}$	1.6e-04
$k_{\text{pt4-pk3h}}$	0.16	$k_{\text{pk3h-pt4}}$	5	$k_{\text{pk3-pk3h}}$	5	$k_{\text{pk3h-pk3}}$	5
$k_{\text{pk1p-pk3h}}$	5	$k_{\text{p3h-pk1p}}$	0.0016	$k_{\text{ph1-ph2}}$	10	$k_{\text{ph2-ph1}}$	5e-03
$k_{\text{pk11-pk0}}$	2.5	$k_{\text{pk0-pk11}}$	5	$k_{\text{pk12-pk2}}$	5	$k_{\text{pk2-pk12}}$	5
$k_{\text{syn-pld}}$	0.01	$k_{\text{deg-pldp}}$	0.005	$k_{\text{deg-pldp}}$	0.005	$k_{\text{phos-ph3}}$	1
$k_{\text{ph3-phos}}$	0.1	$k_{\text{pk1-pk5}}$	10	$k_{\text{pk5-pk1}}$	0.31	$k_{\text{pk5-pt5}}$	10
$k_{\text{pt5-pk5}}$	0.31	$k_{\text{pt5-pk1h}}$	10	$k_{\text{pk1h-pt5}}$	0.31	$k_{\text{pk3-pk6}}$	10
$k_{\text{pk6-pk3}}$	0.31	$k_{\text{pk6-pt6}}$	10	$k_{\text{pt6-pk6}}$	0.31	$k_{\text{pt6-pk3h}}$	10
$k_{\text{pk3h-pt6}}$	0.31	$k_{\text{e-ph3}}$	0.2				
$k_{\text{syn-dk}}$	0.015	$k_{\text{deg-dk}}$	0.005	$k_{\text{deg-dkp}}$	0.005	$k_{\text{h1-h2}}$	1.6e-02
$k_{\text{h2-h1}}$	1.6	$k_{\text{e-jin}}$	0.5	$k_{\text{pk22-pk4}}$	5	$k_{\text{pk4-pk22}}$	5
$k_{\text{dl-dldk}}$	1	$k_{\text{dldk\_dl}}$	0.1	k_{syndl}	0.005	k_{degdl}	0.005
$k_{\text{cp-ck}}$	1	$k_{\text{cp-ck}}$	0.1	$k_{\text{cp-ch2}}$	1	$k_{\text{ch2-cp}}$	0.1
$k_{\text{syn-ctra}}$	0.05	$k_{\text{deg-ctr}}$	0.02	$k_{\text{deg-ctrp}}$	0.02	$k_{\text{syn-cpdr}}$	0.05
$k_{\text{deg-cpdr}}$	0.02	$k_{\text{deg-cpdp}}$	0.02	$k_{\text{ck-ck1}}$	1	$k_{\text{ck1-ck}}$	0.1
$k_{\text{ck1-ct1}}$	1	$k_{\text{ct1-ck1}}$	0.1	$k_{\text{ct1-ck}}$	1	$k_{\text{ck-ct1}}$	0.1
$k_{\text{cp-ch1}}$	1	$k_{\text{ch1-cp}}$	0.1	$k_{\text{e-ch1}}$	1	$k_{\text{ck-ck2}}$	1
$k_{\text{ck2-ck}}$	0.1	$k_{\text{ck2-ct2}}$	1	$k_{\text{ct2-ck2}}$	0.1	$k_{\text{ct2-ck}}$	1
$k_{\text{ck-ct2}}$	0.1	$k_{\text{e-ch2}}$	1				
DivJ_tot	0.5	PleC_tot	1	CckA_tot	1	Phos_tot	0.1
K_{dl}	0.75						

*For each reaction of the form X → Y, the parameters $k_{\text{x-y}}$ and $k_{\text{y-x}}$ are the forward and reverse rate constants (min^{-1}). DivJ_tot, PleC_tot, CckA_tot, Phos_tot and K_{dl} are dimensionless constants representing concentrations.

Table A.8: Parameter values used to simulate mutants*.

$divK_{D53N}$			
$k_{\text{pk2-pt2}}$ 0	$k_{\text{pt2-pk2}}$ 0	$k_{\text{pk3-pt3}}$ 0	$k_{\text{pt3-pk3}}$ 0
$k_{\text{pk4-pt4}}$ 0	$k_{\text{pt4-pk4}}$ 0	$k_{\text{pt4-pk11}}$ 0	$k_{\text{pk11-pt4}}$ 0
$divK_{D90G}$			
$k_{\text{ph1\_pk11}}$ 2.5	$k_{\text{pk11\_ph1}}$ 49	$k_{\text{ph1\_pk12}}$ 0.016	$k_{\text{pk12\_ph1}}$ 16
$k_{\text{ph2\_pk22}}$ 0.025	$k_{\text{pk22\_ph2}}$ 2.5e-03	$k_{\text{ph2\_pk12}}$ 1.6	$k_{\text{pk12\_ph2}}$ 16
$k_{\text{h1\_h2}}$ 0.016	$k_{\text{h2\_h1}}$ 1.6	$k_{\text{dl\_dldk}}$ 0.1	
*pleC:*Tn*5*			
PleC_tot 0			
$\Delta divJ$			
DivJ_tot 0			
$pleC_{F778L}$			
$k_{\text{pk11-pk0}}$ 0	$k_{\text{pk0-pk11}}$ 0	$k_{\text{pk12-pk2}}$ 0	$k_{\text{pk2-pk12}}$ 0
$k_{\text{pk22-pk4}}$ 0	$k_{\text{pk4-pk22}}$ 0		

*Only parameter values deviating from wild type are listed.

Appendix B Supplementary information for chapter 3

B.1 Supplementary Figures

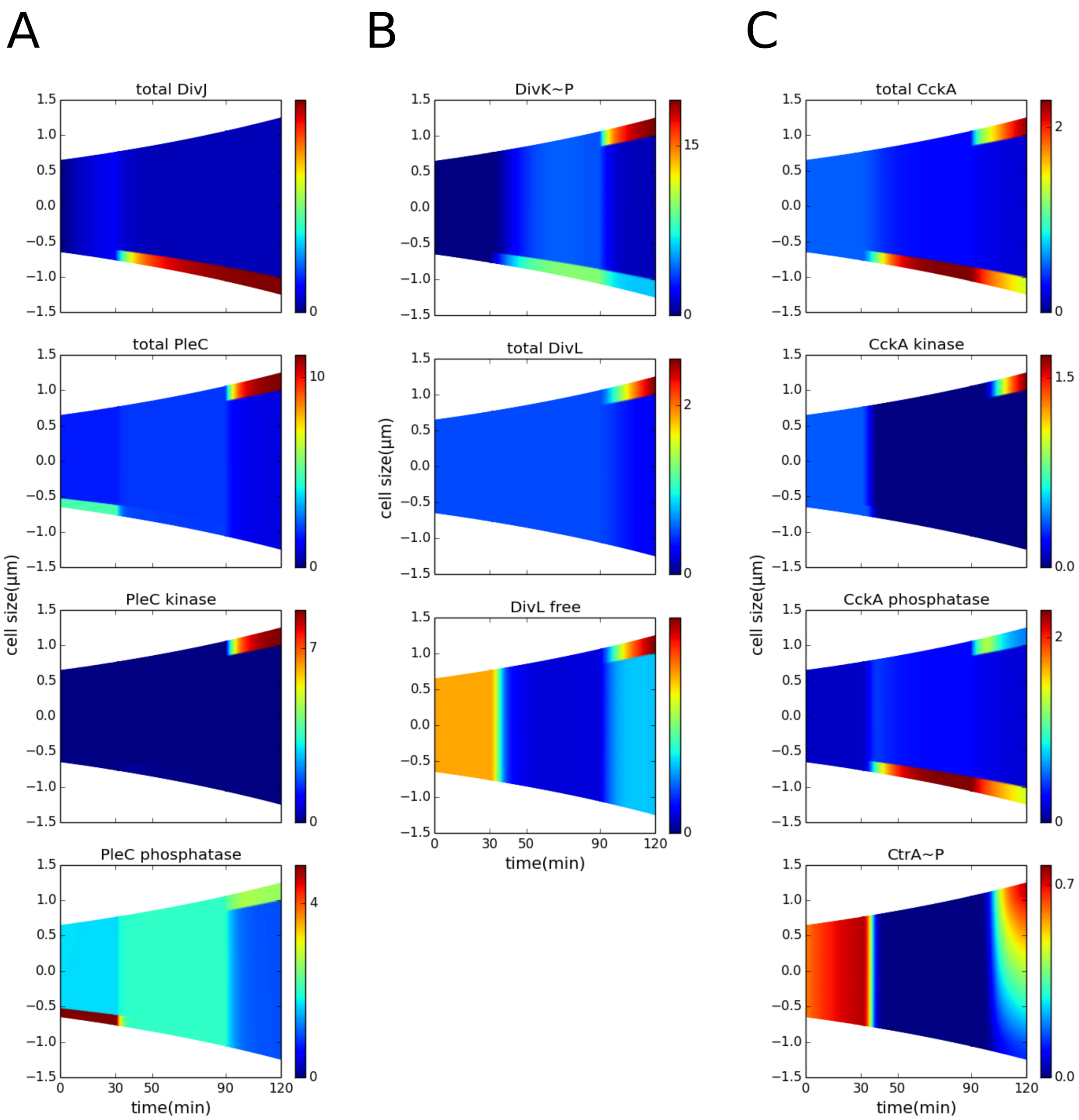

Figure B.1: Spatiotemporal distribution of proteins when PleC is delocalized (at t = 30 min) from the old pole of the stalked cell.

Color indicates concentration gradients from minimum (blue) to maximum (red). (A) DivJ is localized at the old pole (t = 30 – 120 min). PleC is delocalized from the old pole before it can transition to a kinase in the stalked cell. (B) Instead, PleC transitions to the kinase state in the new pole of the predivisional cell, enabling DivL to be in the active form. (C) CckA becoming a kinase, while old-pole CckA remains a phosphatase. Consequently, the predivisional cell establishes a gradient of CtrA~P along its length from high at the new pole to low at the old pole.

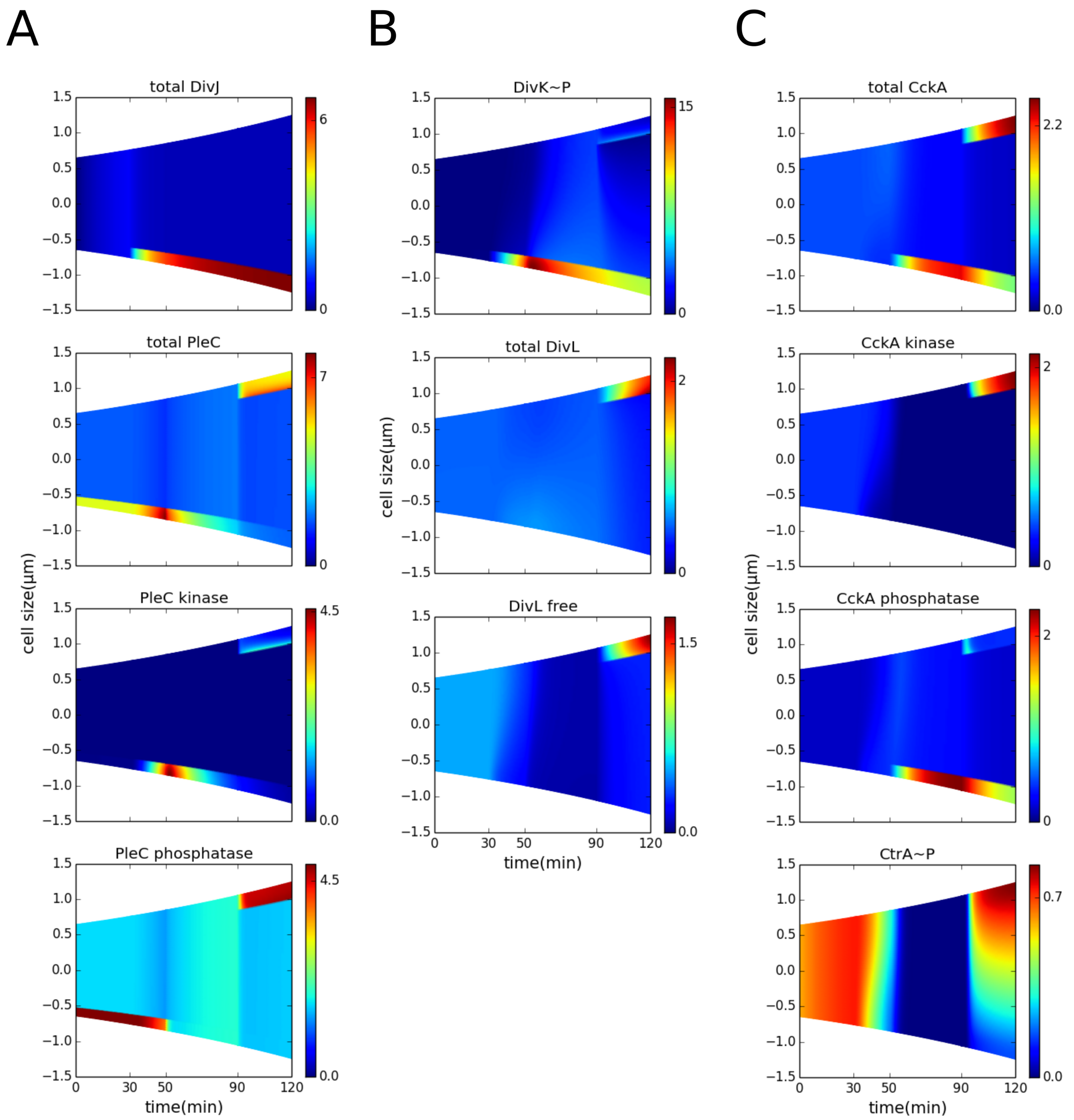

Figure B.2: New-pole PleC is a phosphatase if $D_{\mathrm{DivK}} = D_{\mathrm{DivK\sim P}} = 0.1\ \mu\mathrm{m}^2\ \mathrm{min}^{-1}$.

(A) PleC becomes a kinase in the old pole of the stalked cell (t = 30-70 minutes). Upon relocation to the new pole (t = 90 min), PleC reverts back to phosphatase form because of the slow diffusion of DivK~P. (B) Consequently, DivK is dephosphorylated in the new pole and fails to localize there, and new pole DivL is protected from the inhibitory effect of DivK~P. (C) CckA localized at the new pole is a kinase and the CtrA~P gradient is established in the predvisiional cell.

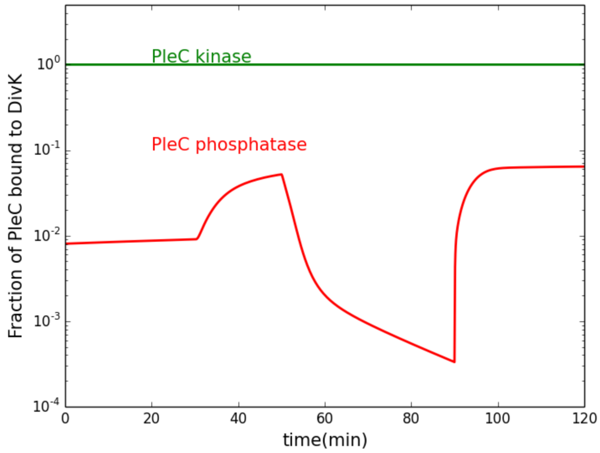

Figure B.3: Fraction of PleC kinase (green curve) and PleC phosphatase (red curve) that is bound to DivK and/or DivK~P is shown in log-scale.

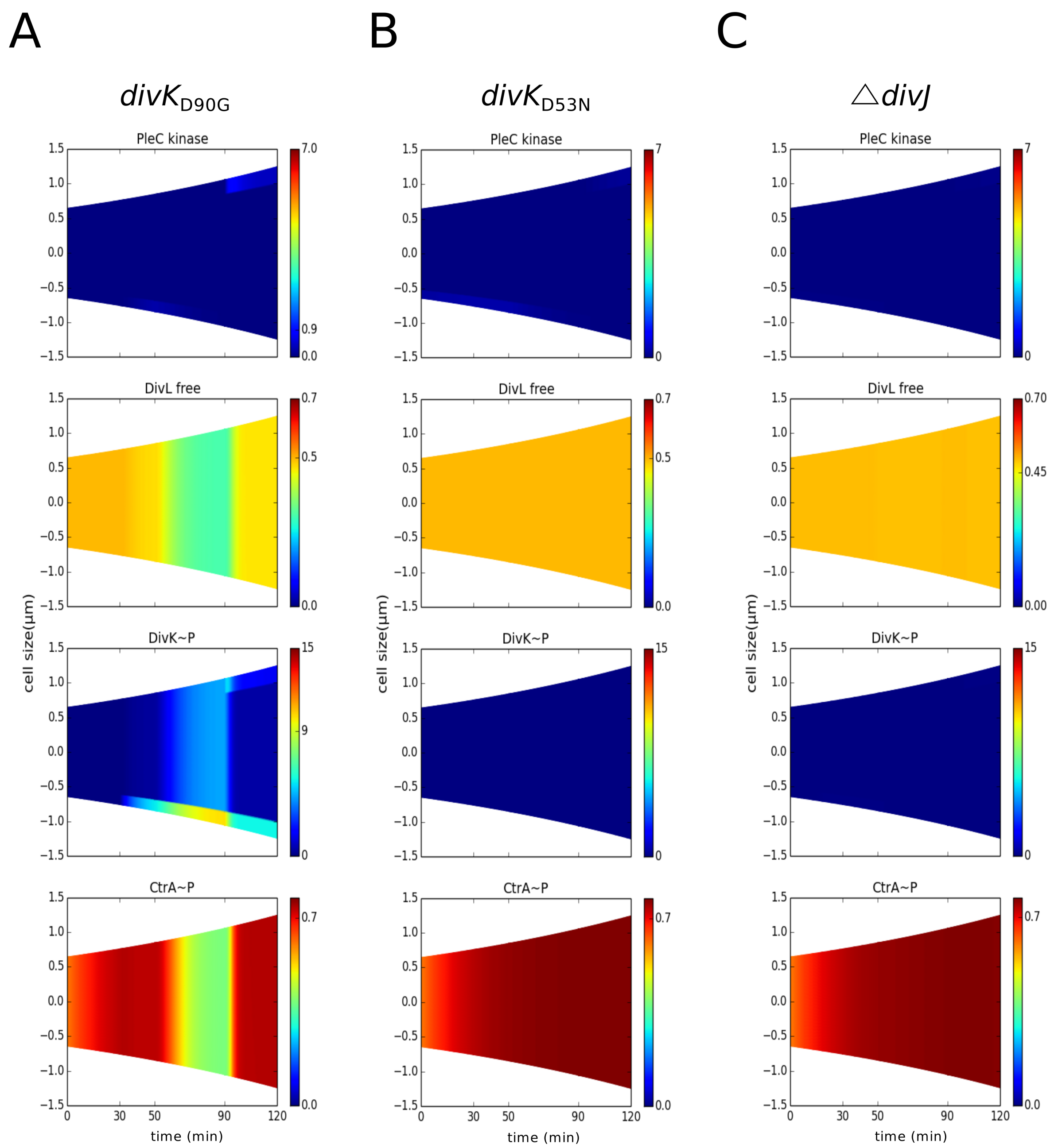

Figure B.4: $divK_{D90G}$, $divK_{D53N}$ and $\Delta divJ$ mutants are characterized by G1-arrest.

(A) In the $divK_{D90G}$ mutant, PleC does not transition to a kinase. Yet, DivL is not inhibited since $DivK_{D90G}$~P cannot bind DivL. (B) In $divK_{D53N}$ and (C) $\Delta divJ$ mutants, DivK remains unphosphorylated throughout the cell cycle. Hence, DivL remains active and the cell is arrested in G1-phase even though PleC does not get up-regulated to the kinase forming. Concentration gradients are color coded as in Figure 3.5.

B.2 Supplementary Tables

Table B.1: Equations governing the model

$\frac{\partial[\mathrm{DivK{\sim}P}]}{\partial \mathrm{t}} = -\left(k_{\mathrm{deg-dkp}} + k_{\mathrm{dil}}\right) \cdot [\mathrm{DivK{\sim}P}] - k_{\mathrm{pc-ph1}} \cdot [\mathrm{PleC}] \cdot [\mathrm{DivK{\sim}P}]$ $+ k_{\mathrm{ph1-pc}} \cdot [\mathrm{PleC_{h1}}] - k_{\mathrm{ph1-pk11}} \cdot [\mathrm{PleC_{ph1}}] \cdot [\mathrm{DivK{\sim}P}]$ $+ k_{\mathrm{pk11-ph1}} \cdot [\mathrm{PleC_{kin11}}] - k_{\mathrm{ph2-pk12}} \cdot [\mathrm{PleC_{ph2}}] \cdot [\mathrm{DivK{\sim}P}]$ $+ k_{\mathrm{pk12-ph2}} \cdot [\mathrm{PleC_{kin12}}] - k_{\mathrm{pk1-pk0}} \cdot [\mathrm{PleC_{kin1}}] \cdot [\mathrm{DivK{\sim}P}]$ $+ k_{\mathrm{pk0-pk1}} \cdot [\mathrm{PleC_{kin0}}] - k_{\mathrm{pk3-pk2}} \cdot [\mathrm{PleC_{kin3}}] \cdot [\mathrm{DivK{\sim}P}]$ $+ k_{\mathrm{pk2-pk3}} \cdot [\mathrm{PleC_{kin2}}] + k_{\mathrm{pt2-pk1h}} \cdot [\mathrm{PleC_{pt2}}]$ $- k_{\mathrm{pk1h-pt2}} \cdot [\mathrm{PleC_{kin1h}}] \cdot [\mathrm{DivK{\sim}P}] - k_{\mathrm{pk2p-pk1}} \cdot [\mathrm{PleC_{kin2p}}] \cdot [\mathrm{DivK{\sim}P}]$ $+ k_{\mathrm{pk1-pk2p}} \cdot [\mathrm{PleC_{kin1}}] - k_{\mathrm{pk1p-pk1h}} \cdot [\mathrm{PleC_{kin1p}}] \cdot [\mathrm{DivK{\sim}P}]$ $+ k_{\mathrm{pk1h-pk1p}} \cdot [\mathrm{PleC_{kin1h}}] + k_{\mathrm{pt3-pk1p}} \cdot [\mathrm{PleC_{pt3}}]$ $- k_{\mathrm{pk1p-pt3}} \cdot [\mathrm{PleC_{kin1p}}] \cdot [\mathrm{DivK{\sim}P}] - k_{\mathrm{j-jkp}} \cdot [\mathrm{DivJ_b}] \cdot [\mathrm{DivK{\sim}P}]$ $+ k_{\mathrm{jkp-j}} \cdot [\mathrm{DivJ{:}DivK{\sim}P}] - k_{\mathrm{pk3h-pt4}} \cdot [\mathrm{PleC_{kin3h}}] \cdot [\mathrm{DivK{\sim}P}]$ $+ k_{\mathrm{pt4-pk3h}} \cdot [\mathrm{PleC_{pt4}}] + k_{\mathrm{h1-h2}} \cdot [\mathrm{PleC_{ph1}}] \cdot [\mathrm{DivK}]$ $- k_{\mathrm{h2-h1}} \cdot [\mathrm{PleC_{ph2}}] \cdot [\mathrm{DivK{\sim}P}] + D_{\mathrm{DivKP}} \cdot \frac{\partial^2[\mathrm{DivK{\sim}P}]}{\partial x^2}$	1
$\frac{\partial[\mathrm{DivK}]}{\partial \mathrm{t}} = k_{syn\mathrm{-dk}} - (k_{\mathrm{deg-dk}} + k_{\mathrm{dil}}) \cdot [\mathrm{DivK}] - k_{\mathrm{pc-ph2}} \cdot [\mathrm{PleC}] \cdot [\mathrm{DivK}] + k_{\mathrm{ph2-pc}} \cdot [\mathrm{PleC_{h2}}]$ $- k_{\mathrm{ph2-pk22}} \cdot [\mathrm{PleC_{ph2}}] \cdot [\mathrm{DivK}] + k_{\mathrm{pk22-ph2}} \cdot [\mathrm{PleC_{kin22}}]$ $- k_{\mathrm{ph1-pk12}} \cdot [\mathrm{PleC_{ph1}}] \cdot [\mathrm{DivK}] + k_{\mathrm{pk12-ph1}} \cdot [\mathrm{PleC_{kin12}}]$ $- k_{\mathrm{pk1-pk2}} \cdot [\mathrm{PleC_{kin1}}] \cdot [\mathrm{DivK}] + k_{\mathrm{pk2-pk1}} \cdot [\mathrm{PleC_{kin2}}]$ $- k_{\mathrm{pk3-pk4}} \cdot [\mathrm{PleC_{kin3}}] \cdot [\mathrm{DivK}] + k_{\mathrm{pk4-pk3}} \cdot [\mathrm{PleC_{kin4}}]$ $- k_{\mathrm{pk2p-pk3}} \cdot [\mathrm{PleC_{pk2p}}] \cdot [\mathrm{DivK}] + k_{\mathrm{pk3-pk2p}} \cdot [\mathrm{PleC_{kin3}}]$ $- k_{\mathrm{j-jk}} \cdot [\mathrm{DivJ}] \cdot [\mathrm{DivK}] + k_{\mathrm{jk-j}} \cdot [\mathrm{DivJ{:}DivK}] - k_{\mathrm{ph1-pk12}} \cdot [\mathrm{PleC_{h1}}] \cdot [\mathrm{DivK}]$ $+ k_{\mathrm{pk12-ph1}} \cdot [\mathrm{PleC_{kin12}}] - k_{\mathrm{pk1p-pk3h}} \cdot [\mathrm{PleC_{kin1p}}] \cdot [\mathrm{DivK}]$ $+ k_{\mathrm{pk3h-pk1p}} \cdot [\mathrm{PleC_{kin3h}}] - k_{\mathrm{h1-h2}} \cdot [\mathrm{PleC_{ph1}}] \cdot [\mathrm{DivK}]$ $+ k_{\mathrm{h2-h1}} \cdot [\mathrm{PleC_{ph2}}] \cdot [\mathrm{DivK{\sim}P}] + D_{\mathrm{DivK}} \cdot \frac{\partial^2[\mathrm{DivK}]}{\partial x^2}$	2

$$\frac{\partial[\mathrm{PleC_f}]}{\partial \mathrm{t}} = k_{\mathrm{syn\_plc}} - (k_{\mathrm{deg-plc}} + k_{\mathrm{dil}}) \cdot [\mathrm{PleC_f}] + D_{\mathrm{PleC}} \cdot \frac{\partial^2[\mathrm{PleC_f}]}{\partial x^2} - k_{\mathrm{pcf-pcb}} \cdot p_{\mathrm{plc}}(x) \cdot [\mathrm{PleC_f}] + k_{\mathrm{pcb-pcf}} \cdot [\mathrm{PleC_b}] \quad 3$$

$$\frac{\mathrm{d}[\mathrm{PleC_b}]}{\mathrm{d}t} = k_{\mathrm{pcf-pcb}} \cdot p_{\mathrm{plc}}(x) \cdot [\mathrm{PleC_f}] - k_{\mathrm{pcb-pcf}} \cdot [\mathrm{PleC_b}] - k_{\mathrm{pc-ph2}} \cdot [\mathrm{PleC_b}] \cdot [\mathrm{DivK}] + k_{\mathrm{ph2-pc}} \cdot [\mathrm{PleC_{h2}}] - k_{\mathrm{pc-ph1}} \cdot [\mathrm{PleC_b}] \cdot [\mathrm{DivK{\sim}P}] + k_{\mathrm{ph1-pc}} \cdot [\mathrm{PleC_{h1}}] + k_{\mathrm{ph2p-pc}} \cdot [\mathrm{PleC_{h2p}}] + k_{\mathrm{ph1p-pc}} \cdot [\mathrm{PleC_{h1p}}] - (k_{\mathrm{deg-plc}} + k_{\mathrm{dil}}) \cdot [\mathrm{PleC_b}] \quad 4$$

$$\frac{\mathrm{d}[\mathrm{PleC_{ph1}}]}{\mathrm{d}t} = k_{\mathrm{pc-ph1}} \cdot [\mathrm{PleC_b}] \cdot [\mathrm{DivK{\sim}P}] - k_{\mathrm{ph1-pc}} \cdot [\mathrm{PleC_{h1}}] - k_{\mathrm{ph1-pk11}} \cdot [\mathrm{PleC_{ph1}}] \cdot [\mathrm{DivK{\sim}P}] + k_{\mathrm{pk11-ph1}} \cdot [\mathrm{PleC_{kin11}}] - k_{\mathrm{ph1-pk12}} \cdot [\mathrm{PleC_{ph1}}] \cdot [\mathrm{DivK}] + k_{\mathrm{pk12-ph1}} \cdot [\mathrm{PleC_{kin12}}] - k_{\mathrm{h1-h2}} \cdot [\mathrm{PleC_{ph1}}] \cdot [\mathrm{DivK}] + k_{\mathrm{h2-h1}} \cdot [\mathrm{PleC_{ph2}}] \cdot [\mathrm{DivK{\sim}P}] - k_{\mathrm{ph1-ph2}} \cdot [\mathrm{PleC_{ph1}}] + k_{\mathrm{ph2-ph1}} \cdot [\mathrm{PleC_{ph2}}] - (k_{\mathrm{deg-plc}} + k_{\mathrm{dil}}) \cdot [\mathrm{PleC_{ph1}}] \quad 5$$

$$\frac{\mathrm{d}[\mathrm{PleC_{ph2}}]}{\mathrm{d}t} = k_{\mathrm{pc-ph2}} \cdot [\mathrm{PleC_b}] \cdot [\mathrm{DivK}] - k_{\mathrm{ph2-pc}} \cdot [\mathrm{PleC_{ph2}}] - k_{\mathrm{ph2-pk22}} \cdot [\mathrm{PleC_{ph2}}] \cdot [\mathrm{DivK}] + k_{\mathrm{pk22-ph2}} \cdot [\mathrm{PleC_{kin22}}] - k_{\mathrm{ph2-pk12}} \cdot [\mathrm{PleC_{ph2}}] \cdot [\mathrm{DivK{\sim}P}] + k_{\mathrm{pk12-ph2}} \cdot [\mathrm{PleC_{kin12}}] + k_{\mathrm{h1-h2}} \cdot [\mathrm{PleC_{ph1}}] \cdot [\mathrm{DivK}] - k_{\mathrm{h2-h1}} \cdot [\mathrm{PleC_{ph2}}] \cdot [\mathrm{DivK{\sim}P}] + k_{\mathrm{ph1-ph2}} \cdot [\mathrm{PleC_{ph1}}] - k_{\mathrm{ph2-ph1}} \cdot [\mathrm{PleC_{ph2}}] - (k_{\mathrm{deg-plc}} + k_{\mathrm{dil}}) \cdot [\mathrm{PleC_{ph2}}] \quad 6$$

$$\frac{\mathrm{d}[\mathrm{PleC_{kin11}}]}{\mathrm{d}t} = k_{\mathrm{ph1-p11}} \cdot [\mathrm{PleC_{ph1}}] \cdot [\mathrm{DivK{\sim}P}] - k_{\mathrm{pk11-ph1}} \cdot [\mathrm{PleC_{kin11}}] - k_{\mathrm{pk11-pk0}} \cdot [\mathrm{PleC_{kin11}}] + k_{\mathrm{pk0-pk11}} \cdot [\mathrm{PleC_{kin0}}] + k_{\mathrm{pt4-pk11}} \cdot [\mathrm{PleC_{pt4}}] - k_{\mathrm{pk11-pt4}} \cdot [\mathrm{PleC_{kin11}}] - (k_{\mathrm{deg-plc}} + k_{\mathrm{dil}}) \cdot [\mathrm{PleC_{kin11}}] \quad 7$$

$$\frac{\mathrm{d}[\mathrm{PleC_{kin12}}]}{\mathrm{d}t} = k_{\mathrm{ph2-pk12}} \cdot [\mathrm{PleC_{ph2}}] \cdot [\mathrm{DivK{\sim}P}] - k_{\mathrm{pk12-ph2}} \cdot [\mathrm{PleC_{kin12}}] + k_{\mathrm{ph1-pk12}} \cdot [\mathrm{PleC_{ph1}}] \cdot [\mathrm{DivK}] - k_{\mathrm{pk12-ph1}} \cdot [\mathrm{PleC_{kin12}}] - k_{\mathrm{pk22-pk2}} \cdot [\mathrm{PleC_{kin22}}] + k_{\mathrm{pk2-pk22}} \cdot [\mathrm{PleC_{kin2}}] - (k_{\mathrm{deg-plc}} + k_{\mathrm{dil}}) \cdot [\mathrm{PleC_{kin12}}] \quad 8$$

$$\frac{\mathrm{d}[\mathrm{PleC_{kin22}}]}{\mathrm{d}t} = k_{\mathrm{ph2-pk22}} \cdot [\mathrm{PleC_{h2}}] \cdot [\mathrm{DivK}] - k_{\mathrm{pk22-ph2}} \cdot [\mathrm{PleC_{kin22}}] - k_{\mathrm{p22-pk4}} \cdot [\mathrm{PleC_{kin22}}] + k_{\mathrm{pk4-pk22}} \cdot [\mathrm{PleC_{kin4}}] - (k_{\mathrm{deg-plc}} + k_{\mathrm{dil}}) \cdot [\mathrm{PleC_{kin22}}] \quad 9$$

$$\frac{\mathrm{d}[\mathrm{PleC_{kin0}}]}{\mathrm{d}t} = k_{\mathrm{pk11-pk0}} \cdot [\mathrm{PleC_{kin11}}] - k_{\mathrm{pk0-pk11}} \cdot [\mathrm{PleC_{kin0}}] - k_{\mathrm{pk0-pk1}} \cdot [\mathrm{PleC_{kin0}}] + k_{\mathrm{pk1-pk0}} \cdot [\mathrm{PleC_{kin1}}] \cdot [\mathrm{DivK{\sim}P}] - (k_{\mathrm{deg-plc}} + k_{\mathrm{dil}}) \cdot [\mathrm{PleC_{kin0}}] \quad 10$$

$$\frac{\mathrm{d}[\mathrm{PleC_{kin2}}]}{\mathrm{d}t} = k_{\mathrm{pk12-pk2}} \cdot [\mathrm{PleC_{kin12}}] - k_{\mathrm{pk2-pk11}} \cdot [\mathrm{PleC_{kin2}}] - k_{\mathrm{pk2-pk1}} \cdot [\mathrm{PleC_{kin2}}] + k_{\mathrm{pk1-pk2}} \cdot [\mathrm{PleC_{kin1}}] \cdot [\mathrm{DivK}] - k_{\mathrm{pk2-pk3}} \cdot [\mathrm{PleC_{kin2}}] + k_{\mathrm{pk3-pk2}} \cdot [\mathrm{PleC_{kin3}}] \cdot [\mathrm{DivK{\sim}P}] + k_{\mathrm{pt2-pk2}} \cdot [\mathrm{PleC_{pt2}}] - k_{\mathrm{pk2-pt2}} \cdot [\mathrm{PleC_{kin2}}] - (k_{\mathrm{deg-plc}} + k_{\mathrm{dil}}) \cdot [\mathrm{PleC_{kin2}}] \quad (11)$$

$$\frac{\mathrm{d}[\mathrm{PleC_{kin4}}]}{\mathrm{d}t} = k_{\mathrm{pk22-pk4}} \cdot [\mathrm{PleC_{kin22}}] - k_{\mathrm{pk4-pk22}} \cdot [\mathrm{PleC_{kin4}}] - k_{\mathrm{pk4-pk3}} \cdot [\mathrm{PleC_{kin4}}] + k_{\mathrm{pk3-pk4}} \cdot [\mathrm{PleC_{kin3}}] \cdot [\mathrm{DivK}] + k_{\mathrm{pt4-pk4}} \cdot [\mathrm{PleC_{pt4}}] - k_{\mathrm{pk4-pt4}} \cdot [\mathrm{PleC_{kin4}}] - (k_{\mathrm{deg-plc}} + k_{\mathrm{dil}}) \cdot [\mathrm{PleC_{kin4}}] \quad (12)$$

$$\frac{\mathrm{d}[\mathrm{PleC_{kin1}}]}{\mathrm{d}t} = -k_{\mathrm{pk1-pk0}} \cdot [\mathrm{PleC_{kin1}}] \cdot [\mathrm{DivK{\sim}P}] + k_{\mathrm{pk0-pk1}} \cdot [\mathrm{PleC_{kin0}}] - k_{\mathrm{pk1-pk2}} \cdot [\mathrm{PleC_{kin1}}] \cdot [\mathrm{DivK}] + k_{\mathrm{pk2-pk1}} \cdot [\mathrm{PleC_{kin2}}] + k_{\mathrm{pk2p-pk1}} \cdot [\mathrm{PleC_{kin2p}}] \cdot [\mathrm{DivK{\sim}P}] - k_{\mathrm{pk1-pk2p}} \cdot [\mathrm{PleC_{kin1}}] + k_{\mathrm{pk1h-pk1}} \cdot [\mathrm{PleC_{kin1h}}] - k_{\mathrm{pk1-pk1h}} \cdot [\mathrm{PleC_{kin1}}] - k_{\mathrm{pk1-pk5}} \cdot [\mathrm{PleC_{kin1}}] \cdot [\mathrm{PleD}] + k_{\mathrm{pk5-pk1}} \cdot [\mathrm{PleC_{kin5}}] - (k_{\mathrm{deg-plc}} + k_{\mathrm{dil}}) \cdot [\mathrm{PleC_{kin1}}] \quad (13)$$

$$\frac{\mathrm{d}[\mathrm{PleC_{kin3}}]}{\mathrm{d}t} = -k_{\mathrm{pk3-pk2}} \cdot [\mathrm{PleC_{kin3}}] \cdot [\mathrm{DivK{\sim}P}] + k_{\mathrm{pk2-pk3}} \cdot [\mathrm{PleC_{kin2}}] - k_{\mathrm{pk3-pk4}} \cdot [\mathrm{PleC_{kin3}}] \cdot [\mathrm{DivK}] + k_{\mathrm{pk4-pk3}} \cdot [\mathrm{PleC_{kin4}}] + k_{\mathrm{pk2p-pk3}} \cdot [\mathrm{PleC_{kin2p}}] \cdot [\mathrm{DivK}] - k_{\mathrm{pk3-pk2p}} \cdot [\mathrm{PleC_{kin3}}] + k_{\mathrm{pk3h-pk3}} \cdot [\mathrm{PleC_{kin3h}}] - k_{\mathrm{pk3-pk3h}} \cdot [\mathrm{PleC_{kin3}}] + k_{\mathrm{pt3-pk3}} \cdot [\mathrm{PleC_{pt3}}] - k_{\mathrm{pk3-pt3}} \cdot [\mathrm{PleC_{kin3}}] - k_{\mathrm{pk3-pk6}} \cdot [\mathrm{PleC_{kin3}}] \cdot [\mathrm{PleD}] + k_{\mathrm{pk6-pk3}} \cdot [\mathrm{PleC_{kin6}}] - (k_{\mathrm{deg-plc}} + k_{\mathrm{dil}}) \cdot [\mathrm{PleC_{kin3}}] \quad (14)$$

$$\frac{\mathrm{d}[\mathrm{PleC_{pt2}}]}{\mathrm{d}t} = k_{\mathrm{pk1h-pt2}} \cdot [\mathrm{PleC_{kin1h}}] \cdot [\mathrm{DivK{\sim}P}] - k_{\mathrm{pt2-pk1h}} \cdot [\mathrm{PleC_{pt2}}] - k_{\mathrm{pt2-pk2}} \cdot [\mathrm{PleC_{pt2}}] + k_{\mathrm{pk2-pt2}} \cdot [\mathrm{PleC_{kin2}}] - (k_{\mathrm{deg-plc}} + k_{\mathrm{dil}}) \cdot [\mathrm{PleC_{pt2}}] \quad (15)$$

$$\frac{\mathrm{d}[\mathrm{PleC_{pt3}}]}{\mathrm{d}t} = k_{\mathrm{pk1p-pt3}} \cdot [\mathrm{PleC_{kin1p}}] \cdot [\mathrm{DivK{\sim}P}] - k_{\mathrm{pt3-pk1p}} \cdot [\mathrm{PleC_{pt3}}] - k_{\mathrm{pt3-pk3}} \cdot [\mathrm{PleC_{pt3}}] + k_{\mathrm{pk3-pt3}} \cdot [\mathrm{PleC_{kin3}}] - (k_{\mathrm{deg-plc}} + k_{\mathrm{dil}}) \cdot [\mathrm{PleC_{pt3}}] \quad (16)$$

$$\frac{\mathrm{d}[\mathrm{PleC_{pt4}}]}{\mathrm{d}t} = k_{\mathrm{pk3h-pt4}} \cdot [\mathrm{PleC_{kin3h}}] \cdot [\mathrm{DivK{\sim}P}] - k_{\mathrm{pt4-pk3h}} \cdot [\mathrm{PleC_{pt4}}] - k_{\mathrm{pt4-pk4}} \cdot [\mathrm{PleC_{pt4}}] + k_{\mathrm{pk4-pt4}} \cdot [\mathrm{PleC_{kin4}}] - k_{\mathrm{pt4-p11}} \cdot [\mathrm{PleC_{pt4}}] + k_{\mathrm{p11-pt4}} \cdot [\mathrm{PleC_{kin11}}] - (k_{\mathrm{deg-plc}} + k_{\mathrm{dil}}) \cdot [\mathrm{PleC_{pt4}}] \quad (17)$$

$$\frac{d[\mathrm{PleC_{kin1h}}]}{dt} = -k_{\mathrm{pk1h-pt2}} \cdot [\mathrm{PleC_{kin1h}}] \cdot [\mathrm{DivK{\sim}P}] + k_{\mathrm{pt2-pk1h}} \cdot [\mathrm{PleC_{pt2}}] - k_{\mathrm{pk1h-pk1}} \cdot [\mathrm{PleC_{kin1h}}] + k_{\mathrm{pk1-pk1h}} \cdot [\mathrm{PleC_{kin1}}] + k_{\mathrm{pk1p-pk1h}} \cdot [\mathrm{PleC_{kin1p}}] \cdot [\mathrm{DivK{\sim}P}] - k_{\mathrm{pk1h-pk1p}} \cdot [\mathrm{PleC_{kin1h}}] - (k_{\mathrm{deg-plc}} + k_{\mathrm{dil}}) \cdot [\mathrm{PleC_{kin1h}}] \quad 18$$

$$\frac{d[\mathrm{PleC_{kin3h}}]}{dt} = -k_{\mathrm{pk3h-pk3}} \cdot [\mathrm{PleC_{kin3h}}] + k_{\mathrm{pk3-pk3h}} \cdot [\mathrm{PleC_{kin3}}] + k_{\mathrm{pk1p-pk3h}} \cdot [\mathrm{PleC_{kin1p}}] \cdot [\mathrm{DivK}] - k_{\mathrm{pk3h-pk1p}} \cdot [\mathrm{PleC_{kin3h}}] - k_{\mathrm{pk3h-pt4}} \cdot [\mathrm{PleC_{kin3h}}] \cdot [\mathrm{DivK{\sim}P}] + k_{\mathrm{pt4-pk3h}} \cdot [\mathrm{PleC_{pt4}}] - (k_{\mathrm{deg-plc}} + k_{\mathrm{dil}}) \cdot [\mathrm{PleC_{kin3h}}] \quad 19$$

$$\frac{d[\mathrm{PleC_{kin2p}}]}{dt} = -k_{\mathrm{pk2p-pk1}} \cdot [\mathrm{PleC_{kin2p}}] \cdot [\mathrm{DivK{\sim}P}] + k_{\mathrm{pk1-pk2p}} \cdot [\mathrm{PleC_{kin1}}] - k_{\mathrm{pk2p-pk3}} \cdot [\mathrm{PleC_{pk2p}}] \cdot [\mathrm{DivK}] + k_{\mathrm{pk3-pk2p}} \cdot [\mathrm{PleC_{kin3}}] - k_{\mathrm{pk2p-pc}} \cdot [\mathrm{PleC_{kin2p}}] - (k_{\mathrm{deg-plc}} + k_{\mathrm{dil}}) \cdot [\mathrm{PleC_{kin2p}}] \quad 20$$

$$\frac{d[\mathrm{PleC_{kin1p}}]}{dt} = -k_{\mathrm{pk1p-pk1h}} \cdot [\mathrm{PleC_{kin1p}}] \cdot [\mathrm{DivK{\sim}P}] + k_{\mathrm{pk1h-pk1p}} \cdot [\mathrm{PleC_{kin1h}}] - k_{\mathrm{pk1p-pt3}} \cdot [\mathrm{PleC_{pk1p}}] \cdot [\mathrm{DivK}] + k_{\mathrm{pt3-pk1p}} \cdot [\mathrm{PleC_{pt3}}] - k_{\mathrm{pk1p-pc}} \cdot [\mathrm{PleC_{kin1p}}] - k_{\mathrm{pk1p-pk3h}} \cdot [\mathrm{PleC_{kin1p}}] \cdot [\mathrm{DivK}] + k_{\mathrm{pk3h-pk1p}} \cdot [\mathrm{PleC_{kin3h}}] - (k_{\mathrm{deg-plc}} + k_{\mathrm{dil}}) \cdot [\mathrm{PleC_{kin1p}}] \quad 21$$

$$\frac{\partial[\mathrm{DivJ_f}]}{\partial \mathrm{t}} = k_{\mathrm{syn\_dj}} - (k_{\mathrm{deg-dj}} + k_{\mathrm{dil}}) \cdot [\mathrm{DivJ_f}] + D_{\mathrm{DivJ}} \cdot \frac{\partial^2[\mathrm{DivJ_f}]}{\partial x^2} - k_{\mathrm{djf-djb}} \cdot p_{\mathrm{dj}}(x) \cdot [\mathrm{DivJ_f}] + k_{\mathrm{djb-djf}} \cdot [\mathrm{DivJ_b}] \quad 22$$

$$\frac{d[\mathrm{DivJ_b}]}{dt} = k_{\mathrm{djf-djb}} \cdot p_{\mathrm{dj}}(x) \cdot [\mathrm{DivJ_f}] - k_{\mathrm{djb-djf}} \cdot [\mathrm{DivJ_b}] - k_{\mathrm{j-jk}} \cdot [\mathrm{DivJ_b}] \cdot [\mathrm{DivK}] + k_{\mathrm{jk-j}} \cdot [\mathrm{DivJ{:}\,DivK}] - k_{\mathrm{j-jkp}} \cdot [\mathrm{DivJ_b}] \cdot [\mathrm{DivK{\sim}P}] + k_{\mathrm{jkp-j}} \cdot [\mathrm{DivJ{:}\,DivK{\sim}P}] - (k_{\mathrm{deg-dj}} + k_{\mathrm{dil}}) \cdot [\mathrm{DivJ_b}] \quad 23$$

$$\frac{d[\mathrm{DivJ{:}\,DivK}]}{dt} = k_{\mathrm{j-jk}} \cdot [\mathrm{DivJ}] \cdot [\mathrm{DivK}] - k_{\mathrm{jk-j}} \cdot [\mathrm{DivJ{:}\,DivK}] - k_{\mathrm{jk-jkp}} \cdot [\mathrm{DivJ{:}\,DivK}] + k_{\mathrm{jkp-jk}} \cdot [\mathrm{DivJ{:}\,DivK{\sim}P}] - (k_{\mathrm{deg-dj}} + k_{\mathrm{dil}}) \cdot [\mathrm{DivJ{:}\,DivK}] \quad 24$$

$$\frac{d[\mathrm{DivJ{:}\,DivK{\sim}P}]}{dt} = k_{\mathrm{jk-jkp}} \cdot [\mathrm{DivJ{:}\,DivK}] - k_{\mathrm{jkp-jk}} \cdot [\mathrm{DivJ{:}\,DivK{\sim}P}] + k_{\mathrm{j-jkp}} \cdot [\mathrm{DivJ_b}] \cdot [\mathrm{DivK{\sim}P}] - k_{\mathrm{jkp-j}} \cdot [\mathrm{DivJ{:}\,DivK{\sim}P}] - (k_{\mathrm{deg-dj}} + k_{\mathrm{dil}}) \cdot [\mathrm{DivJ{:}\,DivK{\sim}P}] \quad 25$$

$$\frac{\partial[\mathrm{DivL_f}]}{\partial \mathrm{t}} = k_{\mathrm{syn\_dl}} - (k_{\mathrm{deg}} + k_{\mathrm{dil}}) \cdot [\mathrm{DivL_f}] + D_{\mathrm{DivL}} \cdot \frac{\partial^2[\mathrm{DivL_f}]}{\partial x^2} - k_{\mathrm{dlf-dlb}} \cdot p_{\mathrm{dl}}(x) \cdot [\mathrm{DivL_f}] + k_{\mathrm{dlb-dlf}} \cdot [\mathrm{DivL_b}] \tag{26}$$

$$\frac{\mathrm{d}[\mathrm{DivL_b}]}{\mathrm{d}t} = k_{\mathrm{dlf-dlb}} \cdot p_{\mathrm{dl}}(x) \cdot [\mathrm{DivL_f}] - k_{\mathrm{dlb-dlf}} \cdot [\mathrm{DivL_b}] - k_{\mathrm{dl-dldk}} \cdot [\mathrm{DivL_b}] \cdot [\mathrm{DivK{\sim}P}] + k_{\mathrm{dldk-dl}} \cdot [\mathrm{DivL{:}\,DivK{\sim}P}] - (k_{\mathrm{deg}} + k_{\mathrm{dil}}) \cdot [\mathrm{DivL_b}] \tag{27}$$

$$\frac{\mathrm{d}[\mathrm{DivL{:}\,DivK{\sim}P}]}{\mathrm{d}t} = k_{\mathrm{dl-dldk}} \cdot [\mathrm{DivL}] \cdot [\mathrm{DivK{\sim}P}] - k_{\mathrm{dldk-dl}} \cdot [\mathrm{DivL{:}\,DivK{\sim}P}] - (k_{\mathrm{deg}} + k_{\mathrm{dil}}) \cdot [\mathrm{DivL{:}\,DivK{\sim}P}] \tag{28}$$

$$\frac{\partial[\mathrm{CtrA}]}{\partial \mathrm{t}} = k_{\mathrm{syn-ctr}} - (k_{\mathrm{deg-ctr}} + k_{\mathrm{dil}}) \cdot [\mathrm{CtrA}] - k_{\mathrm{ctr_{kin}}} \cdot [\mathrm{CckA_{kin}}] \cdot [\mathrm{CtrA}] + k_{\mathrm{ctr\_phos}} \cdot \left[\mathrm{CckA_{phos}}\right] \cdot [\mathrm{CtrA{\sim}P}] + D_{\mathrm{CtrA}} \cdot \frac{\partial^2[\mathrm{CtrA}]}{\partial x^2} \tag{29}$$

$$\frac{\partial[\mathrm{CtrA{\sim}P}]}{\partial \mathrm{t}} = -(k_{\mathrm{deg-ctr}} + k_{\mathrm{dil}}) \cdot [\mathrm{CtrA{\sim}P}] + k_{\mathrm{ctr_{kin}}} \cdot [\mathrm{CckA_{kin}}] \cdot [\mathrm{CtrA}] - k_{\mathrm{ctr\_phos}} \cdot \left[\mathrm{CckA_{phos}}\right] \cdot [\mathrm{CtrA{\sim}P}] + D_{\mathrm{CtrAP}} \cdot \frac{\partial^2[\mathrm{CtrA{\sim}P}]}{\partial\, x^2} \tag{30}$$

$$\frac{\partial[\mathrm{CckA_f}]}{\partial \mathrm{t}} = k_{\mathrm{syn\_ccka}} - k_{\mathrm{deg}} \cdot [\mathrm{CckA_f}] + D_{\mathrm{CckA}} \cdot \frac{\partial^2[\mathrm{CckA_f}]}{\partial x^2} - k_{\mathrm{ckf-ckb}} \cdot p_{\mathrm{ccka}}(x) \cdot [\mathrm{CckA_f}] + k_{\mathrm{ckb-ckf}} \cdot \left[\mathrm{CckA_{phos}}\right] \tag{31}$$

$$\frac{\mathrm{d}\left[\mathrm{CckA_{phos}}\right]}{\mathrm{d}t} = k_{\mathrm{ckf-ckb}} \cdot p_{\mathrm{ccka}}(x) \cdot [\mathrm{CckA_f}] - k_{\mathrm{ckb-ckf}} \cdot \left[\mathrm{CckA_{phos}}\right] - k_{\mathrm{cp-ck}} \cdot \left[\mathrm{CckA_{phos}}\right] \cdot \frac{[\mathrm{DivL_b}]^2}{K_{\mathrm{m-dl}}^2 + [\mathrm{DivL_b}]^2} + k_{\mathrm{ck-cp}} \cdot [\mathrm{CckA_{kin}}] - (k_{\mathrm{deg}} + k_{\mathrm{dil}}) \cdot \left[\mathrm{CckA_{phos}}\right] \tag{32}$$

$$\frac{\mathrm{d}[\mathrm{CckA_{kin}}]}{\mathrm{d}t} = k_{\mathrm{cp-ck}} \cdot \left[\mathrm{CckA_{phos}}\right] \cdot \frac{[\mathrm{DivL_b}]^2}{K_{\mathrm{m-dl}}^2 + [\mathrm{DivL_b}]^2} - k_{\mathrm{ck-cp}} \cdot [\mathrm{CckA_{kin}}] - (k_{\mathrm{deg}} + k_{\mathrm{dil}}) \cdot [\mathrm{CckA_{kin}}] \tag{33}$$

Table B.2: Parameters for wild type simulations

Synthesis and degradation rate constants (min^{-1})

DivJ	$k_{syn\_dj} = 0.05$	$k_{deg\_dj} = 0.05$
DivK	$k_{syn\_dk} = 0.05$	$k_{deg\_dk} = 0.005$
	$k_{deg\_dkp} = 0.005$	
PleC	$k_{syn\_plc} = 0.1$	$k_{deg\_plc} = 0.05$
	$k_{deg\_dkp} = 0.005$	
DivL	$k_{syn\_dl} = 0.025$	$k_{deg\_dl} = 0.05$
CckA	$k_{syn\_ccka} = 0.025$	$k_{deg\_ccka} = 0.05$
CtrA	$k_{syn\_ctr} = 0.05$	$k_{deg\_ctr} = 0.05$

Polar binding rate constants (min^{-1})

DivJ	$k_{djf\_djb} = 1$	$k_{djb\_djf} = 0$
PleC	$k_{pcf\_pcb} = 1$	$k_{pcb\_pcf} = 0.5$
DivL	$k_{dlf\_dlb} = 1$	$k_{dlb\_clf} = 0.1$
CckA	$k_{ckf\_ckb} = 1$	$k_{ckb\_ckf} = 0.1$

Phosphatase-kinase transition, autophosphorylation & phosphotransfer rate constants (min^{-1})

DivJ	$k_{j\_jk} = 5$	$k_{jk\_j} = 0.0016$
	$k_{jk\_jkp} = 5$	$k_{jkp\_jk} = 0.16$
	$k_{jkp\_dj} = 1$	$k_{dj\_jkp} = 5$
PleC	$k_{pc\_ph1} = 5$	$k_{ph1\_pc} = 5$
	$k_{ph1\_p11} = 5$	$k_{pk11\_ph1} = 2.5$
	$k_{p11\_pk0} = 2.5$	$k_{pk0\_p11} = 5$
	$k_{pk0\_pk1} = 0.16$	$k_{pk1\_pk0} = 5$
	$k_{pk1\_pk2} = 5$	$k_{pk2\_pk1} = 0.0016$
	$k_{pk1\_pk1h} = 5$	$k_{pk1h\_pk1} = 5$
PleC	$k_{pk1p\_1h} = 5$	$k_{1h\_pk1p} = 0.16$
	$k_{pk3\_pk2p} = 0.0016$	$k_{pk2p\_pk3} = 5$
	$k_{pk3\_pk4} = 5$	$k_{pk4\_pk3} = 0.0016$
	$k_{pk4\_pt4} = 5$	$k_{pt4\_pk4} = 0.16$
	$k_{pc\_ph2} = 0.05$	$k_{ph2\_pc} = 5$
	$k_{ph2\_p22} = 0.016$	$k_{p22\_ph22} = 1.6e\text{-}08$
	$k_{p22\_pk4} = 5$	$k_{pk4\_p22} = 5$
	$k_{pt4\_pk3h} = 0.16$	$k_{pk3h\_pt4} = 5$
	$k_{pk3\_pk3h} = 5$	$k_{pk3h\_pk3} = 5$
	$k_{pk1p\_p3h} = 5$	$k_{p3h\_pk1p} = 0.0016$
	$k_{ph1\_p12} = 0.0016$	$k_{p12\_ph1} = 1.6e\text{-}04$
	$k_{p12\_pk2} = 5$	$k_{pk2\_p12} = 5$
	$k_{ph2\_p12} = 1.6$	$k_{p12\_ph2} = 1.6e\text{-}04$
	$k_{h1\_h2} = 0.0016$	$k_{h2\_h1} = 1.6$
	$k_{p11\_pt4} = 0.0075$	$k_{pt4\_p11} = 5$
	$k_{ph1\_ph2} = 10$	$k_{ph2\_ph1} = 5e\text{-}03$
	$k_{pt3\_pk1p} = 0.16$	$k_{pk1p\_pt3} = 5$
CckA	$k_{cp\_ck} = 10$	$k_{ck\_cp} = 1$
CtrA	$k_{ctr\_kin} = 600$	$k_{ctr\_phos} = 600$
DivL	$k_{bdl\_dldk} = 2.5$	$k_{dldk\_dl} = 0.5$

Diffusion rate constants ($\mu\mathrm{m}^2\ \mathrm{min}^{-1}$)

$D_{DivK} = 100$	$D_{DivKP} = 100$
$D_{DivJ} = 100$	$D_{DivL} = 100$
$D_{PleC} = 10$	$D_{CckA} = 100$
$D_{CtrA} = 100$	$D_{CtrAP} = 100$

$k_{pk1\_pk2p} = 0.16$	$k_{pk2p\_pk1} = 5$	
$k_{pk2\_pt2} = 5$	$k_{pt2\_pk2} = 0.16$	*Growth rate constant* (min^{-1})
$k_{pt2\_pk1h} = 0.16$	$k_{pk1h\_pt2} = 5$	$k_{growth} = 0.0055$
$k_{pk2p\_pc} = 5$	$k_{pk1p\_pc} = 5$	
$k_{pk2\_pk3} = 0.16$	$k_{pk3\_pk2} = 5$	Equilibrium constant (dimensionless)
$k_{pk3\_pt3} = 5$	$k_{pt3\_pk3} = 0.16$	$K_{mdl} = 0.5$

Table B.3: Rate constants for mutant simulations*

Δ*pleC*	$k_{syn\_plc} = 0$	*pleC*$_{H610A}$	$k_{p11\_pk0} = 0$
			$k_{pk0\_p11} = 0$
pleC$_{F778L}$	$k_{p11\_pk0} = 0$		$k_{p22\_pk4} = 0$
	$k_{pk0\_p11} = 0$		$k_{pk4\_p22} = 0$
	$k_{p22\_pk4} = 0$		$k_{p12\_pk2} = 0$
	$k_{pk4\_p22} = 0$		$k_{pk2\_p12} = 0$
	$k_{p12\_pk2} = 0$		$k_{pk2\_pt2} = 0$
	$k_{pk2\_p12} = 0$		$k_{pt2\_pk2} = 0$
	$k_{pk2\_pt2} = 0$		$k_{pk3\_pt3} = 0$
	$k_{pt2\_pk2} = 0$		$k_{pt3\_pk3} = 0$
	$k_{pk3\_pt3} = 0$		$k_{pk4\_pt4} = 0$
	$k_{pt3\_pk3} = 0$		$k_{pt4\_pk4} = 0$
	$k_{pk4\_pt4} = 0$		$k_{p11\_pt4} = 0$
	$k_{pt4\_pk4} = 0$		$k_{pt4\_p11} = 0$
	$k_{p11\_pt4} = 0$		$k_{ph1\_ph2} = 0$
	$k_{pt4\_p11} = 0$		$k_{ph2\_ph1} = 0$
Δ*divJ*	$k_{syn\_dk} = 0$	*divJ*$_{H338A}$	$k_{jk\_jkp} = 0$
			$k_{jkp\_jk} = 0$
DivK overexpression	$k_{syn\_dk} = 0.2$ (4X)	*divK*$_{D90G}$	$k_{bdl\_dldk} = 0.1$
	$k_{syn\_dk} = 0.4$ (8X)		$k_{udl\_dldk} = 0.5$
			$k_{ph1\_p11} = 2.5$
divK$_{D53N}$	$k_{jk\_jkp} = 0$		$k_{p11\_ph1} = 50$
	$k_{jkp\_jk} = 0$		$k_{ph2\_p22} = 0.025$
	$k_{pk2\_pt2} = 0$		$k_{p22\_ph2} = 0.002$
	$k_{pt2\_pk2} = 0$		$k_{ph1\_p12} = 0.016$
	$k_{pk3\_pt3} = 0$		$k_{p12\_ph1} = 16$

$k_{pt3\_pk3} = 0$	$k_{ph2\_p12} = 1.6$
$k_{pk4\_pt4} = 0$	$k_{p12\_ph2} = 16$
$k_{pt4\_pk4} = 0$	
$k_{p11\_pt4} = 0$	
$k_{pt4\_p11} = 0$	
* All rate constants have units of min^{-1}	

Table B.4: Values of indicator functions p_i

	t = 0 – 30 min	t = 30 – 50 min	t = 50 – 90 min	t = 90 – 120 min	t = 120 – 150 min
DivJ	$p_i^{dj} = 0$ *	p_i^{dj}= 1 for 1 ≤ i ≤ 10 (old pole) and p_i^{dj}= 0 for i > 10			
PleC	p_i^{plc} = 1 for 1 ≤ i ≤ 10 (old pole) and p_i^{plc} = 0 for i > 10		$p_i^{plc} = 0$*	p_i^{plc}= 1 for 91 ≤ i ≤ 100 (new pole) and p_i^{plc}= 0 for i < 91	
DivL	$p_i^{dl} = 1$*			p_i^{dl}= 1 for 91 ≤ i ≤ 100 (new pole) and p_i^{dl}= 0 for i < 91	
CckA	$p_i^{ccka} = 1$*	p_i^{ccka} = 1 for 1 ≤ i ≤ 10 (old pole) and p_i^{ccka} = 0 for i > 10		p_i^{ccka} = 1 for 91 ≤ i ≤ 100 (new pole); p_i^{ccka} = 1 for 1 ≤ i ≤ 10 (old pole) and p_i^{ccka} = 0 for 10 < i < 91	
pleC$_{H610A}$ *mutant*◆					
PleC	p_i^{plc}= 1 for 1 ≤ i ≤ 10 (old pole) and p_i^{plc}= 0 for i > 10			p_i^{plc}= 1 for 1 ≤ i ≤ 10 (old pole) p_i^{plc} = 1 for 91 ≤ i ≤ 100 (new pole) and p_i^{plc} = 0 for 10 < i < 91	
divK$_{D90G,}$ *divK*$_{D53N,}$ Δ*divJ* *mutants*◆					
DivL	p_i^{dl} = 1*				
CckA	p_i^{ccka}= 1*				

* For all i

◆ Unless specified, values of p_i in the mutants are the same as that of wild type

Appendix C Supplementary information for Chapter 5

C.1 Supplementary text

Given the possibility of slow diffusing *popZ* mRNA, can PopZ form polymers at the poles when the gene is positioned away from the poles? To answer this question, we initially varied the position of a single *popZ* gene in a non-growing domain 1.3 µm in size. When the middle two compartments were allowed to produce mRNA, the polymer also aggregated mid-cell (Figure C.2 A). However, if two neighboring compartments located either within the right 40 or left 40 compartments were allowed to produce mRNA, then the focus of PopZ polymer formed at the corresponding pole (Figure C.2 B). The result indicates that the *popZ* gene need not be localized at the pole in order for PopZ protein to polymerize at the pole. Rather, it is sufficient for PopZ polymerization at the old pole that the single *popZ* gene in a newborn cell be located away from the mid-cell and towards the old pole. We performed similar analysis of bipolar PopZ localization in *Caulobacter* cells after replication of the *popZ* gene by assuming the presence of two *popZ* genes in opposite halves of a domain of length 2.5 µm. Our simulations showed a single central peak of PopZ polymer if the two genes were close to the mid-cell (Figure C.2 C), while positioning the genes within a distance of $0.2 \cdot L(t)$ from the poles allowed bipolar PopZ localization (Figure C.2 D).

We carried out similar simulations on growing domains with varying numbers of *popZ* genes. In a representative simulation (Figure 6, described in the main text), with the genes placed at a distance 0.2 $L(t)$ from the poles, PopZ polymerized properly at the poles of the cell. If the mRNA producing compartments are shifter further inwards, the resultant PopZ polymer pattern also moves slightly inwards (Figure C.3). In order to confirm that bipolarity was not a result of an increased concentration of PopZ an older cell with two copies of the *popZ* gene, PopZ monomers were expressed at twice the normal rate from a single *popZ* gene. In this case, a unipolar pattern of PopZ polymer of greater density was obtained (Figure C.4). This result is consistent with experiments showing that increased levels of PopZ protein affect the size of PopZ foci [15] but not their number [18].

C.2 Supplementary Figures

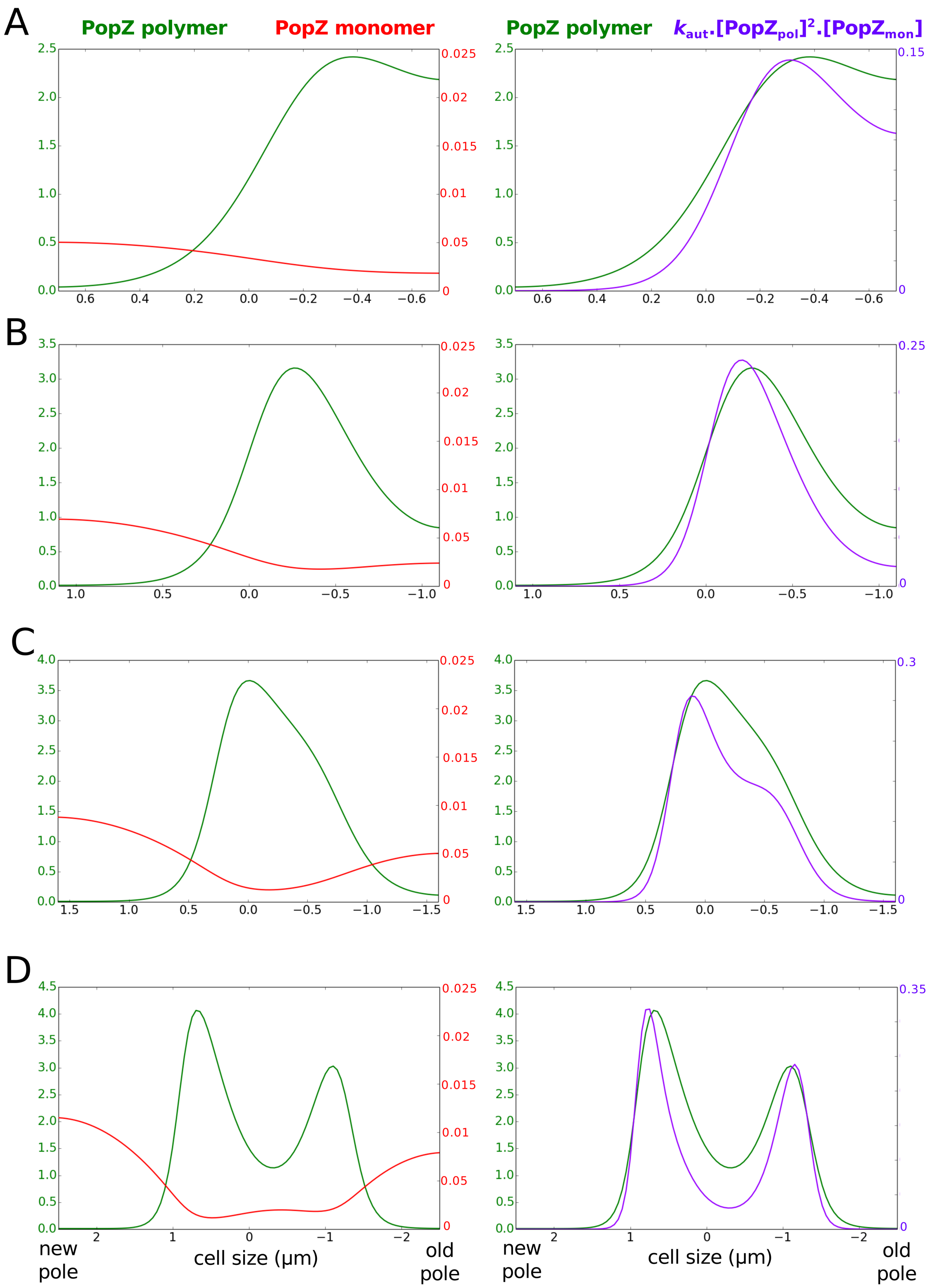

Figure C.1: The autocatalytic reaction promotes localization of the PopZ polymer peak away from the cell poles.

Left panel: Plot of PopZ polymer concentration (green) versus the PopZ monomer concentration (red). Right panel: Plot of PopZ polymer concentration (red) versus the autocatalytic growth rate (min^{-1}; purple). (A) At *t* = 20 min, the PopZ polymer peak is located close to the old pole, while the PopZ monomer gradient is highest towards the new pole. The rate of autocatalytic growth is highest at the PopZ polymer peak boundary facing mid-cell. (B) At *t* = 100 min, and (C) at *t* = 170 min, the PopZ polymer peak and the highest value of autocatalytic growth rate shifts close to mid-cell. (D) At *t* = 250 min, the monomer concentration is lowest at mid-cell and higher towards the poles. Since the cell is large enough to hold two PopZ polymer foci, the original PopZ polymer peak splits into two new peaks. At this stage, the autocatalytic growth rate is higher at the PopZ polymer peak boundaries that are facing towards the poles. Hence, as the cell grows further, the PopZ polymer foci move away from each other and from mid-cell position.

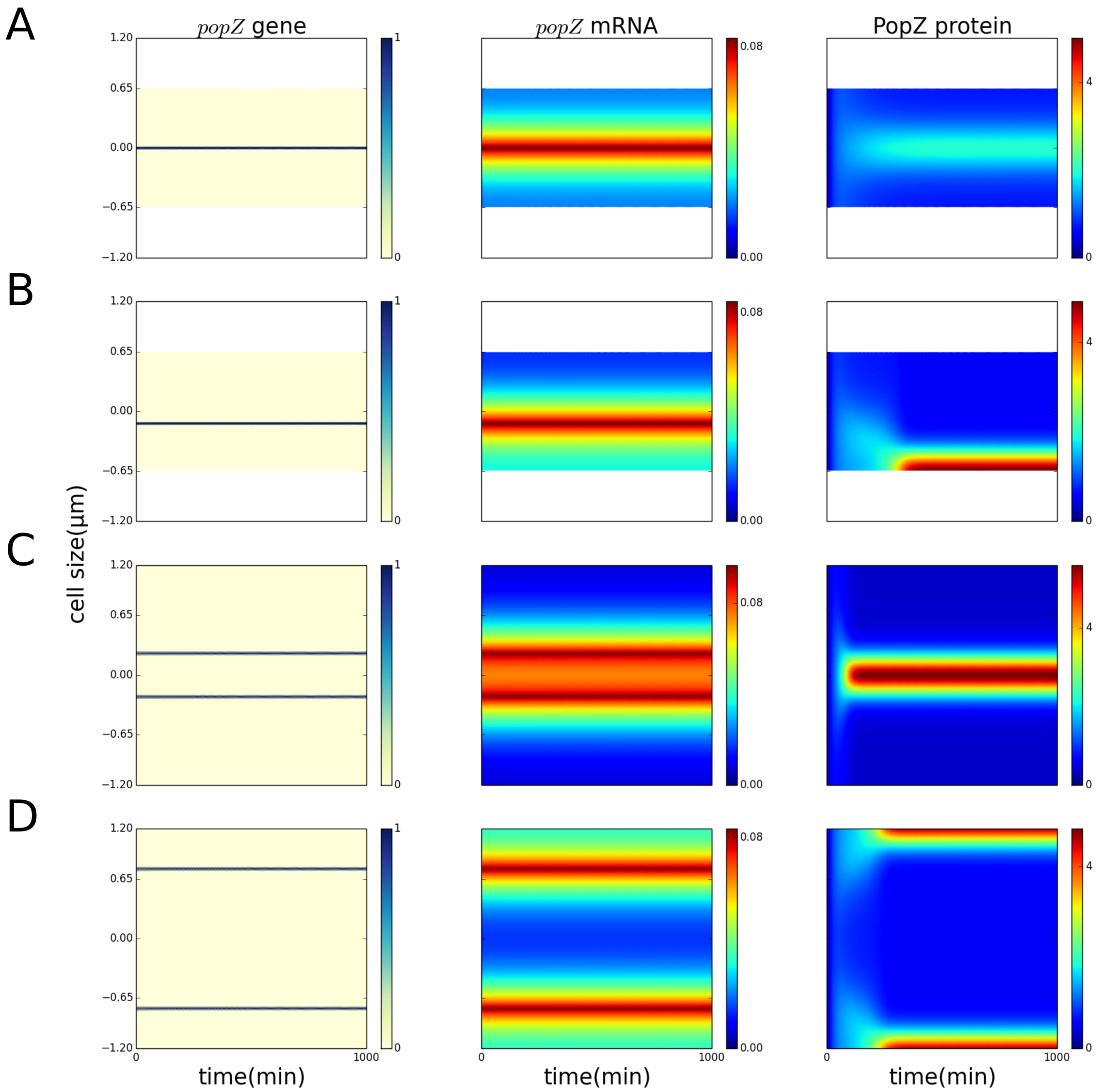

Figure C.2: Polar localization of PopZ polymer is sensitive to the location of the *popZ* genes.

(A) *popZ* gene located in the middle of the swarmer cell (L = 1.3 µm) gives rise to a single focus of PopZ polymer at the cell center. (B) *popZ* gene located at a distance less than $0.4 \cdot L$ from a pole gives rise to a single focus of PopZ polymer at the closer pole. (C) Two *popZ* genes located at a distance of $0.4 \cdot L$ from both poles of a stalked cell (L = 2.5 µm) gives rise to a single focus of PopZ polymer at the cell center. **(D)** Two *popZ* genes located at a distance of $0.2 \cdot L$ from both poles of a stalked cell (L = 2.5 µm) gives rise to bipolar PopZ foci.

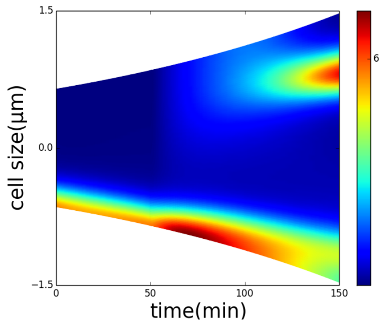

Figure C.3: PopZ localizes away from the poles in the case two *popZ* genes are positioned at a distance greater than $0.25 \cdot L(t)$ from both poles.

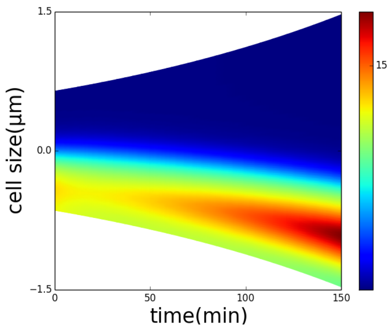

Figure C.4: PopZ shows unipolar old pole localization in the case where a single overexpressing *popZ* gene ($k_{\text{syn-mRNA}}$ = 10 min^{-1}) is positioned at a distance of $0.2 \cdot L(t)$ from the old pole.

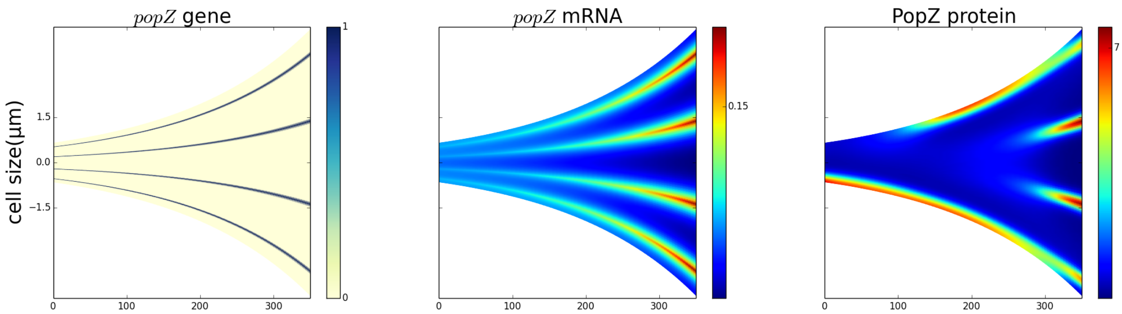

Figure C.5: The appearance of multiple PopZ foci in filamentous cells depends on the number of *popZ* genes present and on the length of the *Caulobacter* cell.

C.3 Supplementary Tables

Table C.1: Equations governing the nucleation-assisted PopZ assembly model

$\frac{\partial[\mathrm{PopZ_{mon}}]}{\partial t} = k_{\mathrm{syn\_prtn}} - k_{\mathrm{degprtn}} \cdot [\mathrm{PopZ_{mon}}] - k_{\mathrm{dnv}} \cdot [\mathrm{PopZ_{mon}}] - k_{\mathrm{aut}} \cdot [\mathrm{PopZ_{pol}}]^2 \cdot [\mathrm{Ncf}] \cdot [\mathrm{PopZ_{mon}}] + k_{\mathrm{depol}} \cdot [\mathrm{PopZ_{pol}}] - k_{growth} \cdot [\mathrm{PopZ_{mon}}] + D_{\mathrm{mon}} \cdot \frac{\partial^2[\mathrm{PopZ_{mon}}]}{\partial x^2}$	1
$\frac{\partial[\mathrm{PopZ_{pol}}]}{\partial t} = -k_{\mathrm{deg\ \_prtn}} \cdot [\mathrm{PopZ_{pol}}] + k_{\mathrm{dnv}} \cdot [\mathrm{PopZ_{mon}}] + k_{\mathrm{aut}} \cdot [\mathrm{PopZ_{pol}}]^2 \cdot [\mathrm{Ncf}] \cdot [\mathrm{PopZ_{mon}}] - k_{\mathrm{depol}} \cdot [\mathrm{PopZ_{pol}}] - k_{growth} \cdot [\mathrm{PopZ_{pol}}] + D_{\mathrm{pol}} \cdot \frac{\partial^2[\mathrm{PopZ_{pol}}]}{\partial x^2}$	2

Table C.2: Equations governing the PopZ self-assembly model

$\frac{\partial[\mathrm{PopZ_{mon}}]}{\partial t} = k_{\mathrm{syn-prtn}} - k_{\mathrm{deg-prtn}} \cdot [\mathrm{PopZ_{mon}}] - k_{\mathrm{dnv}} \cdot [\mathrm{PopZ_{mon}}] - k_{\mathrm{aut}} \cdot [\mathrm{PopZ_{pol}}]^2 \cdot [\mathrm{PopZ_{mon}}] + k_{\mathrm{depol}} \cdot [\mathrm{PopZ_{pol}}] - k_{growth} \cdot [\mathrm{PopZ_{mon}}] + D_{\mathrm{mon}} \cdot \frac{\partial^2[\mathrm{PopZ_{mon}}]}{\partial x^2}$	1
$\frac{\partial[\mathrm{PopZ_{pol}}]}{\partial t} = -k_{\mathrm{deg-prtn}} \cdot [\mathrm{PopZ_{pol}}] + k_{\mathrm{dnv}} \cdot [\mathrm{PopZ_{mon}}] + k_{\mathrm{aut}} \cdot [\mathrm{PopZ_{pol}}]^2 \cdot [\mathrm{PopZ_{mon}}] - k_{\mathrm{depol}} \cdot [\mathrm{PopZ_{pol}}] - k_{growth} \cdot [\mathrm{PopZ_{pol}}] + D_{\mathrm{pol}} \cdot \frac{\partial^2[\mathrm{PopZ_{pol}}]}{\partial x^2}$	2

Table C.3: Equations governing the PopZ self-assembly model with *popZ* mRNA

$\frac{\partial[\mathrm{PopZ_{mon}}]}{\partial t} = k_{\mathrm{syn\_prtn}} \cdot [popZ_{\mathrm{mRNA}}] - k_{\mathrm{deg_{prtn}}} \cdot [\mathrm{PopZ_{mon}}] - k_{\mathrm{dnv}} \cdot [\mathrm{PopZ_{mon}}] - k_{\mathrm{aut}} \cdot [\mathrm{PopZ_{pol}}]^2 \cdot [\mathrm{PopZ_{mon}}] + k_{\mathrm{depol}} \cdot [\mathrm{PopZ_{pol}}] - k_{growth} \cdot [\mathrm{PopZ_{mon}}] + D_{\mathrm{mon}} \cdot \frac{\partial^2[\mathrm{PopZ_{mon}}]}{\partial t}$	1
$\frac{\partial[\mathrm{PopZ_{pol}}]}{\partial t} = -k_{\mathrm{deg_{prtn}}} \cdot [\mathrm{PopZ_{pol}}] + k_{\mathrm{dnv}} \cdot [\mathrm{PopZ_{mon}}] + k_{\mathrm{aut}} \cdot [\mathrm{PopZ_{pol}}]^2 \cdot [\mathrm{PopZ_{mon}}] - k_{\mathrm{depol}} \cdot [\mathrm{PopZ_{pol}}] - k_{growth} \cdot [\mathrm{PopZ_{pol}}] + D_{\mathrm{pol}} \cdot \frac{\partial^2[\mathrm{PopZ_{pol}}]}{\partial x^2}$	2
$\frac{\partial[popZ_{\mathrm{mRNA}}]}{\partial t} = k_{\mathrm{syn\_mRNA}} \cdot [popZ_{\mathrm{gene}}] - k_{\mathrm{deg\_mRNA}} \cdot [popZ_{\mathrm{mRNA}}] - k_{growth} \cdot [popZ_{\mathrm{mRNA}}] + D_{\mathrm{mRNA}} \cdot \frac{\partial^2[popZ_{\mathrm{mRNA}}]}{\partial x^2}$	3
$\frac{\partial[\mathrm{FtsZ_{mon}}]}{\partial t} = k_{\mathrm{syn\_fts}} - k_{\mathrm{deg_{fts}}} \cdot [\mathrm{FtsZ_{mon}}] - k_{\mathrm{dnv}} \cdot [\mathrm{FtsZ_{mon}}] - k_{\mathrm{aut}} \cdot [\mathrm{FtsZ_{pol}}]^2 \cdot [\mathrm{FtsZ_{mon}}] + k_{\mathrm{depol}} \cdot [\mathrm{FtsZ_{pol}}] - k_{growth} \cdot [\mathrm{FtsZ_{mon}}] + D_{\mathrm{fts-mon}} \cdot \frac{\partial^2[\mathrm{FtsZ_{mon}}]}{\partial x^2}$	4
$\frac{\partial[\mathrm{FtsZ_{pol}}]}{\partial t} = -k_{\mathrm{deg-fts}} \cdot [\mathrm{FtsZ_{pol}}] + k_{\mathrm{dnv}} \cdot [\mathrm{FtsZ_{mon}}] + k_{\mathrm{aut}} \cdot [\mathrm{FtsZ_{pol}}]^2 \cdot [\mathrm{FtsZ_{mon}}] - k_{\mathrm{depol}} \cdot [\mathrm{FtsZ_{pol}}] - k_{\mathrm{depol-mz}} \cdot ([\mathrm{MipZ_f}] + [\mathrm{MipZ_b}]) \cdot [\mathrm{FtsZ_{pol}}] - k_{growth} \cdot [\mathrm{FtsZ_{pol}}] + D_{\mathrm{fts-pol}} \cdot \frac{\partial^2[\mathrm{FtsZ_{pol}}]}{\partial x^2}$	5
$\frac{\partial[\mathrm{MipZ_f}]}{\partial t} = k_{\mathrm{syn\_mz}} - k_{\mathrm{deg-mz}} \cdot [\mathrm{MipZ_f}] - k_{\mathrm{mzf-mzb}} \cdot [\mathrm{MipZ_f}] \cdot [\mathrm{MipZ_b}] + k_{\mathrm{mzb-mzf}} \cdot [\mathrm{MipZ_b}] - k_{growth} \cdot [\mathrm{MipZ_f}] + D_{\mathrm{mzf}} \cdot \frac{\partial^2[\mathrm{MipZ_f}]}{\partial x^2}$	6
$\frac{\partial[\mathrm{MipZ_b}]}{\partial t} = -k_{\mathrm{deg-mz}} \cdot [\mathrm{MipZ_b}] + k_{\mathrm{mzf-mzb}} \cdot [\mathrm{MipZ_f}] \cdot [\mathrm{MipZ_b}] - k_{\mathrm{mzb-mzf}} \cdot [\mathrm{MipZ_b}] - k_{growth} \cdot [\mathrm{MipZ_b}] + D_{\mathrm{mzb}} \cdot \frac{\partial^2[\mathrm{MipZ_b}]}{\partial x^2}$	7

Table C.4: Parameters for the PopZ self-assembly model (Table C.1 & C.2)*

$k_{syn\text{-}prtn}$	0.1	$k_{deg\text{-}prtn}$	0.05	k_{dnv}	1	k_{aut}	12
k_{depol}	0.1	k_{growth}	0.005	D_{mon}	10	D_{pol}	0.001

*Parameters of the form k_{sub} have units of min^{-1}, D_{sub} have units of $\mu m^2\ min^{-1}$

Table C.5: Parameters for the PopZ self-assembly model with *popZ* mRNA (Table C.3)*

Wild type parameters

k_{syn_prtn}	1	k_{deg_prtn}	0.05	k_{dnv}	12	k_{aut}	12
k_{depol}	0.1	k_{growth}	0.005	D_{mon}	10	D_{pol}	0.001
k_{syn_mRNA}	2	k_{deg_mRNA}	0.5	D_{mRNA}	0.05	$k_{depol\text{-}mz}$	5
k_{syn_fts}	0.5	k_{deg_fts}	0.05	k_{dnv}	12	k_{aut}	12
k_{depol}	3	$k_{syn\text{-}mz}$	1	$k_{deg\text{-}mz}$	0.5	$k_{mzf\text{-}mzb}$	1
$k_{mzb\text{-}mzf}$	0.1	D_{fzm}	100	D_{fzp}	0.1	D_{mzf}	100
PopZ Overexpression		MipZ deletion		DNA replication mutant			
k_{syn_mRNA}	10	$k_{syn\text{-}mz}$	0	k_{syn_mRNA}	3	D_{mRNA}	0.5

*Parameters of the form k_{sub} have units of min^{-1}, D_{sub} have units of $\mu m^2\ min^{-1}$

Appendix D Supplementary information for Chapter 6

D.1 Supplementary Tables

Table D.1: Equations for the model *

$$\frac{\partial[\mathrm{ParA}]}{\partial t} = k_{\mathrm{syn-pa}} - k_{deg-\mathrm{pa}} \cdot [\mathrm{ParA}] - k_{\mathrm{pa-patn}} \cdot [\mathrm{ParA}] \cdot [\mathrm{TipN}] + k_{\mathrm{patn-pa}} \cdot [\mathrm{ParA_{tn}}] - k_{\mathrm{pa-pa2}} \cdot [\mathrm{ParA}] \cdot [\mathrm{ParA}] + k_{\mathrm{pa2-pa}} \cdot [\mathrm{ParA_{dim}}] + k_{\mathrm{hyd}} \cdot [\mathrm{ParA_{pb}}] - k_{d\mathrm{il}} \cdot [\mathrm{ParA}] + D_{pa} \cdot \frac{\partial^2[\mathrm{ParA}]}{\partial x^2}$$	1
$$\frac{\mathrm{d}[\mathrm{ParA_{tn}}]}{\mathrm{d}t} = -k_{deg-\mathrm{patn}} \cdot [\mathrm{ParA}] + k_{\mathrm{pa-patn}} \cdot [\mathrm{ParA}] \cdot [\mathrm{TipN}] - k_{\mathrm{patn-pa}} \cdot [\mathrm{ParA_{tn}}] - k_{d\mathrm{il}} \cdot [\mathrm{ParA_{tn}}]$$	2
$$\frac{\partial[\mathrm{ParA_{dim}}]}{\partial t} = -k_{deg-\mathrm{pa2}} \cdot [\mathrm{ParA_{dim}}] + k_{\mathrm{pa-pa2}} \cdot [\mathrm{ParA}] \cdot [\mathrm{ParA}] - k_{\mathrm{pa2-pa}} \cdot [\mathrm{ParA_{dim}}] - k_{\mathrm{pa2-pa2D}} \cdot [\mathrm{ParA_{dim}}] + k_{\mathrm{pa2D-pa2}} \cdot [\mathrm{ParA_{dna}}] - k_{\mathrm{pa2-pa2Z}} \cdot [\mathrm{ParA_{dim}}] \cdot [\mathrm{PopZ_p}] + k_{\mathrm{pa2Z-pa2}} \cdot [\mathrm{ParA_{pz}}] - k_{\mathrm{dil}} \cdot [\mathrm{ParA_{dim}}] + D_{\mathrm{pa2}} \cdot \frac{\partial^2[\mathrm{ParA_{dim}}]}{\partial x^2}$$	3
$$\frac{\mathrm{d}[\mathrm{ParA_{pz}}]}{\mathrm{d}t} = -k_{\mathrm{deg-pa2Z}} \cdot [\mathrm{ParA_{pz}}] + k_{\mathrm{pa2-pa2Z}} \cdot [\mathrm{ParA_{dim}}] \cdot [\mathrm{PopZ_p}] - k_{\mathrm{pa2Z-pa2}} \cdot [\mathrm{ParA_{pz}}] - k_{d\mathrm{il}} \cdot [\mathrm{ParA_{pz}}]$$	4
$$\frac{\mathrm{d}[\mathrm{ParA_{pzm}}]}{\mathrm{d}t} = -k_{\mathrm{deg-paZ}} \cdot [\mathrm{ParA_{pzm}}] + k_{\mathrm{pa-paZ}} \cdot [\mathrm{ParA}] \cdot [\mathrm{PopZ_p}] - k_{\mathrm{paZ-pa}} \cdot [\mathrm{ParA_{pzm}}] - k_{d\mathrm{il}} \cdot [\mathrm{ParA_{pzm}}]$$	5
$$\frac{\mathrm{d}[\mathrm{ParA_{dna}}]}{\mathrm{d}t} = -k_{\mathrm{deg-pa2D}} \cdot [\mathrm{ParA_{dna}}] + k_{\mathrm{pa2-pa2D}} \cdot [\mathrm{ParA_{dim}}] - k_{\mathrm{pa2D-pa2}} \cdot [\mathrm{ParA_{dna}}] - k_{\mathrm{pa2D-pa2B}} \cdot [\mathrm{ParA_{dna}}] \cdot [\mathrm{SBZ_P}] + k_{\mathrm{pa2B-pa2}} \cdot [\mathrm{ParA_{pb}}] - k_{\mathrm{dil}} \cdot [\mathrm{ParA_{dna}}]$$	6

$\frac{\mathrm{d}[\mathrm{ParA_{pb}}]}{\mathrm{d}t} = -k_{\mathrm{deg-pa2B}} \cdot [\mathrm{ParA_{pb}}] + k_{\mathrm{pa2D-pa2B}} \cdot [\mathrm{ParA_{dna}}] \cdot [\mathrm{SBZ_p}] - k_{\mathrm{pa2B-pa2D}} \cdot [\mathrm{ParA_{pb}}] - k_{\mathrm{hyd}} \cdot [\mathrm{ParA_{pb}}] - k_{\mathrm{dil}} \cdot [\mathrm{ParA_{dna}}]$	7
$\frac{\partial[\mathrm{SB_p}]}{\partial t} = -k_{\mathrm{deg-sb_p}} \cdot [\mathrm{SB_p}] + \left(k_{\mathrm{dnv_{sb}}} + k_{\mathrm{aut_{sb}}} \cdot [\mathrm{SB_p}]^2\right) \cdot [\mathrm{SB_m}] - k_{\mathrm{depol_{sb}}} \cdot [\mathrm{SB_p}] + D_{\mathrm{sb_p}} \cdot \frac{\partial^2[\mathrm{SB_p}]}{\partial x^2} + v \cdot \frac{\partial[SB_p]}{\partial x} \cdot (1 - \frac{\mathrm{ParA_d}}{\mathrm{ParA_{tot}}}) \cdot (1 - \frac{\mathrm{PopZ_{pol}}}{\mathrm{PopZ_{tot}}})$	8
$\frac{\partial[\mathrm{SB_m}]}{\partial t} = k_{\mathrm{syn-sb_m}} - k_{\mathrm{deg-sb_m}} \cdot [\mathrm{SB_m}] - \left(k_{\mathrm{dnv\_sb}} + k_{\mathrm{aut)sb}} \cdot [\mathrm{SB_p}]^2\right) \cdot [\mathrm{SB_m}] + k_{\mathrm{depol\_sb}} \cdot [\mathrm{SB_p}] + D_{\mathrm{sb_m}} \cdot \frac{\partial^2[\mathrm{SB_m}]}{\partial x^2}$	9
$\frac{\partial[\mathrm{PopZ_m}]}{\partial t} = k_{\mathrm{syn-pz_m}} \cdot [\mathrm{SB_p}] \cdot \sigma(x) - k_{\mathrm{deg-pz_m}} \cdot [\mathrm{PopZ_m}] - \left(k_{\mathrm{dnv\_pz}} + k_{\mathrm{aut\_pz}} \cdot [\mathrm{PopZ_p}]^2\right) \cdot [\mathrm{PopZ_m}] + k_{\mathrm{depol\_pz}} \cdot [\mathrm{PopZ_p}] - k_{dil} \cdot [\mathrm{PopZ_m}] + D_{\mathrm{pz_m}} \cdot \frac{\partial^2[\mathrm{PopZ_m}]}{\partial x^2}$	10
$\frac{\partial[\mathrm{PopZ_p}]}{\partial t} = -k_{\mathrm{deg-pz_p}} \cdot [\mathrm{PopZ_p}] + \left(k_{\mathrm{dnv\_pz}} + k_{\mathrm{aut\_pz}} \cdot [\mathrm{PopZ_p}]^2\right) \cdot [\mathrm{PopZ_m}] - k_{\mathrm{depol\_pz}} \cdot [\mathrm{PopZ_p}] - k_{dil} \cdot [\mathrm{PopZ_p}] + D_{\mathrm{pz_p}} \cdot \frac{\partial^2[\mathrm{PopZ_p}]}{\partial x^2}$	11
$\frac{\partial[\mathrm{FtsZ_m}]}{\partial t} = k_{\mathrm{syn-fz_m}} - k_{\mathrm{deg-fz_m}} \cdot [\mathrm{FtsZ_m}] - \left(k_{\mathrm{dnv_{fz}}} + k_{\mathrm{aut_{fz}}} \cdot [\mathrm{FtsZ_p}]^2\right) \cdot [\mathrm{FtsZ_m}] + k_{\mathrm{depol-fz}} \cdot [\mathrm{FtsZ_p}] \cdot [\mathrm{MipZ_p}] - k_{dil} \cdot [\mathrm{FtsZ_m}] + D_{\mathrm{fz_m}} \cdot \frac{\partial^2[\mathrm{FtsZ_m}]}{\partial x^2}$	12
$\frac{\partial[\mathrm{FtsZ_p}]}{\partial t} = -k_{\mathrm{deg-fz_p}} \cdot [\mathrm{FtsZ_m}] + \left(k_{\mathrm{dnv\_fz}} + k_{\mathrm{aut\_fz}} \cdot [\mathrm{FtsZ_p}]^2\right) \cdot [\mathrm{FtsZ_m}] - k_{\mathrm{depol\_fz}} \cdot [\mathrm{FtsZ_p}] \cdot [\mathrm{SBZ_p}] - k_{dil} \cdot [\mathrm{FtsZ_p}] + D_{\mathrm{fz_p}} \cdot \frac{\partial^2[\mathrm{FtsZ_m}]}{\partial x^2}$	13
$\frac{\partial[\mathrm{TipN_f}]}{\partial t} = k_{syn-\mathrm{tn}} - k_{deg-\mathrm{tn}} \cdot [\mathrm{TipN_f}] - k_{\mathrm{tnf-tnp}} \cdot [\mathrm{TipN_f}] \cdot [\mathrm{FtsZ_p}] + k_{\mathrm{tnp-tnf}} \cdot [\mathrm{TipN_p}] - k_{dil} \cdot [\mathrm{TipN_f}] + D_{\mathrm{tn}} \cdot \frac{\partial^2[\mathrm{TipN_f}]}{\partial x^2}$	14
$\frac{\mathrm{d}[\mathrm{Tip_b}]}{\mathrm{d}t} = k_{\mathrm{tnf-tnp}} \cdot [\mathrm{TipN_f}] \cdot [\mathrm{FtsZ_p}] - k_{\mathrm{tnp-tnf}} \cdot [\mathrm{TipN_p}] - k_{deg-\mathrm{tn}} \cdot [\mathrm{TipN_p}] - k_{\mathrm{pa-patn}} \cdot [\mathrm{ParA}] \cdot [\mathrm{TipN_p}] + k_{\mathrm{patn-pa}} \cdot [\mathrm{ParA_{tn}}] - k_{dil} \cdot [\mathrm{TipN_p}]$	15

$\frac{\partial[\mathrm{MipZ_f}]}{\partial t} = k_{syn-\mathrm{mz}} - k_{deg-\mathrm{mzf}} \cdot [\mathrm{MipZ_f}] - k_{\mathrm{mzf-mzb}} \cdot [\mathrm{MipZ_f}] \cdot [\mathrm{SB_p}] + k_{\mathrm{mzb-mzf}} \cdot [\mathrm{MipZ_b}] - k_{dil} \cdot [\mathrm{MipZ_f}] + D_{\mathrm{mz}} \cdot \frac{\partial^2[\mathrm{MipZ_f}]}{\partial x^2}$	16
$\frac{\mathrm{d}[\mathrm{MipZ_b}]}{\mathrm{d}t} = -k_{deg-\mathrm{mzp}} \cdot [\mathrm{MipZ_b}] + k_{\mathrm{mzf-mzp}} \cdot [\mathrm{MipZ_f}] \cdot [\mathrm{SB_p}] - k_{\mathrm{mzp-mzf}} \cdot [\mathrm{MipZ_b}] - k_{dil} \cdot [\mathrm{MipZ_b}]$	17

*Indicator function $\sigma(x) = 1$ within a distance of $0.2 \cdot L(t)$from either poles .

Table D.2: Parameters used in the model*

ParA			
$k_{\text{syn-pa}} = 1$	$k_{\text{deg-pa}} = 0.1$	$k_{\text{pa\_patn}} = 2$	$k_{\text{patn-pa}} = 0.1$
$k_{\text{pa-pa2}} = 50$	$k_{\text{pa2-pa}} = 0.1$	$k_{\text{pa2-pa2D}} = 1$	$k_{\text{pa2D-pa2}} = 1$
$k_{\text{pa2-pa2B}} = 0.01$	$k_{\text{pa2B-pa2}} = 0.05$	$k_{\text{pa2-pa2Z}} = 0.05$	$k_{\text{pa2Z-pa2}} = 0.25$
$k_{\text{pa-paZ}} = 0.05$	$k_{\text{paZ-pa}} = 0.25$	$k_{\text{hyd}} = 5$	$k_{\text{deg-patn}} = 0.01$
$k_{\text{deg-pa2}} = 0.01$	$k_{\text{deg-pa2D}} = 0.01$	$k_{\text{deg-pa2B}} = 0.01$	$k_{\text{deg-pa2Z}} = 0.01$
$D_{\text{pa}} = 2$	$D_{\text{pa2}} = 0.1$		
SB (*parS*/ParB)			
$k_{\text{syn-sbm}} = 1.5$	$k_{\text{deg-sbm}} = 0.25$	$k_{\text{deg-sbp}} = 0.075$	$k_{\text{dnv\_sb}} = 20$
$k_{\text{aut\_sbl}} = 1.5$	$k_{\text{depol\_sb}} = 1$	$D_{\text{sbm}} = 100$	$D_{\text{spp}} = 0.005$
$v = 0.8$			

PopZ			
$k_{syn\text{-}pzm} = 20$	$k_{deg\text{-}pzm} = 0.25$	$k_{deg\text{-}pzp} = 0.075$	$k_{dnv\_pz} = 300$
$k_{aut\_pz} = 1.5$	$k_{depol\_pz} = 1$	$D_{pzm} = 100$	$D_{pzp} = 0.01$
FtsZ			
$k_{syn\text{-}fzm} = 0.8$	$k_{deg\text{-}fzm} = 0.05$	$k_{deg\text{-}fzp} = 0.05$	$k_{dnv\_fz} = 80$
$k_{aut\_fz} = 10$	$k_{depol\_fz} = 5$	$D_{fzm} = 100$	$D_{fzp} = 0.1$
TipN			
$k_{syn\text{-}tpn} = 0.8$	$k_{deg\text{-}tpn} = 0.5$	$k_{tnf\text{-}tnp} = 1$	$k_{tnp\text{-}tnf} = 0.1$
$D_{tn} = 100$			
Cell growth			
$k_{growth} = 0.0055$	$k_{dil} = 0.0055$		
MipZ			
$k_{syn\text{-}mz} = 1$	$k_{deg\text{-}mz} = 0.1$	$k_{deg\_mzp} = 0.1$	$D_{mz} = 100$
$k_{mzf\text{-}mzb} = 1$	$k_{mzb\text{-}mzf} = 0.1$		

* Parameters of the form k_{sub} have units of min^{-1}, v has units of $\mu m\ min^{-1}$, D_{sub} has units of $\mu m^2\ min^{-1}$

Table D.3: Parameters used in the mutant simulations.

Δ*tipN*	$k_{syn\text{-}tpn} = 0$	*parA* overexpression	$k_{syn\text{-}tpn} = 10$
popZ-S1	$k_{pa\text{-}paZ} = 0.05$	*popZ*-S2	$k_{pa2\text{-}pa2Z} = 0.05$
parA$_{D44A}$	$k_{hyd} = 0$	*parA*$_{G16V}$	$k_{pa\text{-}pa2} = 0$
parA$_{R195E}$	$k_{pa2\_pa2D} = 0$		